

**TRANSMYOCARDIAL ST POTENTIAL
DISTRIBUTIONS IN ISCHAEMIC HEART DISEASE**

Qin Li
2005

**TRANSMYOCARDIAL ST POTENTIAL
DISTRIBUTIONS IN ISCHAEMIC HEART DISEASE**

by
Qin Li
M.B., B.S. (China)

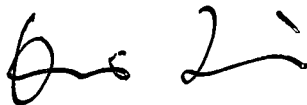
Submitted in fulfillment of the requirements for the degree of
Doctor of Philosophy

Medicine

Faculty of Health Science, University of Tasmania
January, 2005

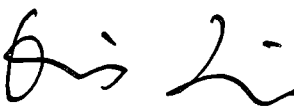
DECLARATION

The investigations described in this thesis constitute my own work. This thesis contains no material which has been accepted for the award of any other higher degree or graduate diploma in any tertiary institution. To the best of my knowledge and belief, this thesis contains no material previously published or written by another person, except where due acknowledgement and reference are made in the text of the thesis.

Signed: 

Date: December, 2004

This thesis may be made available for loan and limited copying in accordance with the *Copyright Act 1968*.

Signed: 

Date: December, 2004

To my husband, Changhai, and my son, Xiaoxuan.

ABSTRACT

The origin of electrocardiographic ST segment depression in subendocardial ischaemia remains unclear. The location of ST depression does not enable the localization of an ischemic region. Previous studies showed that the current path was within the intramyocardium, and there was a current sink at the boundary of the ischaemic area which caused the ST depression on the epicardium. Thus, it is vital to explore the intramyocardial potential distributions during subendocardial ischaemia. Different subendocardial ischaemia animal models were produced in the present study as well as acute myocardial ischaemia model.

(1) SUBENDOCARDIAL ISCHAEMIA MODEL

The subendocardial ischaemia was produced by combining left atrium pacing with partial occlusion of the left anterior descending coronary artery (LAD) and/or the left circumflex coronary artery (LCX). ST potentials were collected simultaneously from epicardial, endocardial and three different layers of the intramyocardium of the left ventricular wall. Regional myocardial blood flow (RMBF) was also measured in the inner one-third, mid one-third and outer one-third of the left ventricular wall by fluorescent microspheres.

The RMBF results showed that there was a decrease of endocardial RMBF in the ischaemic region during subendocardial ischaemia.

In subendocardial ischaemia of alternate LAD or LCX areas, ST depression occurred on the epicardium, the distributions of the ST potential on the epicardium from either ischaemic region were very similar. At the same time, endocardial potentials showed ST elevation which was directly associated with the ischaemic area. In the intramyocardium, both ST elevation and ST depression occurred in different layers from the subendocardium to the subepicardium. Epicardial ST depression can not predict the ischaemic area, however, ST distribution patterns in different layers of intramyocardium during subendocardial ischaemia can be predicted from electrocardiographic theory. Thus, it is suggested that the intramyocardial electrical current path might be altered towards the epicardium.

(2) SUBENDOCARDIAL ISCHAEMIA MODEL: TRANSITION FROM MILD TO SEVERE DEGREE

Further experiments were performed to transit ischaemia from mild degree to severe

degree, and finally to full thickness ischaemia, in an attempt to explain how the intramyocardial electrical current path altered when spread towards the epicardium. ST potentials were also recorded simultaneously from epicardium, endocardium and three different layers of the left ventricular wall. By combining occlusion of the LAD or LCX by 30% and 70% of its original blood flow with left atrium pacing, mild and severe ischaemia were produced, full thickness ischaemia was produced by total occlusion of the LAD or LCX.

Measurement of RMBF showed that RMBF in the inner one-third layer decreased, while RMBF in the mid and outer one-third layers remained unchanged in mild ischaemia. RMBF in every layer decreased in severe ischaemia in the ischaemic regions, with RMBF decreasing most in the inner one-third layer and least in the outer one-third layer. Although it was expected that, with 70% occlusion of the coronary artery, there would be an abrupt transition of RMBF between the mid and outer one-third layer of the left ventricular wall, the RMBF of the entire left ventricular wall was affected in the severe ischaemia.

In the mild ischaemia group in either the LAD or LCX area, epicardial ST depression occurred after ischaemia and it was not related to the ischaemic region. Simultaneously recorded endocardial potentials showed ST elevation which was related to the ischaemic area. Intramyocardial ST potentials showed both ST elevation and ST depression in different layers of the LV wall, with ST elevation occurring in the ischaemic centre and ST depression occurring on the boundary of the ischaemic and non-ischaemic area.

In severe subendocardial ischaemia of either the LAD or LCX area, both ST elevation and ST depression occurred on epicardium and different layers of intramyocardium, as in mild ischaemia, ST elevation appeared in ischaemic area, with the maximal magnitude occurring in the ischaemic centre; ST depression appeared in the non-ischaemic area, the magnitude of ST depression decreased towards the ischaemic boundary. Endocardial ST elevation in severe ischaemia occurred in the ischaemic region. The different epicardial ST distribution between the mild and the severe ischaemic groups led to a postulate that the current path might breakthrough towards the epicardium during severe subendocardial ischaemia.

When the ischaemia became full thickness, ST elevation appeared on the ischaemic area, and ST depression occurred on the non-ischaemic area in every layer of the left ventricle. However, the maximal ST elevation and ST depression occurred on the boundary of the ischaemic and the non-ischaemic regions. The ST distribution patterns between severe and full thickness ischaemia were totally different.

(3) ACUTE MYOCARDIAL ISCHAEMIA MODEL

Acute transmural ischaemia was developed by ligating either the LAD or the LCX. ST potentials and RMBF were recorded and measured in the same way as that in subendocardial ischaemia.

After acute ischaemia, RMBF in different layers of the left ventricular wall in the ischaemic region decreased significantly, and RMBF in the inner and mid one-third layers in the non-ischaemic region also decreased.

Similar ST potential distributions were obtained on different layers of the heart, *i.e.*, ST elevation occurred on the acute ischaemic region while ST depression occurred on the non-ischaemic region. The highest magnitude of maximal and minimal ST potential occurred on the boundary of the ischaemic and the non-ischaemic areas. ST shift had a positive relationship with RMBF. However, ST depression did not relate to the corresponded RMBF decrease. The results supported that some basic balance between ST elevation and ST depression existed during ischaemia, the total current flowing out of the heart must flow back into the heart. The ST depression was also a part of the source.

ACKNOWLEDGEMENT

I wish to sincerely thank my supervisor, **Professor David Kilpatrick**, for his constant guidance, invaluable advice and encouragement throughout the whole project, in the preparation of this thesis and his support for this project.

I am grateful to **Dr. Ah Chot Yong** for his continuous help in the laboratory and in checking and proofreading the manuscripts; for his encouragement and understanding throughout the project.

Grateful thanks to **Dr. Stuart Corney** for his technical and computer skill assistance, and his hard work in computer program related to this project; for his proofreading the manuscripts.

My thanks also extended to Ms **Linxin Guo** and Ms **Rita Corney** for their computer skill help; and for Ms **Rita Corney's** proofreading the manuscripts.

Thanks to Miss **Jan Walsh** for her encouragement.

Discipline of **Biochemistry** in the University of Tasmania for the use of their spectrophotofluorometer. Mr **Jeffrey Appleby** in Discipline of Biochemistry for his kind arrangement of using the spectrophotofluorometer.

Catheterisation Laboratory in the Royal Hobart Hospital for their support of catheters.

All the staff in Faculty of Health Science who provided a congenial and friendly atmosphere in which to work.

Special thanks to my husband **Dr. Changhai Ding** for his understanding, support and continuous encouragement throughout my study, and my son **Xiaoxuan Ding** who made this project full of joy.

CONTENTS

CHAPTER ONE	INTRODUCTION	1
1.1	RESEARCH BACKGROUND	1
1.2	RESEARCH PROPOSAL AND ORGANIZATION OF THE THESIS	4
CHAPTER TWO	LITERATURE EVIEW	6
2.1	FUNDAMENTALS OF ELECTROCARDIOGRAPHY	6
2.1.1	The genesis of the ECG	6
2.1.2	Cellular basis of ECG	8
2.1.2.1	<i>Resting membrane potential</i>	8
2.1.2.2	<i>Action potential</i>	11
2.1.2.3	<i>Conduction of action potential in cardiac fibre—local circuit currents</i>	12
2.1.3	Cardiac electrical field	14
2.1.4	The relationship between electrocardiogram and cardiac electric field	14
2.1.5	Relationship between action potential and ECG	17
2.2	ST SEGMENT SHIFT IN ISCHAEMIC HEART DISEASE	18
2.2.1	ST segment in ECG	18
2.2.2	ST segment shift in ischaemic heart disease	18
2.2.2.1	<i>ST segment elevation in ischaemic heart disease</i>	18
2.2.2.2	<i>ST segment depression in ischaemic heart disease</i>	21
2.2.3	Cellular basis of ischaemic electrocardiographic changes	24
2.2.4	Injury current and its relationship with ischaemic electrocardiographic changes	25
2.2.5	Mechanism of electrocardiographic patterns in myocardial ischaemia	29
2.2.5.1	<i>The mechanism of ST segment elevation</i>	29
2.2.5.2	<i>The mechanism of ST segment depression</i>	29
2.2.5.3	<i>Theoretical analysis of ST segment shift —the solid angle theory</i>	36
2.2.6	Ions changes underlying ST segment shift	46
2.3	PHYSIOLOGY, PATHOPHYSIOLOGY AND ST SEGMENT DISTRIBUTION IN MYOCARDIAL ISCHAEMIA	47
2.3.1	Myocardial blood flow and myocardial metabolism	47
2.3.1.1	<i>Methods of measuring transmural myocardial blood flow</i>	47
2.3.1.2	<i>Blood flow distribution in normal heart</i>	48
2.3.1.3	<i>Determinants of myocardial metabolic rate and coronary blood flow</i>	49

2.3.2 Transmural progress of ischaemic cell death	50
2.3.2.1 <i>Consequences of myocardial ischaemia</i>	50
2.3.2.2 <i>Transmural progress of ischaemic cell death</i>	51
2.3.2.3 <i>Mechanism of transmural progress of ischaemia pattern</i>	52
2.3.3 Lateral boundaries of ischaemia	54
2.3.4 Transmural ST segment distribution in myocardial ischaemia	56
2.3.5 Translateral ST segment shift in myocardial ischaemia	58
2.3.6 ST segment shift in myocardial ischaemia and its relationship to myocardial blood flow	61
2.3.6.1 <i>ST segment shift in transmural myocardial infarction and its relationship to myocardial blood flow</i>	61
2.3.6.2 <i>ST segment shift in subendocardium and its relationship to myocardial blood flow</i>	62
2.4 MODELS AND SIMULATION OF ELECTROCARDIOGRAPH	65
2.4.1 Consideration related to electrocardiograph study	65
2.4.2 Sources of the models	65
2.4.3 Volume-conductor problem	68
2.4.4 Models and simulation of electrocardiograph for forward problems	68
2.4.5 Models and simulation of electrocardiograph for inverse problem	71
2.4.6 Electrocardiograph models for myocardial ischaemia study	73
2.5 APPLICATION OF MAPPING TECHNIQUES	77
2.5.1 Application of electrodes for mapping purpose	77
2.5.2 Analysis of mapping	80
2.5.3 Application of mapping	82
2.5.3.1 <i>Application of body surface mapping</i>	82
2.5.3.2 <i>Application of epicardial, endocardial and intramyocardial mappings</i>	85
CHAPTER THREE MATERIALS AND METHODS	90
3.1 EXPERIMENTAL ANIMALS	90
3.2 ANIMAL PREPARATION AND SURGICAL PROCEDURES	91
3.3 DRUGS AND CHEMICALS	92
3.4 EXPERIMENTAL INSTRUMENTS	93
3.5 REGIONAL MYOCARDIAL BLOOD FLOW MEASUREMENT	94
3.5.1 Preparation of fluorescent microspheres	95
3.5.2 Injection of fluorescent microspheres	96
3.5.3 Digestion of tissue samples and the dissolve of microspheres	96

3.5.4 Measurement of fluorescent intensity	97
3.5.5 Analysis and calculation of the results	98
3.5.6 Evaluation of fluorescence of microspheres and intrinsic fluorescence of myocardium and solvents	98
3.6 POTENTIAL RECORDING AND MAP CONSTRUCTION	100
3.6.1 Potential recording	100
3.6.1.1 <i>Epicardial sock</i>	100
3.6.1.2 <i>Endocardial basket</i>	101
3.6.1.3 <i>Intramyocardial needles</i>	102
3.6.1.4 <i>Potentials recording system</i>	105
3.6.2 Construction of isopotential maps and map display	106
3.6.2.1 <i>Corroboration of the electrode position and reconstruction of the heart outline</i>	106
3.6.2.2 <i>Data analysis</i>	107
3.6.2.3 <i>Computer programs</i>	109
3.7 HAEMODYNAMIC MEASUREMENTS	109
3.7.1 Left ventricular, carotid artery and left atrium pressure	109
3.7.2 Coronary artery blood flow	109
3.7.3 Data recording	110
3.8 STATISTICAL ANALYSIS	110
 CHAPTER FOUR INTRAMYOCARDIAL ST SEGMENT POTENTIAL DISTRIBUTION IN SUBENDOCARDIAL ISCHEMIA	 111
 4.1 MATERIALS AND METHODS	 111
4.1.1 Experimental animals and protocols	111
4.1.2 Experimental procedures and subendocardial ischaemia	112
4.1.3 Regional myocardial blood flow measurement	112
4.1.4 Potentials recording and map construction	113
4.2 RESULTS	114
4.2.1 Haemodynamic response	114
4.2.1.1 <i>Haemodynamic response to pacing</i>	114
4.2.1.2 <i>Haemodynamic response to subendocardial ischemia</i>	115
4.2.2 RMBF response	116
4.2.2.1 <i>RMBF response to pacing</i>	116
4.2.2.2 <i>RMBF response to subendocardial ischemia</i>	118
4.2.3 ST potential distribution	121
4.2.3.1 <i>ST potential distribution in pacing alone group</i>	121

4.2.3.2 <i>ST potential distribution in subendocardial ischaemia in either LAD or LCX area</i>	124
4.2.3.3 <i>ST potential distribution in subendocardial ischaemia in alternation of LAD area and LCX area</i>	134
4.2.3.4 <i>Relationship between ST potential distribution and RMBF in subendocardial ischaemia</i>	143
4.3 DISCUSSION	148
4.3.1 Subendocardial ischaemia model	148
4.3.2. Potential recording method	150
4.3.3 Potential distributions and intramyocardial electrical current path	152
 CHAPTER FIVE INTRAMYOCARDIAL ST SEGMENT POTENTIAL DISTRIBUTION: TRANSITION FROM MILD TO SEVERE SUBENDOCARDIAL ISCHAEMIA	 159
5.1 MATERIALS AND METHODS	159
5.1.1 Experimental animals and protocols	159
5.1.2 Experimental procedures and subendocardial ischaemia	160
5.1.3 RMBF measurement	160
5.1.4 Potentials recording and map construction	160
5.2 RESULTS	161
5.2.1 Haemodynamic response	161
5.2.2 RMBF response	162
5.2.3 ST potential distribution: transition from mild to severe subendocardial ischaemia	167
5.2.4 Relationship between ST potential distributions and RMBF in mild and severe ischaemia in either LAD or LCX area	174
5.3 DISCUSSION	177
 CHAPTER SIX INTRAMYOCARDIAL ST SEGMENT POTENTIAL DISTRIBUTION IN ACUTE TRANSMURAL ISCHAEMIA	 182
6.1 MATERIALS AND METHODS	182
6.1.1 Experimental animals and protocols	182
6.1.2 Experimental procedures and acute transmural ischaemia	183
6.1.3 RMBF measurement	183
6.1.4 Potentials recording and map construction	183

6.2 RESULTS	184
6.2.1 Haemodynamic changes in acute transmural ischaemia	184
6.2.2 RMBF changes in acute transmural ischaemia	185
6.2.3 ST potential distribution in acute transmural ischaemia	188
6.2.3.1 <i>ST potential distributions in acute transmural ischaemia in LAD ligation</i>	188
6.2.3.2 <i>ST potential distributions in acute transmural ischaemia in LCX ligation</i>	191
6.2.4 Time course of ST potential distributions in acute transmural ischaemia	194
6.2.4.1 <i>Time course of ST potential distributions in acute transmural ischaemia in LAD ligation</i>	194
6.2.4.2 <i>Time course of ST potential distributions in acute transmural ischaemia in LCX ligation</i>	197
6.2.5 Relationship between ST potential distributions and RMBF in acute transmural ischaemia	200
6.2.5.1 <i>Relationship between ST potential distributions and RMBF in acute transmural ischaemia in LAD ligation</i>	200
6.2.5.2 <i>Relationship between ST potential distributions and RMBF in acute transmural ischaemia in LCX ligation</i>	202
6.2.5.3 <i>Correlation between ST potential shift and RMBF in acute transmural ischaemia</i>	204
6.2.6 Relationship between ST elevation and ST depression	207
6.3 DISCUSSION	209
6.3.1 Haemodynamic response in acute myocardial ischaemia	209
6.3.2 RMBF in acute myocardial ischaemia	210
6.3.3 Epicardial, endocardial and intramyocardial ST potential distributions during acute myocardial ischaemia	210
6.3.4 ST depression in acute myocardial ischaemia	212
CHAPTER SEVEN CONCLUSION	216
7.1 SUMMARY OF THE STUDY	216
7.2 SUBENDOCARDIAL ISCHAEMIA MODEL	217
7.3 TRANSITION FROM MILD TO SEVERE SUBENDOCARDIAL ISCHAEMIA	218
7.4 ACUTE MYOCARDIAL ISCHAEMIA MODEL	220

ABBREVIATIONS

AC	alternating current
bmp	beats per minute
BF	blood flow
BSPM	body surface potential mapping
CAP	carotid artery pressure
DC	direct current
ECG	electrocardiogram
endo	endocardium or endocardial
endo/epi	endocardial/epicardial
epi	epicardium or epicardial
LA	left atrial or left atrium
LAD	left anterior descending coronary artery
LAP	left atrial pressure
LCX	left circumflex coronary artery
LV	left ventricular or left ventricle
LVDP	left ventricular end diastolic pressure
LVP	left ventricular pressure
LVSP	left ventricular systolic pressure
MCG	magnetocardiography
PDA	posterior descending coronary artery
RMBF	regional myocardial blood flow
RV	right ventricular or right ventricle

CHAPTER ONE INTRODUCTION

1.1 RESEARCH BACKGROUND

The historical development of the electrocardiogram has resulted in a clinical diagnostic tool, the 12-lead electrocardiogram (ECG).

Electrocardiographic ST segment deviation, including ST elevation and ST depression, has been long regarded as a sign of ischaemic heart disease (Pardee, 1920; Wilson et al., 1933d; Kmekci et al., 1961; Kleber et al., 1978).

The cellular mechanism of electrocardiographic ST elevation has been well studied (Samson and Scher, 1960; Prinzmetal 1961; Shaefer and Hass, 1962; Kleber, 1978). In an elaborately designed animal experiment, Kleber (Kleber et al., 1978) studied ischaemic ST deviation on a cellular level. In Kleber's experiment, both transmembrane potentials from the subepicardial ventricular cells and local extracellular DC electrograms in isolated perfused pig hearts were recorded before and after the occlusion of the LAD. Two mechanisms have been put forward to explain the ischaemic ST deviation. Firstly, the ischaemic cardiac cells were less depolarised (i.e., relatively positive compared to normal cells) during the resting phase of action potential compared to the normal heart muscle, which results in injury current flowing from the ischaemic tissue to normal heart tissue with depression of the QT segment of the extracellular potential, which on normal alternating coupled (AC) amplifiers, is represented by ST elevation. Secondly, it was found that during the active phase of action potential, the action potential duration shortened, the upstroke velocity and the amplitude of action potential diminished in ischaemic cardiac cells, the intracellular potential of ischaemic tissue was electrically lower than the normal tissue, which resulted in a systolic injury current flowing from the normal tissue to the ischaemic tissue, also producing ST elevation on surface electrocardiogram.

The mechanism of ST depression in ischaemic heart disease has been controversial (Prinzmetal et al., 1959 and 1961; Ekmekci, 1961; Toyoshima et al., 1964; Holland and Brooks, 1975; Vincent et al., 1977). Wilson (Wilson et al., 1933a) used dipole theory to interpret the electrocardiogram information in ischaemic heart disease. The dipole model considered the active myocardial event as a single dipole source that contained both the maximum and the minimum potentials. Accordingly, an injured tissue of the myocardium acts in systole as the positive pole of dipoles situated on its

boundary with the normal myocardium, and the latter acts as the negative pole. In the event of subendocardial ischaemia, the epicardium over the ischaemic region faces the negative pole of the dipole; the cavity faces the positive pole. Thus, the electrodes over the ischaemic region will record depressed ST and the cavity will yield elevated ST (Bayley, 1946; Yu and Stewart, 1950; Cook et al., 1958). The dipole theory was expanded into the solid angle electrocardiogram theory by Holland and Brooks (Holland and Brooks, 1975). They suggested that ST deflection in ischaemic heart disease is a boundary phenomenon that depended on the diastolic and the systolic injury currents flowing at the boundary between the ischaemic myocardium and the normal myocardium. The electrocardiographically recorded potential was directly proportional to both solid angle and the difference in transmembrane potentials between the normal and the ischaemic regions. Thus, according to this theory, endocardial ischaemia would cause relative depression of the ST segment in the epicardium due to the reversed current flow at the boundary of the normal and the ischaemic myocardium, and that this ST depression should provide the means for localizing ischaemia. However, Holland and Brooks failed to produce subendocardial ischaemia in the porcine model and were unable to confirm their theoretical prediction of subendocardial ischaemia. Clinical research has also shown that ST depression can not localise the ischaemic region (Dunn et al., 1981; Ikeda et al., 1985; Mark et al., 1987), this inability of ST depression to localise the ischaemic region cannot be explained by classical theoretical analysis (Wilson et al., 1933a; Holland and Brooks, 1975 and 1977; Tung, 1978).

In a recent study exploring the origin of ST depression in subendocardial ischaemia, both epicardial and endocardial potential distributions were recorded (Li et al., 1998). With subendocardial ischaemia produced in either the LAD or LCX area, the epicardial ST depression distribution looked very similar, and did not localise the ischaemic area, even though simultaneous recorded endocardial ST elevation occurred on the ischaemic region. These results were not consistent with classical electrocardiogram theories (Wilson et al., 1933a; Holland and Brooks, 1975 and 1977).

To understand the origin of ST depression on the epicardium during subendocardial ischaemia, it is important to trace the electrical path. Kilpatrick (Kilpatrick et al., 1990) postulated that ST depression on the surface ECG originates from current flowing from an endocardial ischaemic region to the outside of the heart through the great vessels and atria. This hypothesis explained the difficulty in localising ischaemia from body surface ST depression. To test this hypothesis, a further study

was carried out by insulating the heart from the return current (Li et al., 1998), the results showed that there was an increase of the magnitude of ST depression on epicardium and a decrease of magnitudes of the QRS complex and T wave in the routine ECG limb leads, whereas the ST depression distribution on the epicardium remained unchanged. This result suggested that the source of ST depression is intramyocardial, rather than involving external paths. This contention was further tested by the transition of subendocardial ischaemia to transmural ischaemia (Li et al., 1998). From the transition of subendocardial ischaemia to full-thickness ischaemia, it was found that epicardial ST depression increased gradually over the boundary region as the ischaemia progressed until ST elevation ensued over the ischaemic region as the ischaemia became transmural. The increase of ST depression before the occurrence of ST elevation was also observed in a study with a perfused canine heart by Guyton et al in 1997 (Guyton et al., 1977). In another study on the effects of conducting media on cardiac potential (Green et al., 1991), it was found that the amplitude of the epicardial QRS potentials from both intact and isolated hearts was markedly higher when the heart was surrounded by an insulating medium but that the QRS potential distribution patterns were less affected. This also supports that the electrical path of the active heart is within the heart muscle.

A mathematical model of the whole heart was constructed by Li and co-workers (Li et al., 1998) to explain the experimental results. From the bidomain model, epicardial ST depression was obtained over the lateral region in either the LAD or the LCX partial occlusion, and endocardial ST elevation over the ischaemic region, which correlated well with the experimental results. It showed that there was a powerful current sink at the boundary of the ischaemic and the non-ischaemic tissues. The model effectively predicted that the major current flow would occur over the boundary. Since the LAD and the LCX share their boundary at the lateral wall, no matter which side of the boundary was involved, there would be similar ST depression distribution on the epicardium. However, further more simple simulations in a block with anisotropy of myocardium suggested that the ischaemic region could be predicted from the region of ST depression, which was discrepant to Li's study (Johnston et al., 2001).

Since the electrical path is within the myocardium, it is necessary to look at the intramyocardial potential distribution, this data will be vital for understanding the current flowing at the ischaemic boundary, and thus to further analyze the source of ST depression.

Acute myocardial ischaemia is commonly associated with ST elevation in ECG leads over the damaged region, “reciprocal” ST depression may appear in ECG leads remote from the infarction region. The origin and significance of ST depression associated with acute myocardial infarction is controversial (Gibson et al., 1982; Ferguson et al., 1984; Roubin et al., 1984; Mirvis, 1988; Bates et al., 1990; Krone et al., 1993; Wong et al., 1993; Edmunds et al., 1994). Animal models of small size of acute myocardial infarction showed uniform ST elevation over the infarcted region with little change over the remaining epicardium (Holland and Brooks, 1975; Smith et al., 1979; Kleber et al., 1978). However, in Li and co-workers’ (Li, et al., 1999) experimental sheep model, they found that ST depression always accompanied ST elevation in large size of acute transmural ischaemia whereas in small size of acute transmural ischaemia, ST depression was almost invisible. They explained this phenomenon by constructing a concentric sphere model which suggested that some basic balance between size of ischaemia and ST elevation to ST depression ratio exists. The total current flowing out of the heart must flow back into the heart, *i.e.*, the overall current out of the heart must be zero. This study was analysed using the data from both epicardial and endocardial ST potentials. Because the current path is within the myocardium, it is essential to take the intramyocardial potential into account when trying to define the origin of ST depression in acute myocardial ischaemia.

1.2 RESEARCH PROPOSAL AND ORGANIZATION OF THE THESIS

Based on the above knowledge, this study was carried out to detect why electrical current, at the boundaries of subendocardial ischaemia, flows in such a manner as to cause epicardial ST depression over the boundary. A series of experiments measuring potentials simultaneously from intramyocardial electrodes, in addition to the epicardial and endocardial electrodes, were performed in ischaemic sheep models. Epicardial and endocardial potentials were recorded from the entire left ventricle surface of both epicardium and endocardium. Intramyocardial potentials were recorded with 29 needles scattered on the boundary of the myocardium supplied by the LAD and LCX. Each needle has three electrodes of different depth when inserted into the heart muscle. The design of the experiments aimed to give as much information as required to understand the electrical path of the heart.

Firstly, animal models of subendocardial ischaemia of either the LAD or LCX area were constructed and confirmed by measuring regional myocardial blood flow (RMBF) using fluorescent microspheres. This kind of experiment model would give

an overall view of potential distributions at different layers of the heart. Subendocardial ischaemia regions were further induced sequentially in both the LAD and the LCX area in the same sheep, with a stable period of 30 minutes between the two manipulations in either order. By comparing the potential distributions in different areas of ischaemia in single experiment, convincing results should be achieved.

Secondly, transition of subendocardial ischaemia from mild degree to severe degree was performed in either the LAD or LCX area. Because the electrical path is within the myocardium, more detail about the potential distributions with the progress of subendocardial ischaemia would be obtained.

Finally, as a part of studying the origin of ST depression in subendocardial ischaemia, ST depression accompanying acute myocardial ischaemia was also studied.

This thesis is composed of seven chapters. Chapter one concludes the research background and the organization of the thesis. Chapter two is a literature review, covering the basic knowledge of electrophysiology of the heart, principal of the ECG, ECG manifestation of ischaemic heart disease and its mechanism. It also reviews the mapping technique in cardiac disease and simulation study of the heart. Chapter three describes the general methodology of this study. Chapter four studies the potential distributions in different layers of the heart in subendocardial ischaemia. Chapter five studies the potential distributions in different layers of the heart during transition of subendocardial ischaemia from mild to severe degree. Chapter six studies the potential distributions in different layers of the heart in acute myocardial ischaemia. Chapter seven gives an overall conclusion to the study.

CHAPTER TWO LITERATURE REVIEW**2.1 FUNDAMENTALS OF ELECTROCARDIOGRAPHY**

The primary function of the heart is to contract so that it can fulfill its role as a pump. The myocardium is unique among the muscles of the body in that it possesses the property of automatic rhythmic contraction, each contraction triggered by excitation waves of electrical activity. The electrical activity arises in the conduction system of the heart, which results in excitation throughout the myocardium. The formation and conduction of the electrical activity of the heart produces weak electrical currents that spread through the whole body. The electrocardiograph (ECG) is a graphic recording of the electrical potential differences, between any two points on the body surface produced by the electrical activity of the heart.

2.1.1 THE GENESIS OF THE ECG

In the genesis of ECG, several factors are involved: (1) initiation of impulse formation in the primary pacemaker (sinoatrial node); (2) transmission of the impulse through the specialized conduction system of the heart; (3) activation (depolarisation) of the atrial and ventricular myocardium; (4) recovery (repolarization) of all the above areas. (Goldman, 1986)

The initial impulse in the cardiac cycle begins in the sinoatrial node which has the most rapid rate of spontaneous depolarisation. In the normal heart, the sinoatrial node cells trigger the contraction, the impulse traverses the internodal pathways to depolarise the atria, producing the P wave. Atrial depolarisation is followed by atrial repolarization. The potentials generated by the atrial repolarization are not usually seen on the surface ECG because of their low amplitude and they are superimposed on the much higher amplitude QRS complex. After atrial repolarisation, the impulse reaches the atrioventricular node. Normally, the impulse is “delayed” in the atrioventricular node for 0.07 second before passing on to the bundle of His, the right and left bundle branches and the ramifications of the Purkinje system. Conduction through this electrical pathway is much more rapid than through ordinary heart muscle. The excitation of these structures is too small to produce detectable potentials on the body surface at the normal amplifier gains used in the clinical ECG, so it appears isoelectric which in normal ECG is represented by the PR segment. The impulse is then passed by the electrical pathway to the ventricular muscle.

The spread of excitation through the ventricular myocardium is from the endocardial to the epicardial surface. The broadly dispersed ramifications of the treelike or fractal Purkinje system and the rapid conduction within it result in depolarisation of most of the endocardial surfaces of both ventricles within several milliseconds and the simultaneous activation of multiple endocardial sites. Earliest activity begins in three sites: (1) the anterior paraseptal wall of the left ventricle, (2) the posterior paraseptal wall of the left ventricle, (3) the center of the left side of the septum. Wave fronts spread from these sites in anterior and superior directions to activate the anterior and lateral walls of the left ventricle. The posterobasal areas of the left ventricle are the last to be activated. Septal activation begins in the middle third of the left side and spreads across the septum from left to right and from apex to base. Excitation of the right ventricle begins near the insertion point of the right bundle branch close to the base of the anterior papillary muscle and spreads to the free wall. The final areas to be involved are the pulmonary conus and posterobasal areas. Thus, in both ventricles, the overall endocardial excitation pattern begins on septal surfaces and sweeps down and around the anterior free walls to the posterior and basal regions in an apex-to-base direction. The activation fronts then move from endocardium to epicardium. Excitation of the endocardium begins at sites of Purkinje-ventricular muscle junctions and proceeds with muscle cell-to-muscle cell conduction in an oblique direction toward the epicardium. The sequence of endocardial activation and endocardial-to-epicardial activation results in the characteristic waveforms of the QRS complex.

Following the excitation of the left ventricular muscle, the recovery of the ventricle occurs. Similar to activation, the recovery of the ventricles occurs in a characteristic geometrical pattern. As activation moves from endocardium to epicardium, sites further away from the endocardium are activated later and later in the sequence. However, action potential durations are longest near the endocardium and shortest near the epicardium, which produces a transmural gradient in recovery periods. Differences in action potential duration are greater than differences in activation times, so recovery is completed near the epicardium before it is completed near the endocardium, thus recovery occurs from the epicardial to the endocardial, resulting in T wave concordant with the QRS wave pattern. The period between excitation and recovery of the heart is electrically quiescent, with no regional differences in potentials occurring in the ventricles. This results in the isoelectrical ST segment of the ECG. After ventricular recovery, no current can be recorded and no potential differences exist, until the next impulse reaches the atria. This period is also isoelectrical in the ECG and is termed the TQ segment.

2.1.2 CELLULAR BASIS OF ECG

The behaviour of the transmembrane action potential of the myocardial cells influences the ECG. The character of the transmembrane action potential varies with its site of origin and is different in different cell types of the heart. Generally, the heart is composed of three types of specialized myocardial cells: one group of cells has the primary function of impulse formation (pacemaker cells); another group has the primary function of conduction (Purkinje fibres); and the third group has the primary function of mechanical contraction (Lipman et al, 1984). The third group is further divided into three subgroups in the left ventricular wall, i.e., epicardial cells, M cells and endocardial cells. Each cell type and subtype has different characteristic action potential, and the recorded ECG is a summation of the extracellular potentials generated by these individual action potentials as modified by the instrumentation used for their amplification and recording. The total ECG is also dependent on the sequence of activation, the status of the myocardium, and a variety of factors influencing depolarisation and repolarization.

The myocardial cell membrane is a thin lipid bilayer that separates the aqueous phases inside and outside the cells (Quinn, 1976; Katz, 1986). Many of the components of the bilayer (e.g., the phospholipids) have a hydrophobic portion oriented toward the interior of the lipid membrane and a charged hydrophilic portion oriented toward the internal or external aqueous phase, the lipids of the bilayer can be polarized, permitting the membrane to store charges, so myocardial membrane is a good capacitor. The membrane is selectively permeable to different ionic species that pass through channels controlled by gates which open and close in response to voltage, time, or the presence of a chemical activator, this character gives the membrane a high impedance.

2.1.2.1 Resting membrane potential

If a microelectrode is placed on the surface of a resting myocardial cell and a second (indifferent) microelectrode is placed in a remote location such as the extracellular space, no detectable potential is recorded because of the high impedance of the cell membrane. However, if the cell membrane is penetrated by a microelectrode, a negative potential will be recorded, which represents the potential difference between the inside and the outside of the cell. This potential is known as the “resting membrane potential” (Fig2.1.1) which varies from -60mV to -100mV , depending on

the type of cell and on the cell's state of depolarization. In the non-pacemaker cells of atria and the ventricles, the resting membrane potential remains steady until the cell is depolarized by the spread of excitation. In the pacemaker cell, a continuous slow diastolic depolarization brings the transmembrane potential to a critical level of about -65mV , which is called the "threshold potential", at this level, the depolarization becomes rapid and gives rise to a spontaneous action potential (vide post).

Measurements of the intracellular and extracellular ionic concentrations show a high intracellular potassium concentration and a low extracellular potassium concentration. Similar measurements of sodium concentration show the reverse, with high extracellular and low intracellular sodium levels. These concentrations are maintained by active metabolism of the myocardial cell and by the fact that the myocardial membrane is not completely permeable to these ions. The large ionic gradients across the membrane create the electrochemical potential.

The major factor that determines the resting membrane potential is the potassium ions gradient across the cell membrane. The intracellular concentration of potassium is about 150mEq/L , and the extracellular about 5mEq/L , resulting in a high 30:1 concentration gradient, the $\text{Na}^+\text{-K}^+$ pump, by an active ion transport mechanism, maintains this concentration gradient. During quiescent state, the membrane is of high permeability to potassium compared with other ions. Because of the high intracellular concentration of potassium, there is always a tendency for potassium to diffuse out of the cell down its concentration gradient, via the opening K^+ channels. However, the negative intracellular ions, mainly organic phosphates and charged proteins, can not accompany potassium ions because the cell membrane is impermeable to them. If the negative intracellular potential was big enough, the electrical attraction of the cell interior for the potassium could fully offset the outward diffusion tendency of the ions, creating a dynamic equilibrium in which there would be no further net movement of potassium ion out of the cell. The electrical potential at which this happens is called the potassium equilibrium potential. This electrical potential is, by definition, equal in magnitude to the outward-driving effect of the chemical concentration gradient. The exact relation between the potassium equilibrium potential and the potassium concentration ratio is given by the Nernst equation (Page 1962; Levick 1995),

$$E_{\text{K}^+} = (RT/F) \ln [\text{K}^+]_o / [\text{K}^+]_i$$

CHAPTER TWO

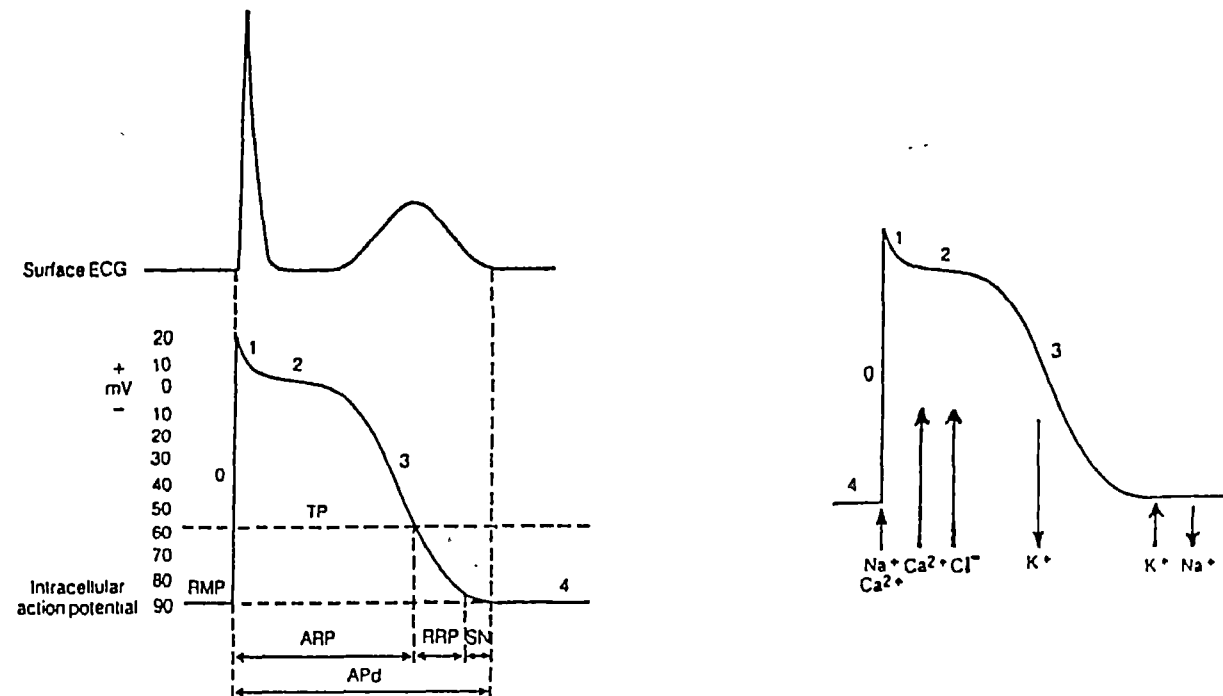


Fig 2.1.1 Left: diagram of transmembrane potential of a ventricular muscle cell and corresponding extracellular electrogram. Right: diagram of ions flux during action potential period and resting membrane potential period.

RMP=resting membrane potential; APd=action potential duration; TP=threshold potential; ARP=absolute refractory period; RRR=relative refractory period; SN=supernormal period of excitability. 0=depolarisation; 1,2,3=phases of repolarisation; 4=diastolic phase.

Phase 0: Rapid depolarisation due to Na^+ (and Ca^{2+}) influx; Phase 2: Plateau phase of repolarisation in which there is a slow influx of Ca^{2+} ; Phase 3: Efflux of K^+ resulting in slow return of intracellular potential to -90mV . At the terminal of phase 3 an active transport system extrudes Na^+ from the cell and pumps K^+ into the cell. Phase 4: Resting membrane potential $\approx -90\text{mV}$

Where R is the universal gas constant, T is the absolute temperature and F is the Faraday's constant. Experimentally, it is found that the myocyte's resting potential is indeed close to the potassium equilibrium potential (Page 1962; Levick 1995). It is also found that when the extracellular potassium concentration increased, as in ischaemia, the myocyte resting potential declines (became more negative) in proportion to the K^+ concentration, and a decreased extracellular K^+ concentration increases the resting membrane potential, as predicted by the Nernst equation (Surawicz, 1967).

2.1.2.2 Action potential

When a pulse reaches a myocyte, it will reduce the cell's transmembrane potential to a critical level known as the threshold potential. The threshold potential is about -65mV in atria and ventricular muscle cells and about -40mV in sinoatrial and atrioventricular nodal cells (Goldschlager and Goldman, 1989). The membrane potential reaching the threshold leads to depolarization of the membrane. At the onset of depolarization of a cardiac muscle cell (e.g. a ventricular muscle cell), there is an abrupt change in permeability of the cell membrane to sodium. As has been mentioned, in a quiescent state, the extracellular Na^+ concentration is relatively high in relation to intracellular Na^+ concentration and the membrane at this period is almost impermeable to Na^+ . This Na^+ concentration gradient across the membrane is also maintained by the $\text{Na}^+\text{-K}^+$ exchange pump. With the change of membrane potential to sodium, Na^+ (and Ca^{2+} to a lesser degree) enter the cell and result in a sharp rise of intracellular potential to positivity (approximately 20mV). This is designated as phase 0 and represents the fast inward current typical of normal myocardial cells and Purkinje fibres. Pacemaker cells of the sinoatrial node and cells in the proximal region of the atrioventricular node are depolarized by a slow inward current of calcium. Under abnormal conditions, cells whose fast inward current via sodium channels is inhibited can be depolarized by the slow inward current via calcium channels. The intracellular potential change to a positive degree is called the "overshoot". At the end of phase 0, all the carrier sites that allow Na^+ to be transported across the membrane have been saturated (inactivated) and the membrane becomes absolutely impermeable to sodium (beginning of the "absolute refractory period"). Therefore, initial depolarization depends on the Na^+ influx.

Following depolarization, there is a relatively slow and gradual return of intracellular potential to the resting membrane potential. This is termed the repolarization time and is divided into 3 phases: Phase 1: an initial rapid return of intracellular potential to 0mV. This is largely the result of abrupt closing of the sodium channels. It has been suggested that chloride ions entering the cell may also contribute to phase 1. Phase 2: a plateau phase of repolarization owing to the slow entrance of calcium ions into the cell. These are the same channels that can result in the slow inward type of depolarization. Phase 3: this represents the slow, gradual return of the intracellular potential to resting membrane potential. It results from extrusion of potassium ions out of the cell, which reestablishes the normal negative resting potential. During repolarization, the sodium carriers are not fully regenerated (activated) during most of the repolarization, hence the cell is partially refractory to stimulation. However, there is a period near the end of repolarization in which there is full reactivation of sodium carriers but the cell has not returned to the resting membrane potential and this is closer to the threshold level. This short period gives rise to the superexcitable (supernormal) period, when a smaller than normal stimulus will result in cellular depolarisation (Fig2.1.1). After repolarization, the cell is again permeable to potassium, there are an excess of sodium ions and a deficit of potassium ions, to restore the original ion concentration, the $\text{Na}^+\text{-K}^+$ pump becomes effective as mentioned before. The energy required pump, which has an adenosine triphosphate (ATP) dependent transport mechanism, removes sodium from the cell and permits potassium influx. The inhibition of the $\text{Na}^+\text{-K}^+$ pump in the early ischaemic stage can cause an increase in extracellular potassium (Kleber, 1983; Wilde and Kleber, 1986). In relation to the action potential, the resting membrane potential period is referred to phase 4.

2.1.2.3 Conduction of action potential in cardiac fibre —local circuit currents

An action potential travelling down a cardiac muscle fibre is propagated by local circuit currents which are shown in Fig2.1.2. Diagram A represents a normal myocardial fibre. In diagram B, there is a depolarized region where the external surface of the membrane is negative compared to the adjacent membrane, and the internal face of the depolarized membrane is positively charged relative to the neighbouring internal areas. These potential differences cause local currents to flow, which depolarize the membrane adjacent to the initial site of depolarisation if the initial electric current is sufficient to bring the adjacent membrane above threshold. The major carrier of this current is K^+ (Horan and Flowers, 1980). These newly

depolarized areas then cause current flows that depolarize other segments of the membrane still further removed from the initial site of depolarization. Diagram C shows the depolarisation is carried on by local circuit currents. Diagram D shows all the myocardial fibre is depolarised. When the depolarising current reaches the end of the cell, propagation of the action potential occurs through the gap junction which is a low-resistance structure responsible for intracellular electrical communication. (Pressler, 1987).

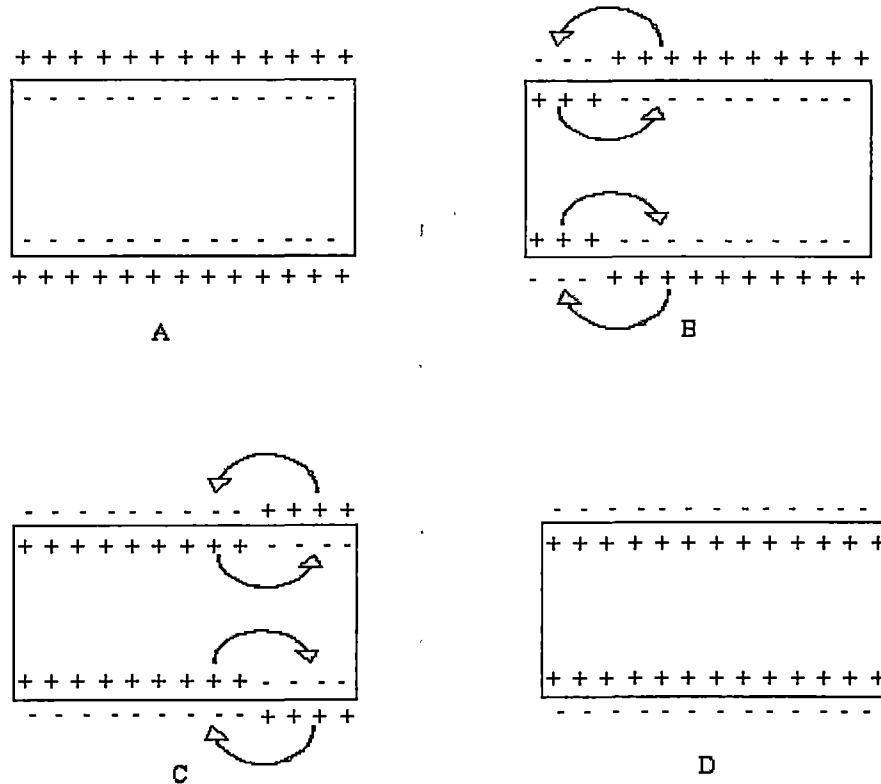


Fig 2.1.2 Mechanism of spread of depolarisation. A: a normal polarised myocardial fibre. B,C: the local circuit currents that flow to adjacent area of the membrane and allow conduction of the depolarisation. D: the reversal of membrane potential in depolarised myocardial fibre.

2.1.3 CARDIAC ELECTRICAL FIELD

Transmembrane potential is, by definition, differences in voltage between the inside and the outside of a cell, but the electrocardiogram records the differences of potential in an electrical field at a distance from the heart, and that electrical field exists because excitation spreads sequentially from one part of the heart to another. At every instant, from the beginning of an action potential in the first myocardial cell to be excited until the complete repolarization of the last one, it is possible to identify a line of demarcation that separates cells that have just been activated from those still in a resting state. This advancing wave front is the origin of the electrical field because the surface of cells just depolarized is electrically negative with respect to the exterior of those not yet activated, where the activated part is served as sink and the non-activated part is served as source, the electrical field generated by such dipole extends outwards. With such a dipole immersed in a conducting medium, an electric current is established which flows through the medium, similar to the magnetic field set up by the positive and negative poles of a magnet, the magnitude and direction of this complex dipole can be recorded and analysed from the body surface leads. The single dipole theory, put forward by Einthoven (Einthoven et al, 1913) and developed by Wilson (Wilson et al, 1933a) is oversimplified, but it is useful for explanation of the electrocardiogram. It is based on three premises: (1) The heart is a single dipole generator; (2) The body is a homogeneous conductor; and (3) All electrodes are equidistant from the dipole generator.

2.1.4 THE RELATIONSHIP BETWEEN ELECTROCARDIOGRAM AND CARDIAC ELECTRICAL FIELD

Depolarization and repolarization of the ventricles occur transversely, i.e. across the thickness of the ventricular myocardium from endocardial to epicardial surfaces. This is illustrated in Fig2.1.3 which, for simplicity, depicts a tissue of four cells extending from endocardium to epicardium. The exploring electrodes are placed on the chest wall (B) and the intracavity (A). Diagram One represents the resting state. All four cells are in the resting state, i.e. they are all in phase 4 of the transmembrane action potential. All the cells of the tissue have positive extracellular potential and negative intracellular potential. There is no difference in potential between the cells, and no current flows.

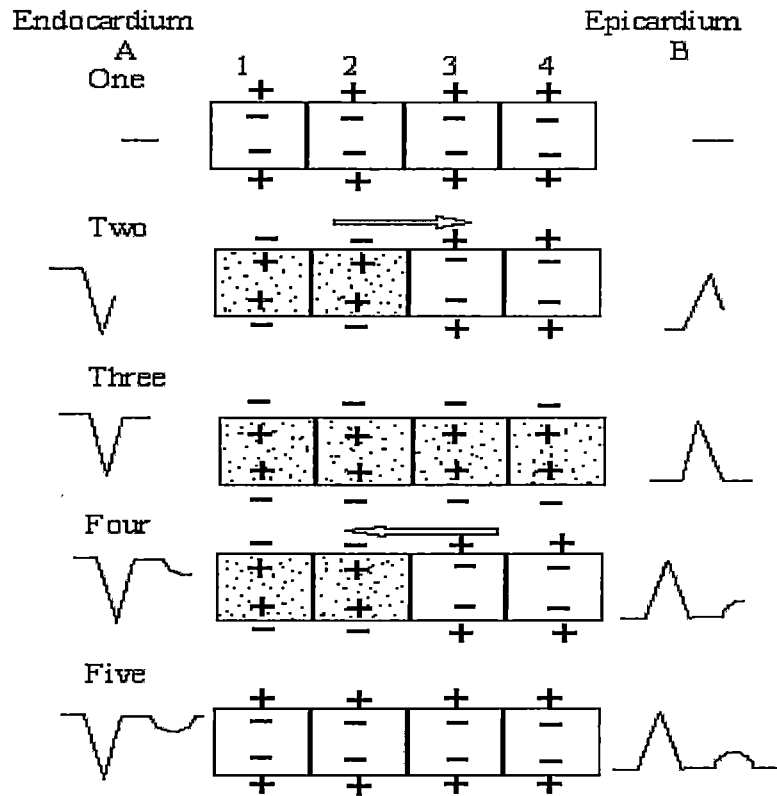


Fig 2.1.3 Process of depolarisation and repolarisation in a series of four cells hypothetically situated from endocardium to epicardium, and corresponding potential recording with exploring electrodes located at endocardium (A) and epicardium (B). The directions of depolarisation and repolarisation are indicated by arrows. (From Schamroth L. *Electrophysiology and electropathology*. In: *The electrocardiology of coronary artery disease*, Schamroth L, ed. Blackwell Scientific Publications, 1975 with modification. See text).

Diagram Two illustrates the process of normal depolarization from endocardium to epicardium, the cells being activated sequentially from cell 1 to cell 4. Cells 1 and 2 have been activated and are in phase 0 of the transmembrane action potential; cell 3 and 4 are still at rest and are in phase 4 of the transmembrane action potential. A doublet exists between cells 2 and 3, the first doublet of the activation process having occurred between cells 1 and 2. The doublet current with a positive head in extracellular space thus flows from endocardium to epicardium, giving rise to a positive QRS deflection in an electrode facing the epicardium, and a negative QRS deflection in an electrode facing the endocardium.

Diagram Three reflects the fully depolarized state, all four cells being in the process of recovery. This state corresponds principally to Phase 2 of the transmembrane action potential, the plateau. Since this is a relatively long phase, there is a large measure of overlap between the cells in this state, and sequential differences are usually not evident. Consequently there is no difference in surface potential, and no current flows. The conventional electrocardiogram therefore reflects no deflection, an isoelectric baseline, which corresponds principally to the ST segment.

As we know, repolarization of the activated cells does not occur in the same sequence as depolarisation. It generally occurs from epicardial to endocardial surfaces instead of from endocardial to epicardial surfaces. The first cell to be depolarized is the last cell to be repolarised, and vice versa. There are several reasons to explain why repolarisation of epicardium occurs earlier than endocardium: the pressure within the endocardial regions is greater compared to the epicardial regions of the myocardium during ventricular systole; different blood supply resulted from specific differences in the distribution of the coronary artery between epicardium and endocardium exists; the endocardium is easy to cool down by dispersing thermal energy to cardiac cavity. This reversed process of repolarization becomes evident when phase 3, the cascade of the transmembrane action potential, is reached. It shows in Diagram Four that cell 4 and 3 have already recovered, being fully polarized with positive extracellular potentials. A doublet exists between cells 2 and 3. The series of doublets so-to-speak proceeds from epicardium to endocardium with a negative head and a positive tail in the extracellular space, giving rise to a positive deflection, an upright T wave in leads orientated to the epicardium and a downward T wave in leads orientated to the endocardium. Diagram Five illustrates the fully repolarised, resting state of the four cells once again.

The measured electrical potential will depend on many factors, including the orientation of the leads with respect to the electrical field generated, rate and number of cells depolarised or repolarised, the nature of the conducting medium surrounding the heart, etc. If all the factors were known, together with the sequence of activation, and the exact intracellular potential of each cell, it would be possible to construct the ECG. This has been nearly done on numerous occasions (Rudy and Plonsey, 1980; Leon and Horacek, 1991; Khoury and Rudy, 1992; Zhou and van Oosterom, 1994; He et al., 1997; Johnston and Kilpatrick, 2003), which provide evidence to better understand the facets of the ECG.

2.1.5 RELATIONSHIP BETWEEN ACTION POTENTIAL AND ECG

The transmembrane action potential reflects the electrical events of a single cell, whereas the electrocardiogram reflects the electrical events of cardiac tissue, from very many cells. Nevertheless, because of the rapid near-synchronous activation of all the cells, the following approximate correlation exists between the two records (on ventricular level):

- | | |
|---------|---|
| Phase 0 | Corresponds to the QRS complex |
| Phase 1 | Corresponds to the J point, the junction of the QRS complex with the ST segment |
| Phase 2 | Corresponds to the ST segment |
| Phase 3 | Corresponds to the T wave |
| Phase 4 | Corresponds to the isoelectric baseline of the resting state, TQ segment |

2.2 ST SEGMENT SHIFT IN ISCHAEMIC HEART DISEASE

2.2.1 ST SEGMENT IN ECG

As has been mentioned, there is a segment in ECG between the QRS complex and T wave which is called ST segment. In a normal ECG, the ST segment has an isoelectric section in most leads. Normal ECG analysis usually regard the TP segment in the ECG (the portion of the ECG tracing that lies between the termination of the T wave and the beginning of the following P wave) or the preceding PR segment as the baseline. The normal variant of the ST segment in the limb leads can be less than 0.1mV above the baseline or less than 0.05mV lower than the baseline; or in the chest leads, within 0.3mV above the baseline in $V_1 \sim V_3$, within 0.1mV above the baseline in leads V_4, V_5 . Normally, the ST segment is not depressed more than 0.05mV in any chest-leads. Any change exceeding the above criteria is regarded as abnormality. The ST segment corresponds to the plateau period in the action potential, any factor affects phase 2 of the action potential will result in ST segment shift. Theoretically, the absence of ST segment deviation from the baseline implies an absence of significant potential differences during phase 2 of ventricular repolarisation. Even under normal circumstances, this condition is not always fulfilled, particularly at the onset of repolarisation. After the end of depolarization, some potential differences do exist before the onset of uniform repolarisation to the level of the plateau. This interval is short but it may cause deviation of the junction (J depression) and of the early portion of the ST segment. As a result of this, measurements of ST segment deviation are usually made about 60-80ms after the end of the QRS complex when all the ventricular fibres are expected to be depolarized (discharged) to the same membrane potentials, before the onset of rapid repolarisation.

2.2.2 ST SEGMENT SHIFT IN ISCHAEMIC HEART DISEASE

ST segment shift, either ST elevation or ST depression, has long been regarded as an indication of ischaemic myocardial injury.

2.2.2.1 ST segment elevation in ischaemic heart disease

According to the classic electrocardiographic theory, ST segment elevation is produced predominantly by acute coronary occlusion. Pardee (Pardee, 1920) first

related ST segment elevation of electrocardiogram to acute myocardial infarction in human, similar results were found by Wilson (Wilson et al, 1933d) who confirmed that with coronary artery ligation, ST segment shift occurred on the epicardial surface of the dog heart. Thus established the theory that ST segment changes in the electrocardiogram is a sign of myocardial ischaemia.

Subsequent researchers have reported a wide range of ST changes after acute coronary occlusion in experimental animals. In Rakita and Ekmekci's experiment with dogs, following the experimental ligation of the left anterior descending coronary artery, unipolar epicardial electrogram leads taken in the center of the cyanotic area showed ST segment elevation within 30~60 seconds, which occurred somewhat later than the regional loss of contraction and tended to reach a maximum in 5 to 7 minutes. Exploration of the epicardial surface in adjacent areas showed more gradual development of ST segment elevation in the peripheral regions, and a gradation of less severe ST segment elevation occurred from central to peripheral cyanotic areas (Rakita et al., 1954; Ekmekci et al., 1961). Reciprocal ST segment depression was noted in leads taken from the posterior wall of the heart (Rakita et al., 1954). This ST segment depression occurred just outside the cyanotic area when only a branch of LAD was ligated, if the small coronary artery supplying such a region of ST segment depression was ligated, ST segment elevation replaced the depression promptly (Ekmekci et al., 1961). When small plunge electrodes were used to record intramural leads across the left ventricular wall, ST segment elevation can also be observed, with less magnitude than that in epicardial leads (Rakita et al., 1954). Intracavity leads immediately beneath the subendocardium also showed ST segment elevation of a slight degree. Nabel studied ST segment shift in human beings with coronary artery disease, rapid atrial pacing confirmed myocardial ischaemia in patients with coronary artery disease when angina was provoked. Before atrial pacing, there was no ST segment shift both in the body surface electrocardiogram and endocardial electrocardiogram; however, after rapid atrial pacing, no abnormalities in the body surface electrocardiogram were apparent, but marked ST elevation was found in 17 of the 21 patients in endocardial leads. This ST elevation was abolished by nitroglycerin. Moreover, in several patients, endocardial ST segment elevation after rapid atrial pacing was abolished after successful percutaneous transluminal coronary angioplasty of the critically stenosed artery supplying the ischaemic region of myocardium (Nabel et al., 1988). These suggested that ST segment elevation in endocardium is a reflection of myocardial ischaemia and may be a sensitive marker compared with the body surface electrocardiogram.

Unlike the above studies, Kleber and his co-workers (Kleber et al., 1978) observed a pattern of uniform ST segment elevation in transmural myocardial ischaemia over the infarcted region and no ST segment depression over the border region following LAD ligation in an isolated pig heart, which led to a current flow just at the border between the normal and the ischaemic tissues, and this agrees with the solid angle model of Holland and Brooks (1975 and 1977).

Smith observed another pattern of ST shift in experiments involving baboons and pigs (Smith et al., 1979 and 1983). A spatially uniform degree of epicardial ST segment elevation overlying the ischaemic area occurred for approximately the first 20 minutes of ischaemia. After 20 minutes of ischaemia, ST segment elevation increased from the periphery to the center of the ischaemic area, this disagreed with the solid angle theory. Smith explained that the entire ischaemic region might be characterized by a uniform dipole moment per unit volume instead of one distributed solely around the border between the normal and the ischaemic tissues (*vide post*).

In addition, ST segment elevation can be recorded with subendocardial and intramural electrodes after coronary occlusion when the ST segment in epicardial leads overlying a site on the periphery of the cyanotic region remained normal (Rakita et al., 1954).

Experimental studies have generally supported the belief that ST segment elevation can localize ischaemic area. It has been shown that ST elevation in precordial leads indicates transmural ischaemia or injury in the LAD distribution, and ST segment elevation in the “inferior” leads (II, III, AVF) indicates transmural ischaemia or injury in the right coronary artery or LCX (Holland and Brooks, 1977; Yasue et al., 1981; Fuchs et al., 1982).

In Fuchs and co-worker’s study (Fuchs et al., 1982) for localizing the site of coronary artery disease in 134 patients with angiographically documented single-vessel coronary disease, they reviewed 10 years of cardiac catheterization to select the studied patients, who had ECGs recorded during myocardial infarction, spontaneous rest angina, and/or treadmill exercise, and found 91% of ST segment elevation correctly identified the location of the coronary lesion. They observed that there was a significant relationship between ST segment elevation and the location of the obstructed coronary artery, ST segment elevation in leads I, avL and $V_1 \sim V_5$ during myocardial infarction correlated with the presence of LAD disease ($p < 0.005$ for each

lead); ST segment elevation in leads II, III and avF was associated with RCA or LCX disease ($p < 0.005$).

Using endocardial potential mapping method, Li (Li, 1997) recorded endocardial potential distribution in subendocardial ischaemia in sheep. It was found that ST segment elevation in the endocardial electrograph can localize ischaemia, that is, partial occlusion of LAD resulted in subendocardial ischaemia and ST elevation over the endocardium in the corresponding area.

2.2.2.2 ST segment depression in ischaemic heart disease

Unlike ST segment elevation which is always an indication of myocardial ischaemia, ST segment depression occurs under different conditions: firstly, it occurs as a benign electrical phenomenon (Mirvis, 1988); secondly, it is a manifestation of myocardial ischaemia caused by acute occlusion of another coronary artery (known as ischaemia at a distance (Schwartz et al., 1983; Haraphongse et al., 1984; Li et al., 1997); furthermore, it is regarded as a primary change of myocardial ischaemia (Ekmekci et al., 1961a; Prinzmetal et al., 1959).

Previous studies have not agreed about a correlation between the site of coronary artery obstruction at arteriography and the site of ST segment depression on exercise electrocardiography.

A positive correlation between ST segment depression on exercise and the site of coronary arterial obstruction has been reported by Robertson (Robertson et al., 1976). He found that exercise-induced ST segment depression in the inferior leads (II, III, avF) indicated right coronary artery disease and ST segment depression in the chest leads I and avL indicated left coronary artery disease, but their investigation included patients with single and multivessel disease. Herman (Herman et al., 1967) found in patients with single and multivessel disease a similar correlation when the site of coronary occlusion was determined from exercise-induced and resting electrocardiographic ST segment depression. Griffith (Griffith et al., 1978) found in 112 patients with single vessel disease that ST segment depression in leads I, avL and V_1 to V_5 reflected myocardium supplied by the LAD and leads II, III and avF reflected myocardium supplied by the LCX or RCA. Because 76 of these patients had myocardial infarction and 36 had angina pectoris, it is difficult to extrapolate these

results to locate coronary artery disease from the site of exercise-induced ST segment depression.

On the other hand, Dunn (Dunn et al., 1981) reported no differences in the distribution of exercise-induced ST segment depression in patients with either isolated left anterior descending artery lesions or in those with single left circumflex or right coronary lesions. ST segment depression in their study in both inferior and anterior leads occurred in 43% of patients with left anterior descending artery disease and in 29% of subjects with right or circumflex artery disease. In Nasmith's study of ST segment deviation with acute coronary syndrome patients which include myocardial infarction patients and unstable angina patients, multiple sites of continuous recording were made with orthogonal X, Y and Z leads. It was evident that ST segment depression vectors were confined to a small, lateral cardiac region despite a variety of cardiac lesions, it is maximal over the left thorax regardless of cardiac lesion location. They suggested that one lateral lead may suffice in monitoring ST segment depression (Nasmith et al., 2001).

In Li's experiments (Li et al., 1998) with sheep, subendocardial ischaemia was induced by partially occluding the LCX or the LAD. Such occlusion induced ischaemia over approximately half of the left ventricle in each instance and there was little overlap between the two regions. The results showed that the epicardial potential distributions were very similar for occlusion of the respective arteries (correlation coefficient was 0.77 ± 0.14), supporting that epicardial ST depression does not predict the location of the ischaemic region. However, further study of the mathematical model designed to understand the relationship between subendocardial ischaemia and the resulting epicardial potential distributions by the same group disagreed with their experimental study (Johnston et al., 2001). In this bidomain model, epicardial potential distribution was simulated on the base of an anisotropic model of the cardiac tissue. It was found from the simulations that it should be possible to predict the region of subendocardial ischaemia from the epicardial potential distribution. The model was an infinite slab of cardiac tissue attached to an infinite amount of blood, whereas the experimental model dealt with finite quantities, and the experimental model induced ischaemia from the middle of the left ventricular free wall to the septum behind which is another blood mass, so difference in the geometries being considered, as well as the relative size of the ischaemic region.

There are several concerns about the lack of capability of ST depression to localise ischaemia. Fuchs (Fuchs et al., 1982) concluded that this is because ST segment depression occurs frequently both as a primary change due to subendocardial ischaemia or infarction and as a secondary “reciprocal” change. Kato (Kato et al., 1968) believed that the non-specific ST segment depression in localizing the site of ischaemia or infarction is due to the multiple ways in which ST segment depression can be produced. Animal experiments have shown that subendocardial ischaemia or injury can produce ST segment depression in leads overlying the area of damage, and transmural ischaemia or injury can produce ST segment depression in distant reciprocal leads (Ekmekci et al., 1961a; Kato et al., 1968). Thus, ST segment depression in leads II, III or avF might be due to subendocardial ischaemia in the distribution of the LCX or RCA or to transmural ischaemia in the distribution of the LAD. There is no clear means of differentiating the two possibilities based on the ECG alone.

Iskandrlan and Segal (1979) postulated that the amount of myocardium supplied by a specific coronary artery varies in each individual patient and is further altered by proximal or distal obstruction. Some myocardial segments that become ischaemic on exercise with associated ST segment depression may be supplied by any one of the three major coronary arteries. They found individual differences of coronary artery anatomy in exercise-induced ischaemia in patients with effort angina pectoris. Myocardial ischaemia may extend from a region supplied by a stenosed vessel to surrounding regions and is prone to take the form of global subendocardial ischaemia (for example, because of elevated left ventricular end-diastolic pressure). Accordingly, the left ventricular apex may be most vulnerable with myocardial ischaemia. This is in agreement with the fact that exercise-induced ST segment depression is most often seen in left chest leads not only in the total study population but also in patients with each one-vessel disease.

The lead position may be another reason for the lack of correlation between ST segment depression and obstructed coronary arteries. If there is a correlation between the distribution of ST segment depression and the site of the ischaemic area, then except for the site of ischaemic area, the position of the heart in relation to the 12 electrocardiographic electrodes will have a definite effect on the distribution of ST depression.

Variations in the extent of collateral blood flow may also explain the lack of correlation between ST segment depression and diseased artery. Berger (Berger et al., 1981) found that regions without collateral vessels distal to an obstruction are more likely than regions with collateral vessels to manifest stress-induced ischaemia as seen on thallium scanning, suggesting that patients without lateral vessels may have more extensive ischaemia and more widespread ST segment depression on exercise ECG. Although collateral vessels may reduce the extent of myocardial ischaemia, Tubau (Tubau et al., 1981) reported no difference in the number of positive leads and the depth of ST segment depression in patients with isolated single vessel disease with and without collateral vessels. Furthermore, Mirvis (1983) found that during 3 months of pacing following ameroid constrictor placement in the LCX in dogs, when collateral formation should be extensive, ST segment depression still occurred. However, collateral blood flow was not measured in Mirvis's study (Mirvis, 1983). This was postulated to demonstrate that collateralization is inadequate to prevent tachycardia-induced ischaemia.

2.2.3 Cellular basis of ischaemic electrocardiographic changes

Classic electrocardiographic theories offered to explain the changes which occur in the ST segments during myocardial ischaemia based on the supposition that a boundary might exist between a region of normal and damaged cells and that an abnormal current might flow between the ischaemic area and the normal area. The injured region is considered to be partially or completely depolarised at rest, the damaged area appears electrically negative with respect to normal regions. Wilson (Wilson et al., 1933b) and Bayley (1942) proposed that ST elevation is a manifestation of this injury current, and Wilson (Wilson et al., 1933a) classified injury currents into two types: injury current at rest or diastolic injury current, and injury current of action or systolic injury current (Fig 2.2.1).

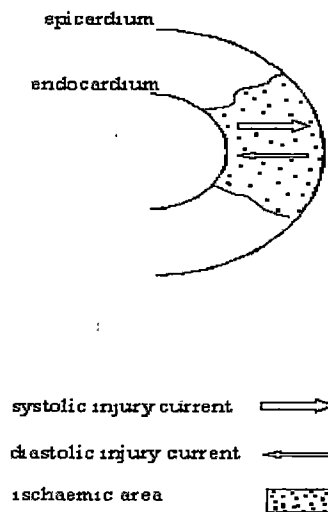


Fig 2.2.1 Effect of systolic and diastolic injury currents on the ST and TQ segments (Modified from Surawicz B et al. Am J Cardiol, 41: 943,1978)

Recent studies of transmembrane action potentials and simultaneously recorded epicardial ECG from the surface of the ventricle have shown the following events during ischaemia: (1) Decrease of resting membrane potential (less negative) occurs in ischaemic tissue results in a diastolic injury current flows from the injured tissue to the healthy tissue, produces depressed QT segment of the surface electrogram, which in clinical ECG using alternating current (AC) coupled amplifiers, is represented by ST elevation (secondary ST elevation). (2) Decrease in the action potential duration and amplitude of the ischaemic tissue results in a systolic injury current flowing from the normal tissue to the injured tissue, produces “primary ST elevation” in the surface electrogram. Further deterioration of the action potential can result in complete loss of the action potential.

2.2.4 INJURY CURRENT AND ITS RELATIONSHIP WITH ISCHAEMIC ELECTROCARDIOGRAPHIC CHANGES

The injury current and its relationship to ST shift have been found by serial researchers (Prinzmetal 1961; Shaefer and Hass, 1962). They were further interpreted by Samson and Scher (1960) and explored by Kleber (1978).

Using intracellular electrodes, Prinzmetal (Prinzmetal et al., 1961) recorded partial diastolic depolarisation from cells within the zone of ischaemia which lead to decreased membrane potential (less negative). In the ECG as recorded from the body surface, the electronic circuit compensates for this baseline shift which would otherwise be recorded as a depression of the TQ segment, and only ST elevation is recorded (secondary ST elevation). Shaefer and Hass (1962) also found that during the diastolic period, when the injured region is partially or completely depolarised, the damaged area appears electrically negative with respect to normal regions, thus resulting in a diastolic injury current.

The conventional ECG recorded with alternating current (AC) coupled amplifiers can't differentiate ST segment shift from QT segment shift (Taccardi, 1967). Using direct current coupled (DC) amplifiers; Samson and Scher (1960) measured the ECG combined with simultaneous intracellular recordings in a model of acute infarction in dogs. The DC recording allowed the differentiation of ST segment shifts from the TQ segment shifts.

When the intracellular electrogram was recorded, Samson and Scher (1960) found that while abnormal resting depolarisation sometimes was the initial event after acute coronary occlusion, more often primary ST segment elevation occurred first in the ischaemic zone within 40 seconds following the occlusion, and abnormal depolarisation during electrical diastole usually became evident 80 seconds later. In addition, they reported that there was an early repolarisation of the ischaemic cells, while cells in the normal myocardial zone were still depolarised, ischaemic cells were partially repolarised, thereby allowing an abnormal current to flow during electric systole and resulting in primary ST elevation.

ST segment shift and its relation to ECG were also supported by Kleber's study which measured intracellular potentials from subepicardial ventricular cells and the local extracellular DC electrogram in isolated pig hearts before and during the LAD occlusion (Kleber et al., 1978; Janse et al., 1980). Kleber and his co-workers observed that the first change was a shift of the resting potential to a more positive value and a concomitant depression of the TQ segment of the extracellular potential, which occurred during the first minute of ischaemia. After 3 minutes, the resting potential decreased further and the upstroke velocity, the amplitude, and the duration of the action potential diminished. The alterations in action potential resulted in ST segment elevation. Finally, the cells in this ischaemic centre became totally

unresponsive at a resting potential of about -65mV . This rendered the extracellular monophasic curve to form (Fig 2.2.2).

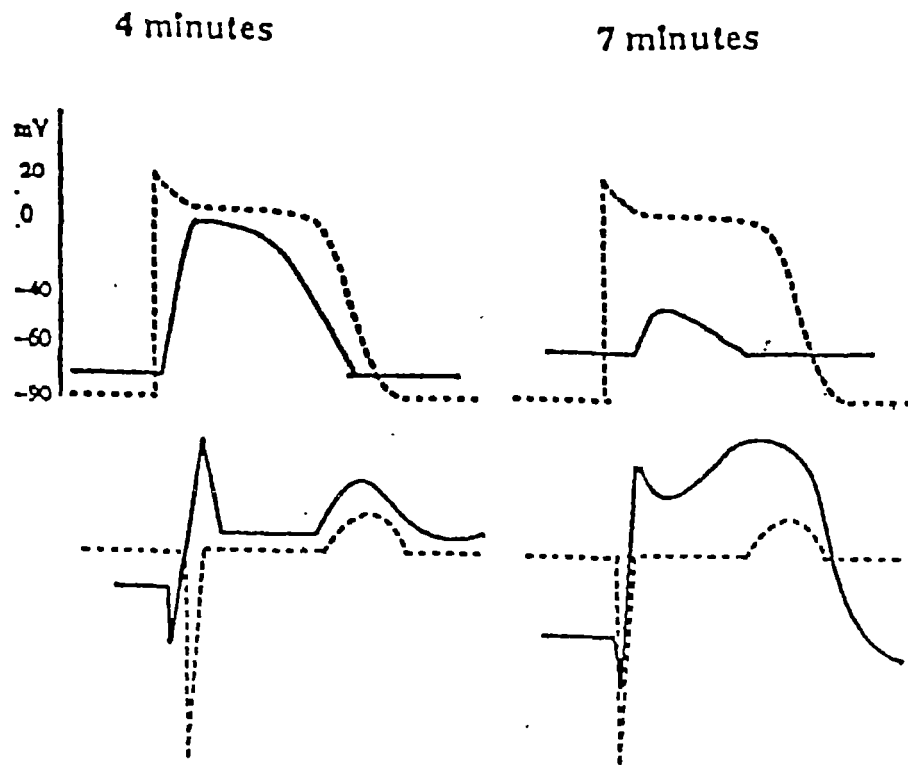


Fig 2.2.2 Transmembrane potentials (up panel) and local DC extracellular Electrograms (low panel) recorded from a single subepicardial cell in the Intact heart during control (dotted line) and ischemia (solid line). (See text For explanation) (Modified from Kleber et al, 1978)

With the use of the Laplacian maps constructed on the basis of the extracellular potential distribution, Kleber also found that during electrical diastole (TQ interval), the injury current flowed from the intracellular compartment of the ischaemic myocardium toward that of the adjacent normal tissue. The diastolic injury current emerged as a current source in the extracellular space at the normal side of the border and flows back into the ischaemic tissue, where it entered, as a current sink, the intracellular space. The distribution of current sources and sinks was localised to the border zone with the extracellular current flowing from the normal zone to the ischaemic zone during the TQ interval, and the current flowing in the opposite direction during the ST interval. Smith and co-workers also showed that the injury current arises at the ischaemic border (Smith et al., 1979). The maximal current density during late systole was $1\mu\text{A}/\text{mm}^2$, flowing in the border zone towards normal myocardium; and during diastole a maximal current of $0.3\mu\text{A}/\text{mm}^2$ flowing in the opposite direction. Cinca (Cinca et al., 1984) measured potential gradients at the "electric border" between the ischaemic and normal myocardium in the dogs during LAD occlusion at 12-20mV. The characteristic of the border zone will be discussed in detail in other section of this thesis.

A comparison between precordial ECG leads recorded during the first minute of acute myocardial infarction in human, and transmembrane potentials and local DC-extracellular electrogram recorded during the first minute following coronary artery occlusion in isolated pig hearts was made by Cinca (Cinca et al., 1980). They found that in the precordial leads in the patient, the configuration of the complexes and the time course of the changes were very similar to the configuration of the extracellular signals in the pig, suggesting that cellular changes in human are similar to those in the pig.

There has been little work with DC coupled amplifiers in human. Studies using the magnetocardiogram which records the same currents as the ECG responds to direct current, have been helpful in separating the systolic injury current from the diastolic injury current (Cohen et al., 1975). Measurements of the magnetic field of patients (Savard et al., 1983; Cohen et al., 1983) have shown that there was an injury current during exercise induced ST segment depression which was comparable to that recorded in animals. Because the magnetocardiogram is currently an impractical device for systematic evaluation of such patients, the results in animals form large part of data on the origin of ST segment potentials.

2.2.5 MECHANISM OF ELECTROCARDIOGRAPHIC PATTERNS IN MYOCARDIAL ISCHAEMIA

2.2.5.1 The mechanism of ST segment elevation

Injury current at rest

During the electric diastolic period, the extracellular space of the injured muscle tissue is electrically negative in relation to the space of the normal resting muscle. Thus, a potential difference between these areas exists, producing current flow from the normal area to the ischaemic area. An electrode overlying the injured area of muscle will record a depression relative to the baseline, which is an isoelectric line recorded when there is no myocardial injury. When the muscle is stimulated, an advancing negative charge (in front of which is a positive charge) is initiated, and the overlying electrode records a positive deflection. When a potential difference no longer exists between the advancing stimulus and the injured area, the recorded deflection returns to the baseline.

Injury current of activity

When injured muscle is stimulated, the extracellular space does not become as electrically negative as normal muscle. Thus, stimulated injured muscle will have less of a negative charge and therefore a relatively larger positive charge than the normal stimulated muscle, producing potential difference between the injured area and the normal area, with current flowing from the ischaemic area to the normal area. An electrode overlying the injured portion of the muscle will face this positive charge, resulting in elevation of the ST segment.

2.2.5.2 The mechanism of ST segment depression

The responsible mechanism of ST depression remains controversial. Two mechanisms are generally discussed. Firstly, ST depression may reflect reciprocal changes of the ST segment elevation. Secondly, it may also be produced by added ischaemia of adjacent myocardium. Furthermore, it is regarded as a primary change of myocardial ischaemia (Ekmekci et al., 1961a; Prinzmetal et al., 1959).

Reciprocal ST depression

Reciprocal ST depression suggests that in acute transmural myocardial ischaemia, ST segment depression occurs in distant “reciprocal” leads, thus, anterior acute

myocardial infarction will cause ST elevation in leads over anterior wall and ST depression in leads over inferior wall, while inferior acute myocardial infarction will cause ST elevation in leads over inferior wall and ST depression in leads over anterior wall. The ST elevation is always termed as "Primary change" and the ST depression is termed as "Reciprocal change". Accordingly, ST depression should always change reciprocally with fluctuations of ST elevation (Mirvis, 1988). This has been observed both in animal experiments and human studies.

Crawford (Crawford et al., 1984) studied inferior electrocardiographic ST depression during acute anterior myocardial infarction in the baboon. Myocardial ischaemia was induced by ligation of the distal third of the LAD and was verified by epicardial ECG mapping and by tissue creatine kinase and histologic study. All baboons had ST depression in leads III and avF of 0.1 to 1.2mV at 30 minutes, and 11 of 13 had similar changes in lead II. 10 of 13 baboons had ST elevation in lead avL and 11 of 13 in lead aVR. The results suggested that the ST vector from the infarct area was directed away from the inferior leads and acute myocardial infarction always resulted in reciprocal ST depression at sites distant from the area of acute infarction.

By analyzing ECG and angiographic results in patients with acute anterior or inferior infarction, Ferguson (Ferguson et al., 1984) verified that ST depression in acute myocardial infarction did not indicate the presence of ischaemia in the remote wall as manifested by segmental wall motion abnormalities. They even found that the degree of ST depression in the remote wall leads correlates with the degree of ST elevation in the infarct wall leads, which supported the idea that reciprocal ST depression was a benign electrical event. Similar conclusions have been proposed by Little and co-workers (Little et al., 1984). In the study of ST depression in acute inferior myocardial infarction patients during thrombolytic therapy, opening of the occluded coronary artery resulted in the resolution of the anterior ST depression whereas failure of streptokinase to open the occluded coronary artery produced no change in the anterior ST depression in patients with a normal LAD. In patients with a diseased LAD, the results also showed that successful reperfusion of the occluded coronary artery caused prompt resolution of both the anterior ST depression and the inferior ST elevation and failure to reopen the occluded coronary artery had no effect on the anterior or inferior ST shifts. By analyzing collateral flow to the anterior wall, aortic blood pressure and heart rate change, the author concluded that even in patients with LAD, the anterior ST depression was due to reciprocal changes from ischaemic injury in the region perfused by the occlude coronary artery other than anterior ischaemia.

Dipole electrocardiographic theory was used to explain the “reciprocal” deduction of ST depression. Reciprocal effects are a direct biophysical consequence of cardiac electrical activity; their properties may be derived directly from concepts of dipole theory. The cardiac electrical sources are located within the units of the electrically polarized cell membrane. For the purpose of evaluating the body surface ECG, an equivalent source or equivalent cardiac generator can be substituted for the actual biologic sources (Vide Section 2.5). The simplest and most widely considered equivalent cardiac generator is an electrical double layer or dipole layer on the surface of the heart. The electrical field generated by a dipole is intrinsically characterized by direct and reciprocal potentials corresponding to the orientation of the dipole. In a dipole model, the maximum positive potentials represent the equivalent of primary ST segment elevation as recorded in leads lying over an injured zone; the minimum represents reciprocal or secondary ST segment depression as seen in leads lying over remote sites. In Li’s (Li et al., 1999) experimental and mathematic model, it was suggested that some basic balance existed between the size of ischaemia and ST elevation to ST depression ratio. They concluded, on the basis of physical factors, that the total current flowing out of the heart must flow back into the heart; the overall current out of the heart must be zero. Hence, all ST balances between elevation and depression are subject to this.

In conclusion, reciprocal ST segment depression is a biophysical phenomenon that is always to be expected to accompany primary ST segment elevation. Both the dipole source strength and the location of the lesion in relation to the body surface electrode position affect its detection on the body surface.

However, Wong (Wong et al., 1993) did not support the proposal that ST depression is a reciprocal phenomenon of ST elevation. By continuous 12-lead ECG recording in patients with acute inferior infarction given intravenous thrombolytic therapy, the results showed that the maximal recorded precordial ST depression correlated inversely with the corresponding inferior ST elevation. Within individual patients, continuous 12-lead monitoring revealed a close negative correlation between the inferior and precordial ST shifts for the entire recording period in most patients, but there was 26% of patients did not have this relation. Moreover, precordial ST depression was not always present during inferior ST elevation, 36% of the patients had ECG showing $<0.1\text{mV}$ precordial ST depression despite summed inferior ST elevation $>0.6\text{mV}$. They suggested that precordial ST depression was not just the simple electrical reciprocal projection of the abnormal inferior wall ST elevation, and

its fluctuation could not be predicted by changes in the inferior ST shifts in every patient. The reciprocal correlation between precordial and inferior ST shifts in the whole group and within most individual patients over time might suggest that precordial ST depression reflected an area of ischaemia adjacent to but anatomically distinct from the inferior wall which shares a common vascular supply from the infarcted-related artery.

Ischaemia at a distance

Under normal conditions, occlusion of one coronary artery produces ischaemia or infarction limited to the subserved myocardium. Even though occlusion of a small coronary artery results in a slight increase of blood flow in non-ischaemic region, occlusion of large coronary artery results in a decrease of blood flow in the non-ischaemic area (Li, 1997). Ischaemia at a distance refers to ischaemia in the myocardium perfused by a stenotic coronary artery produced by acute occlusion of another coronary artery.

Both experimental and clinical studies claim that ST segment depression is due to ischaemia at a distance. Schwartz's (Schwartz et al., 1983) experiment in dogs documented a reduction in flow to the bed perfused by a stenotic artery after acute occlusion of a second major vessel. The reduction is primarily in endocardial regions, with lesser decreases or an increase in epicardial flow, it was found in their experiment that after occlusion of the anterior descending artery, the endocardial/epicardial blood flow ratio in the circumflex zone fell from 0.89 ± 0.07 to 0.04 ± 0.10 . Shah and coworkers (Shah et al., 1980) examined 44 patients with inferior myocardial infarction, and found that those who had anterior reciprocal ST segment changes had reduced contractility in the anterior wall. In another study by Salcedo and coworkers on 45 patients with inferior infarction, 35 exhibited ST depression; among these, 24 had ST depression in precordial leads 1 to 4 and 23 of them had advanced disease in the LAD. Roubin and colleagues (Roubin et al., 1984) performed coronary arteriography in 84 survivors of inferior myocardial infarction and found that absence of reciprocal ST depression precluded the presence of multivessel coronary disease. Haraphongse and associates (Haraphongse et al., 1984) studied 33 patients with anterior myocardial infarction, those who had reciprocal ST depression had higher frequency of right or circumflex coronary artery disease. In Tzivoni's (Tzivoni et al., 1985) study on 137 patients with acute myocardial infarction who underwent right atrial pacing in order to detect residual myocardial ischaemia, they found that patients without reciprocal changes rarely had ischaemia during the

predischARGE pacing. That is, the residual ischaemia in patients without reciprocal changes is extremely rare. However, among patients who exhibited reciprocal changes on admission, Tzivoni found that about half had ischaemia during atrial pacing while the other half did not. The author concluded that two different mechanisms may be responsible for the reciprocal changes: in one half of the patients this is due to a mirror-image phenomenon (those patients with normal response to atrial pacing), while in the other half, the reciprocal changes are due to ischaemia (those patients with ischaemia on right atrial pacing).

There are multiple mechanisms interact to interpret distant ischaemia. First, increased heart rate and increased chamber size following coronary artery ligation may increase oxygen demand of the heart, thus provokes ischaemia in the non-infarcted bed. Second, reduced perfusion due to the drop of the perfusion pressure directly produces ischaemia in the nonischaemic regions. Third, myocardial infarction may result in increase of left ventricular end-diastolic pressure which in turn will increase back pressure on the distal coronary bed; the transcoronary pressure may then be reduced to reduce the coronary blood flow. Fourth, increase of myocardial wall stress to sustain cardiac output by over-compensation by the nonischaemic myocardium may contribute to the relative ischaemia in the nonischaemic regions (Trevi and Sheiban, 1991; Scott and Kerber, 1992).

Under normal conditions ST-T is concordant to the QRS complex and is due to the opposite direction of cardiac activity and recovery (Vide section 2.1). However, this is different during ischaemia. As we know, ischaemia occurs firstly in endocardium, electrocardiophysiologic study shows that ischaemia acts to shorten the action potential durations, thus the action potential in the endocardium is shorter than that in the epicardium, which results in an earlier repolarisation in endocardium than epicardium. This will eventually reverse the normal transmural sequence of repolarisation to produce discordant QRS complex and ST-T, that is, ST segment depression and T wave inversion.

Primary ST depression

Although a lot of research was related to ST segment depression on the epicardium as a result to reciprocal changes of ST segment elevation of endocardial injury, Ekmekci (Ekmekci et al., 1961a) proposed that epicardial ST segment depression might originate from epicardial injury, they called this ST segment displacement as primary ST depression. Prinzmetal (Prinzmetal et al., 1959) found that hemorrhagic

hypotension might produce marked ST segment depression from direct epicardial leads without significant ST elevation from simultaneously recorded subendocardial and cavity leads. These findings were confirmed by Toyoshima and Takakuna (1960) through the use of multiple intramural electrodes. Since no marked ST segment elevation was recorded from subendocardial or cavity leads, the epicardial ST segment depression cannot be explained on the basis of the reciprocal effect of a subendocardial injury current. Massumi (Massumi et al., 1955) made a further demonstration: injury to the outer layers of the myocardium resulting in marked epicardial ST segment depression failed to produce any significant displacement of the ST segment from the subendocardial or cavity leads.

Why does epicardial injury result in different ST segment displacement in ECG. As has been mentioned, epicardial injury will also cause ST segment elevation. In Ekmekci's (Ekmekci et al., 1961a) series of experiment, he found that after the ligation of a coronary artery, ST segment elevation appeared 1~2 minutes later in the centre of the ischaemic area which was cyanotic indicating more severe ischaemia, the amplitude of ST segment elevation decreased as the electrodes moved to the edge of the ischaemic area. About 15 to 20 minutes after ligation of the artery, slight ST segment depression was noted from the periphery of the ischaemic area which was reddish-blue indicating less severe ischaemia.

Following this finding, more detailed experiments done by Ekmekci (Ekmekci et al., 1961a) showed that after the releasing of the ligated coronary artery, the blood flow was re-established in the ischaemic area, and the cyanotic area turned to red. ST segment depression recorded in periphery area during ligation of the coronary artery became an isoelectric line, then previously recorded ST segment elevation in the centre of the ischaemic area also became isoelectric line via a transient ST segment depression. Hemorrhagic hypotension further increased ST segment elevation from the centre part of the ischaemic area, ST segment elevation from the intermediate zone increased slightly. The zone immediately outside the ischaemic area, in which the ST segment had been isoelectric prior to hypotension, also showed slight ST segment elevation, and the area of cyanosis appeared enlarged. Electrocardiographic exploration beyond the large ischaemic area revealed "islands" of ST segment depression scattered over all aspects of both ventricles. It is known that cardiovascular shock leads to further decrease in coronary flow and thereby a further reduction in the blood supply to the ischaemic area. Transfusion resulted in restoration of normal blood pressure. They also found that following transfusion,

elevation of the ST segment decreased from the centre part of the ischaemic area, the scattered ST segment depression that had been recorded over all aspects of both ventricles during hypotension disappeared. So it was concluded that ST segment elevation is associated with more severe ischaemia than ST segment depression.

The conclusion that ST segment elevation is associated with more severe ischaemia than ST segment depression by Ekmekci (Ekmekci et al., 1961a) seems to be contradicted by the observation that ST segment depression never occurred immediately following the ligation of a coronary artery, that is, during the initial period before ischaemia had become severe. If ST segment depression indeed relates to a less severe degree of ischaemia than ST segment elevation, then ST segment depression should have appeared during the initial period of the coronary artery ligation. Ekmekci (Ekmekci et al 1961a) tried to explain this phenomenon by using theory based on cell metabolism (Ekmekci et al 1961a). However, no further experiments are available to support this postulation.

Whilst considering ST depression as a primary change of cardiac injury, Ekmekci (Ekmekci et al., 1961a) did find in one of his experiments that ST segment depression was also recorded from an area of posterior wall of the heart opposite to the ischaemic area in the anterior wall, and this ST segment depression appeared simultaneously with the ST segment elevation from the ischaemic area, which is different from the ST segment depression recorded from around the periphery of the ischaemic area. He concluded that both "reciprocal" and primary ST segment depression exist during myocardial injury.

In MacDonald's study in humans (MacDonald et al., 1986), routine electrocardiographic results were recorded during percutaneous transluminal coronary angioplasty of the LAD. They found that patients developing ST depression (either with or without symptoms), when compared with those evolving ST elevation, commonly have a richer collateral system to the region supplied by the occluded vessel. Thus, the overall response suggests that lesser degrees of ischaemia result in ST depression while more severe and extensive ischaemia produces elevation of ST. Coronary angiography performed during symptomatic episodes of myocardial ischaemia supports this hypothesis (Yasue et al., 1981). Patients with ST depression with chest pain are more likely to have subtotal coronary artery occlusion and/or collaterals to the ischaemic region of myocardium.

2.2.5.3 Theoretical analysis of ST segment shift —the solid angle theory

To relate, in a physiologic and quantitative manner, the electrical activity of the heart to the magnitude and polarity of the deflections in ECG, one needs to know where and when the ionic current originates in the heart and the configuration and electrical properties of the volume conductor. Conversely, the ionic current origination in the heart and the configuration and electrical properties of the volume conductor makes it possible to relate quantitatively the electrical activity of the heart to the magnitude and polarity of the deflections in ECG.

The concept of the solid angle theory was first formulated by Newton in his classic studies on gravitation and was later applied by physicists in the theoretical characterization of a wide variety of electrical phenomenon. The applicability of the solid angle theory to the interpretation of recorded electrocardiographic signals was recognised by Wilson (Wilson et al., 1933a), and was expanded to ECG theory by Holland and Brooks (1975). After Einthoven's establishment of the standard limb lead system, it was soon recognized that electrode location as well as the area of injury was capable of influencing both the magnitude and polarity of the TQ-ST segment deflection (Barnes and Whitten, 1929), the utility of solid angle theory in quantitative TQ-ST segment changes may give rise to a detailed recognition of myocardial injury.

The solid angle model considers each boundary present in the heart to be composed of an infinite number of dipoles, each representing an infinitesimally small region of the boundary. Because more dipoles are considered, this model more accurately represents the electrical activity of the heart, each dipole is permitted to move in the direction of its segment of the boundary and each dipole has exactly the same strength or magnitude which equals the difference in transmembrane voltage across the boundary (Holland and Arnsdorf, 1977). Since this boundary separates two cell populations that differ in transmembrane potential, it has been represented as a distributed dipole layer.

Holland and Brooks' (1977) solid angle model suggested that ST segment deflection is a boundary phenomenon which depends on diastolic and systolic injury currents flowing at the boundary between the ischaemic cells and the normal myocardium. According to the theorem (Holland and Brooks, 1977b) (Fig 2.2.3), the magnitude

and polarity of the TQ-ST segment deflection recorded at an electrode site can be calculated by solid angle formula:

$$E_{QT-ST} = \Omega / 4\pi \cdot (V_{mN} - V_{mI}) \cdot K$$

Where E_{QT-ST} is the potential recorded at a specific electrode point (say, point P); Ω is the solid angle which is defined as the area of spherical surface cut off a unit sphere by the cone formed by drawing lines from P to every point at a boundary of interest. In brief, Ω is the solid angle subtended at P point by the ischaemic boundary; V_{mN} and V_{mI} denote the transmembrane potentials of the normal and ischaemic region during either diastole (TQ segment) or systole (ST segment); K is a term correcting for differences in intracellular and extracellular conductivity and the occupancy of much of the heart muscle by interstitial tissue (Holland and Brooks, 1977a; Holland and Arnsdorf, 1977; Plonsey, 1974). The electrocardiographically recorded potential is thus directly proportional to both solid angle and the difference in transmembrane potentials between the normal and the ischaemic regions.

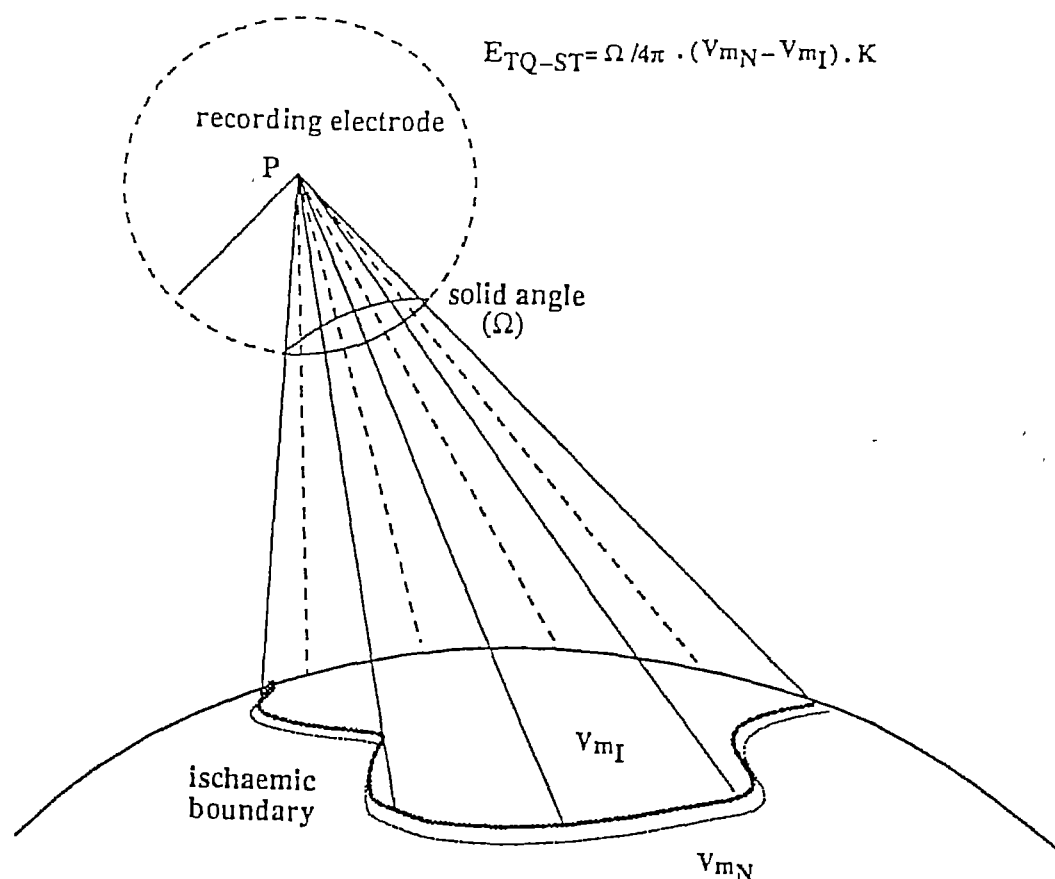


Fig. 2.2.3 Mathematic and pictorial characterization of the solid angle theory. The ischaemic boundary is a source of current flow established by differences in the transmembrane potentials of the normal and ischaemic cells during diastole and systole. The TQ-ST segment potential recorded at the electrode (point P) is given by the above equation. (See text for explanation) (From Holland and Arnsdorf. Prog Cardiovasc Dis, 1977)

*Space factors influence TQ-ST segment shift**Ischaemic position*

Ischaemic position, first considered by Prinzmetal (Prinzmetal et al., 1948), could be a function of solid angle. This is depicted in Fig 2.2.4. Subepicardial ischaemia (A) in which the outer portion of the ventricular wall is involved subtends a positive solid angle and therefore positive ST segment deflections are recorded from leads overlying the ischaemic region. Transmural ischaemia (B) will also yield positive solid angle and ST segment deflections on electrodes overlying ischaemic regions. While with subendocardial ischaemia (C) in which the inner wall is involved, the direction of ionic current flow during systole is away from the recording electrodes, the solid angle and ST segment deflections are negative in all overlying leads.

In Holland and Brooks' (1975 and 1977b) experimental porcine models, they verified that positive ST segment deflection occurred in epicardial and transmural ischaemia produced by ligating different coronary arteries. Although they predicted that ST segment depression in subendocardial ischaemia should be able to localise ischaemia, they failed to produce subendocardial ischaemia in their porcine model (Holland and Brooks 1975), and were unable to confirm their theoretical prediction of subendocardial ischaemia.

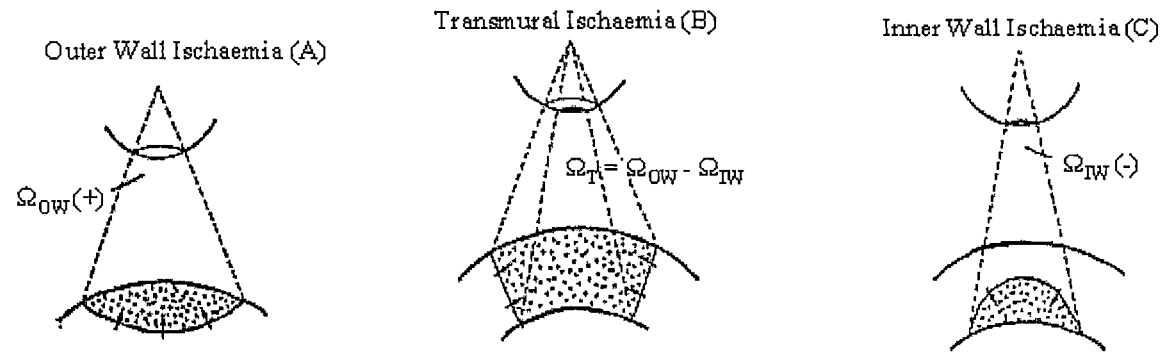


Fig 2.2.4 Magnitude and polarity of the solid angle as a function of ischaemic position. When the region has a transmural ischaemia (Panel B), the resultant solid angle (Ω_T) is equal to the difference in the solid angle computed for ischaemic regions localized to the outer (Ω_{OW}) and inner (Ω_{IW}) layers of the ventricular wall. The direction of current flow (positive to negative) across the ischaemic boundary at midsystole is indicated by arrows. The polarity of the solid angle is then positive at electrode sites overlying outer wall and transmural ischaemic regions and negative at sites overlying inner wall ischaemic regions. (From Holland and Arnsdorf MF. *Prog Cardiovasc Dis*, 1977).

Ischaemic area and the site of the recording electrodes

According to the solid angle theory, an increase of ischaemic area should increase Ω at precordial locations and decrease Ω at epicardial locations overlying the ischaemic region (Fig 2.2.5). Such an increased relationship between precordial and epicardial recordings during an increase in ischaemic area has been demonstrated by Holland and others (Holland and Brooks, 1975 and 1977b). In Holland and Brooks' spherical heart model, they assumed transmural ischaemia with outer and inner wall radii of 3 and 2cm respectively, and the solid angles subtended by transmural ischaemia boundary at centrally overlying precordial and epicardial electrodes were calculated.

The results showed that these solid angles increased with the size of the ischaemic area at the precordial site, and the solid angles decreased with an increase in the ischaemic area at the epicardial site because the ischaemic boundary moves further away from the electrode following an increase of ischaemic area. The relationship of ischaemic area and solid angle was also verified experimentally by Holland and Brooks (1975 and 1977b) in the porcine heart. Sequential coronary ligation was performed in pigs experimentally by ligating different segments of the LAD to produce different sizes of ischaemia. They showed that, when the size of the ischaemic area was increased by ligating the LAD more proximally, the magnitude of precordial TQ-ST segment deflections increased while the magnitude of epicardial TQ-ST segment deflections reduced.

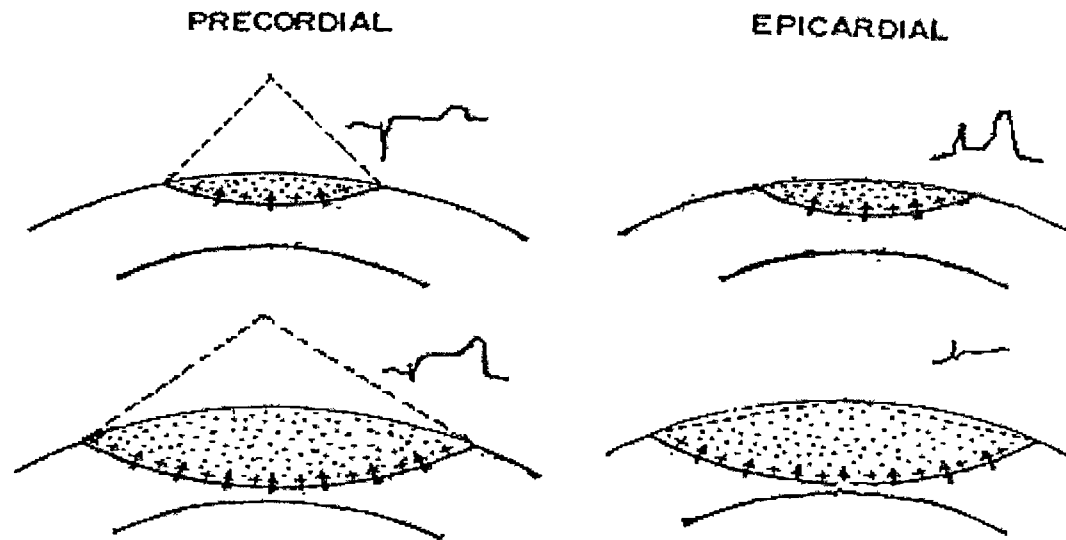


Fig 2.2.5 Effect of electrode location and ischaemic area on the magnitude of the solid angle and the TQ-ST segment deflection. At precordial electrode locations (left), an increase in ischaemic area increases both the solid angle and the TQ-ST deflection. At epicardial locations (right), however, the ischaemic boundary moves further away from the electrode following an increase in ischaemic area and hence the TQ-ST deflection declines in magnitude. The direction of current flow (positive to negative) across the ischaemic boundary at mid-systole is indicated by arrows and is assumed not to be a function of ischaemic area. (From Holland and Arnsdorf, *Prog Cardiovasc Dis*, 1977).

Thickness of the ischaemic wall

Differences in wall thickness exist between the right and left ventricles and the base and apex of the left ventricle, which may account for differences in the TQ-ST segment deflections recorded from these areas (Holland and Brooks, 1977b). As found by Holland and Brooks, thicker-walled ischaemia results in increased magnitude of TQ-ST segment deflection.

Other spatial factor

Other spatial factors which will influence the TQ-ST segment deflection in ischaemia include heart size, location of the electrodes as to if they are centrally or peripherally situated over the ischaemic or the nonischaemic area (Holland and Brooks, 1977b).

Nonspatial factors influence TQ-ST segment shift***Transmembrane potentials in normal or/and ischaemic area***

The change of transmembrane potentials in normal or/and ischaemic area is the mechanism by which nonspatial factors influence TQ-ST segment deflection in ischaemia, as have been discussed in solid angle formula, the TQ-ST segment deflection is a function of the difference in transmembrane voltage (ΔV_m) between the ischaemic and the normal tissue during both systole and diastole. There are a lot of potential agents capable of altering ΔV_m which may be classified into two categories (Holland and Brooks, 1977a): (1) Agents directly alter the transmembrane potential of either the normal or the ischaemic cell. (2) Agents influence the rate and degree of potassium ions accumulation in the extracellular space of the ischaemic tissue. The latter may be accomplished by either altering the rate of potassium ions leakage out of the ischaemic cells or altering the rate of its removal from the extracellular space of the ischaemic tissue.

Potassium ion and TQ-ST segment deflection

In Holland and Brooks' (1977a) opinion, agents as ouabain may influence the ST segment of ischaemic electrogram by shortening (or in other agents, lengthening) the ventricular action potential duration. The ventricular action potential durations are shortened out of proportion in the ischaemic or the normal cells, a difference of transmembrane potential between normal and ischaemic cells may occur resulting in ST segment deflection. The factors which directly modify the transmembrane potentials of either the normal or ischaemic cells during diastole or systole include

electrolytes, temperature, heart rate, metabolic inhibitors, anti-arrhythmia therapy and catecholamine.

According to Nernst equation

$$E_k = RT/F \cdot \ln [K^+]_o / [K^+]_i$$

Where R is the gas constant, T is the absolute temperature, F is the Faraday's constant, and $[K^+]_o$ and $[K^+]_i$ are the respective extracellular and intracellular potassium ions concentrations. Therefore, changes of either extracellular or intracellular potassium concentrations in normal or ischaemic area may result in deflections of resting potentials. Because $[K^+]_o$ is relatively low with respect to $[K^+]_i$, small changes in $[K^+]_o$ will dramatically alter E_k . Calculations indicate that the movement of 1% of the total intracellular potassium ions to the extracellular space will increase $[K^+]_o$ by 140% (1977a). Holland and Brooks (Holland and Brooks, 1977b) found that the decline in the TQ-ST deflection varies with the logarithm of potassium ions level.

Factors affecting the drainage of the ischaemic region such as diffusion and venous efflux will determine how long this gradient will be maintained. Many factors will alter the transmembrane voltage of the ischaemic tissue by changing the degree and rate of potassium leakage out of myocardial cells (Parker et al., 1970; Holland and Brooks, 1976).

It is known that uptake of potassium ion by excitable cells is closely coupled with the active extrusion of sodium ion, this active pumping of sodium ion out and coupled transport of potassium ion into the cell requires the participation of high energy phosphate compounds (ATP). During myocardial ischaemia, hypoxia results in dysfunction of Na^+-K^+-ATP pump, which bring about a rapid block of sodium ion efflux while still permitting the efflux of potassium ion to continue (Caldwell, 1968), thus potassium ion accumulate in extracellular space and cause E_k to decline in the ischaemic cells.

As been found by Samson and Scher (1959), a decreased potassium ion gradient may result in TQ segment shift. Holland and Brooks (1977b) found in their pig model that TQ-ST segment deflections recorded from both the ischaemic and nonischaemic

regions decreased with steadily increasing plasma potassium level. However, other researchers disagree with this opinion (Kleber, 1983; Wilde and Kleber, 1986).

TQ-ST segment deflection is a result of potassium ions accumulation in the extracellular space of the ischaemic tissue is also demonstrated by the phenomenon that potassium ions removal from the ischaemic area will reduce TQ-ST segment deflection. Mechanisms that remove potassium ions from the ischaemic area include diffusion (Kushmerick and Podolsky, 1969), available collateral flow (Schaper, 1971), venous (Datta and Gupta, 1972) and lymphatic drainage (Miller, 1963). For collateral flow to bring about a significant reduction of the TQ-ST segment deflection, it need not necessarily be so great as to sustain the oxygen requirements of the tissue, thereby reversing the ischaemia, but perhaps only great enough to wash out the accumulated potassium ion from the ischaemic tissue into the peripheral circulation. Similarly, hyaluronidase by presumably altering interstitial permeability factors (Maroko et al., 1972) again need only speed up potassium ion removal to bring about an electrocardiographic improvement; significant oxygen and substrate delivery to the ischaemic tissue, although desirable, may not be necessary for this effect. This washout phenomenon has been demonstrated both by Ekmekci and Bodenheimer (Ekmekci et al., 1961b; Bodenheimer et al., 1976).

A recent study on transgenic mice supported the theory that activation of sarcolemmal ATP-sensitive potassium (K_{ATP}) channels by ischaemic ATP depletion played an important role on the ischaemic ST elevation (Li et al., 2000). The Kir6.2 gene in the mice encodes the pore-forming subunit of cardiac surface K_{ATP} channels. Patch-clamp studies in cardiomyocytes confirmed that surface K_{ATP} current was absent in homozygous knockout mice (KO), while robust in cells from wild-type mice (WT). By comparing the electrocardiographic response of both KO and WT mice to the LAD ligation, Li et al found that ST elevation was readily evident in WT following the LAD ligation, whereas it was markedly suppressed in KO. Blocking the surface K_{ATP} channels in WT with HMR1098 (surface K_{ATP} channel blocker) resulted in suppression of early ST elevation in WT. It was concluded that the opening of sarcolemmal K_{ATP} channels underlay ST elevation during ischaemia.

The solid angle theory has provided a geometric ischaemic heart model that quantitatively relates changes of ST segment to the distribution of transmembrane potential changes in the ischaemic region. However, for both theoretical and practical reasons, the solid angle theory does not provide a complete mathematical

representation of the electrical activity of the heart. Solid angle analysis is limited, as is classical dipole theory, by the fact that the thorax is neither a homogeneous nor an infinite volume conductor. The thorax consists of regions of varying conductivity nonhomogeneous. Furthermore, the thorax is irregularly shaped, with the heart occupying an eccentric position with it. These factors make the mathematical formula extremely complex (Bayley and Berry, 1964).

One practical limitation of the solid angle theory approach pertains to the difficulty of calculation. Even when modifications in the theory due to inhomogeneities (Bayley and Berry, 1964), boundaries (Selvester et al., 1967), asymmetric cardiac cell geometry (Plonsey, 1974) and transmembrane potential time dependency (Reimer et al., 1973) are excluded, the solid angle may be computed with relative ease only in those situations where the boundary exhibits a high degree of spherical symmetry. In many instances piecemeal approximations of an irregularly shaped boundary with circular or ellipsoidal boundaries are necessary in order to obtain actual numerical values (Plonsey, 1974).

2.2.6 IONS CHANGES UNDERLYING ST SEGMENT SHIFT

The immediate cause of the ST segment shift during acute myocardial ischaemia has long been presumed to relate to alterations in ion transport which, in turn, would affect the transmembrane potentials of ischaemic cells. Elevation of the K^+ concentration in coronary venous effluent has been observed during ischaemia and was considered likely to reflect loss of intracellular K^+ , accompanied by an increased intracellular Na^+ (Prinzmetal et al., 1961). Recently, myocardial biopsies from both central and border zones of an area of acute myocardial ischaemia showed a striking fall in the ratio of $[K^+]/[Na^+]$ and a drop in the $[Mg^{2+}]/[Ca^{2+}]$ ratio, which started from 15 minutes following the coronary occlusion, progressed over the first hour, and $[K^+]/[Na^+]$ approached that of extracellular fluid at 24 hours (Lie et al., 1975).

It is of interest that perfusion of a coronary artery with a solution high in K^+ (10mEq/l) resulted in ST segment elevations on epicardial electrocardiograph leads accompanied by TQ segment depression on the intracellular electrogram (Prinzmetal et al., 1961). It was proposed that ST segment depression could relate to the opposite effect, that is, an increase in intracellular K^+ with resulting hyperpolarization of the membrane, possibly secondary to an increased flux of K^+ associated with increased glucose uptake in the presence of hypoxemia or ischaemia (Prinzmetal et al., 1961).

2.3 PHYSIOLOGY, PATHOPHYSIOLOGY AND ST SEGMENT DISTRIBUTION IN MYOCARDIAL ISCHAEMIA

2.3.1 MYOCARDIAL BLOOD FLOW AND MYOCARDIAL METABOLISM

2.3.1.1 Methods of measuring transmural myocardial blood flow

Myocardial blood flow can be measured by different methods. It was initially measured by injecting radioactive tracers and recording the rate constants of their wash out (Brandi et al., 1968), by recording the rate constant of the wash out of hydrogen with polarographic electrodes (Howe and Winbury, 1973), by examining the myocardial distribution of infused inert diffusible indicators like tritiated water (Tripp et al., 1977) or antipyrine (Yipintsoi et al., 1973), or by using rubidium or potassium isotopes that exchange with intracellular potassium (Yipintsoi et al., 1973). Lately, a molecular marker, desmethylinipramine has been used (Little, 1983). These methods can not be used to measure flows more than once or twice in the same animal, neither can they measure flows simultaneously in all the regions of the ventricles, without the risk of damaging the tissue locally. Radioactive microsphere methods (Domenech et al., 1969; Hoffman et al., 1983) have been used to measure myocardial blood flow. When used correctly, this method gives flows to small regions with high accuracy (Tripp et al., 1977; Yipintsoi, 1973; Little, 1983). However, radioactive microspheres have disadvantages in that it may pose health risks, requires special precautions for use and disposal, has limited shelf life, and are relatively expensive. Hale (Hale et al., 1988) and Kowallik (Kowallik et al., 1991) reported the use of coloured and heavy metal-labeled microspheres for measuring regional myocardial perfusion, the result correlated well with the radioactive technique, but at high flows, it yielded values greater than those obtained with radioactive microspheres. Recently, fluorescent-labeled microspheres have been used (Glenny et al., 1993; Li et al., 1995). Compared to other methods, blood flow measured by fluorescent microspheres can be repeated in the same experiment, does not have the disadvantage of disposal, and the results correlated well with that measured by radioactive microspheres (Glenny et al., 1993). Regional myocardial blood flow imaging has been accomplished using positron emission tomography (Li et al., 1997), magnetic resonance imaging (Kroll et al., 1996), and ultrasound (Wei et al., 1998). These imaging methods have a potential use in clinical measurements of regional myocardial blood flow.

2.3.1.2 Blood flow distribution in normal heart

Myocardial perfusion is spatially heterogeneous. In research, the myocardium is usually divided into three layers. Subendocardium refers to the deepest one quarter or the one third of the ventricular wall and subepicardium refers to the outer one quarter or the one third, with a middle region between these two layers. No uniformity of blood flow exists in different layers of the heart.

Using fluorescent microspheres, Li and coworkers (Li et al., 1996) measured the endocardial and epicardial blood flow in sheep and found that slight differences of blood flow exist between endocardium and epicardium. The endocardial/epicardial blood flow ratio is 1.23 ± 0.26 in LCX bed and 1.25 ± 0.08 in LAD bed. Previous studies with sheep and lambs (Archie et al., 1974; Fisher et al., 1980 and 1984) found even higher differences of blood flow between different layers. In these studies, flow per gram in the subendocardium is usually 20% to 40% higher than that in the subepicardium, with flow in the midwall usually being between the two. Though it is not yet possible to make blood flow measurement of different layers in human ventricles, it is reasonable to believe that the results of animal experiments can be extrapolated to human.

Systolic contraction of the left ventricular myocardium might be an important reason for the difference between the pattern of blood flow to the subendocardial regions and the subepicardial regions of the left ventricular wall. During ventricular systole, no blood flows to the subendocardium, while blood flow in the subepicardium rises during systole; during diastole, blood flow to the subendocardium rises dramatically, and blood flow to the epicardium remains a high level, blood flow to the midwall region is intermediate between these two patterns. By injecting microspheres to perfuse the coronary arteries only during the ventricular systolic period, Hess and Bache (Hess and Bache, 1976) verified that total coronary blood flow is reduced during systole, with an abrupt rise and then a slow fall during diastole. Under normal conditions, the coronary vascular resistance is lower in the subendocardial layer during diastole so as to compensate for systolic flow limitation. Thus the mean blood flow to the subendocardium is slightly higher than that to the subepicardium, yielding an endocardial/epicardial blood flow ratio of about 1.2:1 (Li et al., 1995). Under normal conditions, it has been postulated that the explanation for this observation is a slightly higher O_2 consumption of the endomyocardium.

The heterogenous nature of regulation of coronary microvascular tone also plays an essential role in determining regional as well as transmural distribution of blood flow (Tiefenbacher and Chilian, 1998). The vascular tone, distributed down to small arterioles, is closely coupled with myocardial O₂ supply and demand (Massie et al., 1994). So the spatial distribution of myocardial flow is most likely to be formed at a precapillary arteriolar level under the influence of the O₂ supply and demand. This is documented in a study which demonstrated that myocardial blood flow distribution was largely altered at arteriolar-capillary levels by a change in arterial O₂ tension (Matsumoto et al., 1996). Thus more workload and myocardial O₂ consumption in the subendocardium than that in the subepicardium will induce differences in a spatial pattern of flow distribution between different layers of myocardium.

Regional differences of vascularity can also make it possible for the subendocardium to receive more blood flow than the subepicardium when other factors are similar. Several studies involved in this condition. The volume of blood in small vessels (mainly capillaries) has been measured in rabbit and dog hearts (Kleinert et al., 1980; Crystal et al., 1981) and it is about 20% greater in subendocardial than in subepicardial vessels. In a study of cardiac vascularity, capillary volume fractions, diameter, numerical density, anisotropy, and sarcomere length were measured using computer analysis of light microscopic images of sections taken transverse or longitudinal to the muscle fibre axis. Capillary volume was 4-6% of myocardial wall volume and exhibited a significant transmural gradient, increasing from epicardium to endocardium (May-Newman et al., 1995).

In a review assessing heterogenous distribution of blood flow and metabolism and their relationship in the heart, the author concluded that blood flow heterogeneity in the heart relates at least in part to heterogeneity of metabolic indicators. The latter may involve regional differences in content of O₂ and energy-consuming mitochondria and contractile elements, and differences in the metabolic rate and requirements of these elements (Groeneveld et al., 2001).

2.3.1.3 Determinants of myocardial metabolic rate and coronary blood flow

The energy requirements of the myocardium include requirements for basal metabolism, for electrical activation, i.e., membrane depolarisation and repolarisation, and for the performance of internal and external mechanical work. The energy required for mechanical work includes the energy required to develop and maintain

systolic tension, as well as the energy required to deactivate the contractile system. Basal oxygen requirements, e.g., the requirements of an electrically arrested, normothermic heart on cardiopulmonary bypass, have been estimated to be 20% of total myocardial oxygen consumption; the energy requirement of electrical activation is about 5% of total oxygen requirements; contractile work accounts for the majority of myocardial oxygen consumption. However, contractile work and consequently total myocardial energy requirements vary greatly. The myocardial energy requirement is determined by the balance of myocardial oxygen demand and oxygen supply. There are three major determinants of myocardial oxygen demands: heart rate, myocardial wall tension, and the intrinsic contractile state of myocardium. Myocardial oxygen supply is determined by oxygen extraction from the vessel and coronary blood flow.

2.3.2 TRANSMURAL PROGRESS OF ISCHAEMIC CELL DEATH

2.3.2.1 Consequences of myocardial ischaemia

Myocardial activity is dependent on aerobic metabolism for the production of energy in the form of ATP. Myocytes contain very limited reserve stores of high-energy phosphates and are dependent on a continuous source of oxygen and metabolic substrate. With the cessation of coronary artery blood flow, the relatively small quantities of oxygen remaining in capillary erythrocytes or attached to myoglobin are rapidly consumed, which results in a rapid drop of ATP production. In the mean while, metabolic catabolites accumulate in the myocytes or in the interstitial space. In ischaemia, both energy insufficiency and catabolite accumulation result in inhibition of cellular function, which includes contractile function and a variety of transport and synthetic functions. Initially, the inhibition of cellular functions is reversible, but eventually damage occurs to some critical subcellular organelle that is irreversible; the myocytes undergo coagulation necrosis, followed by an inflammatory response, macrophage removal of the dead myocytes, and replacement by scar. Ischaemic damage of the microvasculature also occurs; the latter further stimulates the inflammatory response. In addition, the inflammatory response, per se, might further damage myocytes and/or capillaries. If reperfusion occurs, either spontaneously or through experimental or clinical intervention, the consequences depend on the state of the myocardium at the time the reperfusion occurs. If the reperfusion is established when myocytes and microvasculature are still in the “reversible” phase of injury, cell death is prevented, and cellular ultrastructure and metabolic and contractile functions

eventually recover. Conversely, if myocytes have been “irreversibly” injured, restoration of blood flow results not in cellular recovery but rather in explosive swelling of the myocytes, massive calcium overload, and disruption of the myofibrillar apparatus.

2.3.2.2 Transmural progress of ischaemic cell death

By using various periods of temporary coronary occlusion, Jennings (Reimer and Jennings, 1979) studied the time course of ischaemic cell death. They found in anaesthetized, open-chest dogs, ischaemic myocytes remain viable for at least 15 minutes. Beyond 15 minutes of coronary occlusion, increasing numbers of ischaemic myocytes became irreversibly injured, reperfusion does not prevent subsequent infarction. By 40 minutes, much of the subendocardial zone, if severely ischaemic, has been irreversibly injured. Nevertheless, much of the midcardial and subepicardial region is still viable; reperfusion prevents infarction of these zones. With increasing duration of coronary occlusion, a transmural “wavefront” of cell death progresses from the subendocardium to the subepicardium (Reimer et al., 1977; Reimer and Jennings, 1979), and after 3 hours of uninterrupted ischaemia, infarcts eventually involved an average of 80% of the ischaemic region. By 6 hours, infarcts reached their full size. Similar results were found by Fujiwara and co-workers (Fujiwara et al., 1982) in their study of transmural cellular damage in early ischaemia in pig hearts. Using both light microscopy and electron microscopy to determine morphometrically the transmural histological changes of the left ventricle after ischaemia, they also found a “wavefront phenomenon” of ischaemic cellular damage which occurred from inner third to outer third of the left ventricular wall at 20 and 40 minutes of coronary artery occlusion, and became uniform with 120 minutes of ischaemia. Jennings (Jennings et al., 1985) observed in their study of coronary occlusion in dogs that the subendocardial region dies quickly because it is severely ischaemic (flow < 0.15ml/min/g) and that the subepicardial region dies more slowly because it often is only moderately ischaemic (flow 0.15-0.30ml/min/g) or mildly ischaemic (flow > 0.30ml/min/g). In human studies of myocardial infarction, the ischaemic damage is either entirely subendocardial or, in transmural infarcts, is confluent and maximal in the subendocardium and less extensive in the subepicardium (Freifeld et al., 1983). Similar temporal evolution of myocardial infarctions, beginning in the subendocardial region, and only later involving the subepicardial region, has been observed in other experimental models of abrupt coronary occlusion of different species and human as well. (Schaper et al., 1979; Baughman et al., 1981; Lee et al.,

1981; Connelly et al., 1982; Fujiwara et al., 1982; Geary et al., 1982; Wartier et al., 1982; Kloner et al., 1983; Klein et al., 1984). Usually, a higher local flow under normal physiological conditions is associated with a higher demand for oxygen, it might also be hypothesized that the probability of ischaemic injury is higher in high flow region (Deussen et al., 2001). Thus, subendocardial muscle is vulnerable to ischaemia, both when coronary arteries are normal and when they are narrowed.

2.3.2.3 Mechanism of transmural progress of ischaemia pattern

The reasons that ischaemic damage preferentially affects subendocardial muscle may lie in one or more of the following ways: there is a tendency for greater oxygen usage or lower oxygen tensions in subendocardial than epicardial muscle. Subendocardial muscle might use more oxygen, it might be more easily damaged by a decreased oxygen supply, or it might more readily become underperfused. There is evidence that subendocardial oxygen consumption per unit weight is normally about 20% higher than that of subepicardial muscle (Weiss et al., 1978; Weiss, 1979). Some investigators have argued that this increase is because of greater work done by subendocardial muscle fibres, which shorten more in systole than do those in the subepicardium (Yoran et al., 1973). Compared with subepicardial muscle, subendocardial muscle has lower venous oxygen saturations (Weiss et al., 1978) and oxygen tensions (Winbury et al., 1971).

The heart is an organ with an enormous need for oxygen and blood flow. The oxygen consumption of the heart is 20 times more than the whole body at rest, and 5 times more than the whole body even during severe exercise. Oxygen can be obtained by increasing coronary blood flow which will be accomplished by two ways: one is to extract more oxygen from the blood perfusing the heart another way is to increase coronary artery blood flow. The reserve for myocardial oxygen extraction is usually small, so the resultant fall in oxygen tension makes further extraction an inefficient method of delivering oxygen to tissues. As a result, the increased oxygen delivery needed by the heart when its work increases is obtained mainly by an increased coronary blood flow, so the coronary vascular resistance plays an important role in the increasing of coronary blood flow. In Hoffman's experiment (Hoffman, 1978) studying transmural myocardial perfusion with dogs, he found that coronary blood flow can be maintained to each layer of the left ventricle during a certain range of perfusing pressure. When perfusing pressure drops below a certain level, maximal vasodilation takes place first in the deepest, subendocardial muscle and flow there

becomes pressure dependent. Any further fall in perfusing pressure then causes a decreased flow to the subendocardial muscle, while flow remains in the remainder layers of the muscle in which the vessels still retain some vasomotor reserve. Further decreases in perfusing pressure will eventually exhaust the autoregulatory ability in successive layers of the left ventricular wall from inside out, but at each low pressure flows will be lowest in the deepest muscle and will increase progressively the more superficial the muscle layer.

There is a transmural gradient of wall tension, with tension greatest in the subendocardial region and least in the subepicardial region. This transmural gradient of pressure could be another reason for subendocardial ischaemia. At the onset of systole, intramyocardial pressures increase more in the subendocardium than in subepicardium, so intravascular pressures are increased more in the subendocardial where they exceed pressures in the extramural coronary arteries. Although there are intravascular pressures which increase in the subepicardial vessels as well, these pressures remain lower than in the extramural arteries. The resulting pressure gradients permit blood to flow retrogradely from the subendocardial to the subepicardial vessels, but to flow anterogradely in the subepicardial vessels. By the end of systole, the subendocardial arteries are much narrower than they were at the end of diastole. Consequently, at the onset of diastole, blood entering the myocardium from the extramural arteries flows to the most superficial myocardial vessels first (which have the lowest resistance), then to those in the midwall, and last to those in the inner myocardium which have the highest resistance. Reductions in diastolic perfusion time or pressure will thus result in decreased flow to the subendocardium. If the flow reduction is marked, this will cause subendocardial ischaemia. With the dependence of subendocardial blood flow on diastolic perfusion, it is easy to understand why so many studies have shown that reduced coronary perfusing pressures cause profound subendocardial ischaemia.

However, there is evidence that transmural differences in blood flow are not the sole explanation for the transmural wavefront of cell death. Factors other than blood flow are important determinants of the rate of myocardial cell injury during ischaemia. Biochemical studies also indicate a transmural gradient of metabolites during coronary artery occlusion in the dog, where the subendocardium is more vulnerable biochemically to ischaemic injury than is the subepicardium (Griggs et al., 1972). And, in studies in which myocardium has been made totally ischaemic in vivo with no transmural blood flow gradient, ultrastructure and metabolic features of cell injury

have occurred more quickly in the subendocardial region than in the subepicardial region (Lowe, 1983). In Fujiwara's studies of pigs (Fujiwara et al., 1982; Warltier et al., 1982; Klein et al., 1984) and Geary's studies of primates (Geary et al., 1982), the subepicardial zone is as severely ischaemic as the subendocardial region. Nevertheless, analysis of both ultrastructure and infarct location (following reperfusion) in these species indicate the existence of a transmural wavefront of irreversible cellular injury despite the absence of a blood flow gradient.

Tota (1983) has raised the interesting analogy with the anatomy of the heart in fish, most of which have an inner spongy myocardial wall supplied by venous lacunae from the cavity and an outer compact muscle layer that receives blood supply from coronary arteries. In this system, the deepest muscle not only has a different anatomy but also a differently regulated blood supply than has the outer muscle. However, a direct connection between this phylogenetic pattern and the mammalian subendocardium with a normal coronary blood supply has not been made.

In addition, there are also reported differences between subendocardial and subepicardial layers for many metabolites and enzymes. The subendocardium has been found to have greater mitochondrial oxidative activity in some studies but not in others (Tota, 1973). When the ventricles were fibrillated and all coronary inflow was abruptly stopped, a greater accumulation of lactate occurred in the subendocardial than the subepicardial muscle (Dunn and Griggs, 1975). Glycolytic enzyme activities in the subendocardium are altered in ischaemia (Lundsgaard-Hansen, 1967). Consistent differences for many enzymes and substrates have been observed, and differences in redox potential and $\text{NAD}^+/\text{NADH}^+$ ratios (Minamitate et al., 1973) probably do exist across the wall. These findings were reviewed in detail by Feigl (1983). The reasons for these biochemical differences are unknown. The biochemical differences that have been noted may explain why, in experimental animals, in the absence of differences of regional wall tensions or blood flows, sudden cessation of myocardial blood flow leads to the greater production of lactate and to the earlier onset of necrosis in the subendocardium than in more superficial muscle (Dunn and Griggs, 1975; Lowe et al., 1983).

2.3.3 LATERAL BOUNDARIES OF ISCHAEMIA

Controversy exists about the existence and width of ischaemic gradients at the lateral boundaries of an ischaemic region (Hearse and Yellon, 1981). Based on detailed

analyses of such observations, Janse and coworkers (Janse et al., 1979) found that there is a transition composed of interdigitating normal and ischaemic zones rather than a "border zone" between ischaemic and nonischaemic myocardium. In their study, regional ischaemia was produced by LAD occlusion in isolated perfused pig hearts and in hearts in situ; intramural and epicardial direct-coupled electrograms were recorded, subepicardial transmembrane potentials were recorded by floating microelectrodes and tissue ATP, creatine phosphate, lactate glycogen were simultaneously recorded and measured among ischaemic centre, border zone and normal myocardium. Intermediate metabolic values are found in the electrical border zone, and in the border, zones with normal glycogen content interdigitate with zones depleted of glycogen. If the border is reperfused, cells with nearly normal transmembrane action potentials are in close proximity to unresponsive cells with low resting membrane potentials. They suggest that the ischaemic border is composed of interdigitating normal and ischaemic zones sharply demarcated from each other.

Similar results had also previously been found by Cox (Cox et al., 1968). In their study, a border zone in the dog heart was found surrounding severely ischaemic tissue; damage in this border zone was confined to mitochondrial swelling. Brooks (Brooks et al., 1975) found in the pig heart, the zone in which blood flow changed from very low to normal values had an average length of 7.5mm. Hearse (Hearse et al., 1977) concluded from their findings that it was most likely that the border zone consisted of homogeneously damaged cells in which the damage was less severe than in the central ischaemic zone. By measuring blood flow, metabolic and electrocardiographic changes after coronary artery occlusion of dog's hearts, Hearse (Hearse et al., 1977) found gradients in local blood flow, lactate content, high energy phosphate content and ST segment potentials over an area of 8-15mm. They suggested that the finding of an intermediate value for blood flow and metabolic state could be explained when the border tissue was either a mixture of normal and ischaemic cells or uniformly composed of cells with an intermediate degree of change. Kleber (Kleber et al., 1978) also found the zone where extracellular potentials changed from monophasic complexes with maximal TQ depression and ST elevation was of the order of 9mm in the pig heart.

However, Marcus (Marcus et al., 1975) found, on the basis of flow analysis, no evidence for a geometrically well-defined border zone of moderate ischaemic myocardium surrounding and separating severely ischaemic myocardial from normal tissue after a 5 minutes occlusion in the dog heart. In 24-hour infarctions, Hirzel

(Hirzel et al., 1977) found in the dog heart a sharp demarcation between normal tissue and tissue in which creatine phosphokinase depletion was complete. Barlow (Barlow et al., 1977) found a border zone that appeared as a patchwork of ischaemic and normally perfused tissues sharing sharp interfaces.

Schaper (1971b) explained the sharp transition on the basis that the important collateral anastomoses between major coronary arteries are on the epicardial surface of the heart. The myocardium is perfused through smaller penetrating branches of these layer surface arteries. A recent anatomic study of dog by Factor (1981) suggests that the penetrating intramural arteries are essentially end arteries, with few or no interconnections between adjacent capillary beds. So there is no anatomic explanation based on intramural vascular connections for the existence of broad lateral border zones of intermediate severity of ischaemia.

Further studies in dogs showed that, even permanent ligation of a major coronary artery often does not result in complete infarction of the occluded vascular region. In Reimer and Jennings's study (Reimer and Jennings, 1979), they found that after left circumflex artery occlusion, there was persistent viable myocardium in the subepicardial zone, averaging about 20% of the ischaemic vascular bed. In their experimental model, collateral blood flow to the subepicardial zone is quite variable; the amount of subepicardial sparing is inversely related to the amount of collateral blood flow provided to this zone during the early phase of ischaemia. It is concluded that in dogs with permanent coronary artery occlusions, both the size of the ischaemic vascular bed and the amount of subepicardial collateral blood flow are major determinants of infarction size. In contrast, baboons and pigs have few native coronary collateral anastomoses; permanent coronary artery occlusion is followed by severe transmural ischaemia and by solid transmural infarcts (Geary et al., 1982; Warltier et al., 1982). Thus, in these species, infarct size is determined primarily by the size of the occluded vascular bed. Failure to identify the interface between ischaemic and nonischaemic myocardium may explain paradoxical results within the same species.

2.3.4 TRANSMURAL ST SEGMENT DISTRIBUTION IN MYOCARDIAL ISCHAEMIA

To study the origin of ST segment shift, it is important to know the intramural ST segment distribution.

Because endocardium is more vulnerable to ischaemia, occlusion of coronary artery accordingly results in greater regional blood flow reduction and a more pronounced histological damage in endocardium than in epicardium. It is thus conceivable that the electrocardiographic changes occurring at the endocardium may also be more prominent and may precede those of epicardium.

Early research by Sayen (Sayen et al., 1961) observed epicardial and intramyocardial electrocardiograms after coronary artery occlusion in dogs, they recorded ST elevation with intramyocardial electrodes within 12 seconds after ischaemia, and such leads also detected subendocardial ischaemia at the borders of a cyanotic area when the epicardial ST segment was unchanged. In Khuri's (Khuri et al., 1975) study of changes in intramyocardial ST shift and gas tensions with regional myocardial ischaemia in the dog, they found that increases in intramyocardial ST shift are associated with parallel increases in myocardial carbon dioxide tension, the results showed that ST segment shift recorded in unipolar epicardial electrodes were a less-sensitive indicator of myocardial ischaemia than were those recorded in intramyocardial electrodes. Epicardial electrodes sometimes failed to detect the presence of underlying ischaemia, as evidenced by significant changes in local myocardial gas tensions and intramyocardial ST segment shift. The lack of sensitivity of epicardial electrodes may reflect an inability of the epicardial electrodes to sense ischaemic changes in deeper myocardial layers. Similar findings were also supported by O'Riordan. Using multicontact plunge electrodes, O'Riordan (O'Riordan et al., 1977) recorded intramyocardial electrograms at multiple depths within the canine myocardial wall which suggests that the severity of myocardial ischaemia can be assessed by measuring intramyocardial ST magnitude at resting and paced heart rates. They found in the presence of critical stenosis, ST changes recorded in deeper myocardial layers were of greater magnitude than those recorded near the epicardial surface, and the increase of ST magnitude was parallel to that of myocardial carbon dioxide tension with atrial pacing in the presence of different degrees of coronary artery stenosis. They also found that intramyocardial ST magnitude was a more sensitive indicator of the severity of pacing-induced myocardial ischaemia than epicardial ST segment changes.

To analyse the existence of a possible increased electrical vulnerability of the subendocardium during acute myocardial ischaemia in the *in situ* pig heart, Cinca and coworkers (Cinca et al., 1984) recorded epicardial and endocardial electrograms after

LAD occlusion. They found that after LAD occlusion, TQ segment depression and ST segment elevation showed a faster rate of development, and monophasic potentials occurred earlier in the endocardium than in the epicardium. This faster rate of change in endocardial than in epicardial potentials is in agreement with the reported increased vulnerability of the subendocardium to acute myocardial ischaemia.

An early study by Kennamer (Kennamer et al., 1953) reported that coronary occlusion produced less net ST elevation in the inner than in the outer layers of the left ventricle. Using small plunge electrodes, John (1976) recorded intramural ST elevation after coronary artery occlusion in the dogs, and simultaneously epicardial ST elevation was also recorded. The intramural ST elevation is less marked than ST elevation in epicardial leads, similar results to Rakita's (Rakita et al., 1954). In Rakita's experiment of myocardial ischaemia induced by LAD occlusion, they observed that ST segment elevation decreased progressively from epicardium to cavity.

Research has also shown that the electrophysiologic response to ischaemia was greater in the epicardial site than in the endocardial site. This was documented in a study of exploring the effects of ischaemia on transmembrane action potentials and refractory periods of both endocardial and epicardial myocytes in cats (Kimura et al., 1986). In this model, ischaemia was induced by stopping perfusion of the LAD, rapid deterioration of transmembrane action potentials was observed in both endocardial and epicardial cells. The magnitude of the reduction of action potential amplitude and action potential duration was greater in epicardial cells than in endocardial cells, while the change in resting membrane potential was almost the same. However, action potential duration of endocardial cells decreased progressively during 30 minutes of ischaemia, whereas the action potential duration of epicardial cells was reduced maximally at 10 minutes and then partially recovered. The mechanism of the discrepancy of electrophysiologic response and electrocardiograph between endocardium and epicardium is unclear. Further research is needed to explore the time course of both electrophysiologic and electrocardiographic changes in myocardial ischaemia to understand this mechanism.

2.3.5 TRANSLATERAL ST SEGMENT SHIFT OF MYOCARDIAL ISCHAEMIA

According to solid angle theory, an assumption is that the degree of ischaemic cellular injury is uniform in the ischaemic myocardium. Thus, the ischaemia produces two distinct and sharply separated cell populations with respect to action potential morphology. Therefore, a difference in transmembrane potential exists only at the boundary between the ischaemic and normal myocardium so that injury currents originate only at this boundary which means the uniform double layer exists only at the ischaemic boundary. Another assumption is that the conducting medium is infinite, homogeneous and isotropic. Under these assumptions, the distribution of ischaemic ST segment deviation is determined by the ischaemic boundary at any field point, with highest ST segment elevation occurring at the boundary, while a progressive decrease in ST segment elevation is expected to occur approaching the centre of this ischaemic region.

Using isolated, coronary perfused, isovolumic contracting canine hearts in a homogeneous cylindrical volume conductor, Maehara and coworkers (Maehara et al., 1986) recorded ischaemic ST segment deviation at intramyocardial, epicardial and precordial sites to investigate the applicability of solid angle theory to the mechanism of ischaemic ST segment deviation. By comparing experimentally measured ST segment potential distributions and calculated solid angle, they found that there was a high correlation between these two data sets at epicardial, precordial and intramyocardial leads, despite the difference which existed between epicardial and precordial ST segment potential distributions. They concluded that solid angle analysis can be used to approximate the distribution of ischaemic ST segment deviation in acute ischaemia. Furthermore, the results showed that on epicardial ST segment mapping, the higher ST segment elevations occurred near the ischaemic boundary with a small progressive decrease in amplitude as the centre of the ischaemic region was approached, which supports solid angle theory that injury currents arise mainly over the marginal zone in acute ischaemia. This conclusion was further supported by the observation that not only ST segment elevation, but also ST segment depression occurred over the nonischaemic region, with less ST segment depression occurred near the ischaemic boundary and progressively decreased ST segment occurred further away from the ischaemic boundary. However, no indices indicative of the severity of regional myocardial damage were investigated in Maehara's study. Thus, the degree of the inhomogeneity in the ischaemic tissue was unknown. To better understand the translateral ST-shift in different depth of the myocardium, the degree of regional myocardial damage should be considered.

Our recent studies of epicardial ST depression in acute myocardial ischaemia with *in situ* sheep (Li, et al., 1999) observed that occlusion of the big artery (LAD or LCX) produced ST elevation over the infarcted region and ST depression over the noninfarcted region. The highest amplitude of ST elevation is at the boundary, with gradually decreased amplitude of ST segment elevation produced towards the ischaemia centre. Occlusion of small artery (OM) produced a graduated but even peak of ST elevation in the ischaemic centre, with the magnitude decreasing toward the border, and slight reciprocal ST depression occurred at the surrounding region, which is quite different from that of occlusion of the LAD or LCX. The different response of ST in the centre and border zone in smaller ischaemic area was also found by Maehara and coworkers (Maehara et al., 1986). Janse's (Janse et al., 1979) also found in his study of regional myocardial ischaemia in isolated perfused pig hearts that after 8 minutes of ischaemia, highest ST elevation/TQ depression occurred in the centre of ischaemia, ST elevation/TQ depression in the border zone is less than in the centre, while in surrounding normal myocardial showed slight reciprocal TQ elevation/ST depression. After 30 minutes of ischaemia, ST elevation/TQ depression diminished in amplitude in centre zone, and after 2 hours, ST elevation/TQ depression has substantially decreased. However the location of the electrical border zone has remained constant, and even though the electric recording in the border zone showed ischaemic changes (i.e. ST elevation/TQ depression), they were in a lesser degree than in the centre zone. ST/TQ of the normal zone remained either isoelectric or showed slight reciprocal changes.

The different response of ST/TQ in the centre and border zone might be explained that injury currents arise over a marginal zone with a certain width. In Hearse's study, they found that the electrophysiological border zone in dog hearts was over an area of 8~15mm (Hearse et al., 1977). Richeson reported, by the use of solid angle analysis, that epicardial ST segment distributions appear most consistent with the condition in which the injury current source is distributed over a 1 cm border region in the pig heart (Richeson et al., 1978). Miller and Geselowitz (Miller and Geselowitz, 1978) reported that body surface electrocardiograms in acute ischaemia and infarction are well simulated by a model in which action potential morphology is progressively changed from the periphery to the central portion of the ischaemia region. So it may be more realistic to presume that the severity of ischaemic injury increases from the periphery to a central portion over an ischaemic border zone having a certain width. Another explanation is that small regions of infarction lead to stable condition of the animal, which can not produce powerful electrical activities strong enough to lead to

typical ischaemic distribution. The latter was suggested by Li and co-workers (Li et al., 1999) in their animal and modelling study of epicardial ST depression in acute myocardial infarction that the total current flowing out of the heart must flow back into the heart. Thus, the integral of current density over the ischaemic region matches that over the normal region, which was shown by the balance of ST elevation and ST depression during myocardial ischaemia. Smith (Smith et al., 1979) elaborated this discrepancy in his study of epicardial mapping in a myocardial ischaemia injury model. They concluded that early ischaemia (less than 20 minutes) was represented by a model of ischaemia in which injury current arises only at the ischaemic boundary, results in the highest ST segment elevation occurring on the boundary, while later ischaemia (after 20 minutes of ischaemia) may be represented by a model in which ST segment elevation is considered dependent on injury currents generated throughout the ischaemic region, results in a gradient in ST segment elevation from the periphery to the centre of the ischaemic region. An ionic mechanism may be involved in this phenomenon.

2.3.6 ST SEGMENT SHIFT IN MYOCARDIAL ISCHAEMIA AND ITS RELATIONSHIP TO MYOCARDIAL BLOOD FLOW

2.3.6.1 ST segment shift in transmural myocardial infarction and its relationship to myocardial blood flow

Because the degree of ST segment elevation has been used widely as an index of ischaemic injury, it is of particular interest to examine the relationship between ST segment elevation and blood flow in the ischaemia area. Much research has involved in quantitative or qualitative analysis of the relationship between reduction of regional blood flow and myocardial activation recorded in different site of the myocardium.

In Kjekshus and co-worker's study (Kjekshus et al., 1972), myocardial infarction was induced by LAD occlusion in dogs and myocardial blood flow was measured by radioactive-labelled microspheres. They found that blood flow in both the inner and outer portion of myocardium was reduced after coronary artery occlusion, and acute ST elevation on the epicardial was linearly related to reduction of subepicardial blood flow. However, the extent of ST elevation was disproportionately less with respect to the same degree of blood flow reduction in subendocardial portion. Furthermore, epicardial ST changes were less profound and less consistent where local myocardial

flow reduction was present only in the subendocardial region. Comparable ischaemic injury associated with the same extent of reduction of myocardial flow in the outer layer of the heart was associated with more marked ST elevation than that in the inner portion. They also found that epicardial acute ST depression was not associated with reduction of myocardial blood flow in either inner or outer portions of the ventricular wall. In sites with epicardial ST depression, blood flow was normal in both portions. They suggest that ST elevation in the epicardium occurs only with severe myocardial ischaemia, and that ST depression in the epicardial layer might be due to reciprocal changes from reversibly injured subendocardial cells.

In Smith's (Smith et al., 1975) myocardial ischaemia model of LAD ligation in dogs, they found epicardial ST elevations correlate well with myocardial blood flow within two hours, though there was still one third of the areas with myocardial blood flow of 10ml/min/100g or less which had no epicardial ST elevation. After two hours of occlusion, myocardial blood flow in both central and border areas increased, but these increases were not associated with a significant reduction of epicardial ST elevation. Their results didn't show a single quantitative relationship between epicardial ST elevation and myocardial blood flow following acute coronary artery occlusion, the author suggested the reason might be that the critical determinant of ST alteration is the local balance in oxygen demand and supply which affects the functional integrity of the myocardial membrane. It is known that myocardial blood flow has to be reduced to less than 50% of normal before significant ST elevation occurs (Raab et al., 1962). However, they did not measure blood flow in different myocardium layers, which will be vital in determining the relation between myocardial blood flow and ST segment shift. For further understanding of this relationship, more detailed studies need to be designed using intramural plunge electrodes for detailed intramural potential records and with myocardial blood flow recordings in different myocardial layers.

2.3.6.2 ST segment shift in subendocardium and its relationship to myocardial blood flow

As we know, subendocardial ischaemia always produces ST segment elevation in electrodes overlying the subendocardium or in the corresponding area of the ventricular cavity, and overall ST segment depression on the epicardial leads. Subendocardial ischaemia can be induced by partial coronary artery occlusion plus atrial pacing in animal studies. In patients with the presence of coronary artery

stenosis, an exercise test may provoke subendocardial ischaemia. The study of the quantitative relationship between the myocardial blood flow and the electrocardiographic abnormalities in subendocardial ischaemia may lead to an easy way to monitor patients with angina pectoris. Furthermore, the study of quantitative relationship between the myocardial blood flow and the electrocardiographic ST segment elevation in subendocardial ischaemia may be used to predict the prognosis of thrombolytic therapy.

Guyton (Guyton et al., 1977) produced a subendocardial ischaemia model by reducing the subendocardial blood flow to 25% of normal while keeping the subepicardial blood flow normal. They found a significant negative correlation existed between the magnitude of ST abnormality and the endocardial/epicardial coronary pressure. Endocardial ST elevation as well as epicardial ST depression was recorded in subendocardial ischaemia. But when subendocardial ischaemia extended to the outer portion of the left ventricular wall, and ischaemia becomes transmural, epicardial ST elevation occurs. As predicted by Prinzmetal (Prinzmetal et al., 1961) from electrophysiologic considerations, the magnitude of this reciprocal ST depression is small compared with the magnitude of simultaneous subendocardial ST elevation.

In Mirvis and co-worker's study (Mirvis et al., 1986), they produced subendocardial ischaemia in a dog model by chronically constricting the LCX plus atrial pacing at 90 to 210 beats/min. They studied ST shifts by body surface isopotential mapping with an 84-electrode torso grid and ST changes related to myocardial blood flow measured by radiolabelled microspheres. Subendocardial ischaemia was verified by the reduction of endocardial/epicardial blood flow ratios. Logistic regression analysis demonstrated that the magnitude of ST segment depression corresponded to an endocardial/epicardial blood flow ratios of less than 0.57~0.70. An equal likelihood of a normal and an ischaemic response was at an endocardial/epicardial blood flow ratio of 0.67. Ratios of 0.58 and 0.76 predicted abnormal or normal patterns respectively, with probabilities of 95%. The exact value of such an effect may be inaccurate, since recordings and measurements were made intermittently rather than continuously. It may also have varied if compared with contraction and metabolic measures, which may be more sensitive indicators of ischaemia (Markham et al., 1983). Mirvis further documented that the increase of blood flow in both endocardium and epicardium of a dog's heart with dipyridamole, which does not

induce endocardial/epicardial blood flow ratio change, will not result in abnormal body surface potential distribution (Mirvis et al., 1988).

In a recent study by Li (Li et al., 1997), they explored the relationship between epicardial and endocardial potential distributions and regional myocardial blood flow, subendocardial ischaemia was produced by partial LAD or LCX occlusion together with atrial pacing in sheep and was verified by measurement of regional myocardial blood flow with fluorescent microspheres. Both endocardial and epicardial potential distributions were recorded by direct cardiac mapping. Their results showed that the epicardial potential changes at 20 minutes did not correlate with either the endocardial/epicardial blood flow ratio or the percent decrease in the regional myocardial blood flow in the inner third of the myocardium underlying the electrodes. Neither did the peak negative epicardial potential difference correlate with the average endocardial/epicardial blood flow ratio. When the epicardial potential distribution maps were combined with the endocardial regional myocardial blood flow maps, the lowest ST segment depression did not coincide with the lowest flow area. Similar analysis was performed with the endocardial potential changes. It was shown that there was a weak but highly significant negative correlation between the endocardial potential changes and the endocardial/epicardial blood flow ratio, as well as the percent decrease of the control regional myocardial blood flow. When the endocardial potential maps were superimposed with the regional myocardial blood flow maps, a general relationship existed between the positive endocardial ST potentials and the low flow regions. This detailed research indicated that epicardial ST depression in subendocardial ischaemia does not predict the location of ischaemia region, while endocardial ST segment elevation is a direct effect of subendocardial ischaemia.

2.4 MODELS AND SIMULATION OF ELECTROCARDIOGRAPH

2.4.1 CONSIDERATION RELATED TO ELECTROCARDIOGRAPH STUDY

Research into the ECG study can be considered as falling into one of the three areas: (1) The direct problem, which describes the electrical sources in the heart directly; (2) The inverse problem, which involves the quantitative specifications of the parameters of the electrical sources of the heart from potential measurements over the torso; (3) Diagnosis, which is the determination of the pathological state of the heart from a temporal description of the electrical source of the heart as found under the inverse problem.

The simulation of the electrocardiograph involves constructing models for the effective sources of the heart and the surrounding conducting medium that are capable of an accurate simulation of the corresponding ECG. The models, in general, include two independent parts, one is a representation of the cardiac electric sources, the other is the relationship between the sources and the surface potentials (the body-surface ECG) they generate. The sources of the model have been used as single dipoles, multiple dipoles and distributed dipoles etc. (vide infra). The problem of determining the relationship between sources and potentials is referred to as the volume-conductor problem.

2.4.2 SOURCES OF THE MODELS

According to electrocardiographic theory, simulation of the electrocardiograph involves sources of the heart. Many attempts have been made to provide “equivalent cardiac generators” for the bioelectric sources in the heart, these include: single dipoles, multiple dipoles, multipoles and a double layer equivalent cardiac generator.

Single dipole

In the single dipole model, the heart’s electrical activity is represented by a dipole current source that is fixed in position but allowed to vary in magnitude and direction during the heart beat (Geselowitz, 1964). It assumes that the distance from the recording electrode to the heart is large in comparison with the electrically active boundaries of the heart, and that the heart and surrounding thoracic structures together comprise a uniform, homogeneous volume conductor. The limitations of the single dipole model have been demonstrated (Scher et al., 1960) and discussed (Geselowitz,

1964; Horan and Flowers, 1972) extensively. The electrical activity of the heart cannot be considered by a single dipole source with electrodes placed in close proximity to the heart. Experiments in which intramural electrodes were placed in the heart indicated that at any time during the QRS complex interval, multiple boundaries or surfaces are present which separate the resting cells from the cells that are already depolarised. But the size of these boundaries is not small, especially in relation to most electrode distances. Furthermore, the boundaries are also not fixed in position, as is required by the single dipole representation. As time progresses, the boundaries propagate through the ventricular myocardium, generally in an endocardial-to-epicardial and apex-to-base direction in the normal heart (Durrer et al., 1970).

In order for a single dipole model to be a reasonably good approximation, the electrode distance to the heart must be great in relation to the size of the boundary. Taccardi (1958) observed that it is only at a distance equal to five times the radius of the heart that the distribution of electrical potentials recorded are similar to those which may be generated by a single dipole. This requirement is not met by most epicardial, endocardial, intracavitary, esophageal, or precordial recording sites. Furthermore, Horan and Flowers (1972) have pointed out that in the normal heart only during the very early inscription of the QRS complex, when the activation process is taking place in the septum, is the boundary separating the resting and the depolarised tissue small and well localized.

Multiple Dipole

The multiple dipole model more completely represents the electrical activity of the heart (Holt et al., 1969). The boundary is represented by a finite number of discrete dipoles. This model permits the association of each dipole with a particular anatomic segment of the myocardium. In the study of Holt (Holt et al., 1969), the ventricular wall was divided into 12 segments. Unlike the single dipole model, the direction of each of the 12 dipoles is fixed in advance and approximates the average direction of the activation pathway in each particular segment. The magnitude of each dipole is then permitted to vary in time, rising from zero when the wavefront or boundary enters the segment and returning to zero when it leaves. Thus, in this model, the thicker the segment the longer the time the contribution from that segment persists. The magnitude of each dipole is also assumed to be proportional to the area of the activation boundary occupied by that segment at different moments in time as the boundary propagates through the segment. The potential seen at an electrode site is then equal to the sum of potentials contributed by each dipole. With the analog model

of Selvester's (Selvester et al., 1967), it was shown that infarctions of only 1.0 cm^3 in size resulted in identifiable changes in the vectorcardiogram as compared to the control, regardless of location including the supposedly "silent areas" (i.e. basilar portions of the septum and left ventricular wall). They also noted that involvement of the base of the left ventricle resulted in abnormalities of the terminal portions of the QRS complex.

Distributed dipole (Solid angle theory)

The concept of the solid angle theory was first formulated by Newton in his classic studies on gravitation and was later applied by physicists in the theoretical characterization of a wide variety of electrical phenomenon. The applicability of the solid angle theory to the interpretation of recorded electrocardiographic signals was recognised by Wilson (Wilson et al., 1933a), and was expanded to ECG theory by Holland and Brooks (1975). The solid angle model considers each boundary present in the heart to be composed of an infinite number of dipoles, each representing an infinitesimally small region of the boundary. Because more dipoles are considered, this model more accurately represents the electrical activity of the heart. This model differs significantly from the two previously considered not only in the number of dipoles used to represent the heart but because each dipole is permitted to move in the direction of its segment of the boundary and each dipole has exactly the same strength or magnitude which equals the difference in transmembrane voltage (ΔV_m) across the boundary (Holland and Arnsdorf, 1977). Since this boundary separates two cell populations that differ in transmembrane potential, it has been represented as a distributed dipole layer.

The solid angle or distributed dipole layer model of the electrical activity of the heart overcomes many of the limitations of the more conventional single dipole representation. First and foremost, the solid angle approach provides a specific physiologic interpretation of the ECG. All ECG deflections may be categorized as being due to spatial (Ω), nonspatial (ΔV_m), or other (K) factors. These deflections, whether reflecting electrical activity of normal or diseased (ischaemic, hypertrophic, or infarcted) hearts, are due to the presence of boundaries in the heart established by regions having different transmembrane voltages. Second, it is observed that the solid angle approach is valid at all electrode distances from the heart. Since the area represented by each dipole in the distributed dipole layer model is infinitesimally small, an electrode can be placed as close to or as far away from the heart (or, more properly, the boundaries present in the heart) as is desirable and the solid angle

representation remains valid. Third, it is suggested that the solid angle analysis provides a rational basis for the quantitative interpretations of electrocardiographic data. Using this theory, changes in the spatial relationship of the boundary and the electrode site or changes in the transmembrane potential difference of different regions can be directly associated with changes in the magnitude and polarity of the waveforms recorded in the ECG.

However, the solid angle theory has its limitations. For both theoretical and practical reasons, it does not provide a complete mathematical representation of the electrical activity of the heart. The solid angle analysis is limited, as is the classical dipole theory, by the fact that the thorax is neither a homogeneous nor an infinite volume conductor. Furthermore, the thorax is irregularly shaped, with the heart occupying an eccentric position within it. These factors make the mathematical formulations extremely complex (Bayley and Berry, 1964). One practical limitation of the solid angle approach pertains to the difficulty of calculation. In many instances piecemeal approximations of an irregularly shaped boundary with circular or ellipsoidal boundaries are necessary in order to obtain actual numerical values (Plonsey, 1974). Most important of all, the anisotropy of the heart muscle must be taken into account in the solid angle analysis.

2.4.3 VOLUME-CONDUCTOR PROBLEM

The earliest solutions to the ECG volume-conductor problem were analytical. Such solutions are confined to relatively simple shapes such as spheres or ellipsoids. However, they can provide useful information. Analogue computer solutions were induced later to cope with realistic torso geometries. Numerical schemes were developed more recently which enabled the calculations to be carried out on digital computers. In either case, it suggests that realistic geometries be used to avoid restricting electrode sites to the limbs, and to incorporate electrical inhomogeneities in the volume conductor to account for the different conductivities of body tissues such as lung, fat, bone, cardiac muscle, skeletal muscle and blood.

2.4.4 MODELS AND SIMULATION OF ELECTROCARDIOGRAPH FOR FORWARD PROBLEMS

The prototype model of the ECG was put forward by Einthoven (Einthoven et al., 1913). This simplistic model has proved to be extremely useful and still dominates

much of electrocardiographic theory. The source of Einthoven's model is a dipole, the distribution of sources throughout the heart during cardiac cycle can be represented by a single dipole source at a fixed location, thus in Einthoven's model, the heart is localised in the midpoint of a triangle, it is postulated that the electromotive force created by the heart is equivalent at any given moment of the cardiac cycle to a single dipole, this single dipole may be presented by a vector directed from the negative to the positive pole, proportional to the magnitude of the charges and to the distance that separates them, this vector represents the moment of the dipole. Einthoven also postulated that the triangle may be conceived as a homogeneous plane of conducting material, implying that the structures surrounding the heart—bones, muscles, etc are homogeneous from an electrical standpoint. There are limitations of Einthoven's model, the human body is certainly not a symmetric, homogeneous conductor, different specific resistances exist among various tissues of the body, etc.

Einthoven's single dipole model was developed by Wilson (Wilson et al., 1933b and 1933c) who correlated dipole sources to cellular activity. By using a single cylindrical fibre, Wilson showed that the dipole moment was related to the spatial gradient of transmembrane action potential. According to Wilson, a long cylindrical fibre in an infinite volume conductor acts as a distributed current dipole source whose movement is proportional to the product of the area of the fibre, the conductivity and the derivative of the transmembrane potential along the fibre axis.

Researchers used the cable theory with the assumption that the intracellular potential varied along the axis of the cylinder and that the intracellular conductivity was the same throughout the cylinder, it was found that the intracellular potential gradients primarily determine the magnitude of the extracellular potentials during depolarisation (Rall, 1969) and repolarization (Spach and Barr, 1976).

Despite its cellular nature, the heart acts in many respects as a syncytium. Cell-to-cell resistance of the heart is low, therefore intracellular space may be thought of as a "syncytium" occupying the volume of the heart muscle. Interstitial space similarly can be considered a second syncytium. Thus the volume of the heart muscle can be considered to be composed of two syncytia or domains. The two domains (bidomain) or syncytia are everywhere separated by the cell membrane. In Spach's (Spach et al., 1972) "SI model" (spatial intracellular potential), he assumes that a network of cells

can be treated as one large cell so that net membrane currents can be determined from the second spatial derivative.

The “bidomain model” provides a basis for relating cardiac sources to cellular action potentials. The volume conductor problem provides the framework for relating torso potentials to cardiac sources. A model based on the bidomain model has been developed by Miller and Geselowitz (1978). In Miller and Geselowitz’s model which is similar to Spach’s SI model, they applied a general three-dimensional distribution of cells. In this model, the geometry of a human heart was represented by a series of 16 cross-sections along planes perpendicular to the base-to-apex axis. A rectangular grid of discrete points was superimposed on each cross-section, resulting in a three-dimensional array of approximately 4000 points. This was subdivided into 23 regions representing the ventricles of the heart, giving a multiple-dipole model of the heart. On the basis of the bidomain model, the distributed dipole source \vec{J}_i (intracellular current density) is proportional to the spatial derivative of the transmembrane potential. During the heart cycle, the transmembrane potential of each cardiac cell undergoes a variation in time, the resulting waveform being known as the action potential. The distribution of cellular action potentials both spatially and temporally throughout the heart provides sufficient information to determine \vec{J}_i . By summing the spatial gradient of the intracellular potential distribution throughout the region, the moment of the single dipole representing each region is determined. The resulting set of 23 dipoles is then used to calculate the potentials on the surface. The Miller-Geselowitz model of the ECG appears to provide an excellent simulation of the body surface ECG for the normal heart and for a wide variety of examples of ischaemia and infarction. However, inhomogeneity and anisotropy of the body as a volume conductor are ignored in this model.

A more detailed three-dimensional inhomogeneous torso model has been developed by Walker and Kilpatrick (1985). In this torso model, the torso was digitised from the CT scans of human with normal torso geometry. A non-uniform grid was used, grid spacing ranged from 7.5mm to 15mm. The model was made from 25 slices, ranging in thickness from 10mm in the vicinity of the heart to 50mm in the lower part of the torso, resulting in a highly detailed model containing 18924 nodes, encompassing the heart, lungs, spine and sternum. The validity of the modelling procedure has been tested by modelling a homogeneous spherical volume conductor with two point current sources and comparing the model solution with the known analytical solution (Frank, 1952). The isopotential contour maps for both the model and the analytical

result are almost identical. The percentage difference between the two solutions is 1%~2% through the outer half of the sphere and 4%~5% at the surface of the sphere which is relatively small. Using this model, a standard dipole-like source is placed along the axis of the heart. The torso surface potential distributions produced are quite similar in shape to those measured from a normal subject at mid QRS, supporting the idea underlying most conventional electrocardiography and vectorcardiography that the electrical sources in the heart can be approximated by a single dipole source.

However, in multidimensional anisotropic tissue, the relationships exist between the intracellular and the extracellular potentials are considerably more complex. Using the standard equations of cable theory, Jack (Jack et al., 1975) used a core conductor model to explain the origin of extracellular potentials in multidimensional anisotropic tissue. This model provided most of the information that explains the spread of intracellular currents. The concept of using intracellular currents to derive the transmembrane currents, which is an integral part of the core conductor model, has been applied to cardiac muscle in the analysis of extracellular potentials (Spach and Barr, 1976). It provides a way to describe in detail the spread of intracellular currents which, in turn, determine the currents that flow between the intracellular and the extracellular space. Thereby, providing all of the information necessary to develop, evaluate and compose various models of bioelectric sources.

Anisotropy is likely to play a significant role in the case of cardiac ischaemia, this has been documented by Johnston and co-worker's further study of modelling ST segment shift in subendocardial ischaemia (Johnston et al., 2001). In this study, the cardiac tissue is represented by the bidomain model. Tissue anisotropy and fibre rotation have been incorporated with a view to predicting the epicardial surface potential distribution. This model allows differing electrical conductivity in the intracellular and extracellular spaces as well as in the longitudinal and transverse directions. It showed that tissue anisotropy and fibre rotation must be included to obtain meaningful and realistic epicardial potential distributions.

2.4.5 MODELS AND SIMULATION OF ELECTROCARDIOGRAPH FOR INVERSE PROBLEM

In an attempt to improve the clinical utility of electrocardiographic recordings, many groups have attempted to calculate the strength and location of sources within the

heart that give rise to the measured ECG, this is known as the inverse problem of electrocardiography.

A number of methods have been tried in the study of the inverse problem (Barr and Spach, 1978a; Cuppen and VanOosterom, 1984; Walker and Kilpatrick, 1987a). In Barr's study of inverse calculation of QRS-T epicardial potentials from body surface potential distributions in the intact dog, inverse calculations are made to develop mathematical models previously used for forward simulations (Barr and Spach, 1978b). They found that epicardial potential distributions estimated from measured body surface potential distributions correspond well to measured epicardial maps. Moreover, the inverse epicardial maps characterized each sequence of excitation and repolarization to an extent not possible from inspection of the body surface maps alone. This was done by providing information that was sufficient not only to make clear the answers to the question of the site of the stimulus, but also to provide a picture of the development and movement of major features of the sequence of excitation and repolarization events.

Walker and Kilpatrick (1987a) calculated epicardial potential distribution on a resistive network model of the human torso containing approximately 20000 nodes. To calculate epicardial potentials, a model of the torso was constructed and used to determine body surface potentials in terms of the epicardial potentials. Computerised tomographic (CT) scan data were digitised to create a three-dimension resistor network model which approximates the torso. The torso model used here was obtained from the CT scans of a 40-year-old male subject. The model contained 18924 nodes and included the heart, lungs, spine and sternum. There are 736 nodes on the epicardial surface. The epicardial-nodes were grouped into source regions of approximately equal size. Epicardial potential distributions were calculated using 26, 50, 74 and 98 source regions. The epicardial potential distributions calculated from measured body surface data yielded a constant potential with small error. Further research by Walker and Kilpatrick (1987b) showed that using some form of smoothing (regularization) was essential when calculating epicardial potentials. This was previously verified by Barr and Spach (1978b).

Two approaches are immediately evident for modifying the inverse calculation method. The first and most direct approach is to reduce the errors in the epicardial potentials by reducing the noise. The second is to incorporate into the solution procedure additional information about the characteristics of physiologically real

epicardial potential distributions, in addition, to using the same variance for the potential magnitude at all electrodes.

2.4.6 ELECTROCARDIOGRAPH MODELS FOR MYOCARDIAL ISCHAEMIA STUDY

The assessment of alterations in ST segment deflections obtained by electrocardiograph is a valuable experimental and clinical method of dynamical reflection of alterations in the metabolic status of ischaemic myocardial cells. To model ischaemia, the action potentials were modified in the region of injury on the basis of available electrophysiological data. As ischaemia progresses, there are characteristic changes in the action potentials, including a decrease in the magnitude of the resting potential, a decrease in action potential amplitude, and a shortening of the action potential. A cell may eventually become unresponsive and finally die. All these features, as well as ischaemic conduction delay, should be incorporated to the model. Myocardial injuries generally have complex and irregular geometries, however, and vary greatly in location, size, and in the distribution of the severity of injury within the injured region. It is impossible to predict accurately the nature of the changes in the surface ECG without taking all of these factors into account. In addition, volume conductor distance and boundary effects in the torso must be considered. Considerable interest has been focused on defining the relationship between ST elevation and the distribution of transmembrane potential changes within the ischaemic region.

Modelling of electrophysiological events in myocardial ischaemia for interpreting ST segment shift has been reported in many studies (Ekmekci et al., 1961a and 1961b; Holland et al., 1977; Holland and Brooks, 1975 and 1977a; Kleber et al., 1978; Smith et al., 1979 and 1983).

The origin of cardiac injury potentials, manifested as ST elevation in the epicardial ECG, was initially formulated by Wilson and others (Wilson et al., 1933a; Pruitt and Valencia, 1948) by the application of basic principles of field theory. Wilson proposed that the solid angle theory could be used to predict the ST elevation at a given recording site from knowledge of the geometrical configuration of a region of ischaemic injury (Wilson et al., 1933a). This was based on the assumption that transmembrane potential is uniformly altered throughout an ischaemic region such that a difference in transmembrane potential exists only at the boundary between the

ischaemic and the normal myocardium. Thus, the ischaemic boundary has been represented as a polarized surface giving rise to injury potentials measured as ST elevation in the ECG. Holland and Brooks (Holland et al., 1977; Holland and Brooks, 1975 and 1977a) constructed a geometrical ischaemic heart model based on "polarized surface" analysis linking changes in ST elevation to the distribution of transmembrane potential changes in the ischaemic region. In their model, which employed a solid angle theory, the ventricle was represented by a sphere of specified thickness. A transmural region of ischaemia was represented by a wedge throughout the ventricle. The ischaemic boundary is defined as the interface of the ischaemic and normal regions. As this boundary separates the two cell groups that differ in transmembrane potential, it has been represented as a distributed dipole layer. Polarized surface models predict that the ST elevation observed at a given recording site is proportional to the solid angle subtended at that recording site by the polarized surface representing the boundary of ischaemia. According to this model, the degree of ST elevation overlying the ischaemic region is approximately uniform and represents the pattern experimentally observed during early ischaemia. They found that a decrease in ischaemia size results in an increase in ST elevation.

After a more prolonged period of ischaemia, studies showed that a gradient in the transmembrane potential of ischaemic cells occurred that extended from the boundary to the centre of the ischaemic region (Prinzmetal et al., 1968; Mitra, 1968). They found ST elevation showed a progressive increase from the boundary to the centre of the ischaemic region, the lowest ST elevation occurred near the ischaemic boundary and a progressive increase in ST elevation occurred approaching the centre of the ischaemic region, which can't be explained by "polarized surface" model. Furthermore, the decrease in ischaemic size resulted in a decrease in ST elevation and, conversely, an increase in ischaemic size resulted in an increase in ST elevation. They suggested that later ischaemia may be presented by a model in which ST elevation was considered dependent on injury currents generated throughout the ischaemic region. Because cell groups differing in transmembrane potential exist throughout the volume of ischaemia, the gradient of cellular transmembrane potential has been represented by a volume of distributed dipoles.

An electrocardiographic model of ischaemic injury was constructed by Smith (Smith et al., 1983) which accounted for the non-uniform distribution of transmembrane potential changes which occurred throughout a region of ischaemia. In their model, the ventricle was represented by a sphere of specified thickness, and a transmural

region of ischaemia was represented by the intersection of the sphere with a cone, the apex of which lay at the centre of the sphere. The ischaemic boundary was defined as the annular shell that interfaces the cone and the sphere. Such a model is referred to as a “polarized volume” model. This has the capability of representing polarization distributed throughout a volume and affords a method of accurately describing the nonuniformity in transmembrane potential changes occur within the ischaemic region. This model is quite similar to that of Holland and Brooks’ “depolarised surface” model (Holland et al., 1977), only that the total volume of ischaemia was divided into an arbitrarily large number of volume elements. Any given volume element is considered to be polarised in that it exhibits a gradient in transmembrane potential which gives rise to a dipolar field of injury current, and each volume element behaves as a small current dipole. Using this model, Smith compared the theoretical three-dimensional plots of distribution of epicardial ST elevation and the experimental distributions of epicardial ST elevation during the course of myocardial ischaemia in a pig heart, and found a good relationship between them. Similar results were obtained by Kleber (Kleber et al., 1978) who used high resolution ST mapping in the pig. These results are also consistent with previous ST mapping studies conducted in the dog (Redwood et al., 1972; Ergin et al., 1976). Thus a “polarised volume” model can explain the experimental observed increase in the magnitude of epicardial ST elevation from the boundary to the centre of the ischaemic region which is inconsistent with the “polarised surface” model. In addition, the “polarised volume” model also predicts the experimental results that the amplitude and area of ST elevation decreases following a decrease in the size of ischaemia. The “polarised volume” model more accurately reflects the experimental results regarding changes of ST in myocardial ischaemia.

To explain electrocardiographic ST changes in subendocardial ischaemia, a bidomain model was constructed (Li et al., 1998). In the bidomain model, the intracellular and extracellular volumes occupied the same space and were separated everywhere by the membrane. The intracellular space and the extracellular space were coupled through the trans-membrane current; the concept is that the outflow from one region must be equal to inflow to the other. In Li’s model, the geometry of the heart of a normal 58-year-old woman was constructed from a magnetic resonance image scan. Subendocardial ischemia from either LAD or LCX region was simulated. Eight-node brick elements were used to mesh the heart, which was divided into 60661 elements ($2 \times 2 \times 2 \text{ mm}^3$). The source was calculated from the width of the boundary, the given conductivity and the transmembrane potentials. It was found from the model that the

epicardial ST depression in subendocardial ischemia was over the lateral region in either the LAD or the LCX occlusion. Since the LAD and the LCX share their boundary at the lateral wall, ST potentials showed a similar distribution pattern of lateral ST depression.

However, anisotropy of the heart was not taken into account in Li's model. The anisotropy was simulated further in Hopenfeld's model (Hopenfeld et al., 2004). Hopenfeld constructed a geometric model based on the anatomic and fiber structure data of the Auckland canine heart. The localized ischaemia was represented by a path of tissue in the left ventricle, where the transmembrane potentials were 30mV smaller than that in the remaining healthy cells, and the size of the ischaemic patch was altered in the transmural direction to simulate various degrees of transmural ischaemia. The anatomy of the heart was represented by a hexahedral mesh defined by a number of nested, concentric layers. The heart consisted of 60 layers that were weighted averages of the epicardial and endocardial surfaces. The degree of ischemia was defined with respect to the 60 layers. They found from the model study that ST depression along at least one side of the ischaemic patch increased with the degree of transmural ischaemia, and the voltage drop across the ischaemic boundary tended to be greatest along the direction of the fibres. Further model study by Hopenfeld (Hopenfeld et al., 2005) took into account of both the intracellular and extracellular conductivities of the heart and the conductivity of the ventricular blood. The conductivity tensor at each quadrature point was based on the local fibre orientation, which was computed by forming a distance-based weighted average of the fibre orientation data corresponding to the eight points from the canine data. It showed that at medium or high thickness of transmural ischaemia, a consistent pattern of two minima of the epicardial potential over opposite sides of the boundary between healthy and ischaemic tissue appeared on the epicardium over a wide range of conductivity values. The magnitude of the net epicardial potential differences was strongly correlated to the intracellular to extracellular conductivity ratios both along and across fibres. Anisotropy of the ischaemic source region was critical in predicting epicardial potentials. Subendocardial ischaemia is manifest on the epicardium by ST depression located over a boundary between ischaemic and healthy tissue. The magnitude of the ST depression is a function of the bidomain conductivity values. The limitation of Hopenfeld's study is that the heart model has not been linked to the torso. Thus, it is not certain if these findings might serve as a diagnostically meaningful marker of ischaemia.

2.5 APPLICATION OF MAPPING TECHNIQUES

Mapping techniques used in cardiac research and diagnosis include cardiac mapping and body surface mapping. Cardiac mapping is a method by which potentials are recorded directly from the heart, while body surface mapping is defined as the temporal sequence of potential distributions observed on the thorax. The location of the recording electrodes (endocardium, intramyocardium, epicardium, or torso surface), the recording mode used (unipolar or bipolar, or both) as well as the method of display (isopotential or isochronous) depends on the problem under consideration. As we know, the spread of excitation and recovery through the heart gives rise to a three-dimensional time-varying cardiac potential distribution. A complete picture of the cardiac electrical field can be obtained by measuring the potential distribution in the cavity of the heart, on the endocardial surface, in the thickness of the cardiac walls, on the epicardial surface, in the extracardiac conducting media and on the surface of the body. A detailed picture of the cardiac electrical field will give more information in order to understand the cardiac activity and to interpret the underlying mechanism of cardiovascular disease.

2.5.1 APPLICATION OF ELECTRODES FOR MAPPING PURPOSE

The electrode configurations vary significantly between different research groups and with different applications. While epicardial mapping can be done with one probe, and two electrodes can detect a surface electrocardiograph, most mapping systems have a minimum of 32 electrodes. The nature of the electrodes used to measure the myocardial potential determines the nature and quality of the data. Unipolar electrodes yield information about total cardiac electrical activity while bipolar electrodes, when used properly, cancel the effects of activation of tissue far away from the electrode site (Durrer and Van, 1953). The electrode material can influence the amount of direct coupled offset introduced into the recording. The method of application of the electrode influences the amount of mechanical artifact introduced into the electrogram and thus makes the data more or less difficult to analyse. The size of the electrodes, and thus the surface area in contact with the epicardium, also influences the quality of the data.

Epicardial electrodes have been widely used in basic research as well as in clinical research. Different kinds of epicardial electrodes were designed both for animal and human studies. In Muller and co-workers' research (Muller et al., 1975) of

myocardial ischaemic injury in dogs, the epicardial electrograms were recorded with the use of an electrode grid sutured by its corners to the surface of the left ventricle. The grid was composed of 30 multistrand 34 gauge stainless steel wires sutured 0.5cm apart in a 2-by-4cm sheet of silastic. To study the genesis of the electrocardiograms, D'Alche (1976) used stainless steel hooks which were fixed in a homogeneous distribution over the whole pericardial surface as electrodes. Each hook was soldered to an isolated electrical copper wire which came out of the thorax. In a study of analysing cardiac activation during arrhythmia, Gallagher (Gallagher et al., 1982) constructed epicardial mapping with a hand-held probe. In Gallagher's work, a single electrode probe was used to record signals from the epicardium, a reference electrode was also used for timing purpose. Monro and co-workers (Monro et al., 1986) studied epicardial potential distribution in humans during surgery. Three stainless steel pacing wires were used to record the epicardial potential. The bared end of the wire was bent sharply in the middle and sewn to the epicardium. Using a 64-unipolar-electrode sock, the epicardial potential mapping from the isolated whole heart of the dog was constructed by Green and co-workers (Green et al., 1991). The 64 electrodes were mounted on the sock, and the arrangement of the 64 electrodes provided extensive coverage of the epicardial surfaces of the left and right ventricles. Epicardial potential distribution on both left and right ventricular surfaces was recorded from the in situ sheep heart during acute myocardial infarction by using a similar epicardial sock (Li et al., 1999). For coverage of a smaller area with possible higher electrode density, a sock with the configuration of the electrodes modified appropriately or a patch of electrode-carrying material anchored to the epicardial surface was used by Ergin (Ergin et al., 1976) who mounted electrodes on a piece of Mersilene mesh coated with silicone and tailored the mesh to cover the desired part of the epicardium.

Endocardial mapping is widely used in cardiac arrhythmia and ischaemia studies. The application of multiple electrodes to the endocardial surface of the heart chambers can not be carried out as conveniently as with the epicardium. To study endocardial potential distribution, Scherlay (Scherlay et al., 1967) used wires inserted through the myocardial wall, the ends of the wires were hooked and inserted inside the needle into the cavity. The needle was pulled back and the wires gently retracted until the hooks embedded in the endocardial surface. Smith (Smith et al., 1979) used a series of electrodes inserted into a needle curved in the approximate shape of the interventricular septum, the needle was passed longitudinally through the septum and pulled back, and electrodes were left in the cavity along the length of the septum. For

studying ventricular tachycardia, Josephson (Josephson et al., 1982) used intracardiac catheters to record endocardial potential. Beatty (Beatty et al., 1994) used a multiple-electrode array catheter which can be introduced percutaneously through a 9F introducer to record endocardial potential. By using an endocardial basket which has 8 arms, each with five electrodes on it, Li (Li et al., 1999) successfully recorded the global endocardial potential distribution by inserting the basket from the cardiac apex to the cavity where the basket became inflated. A similar basket catheter was used by Zrenner (Zrenner et al., 1999) in his study of atrial arrhythmias. The basket catheter was composed of 64 electrodes mounted on eight flexible, self-expanding nitinol splines; each spline had 8 electrodes on it. The multiple electrograms recorded by this basket catheter were used to analyse the three-dimensional activation patterns of various atrial arrhythmias. Kongstad also used a catheter which was introduced into the left ventricle via the carotid/femoral artery or into the right ventricle via the jugular/femoral vein to record monophasic action potentials, the catheter had a contact ball of length 0.5mm and diameter 1mm at the end surface of the tip electrode (Kongstad et al., 2002).

The intramyocardial potential distribution is not easy to record for the analysis of myocardial injury currents. Kasell and Gallagher (1977) measured intramyocardial electrograms by using a needle with wire electrodes fixed along its length, the ends of 15~20 wires were placed along the open side of the needle at 1mm intervals and were fixed using epoxy or dental acrylic. An automated system for transmural cardiac mapping has been described by Witkowski and Corr (1984). They used plunge needle electrodes to record from up to 240 sites simultaneously. Li (Li et al., 1997) used four quadripolar needle electrodes with a diameter of 0.9mm and a length of 17mm to record intramural potentials. However, the data recorded by Li were not satisfactory due to the strong injury currents produced by the intramural electrodes.

Abraham (1983) designed a suction-electrode net for precordial ECG mapping which included a 19-electrode net and 48-electrode net. The 48-electrode net was a rectangular 6x8 matrix with four pneumatically isolated quadrants. The 19-electrode net had a hexagonal structure around a central electrode. Suction was transmitted from each electrode to its neighbours via holes in the groove surrounding a concave conductive electrode and a soft "Silastic" tubing system which enabled the matrix to conform to the body contours. The dimensions of the net can be easily varied by using sets of connecting tubes of different length. Walker (Walker et al., 1983) constructed a jacket of two layers of closed cell foam, the surface of the inner layer

shows a regular grid of slightly raised nickel plated electrodes 1cm in diameter. The electrodes are distributed regularly on the inner layer of the jacket, with 5 rows of 10 electrodes. Each electrode is connected to a high input impedance unity gain buffer, which lie between the foam layers, behind the electrodes. With this jacket, body surface potential mapping was generated quickly with great success. Other technology for body surface mapping has also been used in the clinical research (Tonooka et al., 1983; Toyama et al., 1984; Osugi et al., 1984). Compared to routine ECG, body surface potential mapping contains more information for diagnosis of myocardial disease, even though the technique is more difficult.

2.5.2 ANALYSIS OF MAPPING

Mapping data can be displayed by conventional potential versus time scale plots, distribution displays such as isopotential contour maps, isointegral contour maps or isochrone contour maps. A variety of graphic techniques is also available for enhancing aspects of the distributions which include the use of colour, either as contours or shading between contours, and nonlinear scaling.

Some of the mapping studies used the trajectories of maxima and minima as diagnostic parameters. According to the trajectory analysis, Hirai found that in 26 out of 32 cases of anterior myocardial infarction with normal ECG, the trajectories of the potential minimum were abnormal and correlated well with the location of the asynergy (Hirai et al., 1984). Similar findings were obtained in inferior myocardial infarction patients with normal 12 lead ECG (Osugi et al., 1984). In angina patients with normal resting ECG, De Ambroggi (De Ambroggi et al., 1977) observed a typically abnormal location of the ST minimum in about one half of the patients. The trajectory analysis was also used in exercise tests by Simoons and Block (1981) who found the optimal electrode location and the optimal criteria for detecting ischaemic changes. Liebman even found that the trajectory of the maxima may reveal the location of focal right bundle branch block in children after surgical repair of congenital heart diseases (Liebman et al., 1984).

Many researchers have used the isopotential analysis technique which allows detailed analysis of sequential changes in the ECG, the disadvantage of isopotential analysis is that the large amount of data makes display cumbersome. Iso-integral analysis technique was introduced by Montague (Montague et al., 1981) and it is a useful and convenient method of data reduction and can provide spatial information. It has the

advantage of summarizing the map information relating to the entire QRST interval, or parts of this interval, into one map. Compared to iso-integral analysis, departure mapping is more accurate in estimating the site and size of myocardial ischaemia. Iso-integral maps, departure maps and departure index maps may be used for mapping analysis to provide information on the location and size of myocardial infarctions. Using iso-integral maps, departure maps and departure index maps, De Ambroggi (De Ambroggi et al., 1986) found that all these indices could be used to localise myocardial infarction.

Quantitative analysis has been recently applied to body surface mapping with interesting results. Peak potential values and the integral of the potential function extended to the entire chest surface have been combined in a multivariate statistical analysis to reveal myocardial infarctions, left ventricular hypertrophy and myocardial ischaemia in 42 patients with left bundle branch block. These conditions were undetectable from the 12-lead ECG (Musso et al., 1987). The same parameters, combined with the location of the ST minimum, enabled myocardial ischaemia to be detected in 80% of angina patients with normal resting ECG.

Quantitative analysis of ST magnitude using discriminant maps was done by Kornreich (Kornreich et al., 1993). In their study, different maps were computed by subtracting at each electrode site the normal group mean voltage from each myocardial infarction group mean voltage for each time instant. Sequential discriminant maps were obtained. The values achieved were referred to as discriminant indices, this was used to assess the effect of thrombolytic therapy in acute myocardial infarction. Hanninen (Hanninen et al., 2001) used body surface potential mapping to evaluate electrocardiographic criteria for ischaemia in stress testing. By introducing the discriminant index suggested by Kornreich (Kornreich et al., 1993), they calculated the group mean ST segment isopotential and isoslope maps. The highest negative discriminant indices indicate the optimal locations for the ST depression and ST-slope decrease and the highest positive discriminant indices indicate the optimal locations for the reciprocal ST elevation and ST-slope increase. The results showed that both ST depression and ST-slope could detect transient myocardial ischaemia in body surface potential mapping. The morphology of the ST, reflected by the ST-slope, appeared to be a sensitive and specific marker of transient myocardial ischaemia, and seemed to perform slightly better than conventional ST depression. Even in the standard ECG, ST-slope seems to be a sensitive marker of myocardial ischaemia (Ribisl et al., 1993).

2.5.3 APPLICATION OF MAPPING

2.5.3.1 Application of body surface mapping

Body surface mapping is the collection of sufficient electrocardiographic potentials from the surface of the body to adequately reconstruct the body surface potential contours for diagnostic purposes.

Body surface mapping has been used in human to study the sequence of atrial activation and the sequence of ventricular activation (Abildskov et al., 1976), to find accessory pathway of arrhythmias (Tilg et al., 2002), and to estimate possible approaches for management of cardiac arrhythmia (Iwai et al., 2002). In addition, body surface potential mapping is also used in other cardiac diseases like reperfusion assessment (Von-Essen et al., 1985), cardiac function estimate (Horan et al., 1988), and hypertrophy (Yamaki et al., 1989). It is widely used in diagnosing myocardial infarction and localizing myocardial infarction (Toyama et al., 1984; Osugi, 1984; Montague et al., 1988; Montague et al., 1990; Hauninen et al., 2001b).

In Abildskov's (Abildskov et al., 1976) study of body surface isopotential maps in dogs, they constructed body surface isopotential maps based on 192~200 body-surface-electrode recordings, and found that body surface potential patterns were substantially influenced by the effects of electrical activity. Different effects of electrical activity in various cardiac regions on body surface potential were seen by the body surface location of potential maxima and minima, and by patterns of isopotential lines during early portions of ventricular excitation initiated at different ventricular sites. Thus cardiac activity can be examined by body surface mapping. Furthermore, to interpret the cardiac activity in more detail, the potential gradients at various locations, the time course of changing potential values can also be referred to.

Body surface mapping has been shown to be superior to 12-lead ECG for detecting myocardial ischaemia. Body surface mapping has been used in human studies during exercise (Miller et al., 1980). Miller recorded the body surface potential distribution from 20 normal young adults during multistage maximal exercise testing on a bicycle ergometer. Body surface potential maps were obtained from 24 electrodes; spatial distributions of the potentials over the surface of the torso have been examined at serial instants of time. The results showed that during and after exercise, consistent changes appeared in the map patterns during early QRS and the ST segment and in

the magnitude of the T-wave potentials. Increases in QRS duration (0-10 msec) also appeared during exercise. They concluded that the changes in map patterns during early QRS in exercise strongly suggested changes in the initial sequence of activation in the ventricles, and that more information was obtained from body surface mapping than clinical ECG. Yanowitz (Yanowitz et al., 1982) recorded body surface maps during exercise in patients with coronary artery disease, torso potential distributions at 192 locations were derived from a 32 lead electrode array. Body surface potential mapping was constructed at ST₈₀ (80ms after the end of the QRS complex —J point), and the most negative ST₈₀ site on the map was called the “ST₈₀ minimum”. They found that the ST₈₀ minima were located 1 or 2 electrode rows away from the standard V₄~V₆ electrode positions in patients who developed ST₈₀ areas of -8mV.ms or greater. The results suggested that standard electrocardiographic leads may not be optimal for identifying ST depression in all patients with coronary disease. Furthermore, body surface mapping during exercise provides a more quantitative and qualitative method for characterizing the ischaemic response to exercise. In Kornreich’s (Kornreich et al., 1993) study of body surface mapping to monitor the effect of thrombolytic therapy in acute myocardial infarction, they compared 120-lead body surface potential mapping data in acute myocardial infarction patients and normal control subjects. The results showed that from the six leads selected for optimal classification of the acute myocardial infarction patients, five are outside the area sampled by the conventional precordial electrodes. It was also found that quantitative analysis of ST magnitude at each electrode site allows determination of best thresholds for ECG criteria. To compare the diagnostic ability of the 12-lead ECG with body surface mapping for early detection of acute myocardial infarction in patients presenting with ST depression in the 12-lead ECG, 54 patients with chest pain and ST depression in ECG were studied (Menown et al., 2001). Acute myocardial infarction occurred in 24/54 patients. Univariate prediction of acute myocardial infarction by the 12-lead ECG, based on the depth or numbers of leads with ST depression, was not improved by assessment of ST elevation outside the conventional 12 leads using body surface mapping. Thus, using body surface mapping may improve the early diagnosis of acute myocardial infarction in patients presenting with chest pain and ST depression only on the 12-lead ECG.

By sampling the ECG over the whole thorax, body surface mapping can be used for spatial analysis of ECG to detect myocardial ischaemia. In Montague’s (Montague et al., 1988) study of body surface potential mapping in patients with isolated LAD coronary artery stenosis during exercise test, they found that ST integral decrease was

higher in LAD patients than that in normal subjects. The author concluded that ischaemic repolarization changes were detectable and quantifiable by body surface mapping.

Researchers also found that body surface mapping can locate myocardial ischaemia. Using isointegral analysis of body surface mapping, Tonooka (Tonooka et al., 1983) estimated the location and size of myocardial infarction in 35 myocardial infarction patients and observed that QRS isointegral mapping is useful and convenient for detecting the location and size of myocardial infarction. A similar result has also been observed by Toyama (Toyama et al., 1984). They used thallium-201 scintigram as a standard method to detect myocardial infarction and found that body surface isopotential mapping is more sensitive than the 12 lead ECG in detecting the location of myocardial infarction. Osugi (1984) compared body surface isopotential maps with 12 lead ECG results in 43 old myocardial infarction patients, and found that body surface maps contained diagnostic information concerning the presence or absence of inferior myocardial infarction which can not be diagnosed by 12 lead ECG. Montague (Montague et al., 1990) recorded body surface ST integral maps in 36 coronary artery disease patients and observed that patients with two and three vessel coronary artery disease had significantly greater decrease in the body surface sum of ST integral values than patients with single vessel coronary artery disease. Thus exercise ST integral body surface mapping allows quantitation of myocardium at ischaemic risk in patients with coronary artery disease, though considerable overlap of ST integral values exist among individuals. Hauninen (Hauninen et al., 2001b) also used body surface potential mapping to detect exercise-induced myocardial ischaemia in coronary artery stenosis patients. The results showed that the optimal location for ST depression was on the left upper anterior thorax for the LAD, left lower anterior thorax for the RCA, and on the lower back for the LCX subgroup. Mean ST amplitudes in coronary artery stenosis patients were lower than that in normal subjects. It concluded that body surface potential recording was sensitive for detecting transient myocardial ischaemia.

Conversely, Thompson and Katavatis (1976) found precordial ST mapping has no use in assessing myocardial infarction size and location. In their study of 78 patients with anterior myocardial infarction or ischaemia, the extent and amplitude of ST elevation was measured on the chest wall with precordial mapping. They found poor relation between the extent and amplitude of ST elevation obtained by precordial mapping and the extent of necrosis measured by the peak levels of creatine kinase (CK). They

found that the only use of precordial ST mapping is to estimate prognosis of early mobilization. They suggested that the standard 12 lead ECG provides sufficient information for clinical evaluation of ST elevation.

Until recently, body surface potential mapping has not been widely used in the clinic as a diagnostic tool. The performance of a body surface map required the individual placement of multiple electrodes sometimes up to 128~256 which will take a much longer time than 12 lead ECG. There is also a large expenditure of recording equipment and analysis software. Moreover, there is no standardization for mapping analysis. However, recent work has shown that only limited electrodes is needed and there are now systems available with which body surface mapping can be performed faster than a routine 12 lead ECG for no greater cost (Walker et al., 1983). Although the initial equipment is moderately expensive, it is quick to use and uses no consumable items.

2.5.3.2 Application of epicardial, endocardial and intramyocardial mappings

There is a great theoretical advantage in looking at epicardial and endocardial potentials; the heart is the source of the electrocardiographic changes and these changes can be directly related to cardiac anatomy. Both epicardial and endocardial mappings have been proven to be a valuable technique in clinical practice as well as in basic research.

The technique of epicardial mapping was first reported in a dog by Rothberger and Winterberg (1913) and by Lewis and Rothschild (1915). After that, Barker (Barker et al., 1930) described the excitatory processes recorded in the exposed heart of a patient with draining purulent pericarditis. Epicardial mapping was first used clinically to localize accessory pathways associated with the Wolff-Parkinson-White syndrome (Burchell et al., 1967). Later on, research on transmural activation in human hearts were reported by Durrer (Durrer et al., 1970) in adults and by Brusca and Rossetani (1973) in the fetus. Epicardial mapping was also used in other applications, including the use of mapping to study atrial activation (Wellens et al., 1971), to delineate the course of the atrioventricular conduction system (Wyndham et al., 1980) and to identify areas of ischaemia and infarction (Daniel et al., 1971). Similar techniques have been used to direct the surgical treatment of ventricular tachyarrhythmia (Gallagher and Cox, 1979). In Li's (Li et al., 1999) study of the origin of epicardial ST depression of acute myocardial infarction in sheep, epicardial ST mapping was

constructed by a 64-electrode sock recording. In the animal study, they found that sheep with small infarcts showed uniform ST elevation over the infarction whereas sheep with larger infarcts showed marked ST depression over the normal myocardium in addition to the ST elevation. The experimental findings were replicated by bidomain models of the heart to explain the results.

Epicardial mapping can be constructed by both direct epicardial potential recordings and calculating from body surface potential mapping. A lot of studies have been done by inverse calculating epicardial mapping from body surface measurements. Barr and Spach (1978) compared directly measured epicardial maps with epicardial maps computed from body surface measurements in an intact dog during cardiac depolarisation and repolarization. They observed that the two correlate well with each other although significant differences occurred occasionally. Oster (Oster et al., 1997) observed that non-invasive electrocardiographic imaging can reconstruct epicardial potential and isochrone mapping over the entire epicardial surface during the cardiac cycle and provide detailed information on local activation of the heart noninvasively. Similar result were found by Tanaka (Tanaka et al., 1982) using the orthogonal expansion method and Yajima (Yajima et al., 1982) who found that the correlation coefficients between the measured and the computed epicardial potentials were from 0.3 to 0.7.

Toyama (Toyama et al., 1987) found in humans that an epicardial map calculated from body surface mapping is adequate to predict the size and the location of the infarcted areas in anterior infarction. In their study, the accuracy of the prediction by the epicardial mapping was assessed by comparing it with findings from thallium-201 scintigraphy (SCG), electrocardiography and vectorcardiography (VCG). It was shown that in anterior infarction patients, the location of the abnormal depolarized areas determined on the epicardial mapping, as localized at the anterior wall along the anterior intraventricular septum, agreed with the location of the abnormal findings obtained by SCG, electrocardiography and VCG. For inferoposterior infarction patients, the abnormal depolarized areas were localized at the posterior wall and the location also coincided with that of the abnormal findings obtained by SCG, electrocardiography and VCG. They also found that the size of the abnormal depolarized areas could be predicted by the epicardial mapping for both anterior and inferoposterior infarction patients. In anterior infarction patients, the size of the abnormal depolarized area by the epicardial mapping was correlated to the size of the abnormal findings by SCG, as well as to the results from Selvester's QRS scoring

system in electrocardiography and to the angle of the maximum QRS vector in the horizontal plane in VCG.

Endocardial mapping has been used in myocardial ischaemia and cardiac arrhythmia studies. With different kinds of endocardial mapping equipment, endocardial electrical activity has been successfully recorded.

In studies of ventricular arrhythmias, animal experiments as well as clinical observations, indicate that the origin of ventricular arrhythmia is often endocardial. Mapping is carried out endocardially rather than epicardially (Spielman et al., 1978). A technique was developed by De Bakker (De Bakker et al., 1983) for the simultaneous recording of 30 endocardial electrograms during cardiac surgery in patients undergoing aneurysmectomy or endocardial resection, endocardial potential was recorded and isochrone contour maps were constructed. The results showed that isochrone contour maps could depict activation sequences during constructive ectopic beats with the same QRS morphologic features. An olive-shaped probe, which was introduced to the left ventricle via the left atria, was used by Taccardi (Taccardi et al., 1987) to record intracavity potential. Isopotential and isochrone contour maps were constructed from records of this probe, on which electrodes were regularly distributed; these maps provide information on the point of origin of ectopic paced beats in a normal dog heart. Multipolar endocardial potential recordings were obtained by Smith (Smith et al., 1994) from electrode arranged on a basket catheter in the left ventricle of swine subjected to anterior myocardial infarction. They suggested that endocardial potential recording permit easier localization of endocardial sites suitable for catheter ablation of ventricular tachycardia. Using a multielectrode basket catheter, Zrenner (Zrenner et al., 1999) recorded the activation pattern in patients with atrial arrhythmia. It revealed that multiple electrograms recorded with the basket catheter were valuable to delineate the three-dimensional activation patterns of various atrial arrhythmias.

Using a homemade basket with 40-electrode, Li (Li et al., 1998) constructed endocardial maps in sheep with subendocardial ischaemia produced by partial occlusion of the LAD or LCX with atrial pacing, their results showed that ST elevation occurred in areas of corresponding partially occluded artery.

To study the sequence of ventricular activation and repolarization, it is necessary to know the intramural electrical activity. Spach and Barr (1975) measured ventricular

intramural and epicardial potential distribution during normal excitation and repolarization in intact dogs; intramural potentials were recorded by intramural plunge needles, each with 15 insulated tungsten wires. Unipolar wave forms were recorded from intramural and epicardial electrodes and converted into potential distributions. Well-known shapes of waveforms recorded at the inner and outer layers of the ventricles as well as peak-to-peak voltages were shown by the potential distributions to be determined primarily by superposition effects of distant excitation waves. It was found that these effects were most prominent before epicardial breakthrough and then receded during the last half of the QRS complex. However, the potential distributions became more complex as excitation waves merged, collided, and terminated. During terminal depolarisation, there were scattered positive repolarization potentials intramurally. Normal repolarization was characterized by positive potentials over the ventricular epicardium while there were changes intramurally and on the atrium. Throughout the T wave, there was a predominant transmural unidirectional gradient with the inner wall being more negative than the outer wall. This finding confirms that the sequence of repolarization is from the epicardium to the endocardium with the middle layers having an intermediate time. A similar study has been done by Van Oosterom and Van Dam (1976) in the dog.

Intramural electrodes were also used in the study of ventricular arrhythmia during acute myocardial ischaemia. In Wu's study of ventricular arrhythmia (Wu et al., 1995), the intramural electrodes were constructed with tungsten wire through 22-gauge needles; each needle had 8 electrodes in it. With the three-dimensional activation maps derived from 240 bipolar sites by 60 plunge needle electrodes, they observed that spontaneously occurring premature ventricular complexes and ventricular tachycardia during acute myocardial ischaemia in dogs display focal excitation with no evidence of macroreentry.

With similar intramural plunge electrodes, the mechanism of ventricular tachycardia in canine and cat myocardial infarction was also studied previously by Pogwizd and Corr (1987) respectively. They found that five minutes after the occlusion of the LAD, activation was delayed during sinus rhythm and was characterized by slow conduction in the endocardial-to-epicardial direction. While the initiation of premature ventricular contractions and ventricular tachycardia resulted from intramural reentry which occurred in the subendocardium, adjacent to the site of delayed subendocardial and midmyocardial activation of the preceding sinus beat. Mechanisms of ventricular arrhythmias in long QT syndrome in puppies were studied

by El-Sherif (1996) using intramural tungsten plunge needles. Analysis of three dimensional activation and repolarization patterns showed that the polymorphic QRS configuration of ventricular tachycardia in the long QT syndrome was due to either changing the site of origin of focal activity, resulting in varying activation patterns, or varying orientations of circulating wave fronts.

There is little research considering using intramural potential mapping to study intramural ST distribution in myocardial ischaemia. Since ST depression occurs on the boundary of ischaemia in subendocardial ischaemia (Li et al., 1998), it is necessary to study the electrical activity on the boundary, which can only be obtained by intramural potential recording.

CHAPTER THREE MATERIALS AND METHODS

3.1 EXPERIMENTAL ANIMALS

A total of 24 (Polworth/Comeback cross) sheep weighing between 26~36kg of both genders were used. All the sheep were bred in the University of Tasmania's animal farm. Table 3.1 shows the groups of animals subjected to different experimental protocols.

Table 3.1 Experimental protocol

animal	
group	number experimental protocol
1	transmural ST segment potential distribution in subendocardial ischaemia.
2	transmural ST segment potential distribution in transition of mild subendocardial ischaemia to severe subendocardial ischaemia.
3	transmural ST segment potential distribution in acute myocardial infarction.

Group 1: Subendocardial ischaemia group. In this group, animals were divided into four subgroups.

Subgroup 1: Cardiac pacing without coronary artery stenosis.

Subgroup 2: Subendocardial ischaemia in LCX area.

Subgroup 3: Subendocardial ischaemia in LAD area.

Subgroup 4: Alternating subendocardial ischaemia in LCX and LAD areas.

Group 2: Transition of mild subendocardial ischaemia to severe subendocardial ischaemia group. This group was divided into two subgroups.

Subgroup 1: Transition of mild subendocardial ischaemia to severe subendocardial ischaemia in LCX area.

Subgroup 2: Transition of mild subendocardial ischaemia to severe subendocardial ischaemia in LAD area.

Group 3: Acute myocardial infarction group. Acute myocardial infarction was

induced by ligating the following coronary artery.

Subgroup 1: Ligation of LCX.

Subgroup 2: Ligation of LAD.

3.2 ANIMAL PREPARATION AND SURGICAL PROCEDURES

Experiments were performed in an open-chest sheep preparation. Anaesthesia was induced intravenously with sodium pentobarbital (30mg/kg) and then maintained at 3~8mg/kg/hour throughout the experiment via a jugular vein catheter. The sheep were artificially ventilated with respirator (Engstrom, Erica, Sweden) at a rate of 12~14 breaths/min via a cuffed tracheal tube with room air. O₂ was added according to blood gas measurements. Tidal volume and respiratory rate were constant during each experiment. The sheep were heparinized prior to instrumentation. A left thoracotomy was performed in the fourth and fifth intercostal space, and the hearts were suspended in a pericardial cradle.

The carotid arterial pressure (CAP) was measured via a 7F catheter introduced to the left carotid artery. The left ventricular systolic and diastolic pressure (LVSP, LVDP) were measured by another 7F catheter introduced through a side hole into the left ventricular cavity through the left carotid artery. The left atrial pressure (LAP) was measured via a PE 90 cannula implanted in the left atrium through the left atrial appendage, this PE 90 cannula was also used for fluorescent microsphere injection. Two pacing wires were sutured to the left atrial appendage for left atrial pacing.

The LCX and LAD were isolated proximally for the Doppler probe (TRITON TECHNOLOGY, INC, SANDIEGO, CA) to measure coronary blood flow, and 10~20mm distal to the probe, LCX and LAD were isolated for the hydraulic occluder (IN VIVO METRIC, Healdsburg, CA) to induce coronary artery stenosis or for coronary artery ligation.

3.3 DRUGS AND CHEMICALS

Drugs and chemicals used in this study are listed below (Table 3.2).

Table 3.2 Drugs and chemicals used in this study

Name	Supplier	Usage
Pentobarbitone sodium	Boehringer Ingelheim	Induce and maintenance of anaesthesia
0.9% physiological Saline	Royal Hobart Hospital Pharmacy	(1) Compensate for body fluid loss during experiments (through jugular vein); (2) Flush catheters to prevent blood clot; (3) Make up drug or chemical solutions; (4) Soak flowmeter probes for calibration;
Heparin	Royal Hobart Hospital Pharmacy	Avoid blood clot formation (administer into jugular vein and coronary artery)
Adrenaline hydrochloride	Royal Hobart Hospital Pharmacy	Drip into jugular vein to maintain blood pressure when necessary
Fluorescent Microspheres	Molecular Probes, Inc	Measure regional myocardial blood flow
Ethyl Acetate	Sigma	Extract fluorescent dye
Potassium hydroxide	Sigma	Digest myocardial tissue
Methylene Blue	Sigma	Delineate ischaemia area
Tween 80	Sigma	Disperse microspheres

3.4 EXPERIMENTAL INSTRUMENTS

Experimental instruments used in the study are listed in Table 3.3.

Table 3.3 Experimental instruments used in this study

Instruments	Location	Usage
F7 fluid filled catheter	carotid artery and LV	pressure measurement
PE 90 cannula	left atrium	pressure measurement/ microsphere injection
2 8/3 2/3.7mm Doppler Flow probes	LCX/LAD	coronary flow measurement
Hydraulic occluder	LCX/LAD/OM	induce coronary artery stenosis
Pacing wires	left atrial appendage	cardiac pacing
Epicardial sock electrodes	ventricular surface	epicardial potential recording
Endocardial basket electrodes	LV cavity	endocardial potential recording
Intramyocardial plunge needles	intramyocardium	transmural potential recording
Spectrophotofluorometer		RMBF measurement

3.5 REGIONAL MYOCARDIAL BLOOD FLOW MEASUREMENT

Regional myocardial blood flow (RMBF) was measured by fluorescent microspheres. The fluorescence microspheres were bought as a kit containing seven vials of different fluorescent dyes from Molecular Probes, Inc., USA. Table 3.4 lists the seven colours with their excitation and emission wavelengths in Ceilosolve acetate (Glenny et al. 1993) and in ethyl acetate (author's measurement).

Table 3.4 Excitation and Emission maximum wavelengths of fluorescete microsphere in Ceilosolve acetate and in ethyl acetate for blood flow determination.

Colour	Excitation wavelength (nm)		Emission wavelength (nm)	
	Ceilosolve acetate	ethyl acetate	Ceilosolve acetate	ethyl acetate
blue	360	360	420	430
blue-green	430	420	457	470
yellow-green	490	490	520	505
orange	530	530	552	550
red	565	565	598	590
crimson	600	600	635	630
scarlet	651	650	680	680

To accurately measure blood flow using fluorescent microspheres, an imperative is an even distribution of microspheres in the myocadium. Two sheep were used to detect whether different fluorescent dyes had stable and even distribution throughout the myocardium. Two fluorescent microspheres were randomly chosen and injected through the left atrium of each sheep. Fig. 3.1 showed that blood flow (BF) measured by blue-green fluorescent microspheres had a significant correlation with blood flow measured by yellow-green fluorescent microspheres. Blood flow measured by orange fluorescent microspheres had a significant correlation with blood flow measured by

crimson fluorescent microspheres. The results indicated that the fluorescent microspheres were evenly distributed throughout the myocardium.

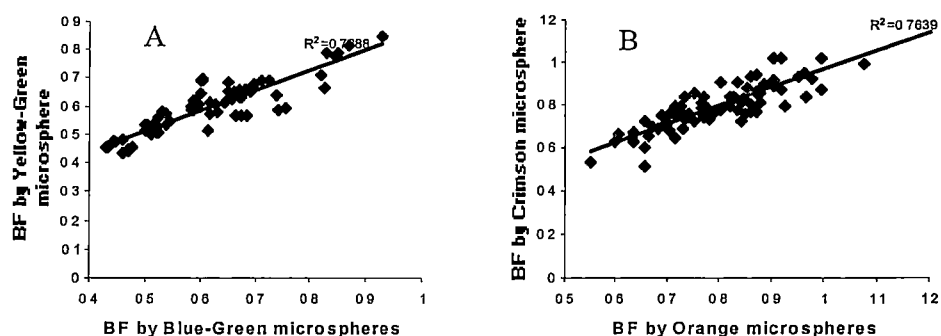


Fig. 3.1 Correlation of distribution of different fluorescent dyes. A: Relationship between blood flow (BF) measured by blue-green fluorescent microspheres and blood flow measured by yellow-green fluorescent microspheres (data from 90 samples in different myocardial layers). B: Relationship between blood flow measured by orange fluorescent microspheres and blood flow measured by crimson fluorescent microspheres (data from 81 samples in different myocardial layers).

3.5.1 PREPARATION OF FLUORESCENT MICROSPHERES

The microspheres were uniform polystyrene microspheres with nominal diameter of $10\mu\text{m}$ and were supplied as suspensions in 10ml of 0.15% NaCl with 0.05% Tween® 20 and 0.02% thimerosal. The suspensions (0.2% solids) contain 3.6×10^6 microspheres per milliliter of solution. Each microsphere reagent contains a single fluorescent dye whose fluorescence is well resolved from all of the others (Fig. 3.2 & Table 3.4).

Due to the weak red signal in the spectrophotofluorometer used in this study, 2~4 times more Orange, Crimson and Scarlet microspheres were used in the experiments. On average, approximately 2500 microspheres for Blue-Green and Yellow-Green, and 5000 microspheres for Orange, Crimson and Scarlet dyes per myocardium sample were used.

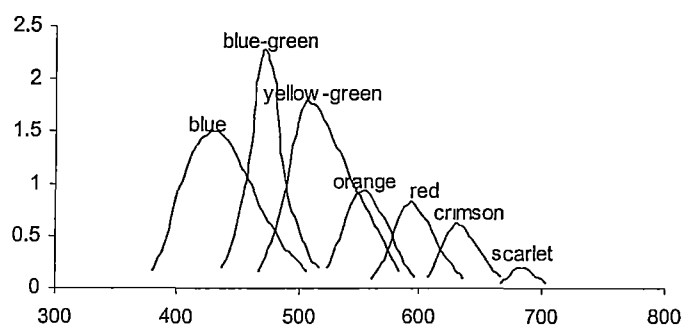


Fig. 3.2 Fluorescence emission spectra of the dyes contained in the polystyrene microsphere components, after extraction into ethyl acetate. The seven types of microspheres represented are: Blue, Blue-Green, Yellow-Green, Orange, Red, Crimson and Scarlet.

The fluorescent dyes were randomly chosen for different experiments. As specified by the spectrophotofluorometer, the following colours of microspheres and optimum excitation/emission wavelengths were used: Blue-Green (420/470nm), Yellow-Green (490/505nm), Orange (530/550nm), Crimson (600/630nm), and Scarlet (650/680nm).

3.5.2 INJECTION OF FLUORESCENT MICROSPHERES

Each color of microspheres was ultrasonically agitated for 5 minutes, followed by a vigorous vortex for 10 minutes, prior to injection. Microsphere suspensions were mixed with 10ml of warm blood and the whole mixture was injected into the left atrium via the implanted cannula over a period of about 10 seconds. The cannula was then flushed with 10ml of saline.

3.5.3 DIGESTION OF TISSUE SAMPLE AND DISSOLVING OF MICROSPHERES

At the end of the experiment, 10ml of 0.1% Methylene blue dye (Sigma) was injected into the culprit coronary artery to delineate the ischaemic from the non-ischaemic area. Each sheep was killed by stopping ventilation and sodium pentobarbital overdose. The heart was carefully taken out of the chest and rinsed with 0.9% saline to remove superficial blood. The left ventricle was isolated, and the epicardial fat and blood vessels were trimmed off. The heart was then stored in a freezer at -10°C to facilitate section. The left ventricle was cut into 4~6 circumferential rings from base to apex. The apex of the left ventricle was ligated to secure the cavity basket, causing blood supply to this area to be disturbed, thus it was trimmed off and blood flow was

not measured in this part (*vide infra*). The circumferential rings were then cut into sections of about 3g each. Each section was then cut into 3 layers, which corresponded to the epicardial, the middle myocardial and the endocardial layers. The anatomic location of each myocardial piece was recorded. The weight of each piece was 0.6~1.2g. Each myocardial piece was placed into a screw-capped polystyrene tube in which 2ml of 4M KOH was added. The polystyrene tubes were then placed in a 37 °C water bath for 12 hours. After the tissue had been digested, 3ml of ethyl acetate was added to dissolve the microspheres, then the tube was vortexed for three minutes to extract the fluorescent dye ethyl acetate. The mixture was allowed to settle for at least 30 minutes. The upper ethyl acetate layer was transferred to a quartz cuvette where fluorescent intensity was determined.

3.5.4 MEASUREMENT OF FLUORESCENT INTENSITY

The tissue fluorescent intensity was measured by Amino-Bowman spectrophotofluorometer. Each fluorescent intensity was read at the appropriate excitation/emission wavelengths. The excitation/emission bandpass was set at 27.5nm/27.5nm. All the samples from the same experiment were measured on the same day. The whole procedure of microspheres injection, tissue sampling and digestion, fluorescence extraction and measurement is illustrated in Fig. 3.3.

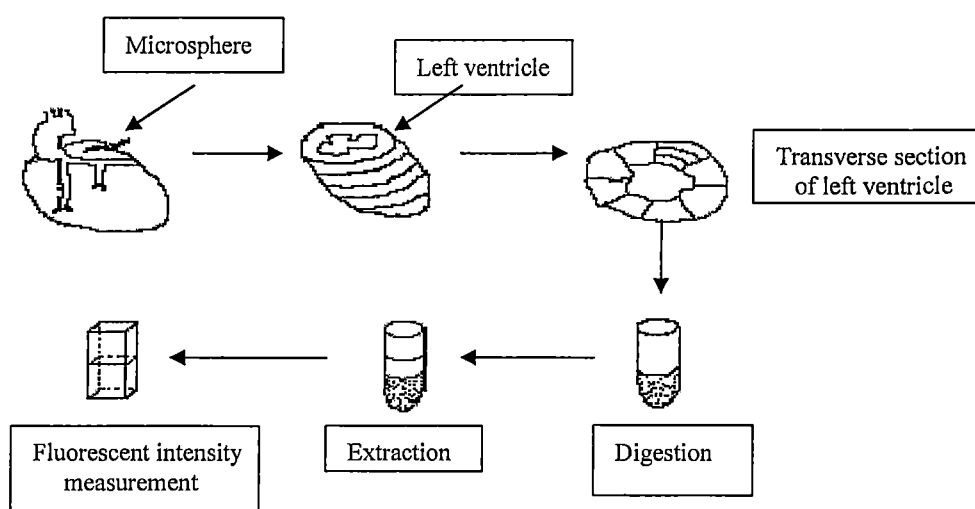


Fig. 3.3 Illustration of the procedure of microspheres injection, tissue sampling and digestion, fluorescence extraction and measurement.

3.5.5 ANALYSIS AND CALCULATION OF THE RESULTS

Reference blood flow rate was used to calculate the flow rate per myocardial tissue sample. Blood flow of LCX and LAD measured by the Doppler flowmeters was used as reference blood flow. The flow rate (ml/min) is calculated as follows:

$$F_i = I_i * F_{ca} / I_{ca}$$

Where: F_i = flow rate of per gram tissue sample (ml/min/g)
 I_i = fluorescence intensity of per gram tissue sample (units/g)
 F_{ca} = flow rate of LCX or LAD area (ml/min)
 I_{ca} = fluorescence intensity of LCX or LAD area (units)

3.5.6 EVALUATION OF FLUORESCENCE OF MICROSPHERES AND INTRINSIC FLUORESCENCE OF MYOCARDIUM AND SOLVENTS

50 μ l of each fluorescent microsphere dye was obtained from each vial of the kit, yielding a 0.35ml solution containing 7 different fluorescent dyes. This was diluted with 9.65ml of 0.9% NaCl. A new solution with 18,000 microspheres per milliliter was obtained. A serial dilution of 9 different fluorescent dye concentrations was made from this new solution. Each dilution was divided into two equal halves and one gram of myocardial tissue was added to each of them.

Two nine-serial dilutions were thus produced, with one containing pure fluorescent dyes and the other a mixture of fluorescent dyes and myocardial tissue. 2ml of 4M KOH and 3ml of ethyl acetate were added to each of the dilutions. After being vortexed for three minutes, the microsphere dyes were extracted by ethyl acetate. The ethyl acetate which contained microsphere fluorescent dyes was transferred to a quartz cuvette where fluorescent intensity was read. The fluorescent intensity of each dilution was measured by the Aminco-Bowman spectrophotofluorometer.

The results were similar to Abel's (Abel et al. 1993). In the serial dilutions without myocardial tissue, the fluorescent intensity showed a linear relationship with microsphere number of all the 7 fluorescent dyes. In the serial dilutions with myocardial tissue, the fluorescent intensity had a linear relationship with the microsphere number of all the fluorescent dyes except blue and red dyes.

Consequently the blue and red fluorescent microspheres were excluded from the subsequent experiments (Fig. 3.4).

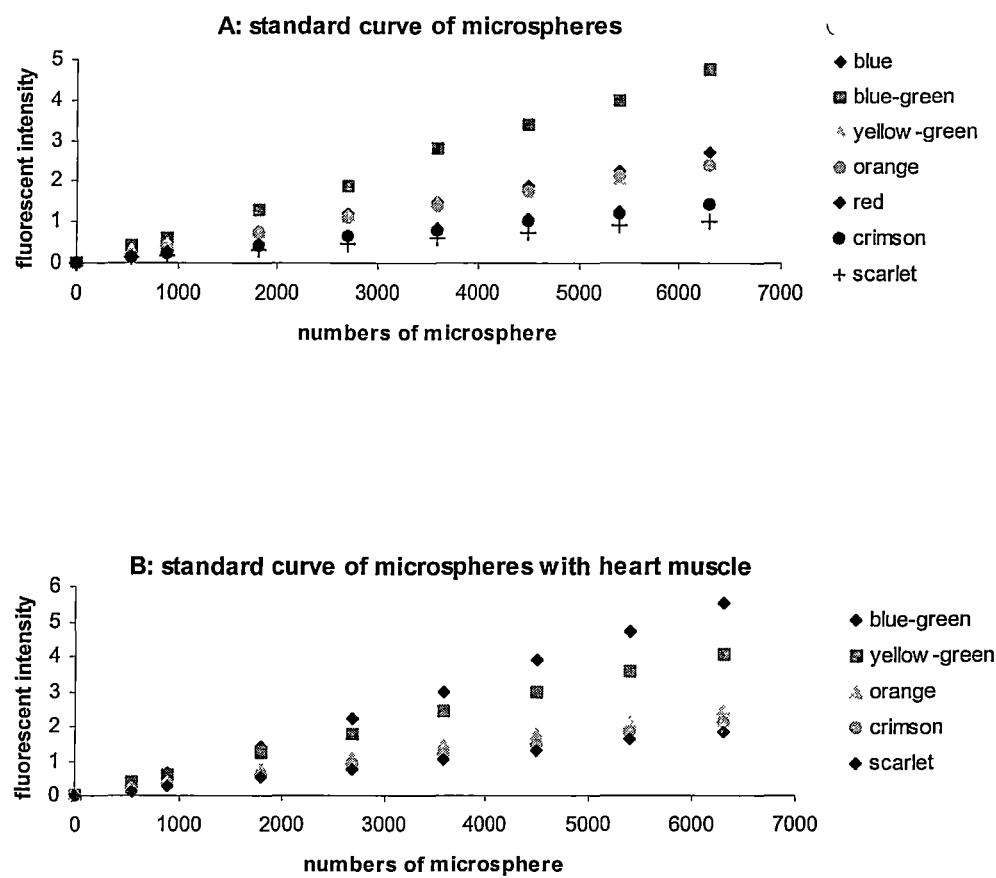


Fig. 3.4 Fluorescence of microspheres, myocardium and solvents. A: Samples were made by 7 mixed dyes. B: Samples were made by 7 mixed dyes and one gram of myocardial tissue.

3.6 POTENTIAL RECORDING AND MAP CONSTRUCTION

3.6.1 POTENTIAL RECORDING

3.6.1.1 Epicardial sock

The epicardial potentials were recorded using an epicardial sock containing 64 electrodes (Cardiovascular Research and Training Institute, the University of Utah, USA). Each electrode is a construction of fine silver wire mounted in a nylon sock. The arrangement of the 64 electrodes provides coverage of the epicardial surface of the left and right ventricles (Fig. 3.5).

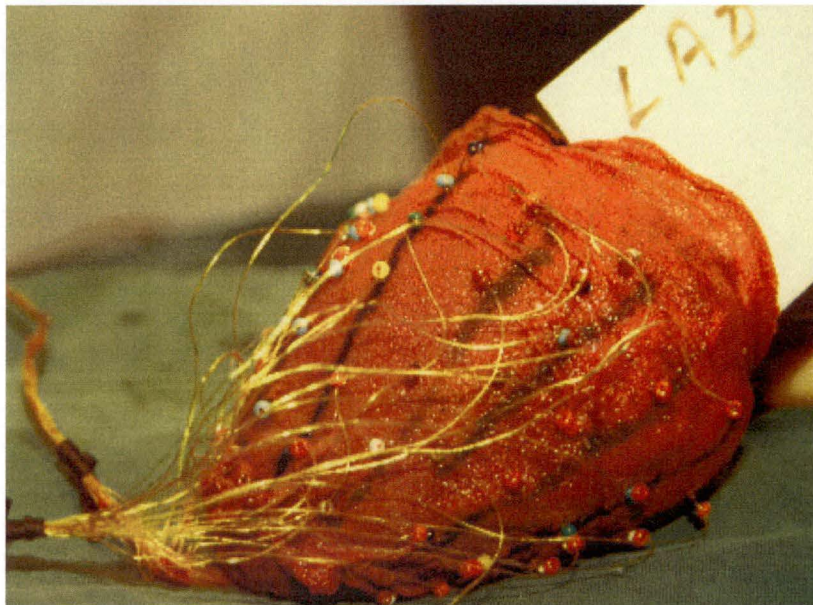


Fig. 3.5 Image of the sock

3.6.1.2 Endocardial basket

The endocardial potentials were recorded using a home-made 40-electrode basket mapping apparatus (Fig. 3.6). The apparatus was oval-shaped and constructed with spring steel wire as the skeleton, and polyethylene tube as the outer covering, on which 40 silver electrodes were mounted. The steel skeleton consisted of 8 arms. Each arm was insulated with a polyethylene tube and mounted with 5 unipolar silver electrodes. To avoid electrical injury current, the electrodes were mounted in such a manner that they were not in direct contact with the endocardium. The 8 arms were equally spaced. This was ensured by using a fine nylon string to tie the middle of each arm sequentially with equal length. And the 8 arms also connected to each other at both ends. Thus, when the apparatus was expanded, a uniform distribution of electrodes resulted. The arms were marked for orientation. The apparatus was 52mm long and 32mm in maximal diameter when fully opened (Fig. 3.6).

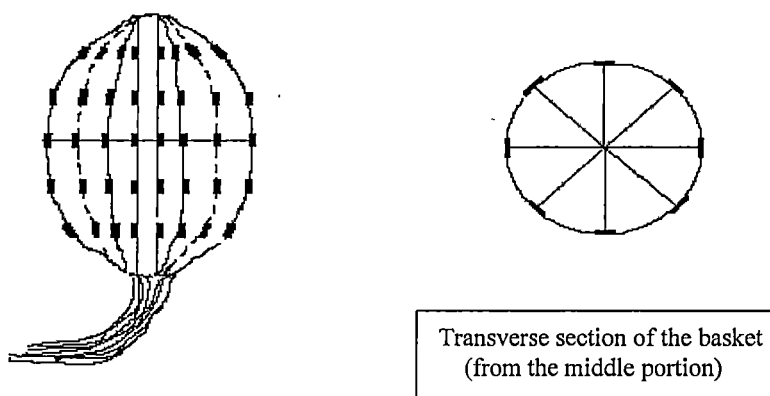


Fig. 3.6 Structure of the basket (black spots are electrodes sites, the middle line is where the string being tied for equal expansion of the basket)

Placement of the apparatus was accomplished by using a thin wall tube (insertor) with an outer diameter of 8mm through the myocardial apex. The closed apparatus was placed inside the insertor; a left apical ventriculotomy of approximately 10mm, simulating the clinical approach, was performed. The insertor was introduced into the

apex, and the apparatus placed into the left ventricle while withdrawing the inserter. The apparatus was secured by a purse string suture around the point of insertion, i.e., the apex of the left ventricle. All this was done as quickly as possible to avoid interfering with the physical activity of the heart. Once inside the left ventricle, the apparatus deploys, with 8 arms placed into position, each maintaining constant contact with the endocardium. The electrodes were not in direct contact with the endocardium, however, they detected the potential changes from the nearest section of the endocardium.

From the postmortem examination, the distance between the electrodes and the endocardium ranged from 1.3~1.5mm. The apparatus enabled recording signals from a working heart, and to allow mapping the whole endocardial surface potentials simultaneously.

Brief hemodynamic measurements during experiments suggested that the insertion of the apparatus into the left ventricle did not cause significant hemodynamic deterioration. The apparatus did not provoke electrical injury currents. All the electrodes remained in their positions throughout the experiments. The quality of all signals remained satisfactory.

3.6.1.3 Intramyocardial needles

Development of intramyocardial plunge needles

Intramyocardial potential recordings require intramyocardial electrodes that do not cause significant injury current. To construct suitable intramyocardial electrodes, techniques such as insulation of the intramyocardial plunge needles, decreasing the size of the intramyocardial plunge needles and use of different materials for the intramyocardial plunge needles were tried.

Stainless steel plunge needles used in this laboratory were found to incur strong injury currents (Li, 1997). These plunge needles were used again in the present study with some modification to avoid the occurrence of injury current. These plunge needles have four quadripolar electrodes on it, with a diameter of 0.9mm and a length of 17mm. A technique was used to restrict the contact of these needles with the cardiac muscle. An insulation material was used to coat these needles, leaving only the electrodes exposed. The results still showed strong injury current which lasted several hours.

In an attempt to improve results, fine-gauge needles (26-gauge) were used. To determine whether insulation affected the results, some needles were insulated, while others were left without insulation. Disappointingly, even these tiny needles, with or without insulation, produced strong injury current.

Given these results, it seemed that the needle material might have an important role in the occurrence of the injury current. Intramyocardial tungsten wires were successfully used to study cardiac electrophysiology (Spach and Barr, 1975; Van Oosterom and van Dam, 1976). Intramyocardial electrodes constructed with tungsten wire introduced through 22-gauge needles were also used in the study of ventricular arrhythmia during acute myocardial infarction (Pogwizd and Corr, 1987; Wu et al., 1995; El-Sherif, 1996). Further experiments were carried out on intramyocardial plunge needles made of different materials such as tungsten, nickel, silver, copper and stainless steel. The results showed that needles made of tungsten, nickel and silver incurred minor injury current. The silver needles gave the best results. Although the injury current did occur immediately following the insertion of the needles, almost all would disappear within 30min, while others took 45~60min. Silver wire was thus chosen to make the intramyocardial plunge needles.

Structure of the silver intramyocardial needles

Transmural potentials were recorded by intramyocardial plunge needles. Each needle consisted of 3 strings of insulated silver wires, the tip of each wire was exposed at a length of 1.0mm for potential recording, the adjacent wire tips were 3.0mm apart. Then the 3-strand wire was inserted into a polyethylene tube (with an outside diameter of 0.8mm). 3 side holes to accommodate the silver wire tips were punctured along the wall of the polyethylene tubing to complete the making of an intramyocardial needle. Finally, the tip of the polyethylene tube was stretched sharp so as to facilitate needle insertion. The base of the needle was bent to a 90-degree angle, giving the needle with a length of 12mm.

The construction of the needle ensured that whenever the needle was inserted into the myocardium, the subepicardial electrodes were 1.5mm, the mid-myocardial electrodes were 4.5mm, and the endocardial electrodes were 7.5mm beneath the epicardium respectively (Fig. 3.7, Fig. 3.8).

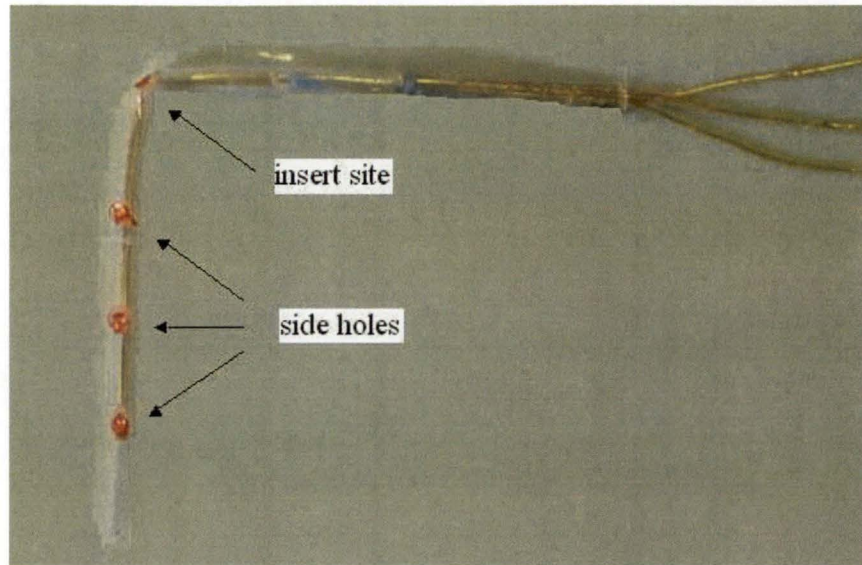


Fig. 3.7 Image of the plunge needle

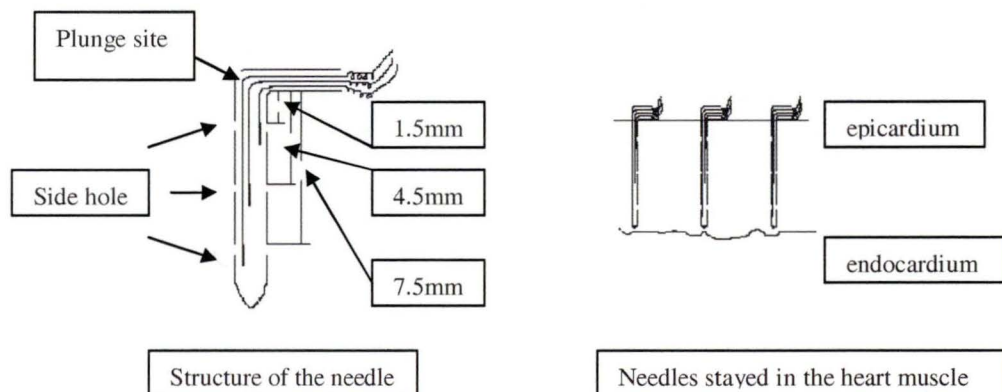


Fig. 3.8 Model structure of the plunge needle

To insert the needles into the heart, a stainless steel wire was inserted through the plunge site at the base of the needle, until it protruded about 3mm from the tip of the needle. This protruded wire punctured the heart muscle with ease, guiding the needles into the heart muscle. Once the whole length of the needle was inserted into the heart muscle, the stainless steel wire was withdrawn, leaving the needle on site. To avoid the needle coming out of the myocardium, a tiny piece of wool was placed around the base of the needles to facilitate clot formation and anchor the needles in position. The

insertion of the needles did not cause haemodynamics deterioration, but did cause brief electrical injury current. After a period of stabilization (1.0~1.5 hours), the electrical injury current would significantly decrease, and the recorded ST potential was fairly close to the isoelectrical line. Any ongoing experiments were carried out at least 1.5 hours after the needle insertion. Altogether 29 needles were used in this study. The needles were inserted randomly into the myocardium, with a greater density of the needle array at the border of myocardium supplied by LAD and LCX. The location of the needles was marked at the end of each experiment.

3.6.1.4 Potential recording system

The epicardial, intramyocardial and endocardial electrodes were connected to a 256-channel system (BDDD-Binary Data Delivery Device). 191 out of 256 channels were used in this study. The signal from each electrode was passed through a differential amplifier with a gain of 1000. The system was controlled by a Field Programmable Gate Array (FPGA) chip. The configuration data were stored in a PROM (XC1765) which delivered the data to the FPGA. A sample and hold on the output of each amplifier allowed the signal of all electrodes to be sampled simultaneously. Potentials were sampled at 1000 samples/second/channel by the data acquisition system directly on to the computer memory (DMA) through an S11w (Engineering Design Team, Inc., 1100NW Compton, Suite 306, Beaverton, Oregon USA 97006) interface to SBus on a computer (Sun Sparc5, SUN Microsystems, Inc., 4150 Network Circle, Santa Clara, CA 95054, USA) (Fig. 3.8). An immediate display of the sampled electrocardiographic signals enabled a check on the data quality. All the potentials were recorded with the reference to the left leg. During data acquisition, the pericardial cradle was released; the opening chest wall was covered by moisturized warm saline pads without touching the myocardium, preventing the anterior wall of the left ventricle from being exposed to air. The left and right atria, the right ventricle and the posterior and lateral walls of the left ventricle were in contact with the lung, the great vessels and the back of the thoracic cavity.

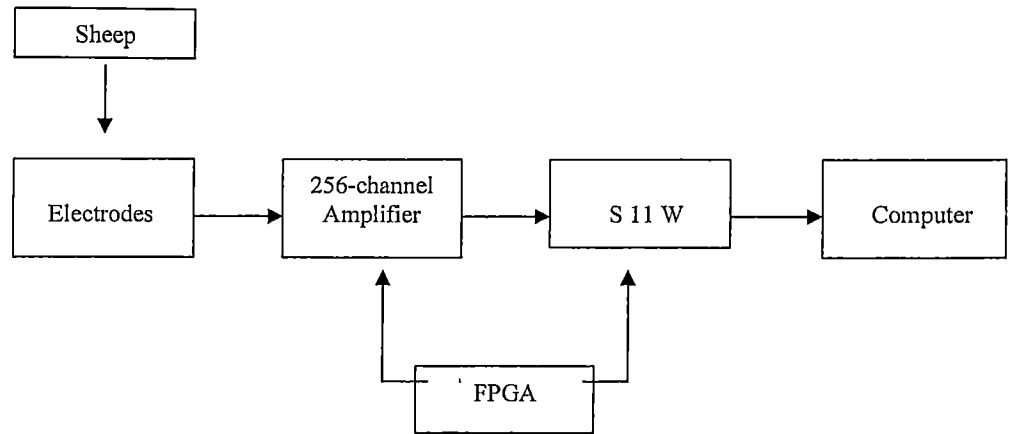


Fig. 3.8 The potential recording system

3.6.2 CONSTRUCTION OF ISOPOTENTIAL MAPS AND MAP DISPLAY

3.6.2.1 Confirmation of the electrode position and reconstruction of the heart outline

At the termination of each experiment, the sheep was sacrificed and the heart was carefully removed from the chest cavity. After both of the epicardial electrode positions and the intramyocardial needle positions were marked with numbered mapping pins, the sock and the needles were removed from the heart. By making an incision from the middle of the septum, the left ventricle was opened and the endocardial electrode positions were verified and marked. The sock electrode positions, the needle electrode positions and the basket electrode positions were linked at different myocardial sites, so the potential transition map could be constructed later. The electrode positions corresponded to the tissue samples subsequently taken for measurement of the RMBF, so that the ST segment potentials following the coronary artery occlusion could be correlated with the blood flow of each sample. From the flatly opened heart, the epicardial and endocardial vascular patterns and the outlines of the ventricle could be traced. The electrode positions, the vascular patterns and the outlines of the ventricle were then traced using transparent plastic paper and transferred to paper, where the coordinates of the whole picture were measured and reconstructed using our own mapping program and the S-plus statistical package. The pictures were then combined with the ST potential maps to give an epicardial, intramyocardial, or an endocardial potential map. The potential

maps were combined with the flow maps constructed from the simultaneously measured RMBF. In some experiments, the blood flow maps were also constructed.

3.6.2.2 Data analysis

Data from the recording system were transferred to a SUN workstation (SUN Microsystems, Inc., 4150 Network Circle, Santa Clara, CA 95054, USA), and then analyzed using the mapping program in this laboratory (Walker et al. 1983 and 1987a) and the S-plus statistical package, which are both run under UNIX. The quality of electrograms was evaluated. Missing or poor electrograms were discarded. Bad leads were picked out and replaced by interpolation from the surrounding leads. The onset of the QRS complex was chosen manually from the plots, and the potentials during a 10msec period of the PR segment were averaged for use as a zero-potential reference level. The ST segment maps were constructed from data averaged over a 40msec interval centered on a point of 80msec after the QRS onset (the QRS interval of the sheep is shorter than that in the human, about 40msec). The epicardial potential maps were constructed from the epicardial ST potentials of both ventricles. The transmural and endocardial potential maps were constructed from the transmural and the endocardial ST potentials of the left ventricle respectively. In some studies, the epicardial, the transmural and the endocardial potential maps were further combined with the flow maps constructed from the simultaneously measured RMBF. The ST segment potential distributions were displayed as isopotential contour maps or image maps.

Maps were also displayed and analyzed in the patterns as described below.

Isopotential maps: Individual maps were constructed as contour lines, connecting the points of equal voltage at the selected time instants, representative of the ST segment. The ST segment was measured over a period of 40msec, after 80msec of QRS onset, subtracted from the PR segment measured over a period of 10msec before 20msec of QRS onset. The latter was used as a zero-potential reference level. This isopotential map construction was used in experiments pacing the sheep heart without occluding the coronary arteries.

Isopotential difference maps: The difference maps were computed by subtracting the baseline potential from each ischaemic potential at each electrode site during the ST segment. This isopotential difference map construction was used in the ischaemic sheep heart model, i.e., pacing the sheep heart at a specific rate plus partial occlusion

of the coronary artery. After the ischaemic heart models were set up, the recorded ST potentials from epicardium, intramyocardium and endocardium were close to but not totally isoelectrical during the baseline recording. Using the TQ segment as a reference for each lead, the baseline ST potentials were usually less than 0.03mV. To get rid of the baseline effect on ischaemic results, the baseline potential from each electrode site during the ST segment was subtracted from the ischaemic potential, i.e.,

$$ST_{\text{potential}} = (ST_{\text{ischaemia}} - QT_{\text{ischaemia}}) - (ST_{\text{baseline}} - QT_{\text{baseline}}),$$

where $ST_{\text{potential}}$ is the calculated ST potential during ischaemia from each electrode, $ST_{\text{ischaemia}}$ is the recorded ST potential during ischaemia, $QT_{\text{ischaemia}}$ is the recorded reference potential during ischaemia, ST_{baseline} is the recorded ST potential at baseline, QT_{baseline} is the recorded reference potential at baseline.

Grouping of map patterns: To group similar ST potential distributions, a hierarchical clustering technique was used. The measure of similarity between two distributions was taken to be their correlation coefficient, which was calculated as follows (two potential distributions A and B are given):

$$\text{Correlation coefficient} = \frac{A \cdot B}{|A| \cdot |B|}$$

$$\text{where } A \cdot B = \sum a_i b_i \quad |A| = \sum a_i a_i \quad |B| = \sum b_i b_i.$$

The correlation coefficient is independent of the magnitude of the two vectors, and gives an indication of the similarities of both pattern and position of maxima and minima. In all correlations, the recorded signals were used without interpolation and the electrode arrays did not shift throughout the procedure. The resulting correlation coefficient is between -1 and 1. A correlation coefficient approaches 1 if the data sets are identically shaped, a zero correlation coefficient implies there is no association between the two data sets. This technique was used previously for analyzing body surface map data (Walker et al. 1987).

Maps were also analyzed on the basis of the magnitude of the maximum ST segment depression or the magnitude of the maximum ST segment elevation from each electrode.

3.6.2.3 Computer programs

Computer programs written on the UNIX system to process data and to display results are as follows:

- premap Extracts ST potential data from the electrogram data collected by the recording system

- get_con Combines ST potential of each channel with its corresponding electrode position, and picks out bad or missing signals

- mycontour Displays the ST potentials or blood flow values in the format of contour map or image map together with the picture of the heart

- subtract Subtracts the control ST potential from each ischaemic ST potential at each electrode site.

- flow-spatial Displays the spatial distribution of regional myocardial blood flow.

3.7 HAEMODYNAMIC MEASUREMENTS

3.7.1 LEFT VENTRICULAR, CAROTID ARTERY AND LEFT ATRIUM PRESSURE

Statham P23ID pressure transducers (Statham Laboratory Inc.) were used for left ventricular, carotid artery and left atrium pressure measurements with size 7 catheters. Each sheep was anticoagulated with heparin sodium (initial dose 10000IU, followed by 5000IU every 2~3 hours) throughout the whole experiment to ensure there was no clot during each experiment.

3.7.2 CORONARY ARTERY BLOOD FLOW

LAD and LCX blood flow were measured by Doppler flow probes (TRITON TECHNOLOGY, INC, SANDIEGO, CA). The probes were cleaned thoroughly and soaked in saline for at least 30min, and then calibrated according to the manufacturer's instructions. The calibration was also performed during the experiment and at the end of each experiment.

3.7.3 DATA RECORDING

The left ventricular pressure, the carotid artery pressure, the left atrium pressure and the coronary artery flows were recorded on a multichannel recorder (Grass Instrument Co., Quincy, Mass, 02169, USA).

3.8 STATISTICAL ANALYSIS

All data were continuous and were checked with SPSS and found to be normally distributed so parametric statistical tests were employed. The data were expressed as the mean \pm standard deviation (SD). The paired data were analyzed by two-tailed Student's paired t-test with the 0.05 level of probability considered as being significant. Simple linear regression and correlation were used to analyze the relationship between two sets of variables. Standard diagnostic checks of model fit and residuals were made.

The following statistical packages were used to analyze data.

- | | |
|---------------|--|
| Excel | was used to calculate regional blood flow and haemodynamic parameters, the mean, the standard deviation (SD) and the P value for student t-test, it was also used to compare two groups of data by linear correlation. |
| S-plus | was used to compare two groups of data by linear correlation, and to do t-tests for correlation coefficient. |
| Cricket Graph | was used to graph data and to compare two groups of data by linear regression and correlation |
| Sigma Plot | was used to graph data. |

CHAPTER FOUR

INTRAMYOCARDIAL ST SEGMENT POTENTIAL DISTRIBUTION IN SUBENDOCARDIAL ISCHAEMIA

To analyse the source of ST depression, a further series of experiments were conducted to measure potentials from intramyocardial electrodes in addition to the epicardial and endocardial electrodes. ST potential distribution maps were constructed from the recorded ST potentials. These data should allow future modeling including anisotropy to explain the source of ST changes in partial thickness ischaemia.

4.1 MATERIALS AND METHODS

4.1.1 EXPERIMENTAL ANIMALS AND PROTOCOLS

A total of 18 (Polworth/Comeback cross) sheep weighing between 26~36kg of both genders were used. All the sheep were bred in the University of Tasmania's animal farm. Table 4.1 shows the groups of animals subjected to different experimental protocols.

- Group 1: Cardiac pacing without coronary artery stenosis (n=6). In this group, the heart was paced at a rate of 120, 140, 150, 160, 180, 200, 220, 240bpm without coronary artery occlusion.
- Group 2: Subendocardial ischaemia in LAD area (n=3). LAD was partially occluded with the blood flow reduced to 50% of the original blood flow plus left atrial pacing at a rate of 180bpm.
- Group 3: Subendocardial ischaemia in LCX area (n=3). LCX was partially occluded with the blood flow reduced to 50% of the original blood flow plus left atrial pacing at a rate of 180bpm.
- Group 4: Alternating subendocardial ischaemia in LAD and LCX areas (n=6). Subendocardial ischaemia were produced both in LAD and LCX area in the same sheep. Alternative occlusion of LAD and LCX reduced the blood flow to 50% of the original level. Each partially occlusion lasted for 20 minutes, the first occlusion was followed by at least 30 minutes of rest before the next occlusion, or until the flow and pressure returned to the control level (normally after 30 minutes of rest).

Table 4.1 *Experimental protocol*

animal		
group	number	experimental protocol
1	6	pacing alone
2	3	LCX occlusion plus left atrial pacing
3	3	LAD occlusion plus left atrial pacing
4	6	alternating of LAD and LCX occlusion plus left atrial pacing

4.1.2 EXPERIMENTAL PROCEDURES AND SUBENDOCARDIAL ISCHAEMIA

Experimental procedures were described in detail in chapter 3. In group 1 (Pacing without coronary artery stenosis group), the heart was paced without coronary artery occlusion at a start rate of 120 beat per minute (bpm). Then the stimulation was gradually increased at a rate of 10bpm every 2 minutes until it reached 180bpm, after that the stimulation rate was increased to 200, 220 and finally 240bpm every 2 minutes. In the subendocardial ischaemia group, the subendocardial ischaemia sheep model was made by combining pacing with partial occlusion of an artery. This technique was previously validated in our laboratory by fluorescent microspheres (Li et al., 1996). In brief, stenosis was achieved by inflating the hydraulic occluder causing a reduction in flow to about 50% of the control level. The left atrium was then paced by a stimulator starting with a rate of 120bpm, and increased gradually by 10bpm every 2 minutes until it reached 180bpm.

4.1.3 REGIONAL MYOCARDIAL BLOOD FLOW MEASUREMENT

The regional myocardial blood flow (RMBF) was measured before ischaemia and at 20 minutes of ischaemia by using fluorescent microspheres (Molecular Probes, Inc., Eugene, OR, USA) as previously described (Li et al., 1996). Instead of using Perkin-Elmer 650-10S fluorescence spectrophotometer (Hitachi Ltd), the tissue fluorescent intensity was measured by Amino-Bowman spectrophoto-fluorometer. Each fluorescent intensity was read at the appropriate excitation/emission wavelengths. The excitation/emission bandpass was set at 27.5nm/27.5nm. All the samples from the same experiment were measured on the same day. The detailed procedure of

microspheres injection, tissue sampling and digestion, fluorescence extraction and measurement has been described in chapter 3.

4.1.4 POTENTIALS RECORDING AND MAP CONSTRUCTION

Potentials recording and map construction are described as in chapter 3. Epicardial potential, endocardial potential and intramyocardial potentials of different depth were simultaneously recorded in each experiment before and after 5min, 10min, 15min and 20min of ischaemia. The epicardial potentials were recorded by using an epicardial sock containing 64 electrodes (Cardiovascular Research and Training Institute, the University of Utah, USA). The endocardial potentials were recorded by using a home-made 40-electrode basket mapping apparatus. Intramyocardial potentials were recorded by intramyocardial plunging needles; each needle had three electrodes as described in chapter 3. Such apparatus enable the recording of signals from a working heart. The locations of all the electrodes were marked at the end of the experiments, and the epicardial vascular pattern and the outlines of the ventricle were also recorded for future map construction.

The potentials from epicardial, intramyocardial and endocardial electrodes were recorded by a 256-channel system. Data from the recording system were transferred to a SUN workstation (SUN Microsystems, Inc., 2550 Garcia Avenue, Mountain View, CA 94043, USA), and then analysed using the mapping program developed in this laboratory (Walker et al. 1983 and 1987a) and the S-plus statistical package, which are both run under UNIX system. The ST segment potential distributions were displayed as isopotential contour maps, and these were further combined with flow maps constructed from the simultaneously measured regional blood flow.

4.2 RESULTS

4.2.1 HAEMODYNAMIC RESPONSE

4.2.1.1 Haemodynamic response to pacing

Haemodynamic parameters were recorded before and during pacing. Pacing the heart at a rate of 180bpm for 20min did not cause significant change in LVDP, LVSP, LAP and CAP ($P>0.05$), (Table 4.2).

Table 4.2 Haemodynamic response to left atrial pacing (n=6)

	control (before pacing)	pacing (180bpm)
LVDP, mmHg	-8.83 ± 3.76	$-5.67 \pm 7.00+$
LVSP, mmHg	106.67 ± 11.69	$94.17 \pm 18.82+$
LAP, mmHg	-0.14 ± 1.95	$3.40 \pm 7.79+$
CAP, mmHg	85.44 ± 9.06	$73.61 \pm 18.54+$

LVDP: left ventricular diastolic pressure LAP: left atrial pressure

LVSP: left ventricular systolic pressure CAP: carotid artery pressure

compared with control group: + $P>0.05$

4.2.1.2 Haemodynamic response to subendocardial ischemia

Partial occlusion of a coronary artery itself did not cause LVDP, LVSP, LAP and CAP changes; partial occlusion of a coronary artery together with left atrial pacing did not cause LVDP, LVSP and CAP change ($P>0.05$), but did increase LAP ($P<0.05$), (Table 4.3).

Table 4.3 Haemodynamic response to partial coronary artery stenosis and subendocardial ischemia (n=12)

	control	stenosis only	subendocardial ischaemia
LVDP, mmHg	-0.06 ± 3.46	1.17 ± 4.81	3.36 ± 5.04
LVSP, mmHg	102.00 ± 9.93	101.9 ± 13.50	91.67 ± 15.15
LAP, mmHg	1.98 ± 2.77	2.77 ± 3.22	$6.81 \pm 5.43^*$
CAP, mmHg	79.61 ± 17.49	79.91 ± 16.96	66.28 ± 15.60

LVDP: left ventricular diastolic pressure LAP: left atrial pressure

LVSP: left ventricular systolic pressure CAP: carotid artery pressure

*Compared to control group: * $P<0.05$*

4.2.2 RMBF RESPONSE

4.2.2.1 RMBF response to pacing

RMBF was measured before pacing and after 20 minutes of pacing the heart at 180bpm. Though pacing the heart at a rate of 180bpm increased blood flow in every layer of the heart, especially in the inner layer, the difference was not significant ($P>0.05$). RMBF in any layer of the heart, and the ratio of RMBF of the inner one-third layer and outer one-third layer of the LV wall (endo/epi ratio) during pacing did not differ significantly from that of before pacing ($P>0.05$), (Table 4.4, Fig. 4.1).

Table 4.4 RMBF response to left atrial pacing ($n=6$)

	LAD area		LCX area		whole LV	
	control	pacing (180bpm)	control	pacing (180bpm)	control	pacing (180bpm)
epi	0.71 ± 0.09	$0.70 \pm 0.11+$	0.74 ± 0.13	$0.77 \pm 0.12+$	0.72 ± 0.11	$0.74 \pm 0.12+$
mid	0.72 ± 0.12	$0.74 \pm 0.11+$	0.77 ± 0.13	$0.83 \pm 0.14+$	0.75 ± 0.12	$0.78 \pm 0.13+$
endo	0.77 ± 0.13	$0.79 \pm 0.13+$	0.82 ± 0.13	$0.87 \pm 0.13+$	0.79 ± 0.13	$0.83 \pm 0.13+$
trans	0.73 ± 0.11	$0.74 \pm 0.12+$	0.78 ± 0.13	$0.82 \pm 0.13+$	0.75 ± 0.11	$0.78 \pm 0.13+$
endo/epi ratio	1.08 ± 0.12	$1.13 \pm 0.04+$	1.12 ± 0.08	$1.13 \pm 0.03+$	1.10 ± 0.10	$1.13 \pm 0.03+$

epi: RMBF in outer one-third layer of LV wall mid: RMBF in middle one-third layer of LV wall

endo: RMBF in inner one-third layer of LV wall trans. RMBF in full thickness of LV wall

endo/epi ratio: ratio of RMBF of inner one-third layer and outer one-third layer of LV wall

Compared with control group: + $P>0.05$

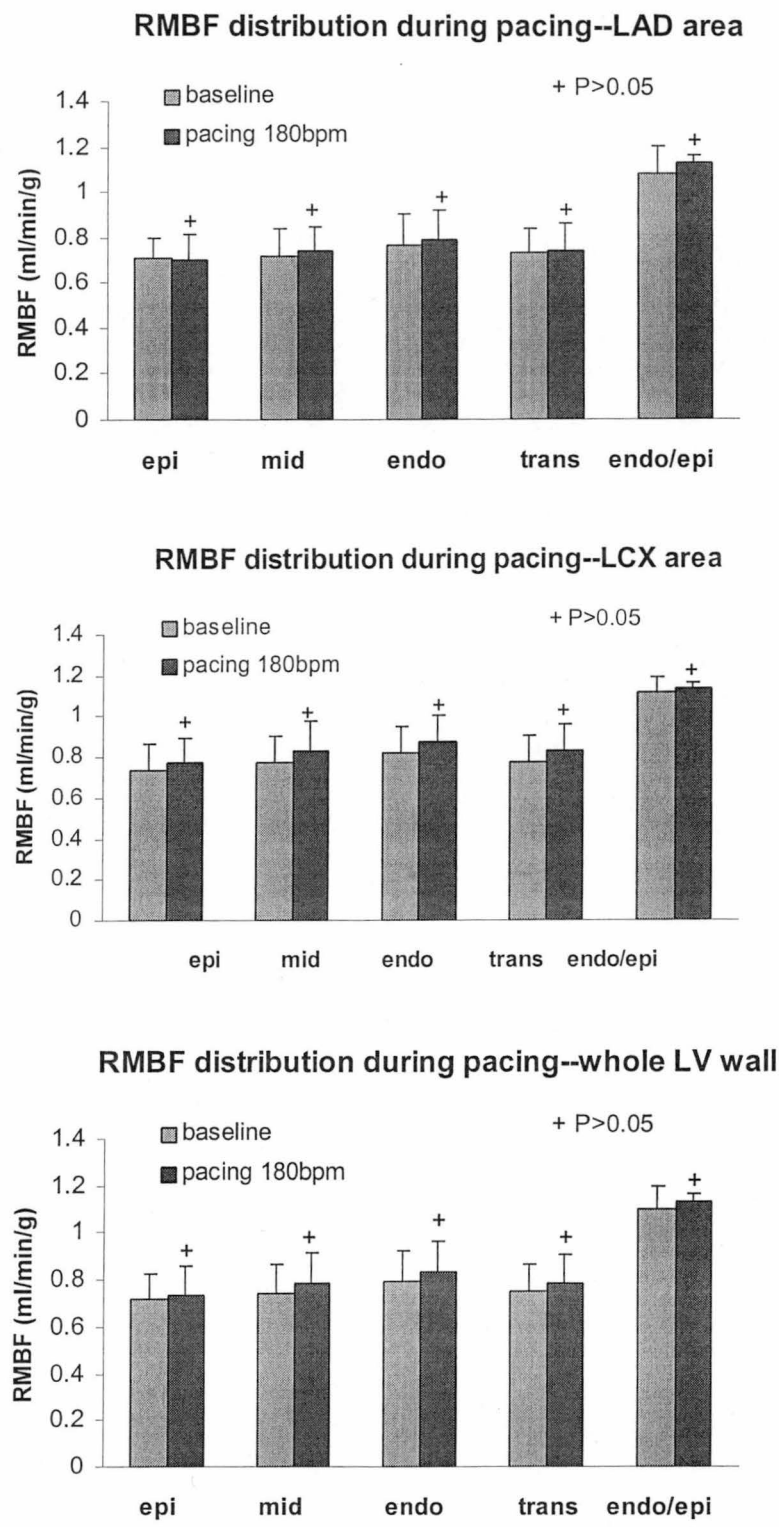


Fig. 4.1 RMBF distributions during left atrial pacing (see Table 4.4 for abbreviation)

4.2.2.2 RMBF response to subendocardial ischemia

RMBF was measured before and after 20min of ischaemia. During subendocardial ischaemia, RMBF in the subendocardial layer of the heart in the ischaemic area was significantly reduced ($P<0.05$). The endo/epi ratio was also decreased significantly ($P<0.001$), while the RMBF in the mid layer and subepicardial layer displaced no significant change. In the non-ischaemic area, subendocardial ischaemia caused a slight increase in the RMBF in the endocardial layer and the mid layer, but the difference was not significant ($P<0.05$), (Table 4.5, Fig. 4.2).

Table 4.5 RMBF response to subendocardial ischemia (n=12)

	control	subendocardial ischaemia
ischaemic area		
epi	0.821 ± 0.089	0.780 ± 0.066+
mid	0.872 ± 0.111	0.763 ± 0.059+
endo	0.916 ± 0.107	0.689 ± 0.079*
trans	0.870 ± 0.100	0.744 ± 0.067*
endo/epi ratio	1.116 ± 0.057	0.882 ± 0.041**
non-ischaemic area		
epi	0.829 ± 0.142	0.827 ± 0.088+
mid	0.835 ± 0.067	0.882 ± 0.111+
endo	0.880 ± 0.092	0.972 ± 0.174+
trans	0.848 ± 0.094	0.893 ± 0.122+
endo/epi ratio	1.073 ± 0.099	1.170 ± 0.095+

epi: RMBF in outer one-third layer of LV wall mid: RMBF in middle one-third layer of LV wall

endo: RMBF in inner one-third layer of LV wall trans: RMBF in full thickness of LV wall

endo/epi ratio. ratio of RMBF of inner one-third layer and outer one-third layer of LV wall

*Compared with control group: + P>0.05, * P<0.05, ** P<0.001*

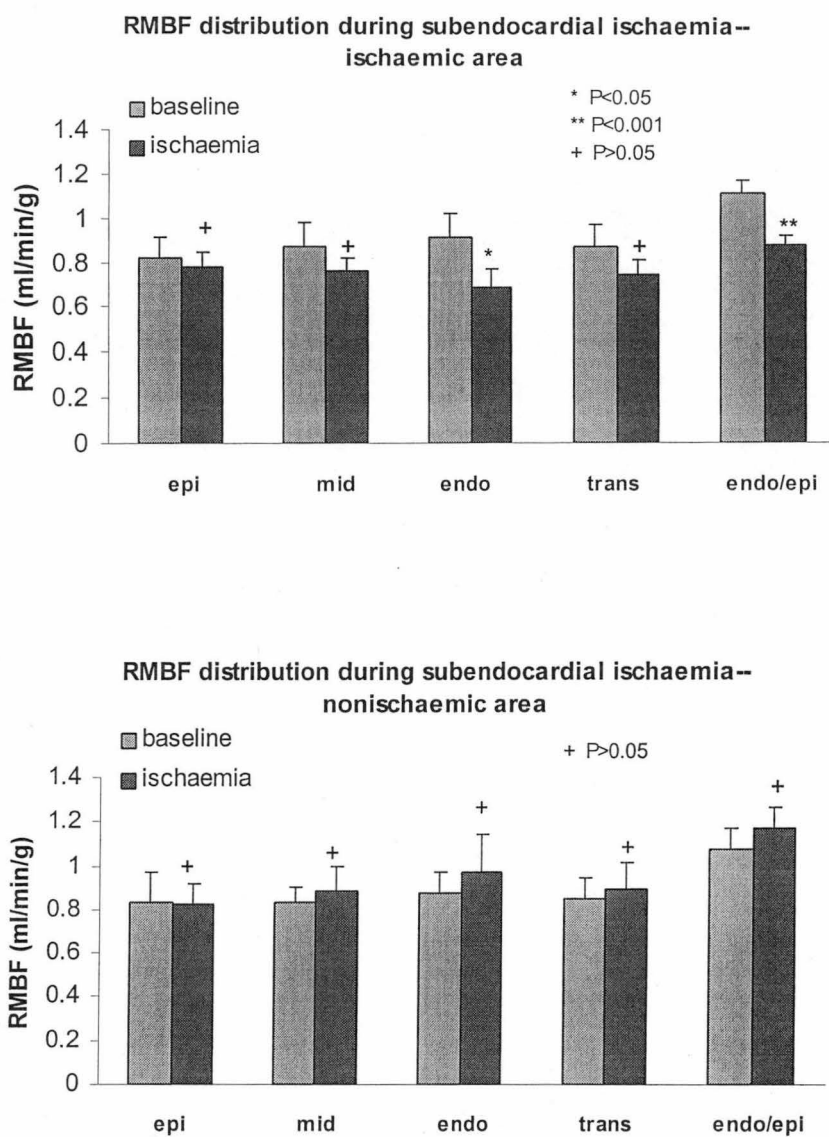


Fig. 4.2 RMBF distributions in subendocardial ischaemia (see Table 4.5 for abbreviation)

4.2.3 ST POTENTIAL DISTRIBUTION

4.2.3.1 ST potential distribution in pacing only group

6 sheep were paced at different rates without ligation of a coronary artery. Pacing the heart up to a rate of 180bpm did not cause significant spatial ST potential distribution changes and ST magnitude changes in the epicardial, subepicardial, mid layer of the heart, subendocardial and endocardial potential recordings. When the heart rate reached 220bpm, ST potential magnitude in the epicardial and subepicardial layers increased compared to that of before pacing ($P<0.05$); Pacing the heart up to a rate of 240bpm resulted in increased ST potential magnitude in the mid, subendocardial and endocardial layers ($P<0.05$). ST potential distributions in different layers at pacing rate of 160bpm, 180bpm and 220bpm are shown in Fig. 4.3. ST potential magnitudes in different layers before and after left atrial pacing were shown in Table 4.6.

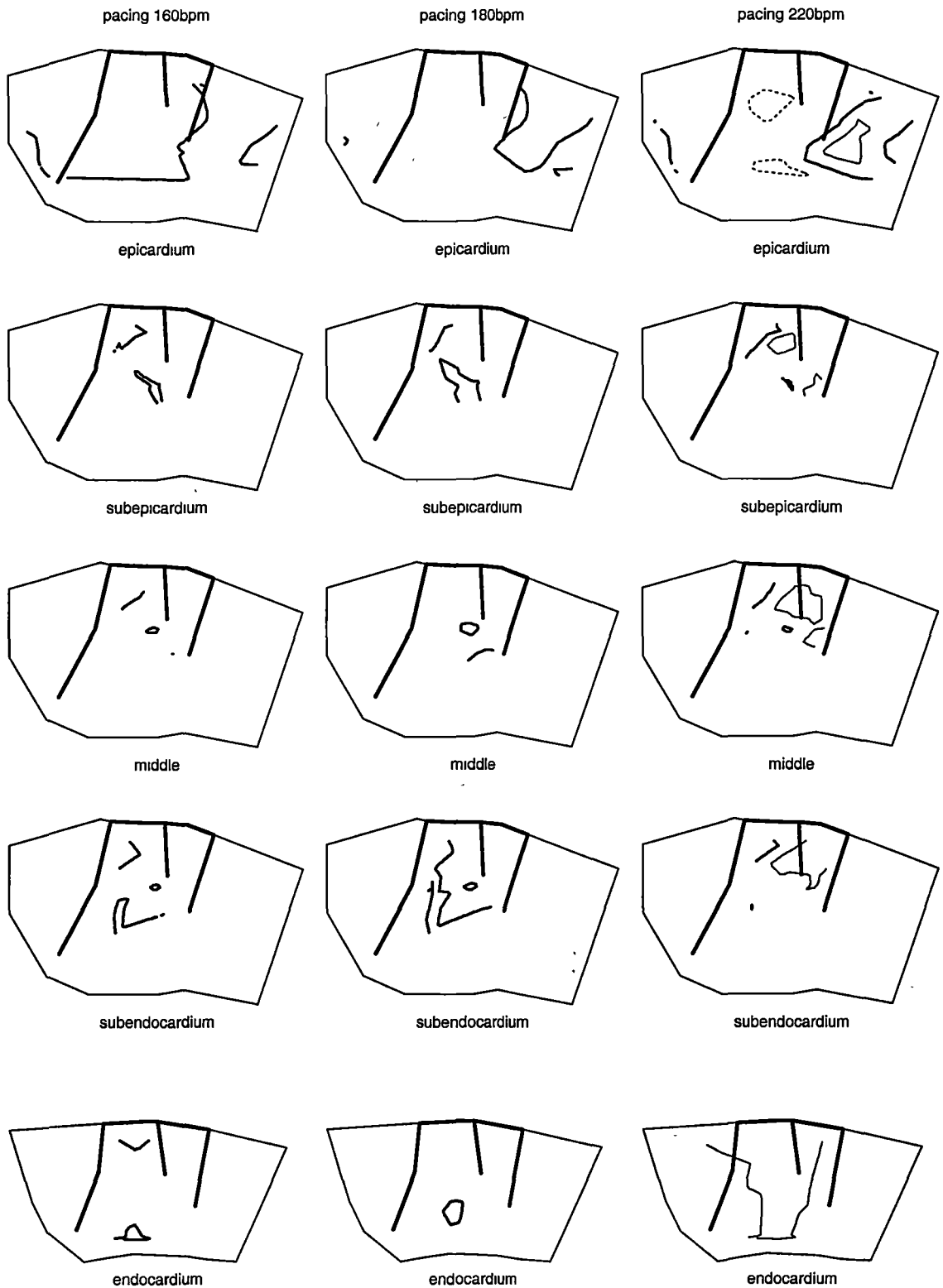


Fig. 4.3 ST potential distributions in different layers of the heart at a pacing rate of 160bpm, 180bpm and 220bpm.. The thickest solid lines reflect the position of the coronary arteries, the thick solid lines indicate zero potential, the thin solid and the dashed lines indicate ST elevation and ST depression respectively. Maps are plotted from data of one of the animals in group 1. Contour interval=0.2mV.

CHAPTER FOUR

Table 4.6 ST potential magnitudes (microvolt) before and during pacing (n=6)

	baseline	140bpm	150bpm	160bpm	180bpm	200bpm	220bpm	240bpm
epi	-47.9±15.4	-34.3±26.3	-38.7±15.2	-35.9±21.2	-54.9±27.9	-60.2±39.1	-103.5±48.1*	-153.3±59.0*
sub-epi	-31.8±32.4	-30.3±38.6	-29.0±35.4	-29.9±43.6	-26.7±54.0	-13.5±46.8	34.7±61.5*	33.8±60.9*
mid	-23.1±54.8	-24.3±48.3	-19.2±41.1	-17.8±50.2	-23.6±61.4	-4.91±47.3	51.6±64.6	71.1±76.3*
sub-endo	-36.1±79.9	-31.9±41.3	-35.3±35.4	-27.0±28.9	-27.4±52.7	-17.3±45.6	17.5±82.0	101.3±107.2*
endo	46.8±29.2	46.3±25.5	48.2±34.3	55.1±37.7	50.4±22.0	69.2±48.7	102.3±62.7	175.6±97.8*

epi: ST potential magnitude from epicardial recording

sub-epi: ST potential magnitude from subepicardial recording

mid: ST potential magnitude from mid-layer of LV wall recording

sub-endo: ST potential magnitude from subendocardial recording

endo: ST potential magnitude from endocardial recording

*Compared with baseline: *P<0.05*

4.2.3.2 ST potential distribution in subendocardial ischaemia in either LAD or LCX area

Subendocardial ischaemia was produced in the LAD area in 3 sheep and in the LCX area in another 3 sheep. In either the LAD or the LCX subendocardial ischaemia area, epicardial ST depression occurred following ischaemia. Subendocardial ischaemia in either the LAD or the LCX area caused similar epicardial ST potential distributions. Simultaneously recorded endocardial potentials showed ST elevation which was related to the area supplied by the culprit coronary artery. Intramyocardial ST potential recordings showed both ST elevation and ST depression in different layers of the heart, with ST elevation occurring in the ischaemic centre and ST depression on the boundary of the ischaemic and non-ischaemic areas, the distribution of the ST depression extended slightly towards the ischaemic area from subendocardium to subepicardium (Fig. 4.4, Fig. 4.5).

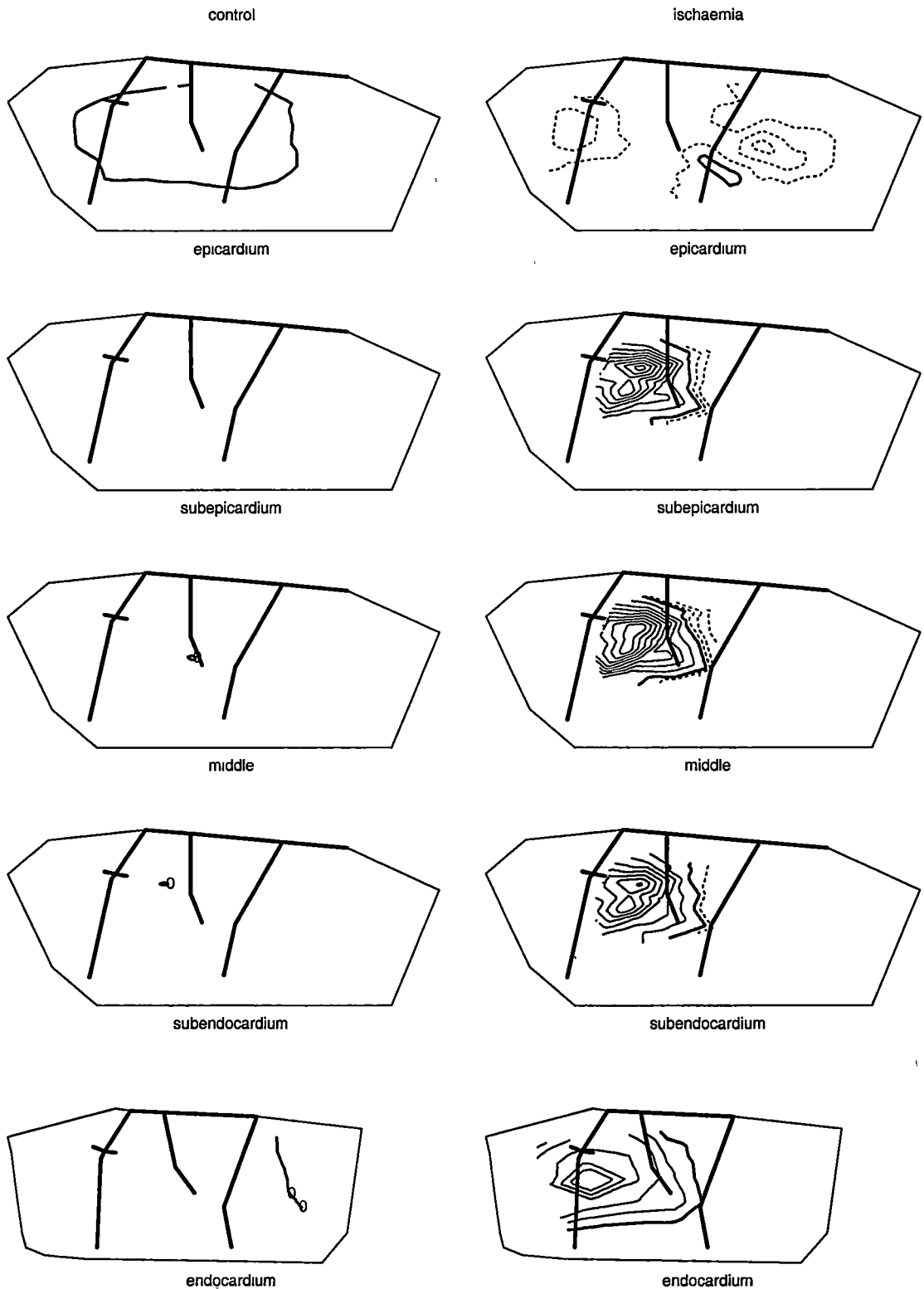


Fig. 4.4 ST potential distributions in different layers of the heart before and at 20min of subendocardial ischaemia of LAD area. The thickest solid lines reflect the position of the coronary arteries, the thick solid lines indicate zero potential, the thin solid and the dashed lines indicate ST elevation and ST depression respectively, with the occluded arteries indicated by bars across the coronary arteries. Maps are plotted from data of one of the animals in group 2. For negative ST, contour interval=0.2mV; for positive ST, contour interval=0.2mV in endocardium, contour interval=0.5mV in epicardium and intramyocardium (subepicardium, middle and subendocardium).

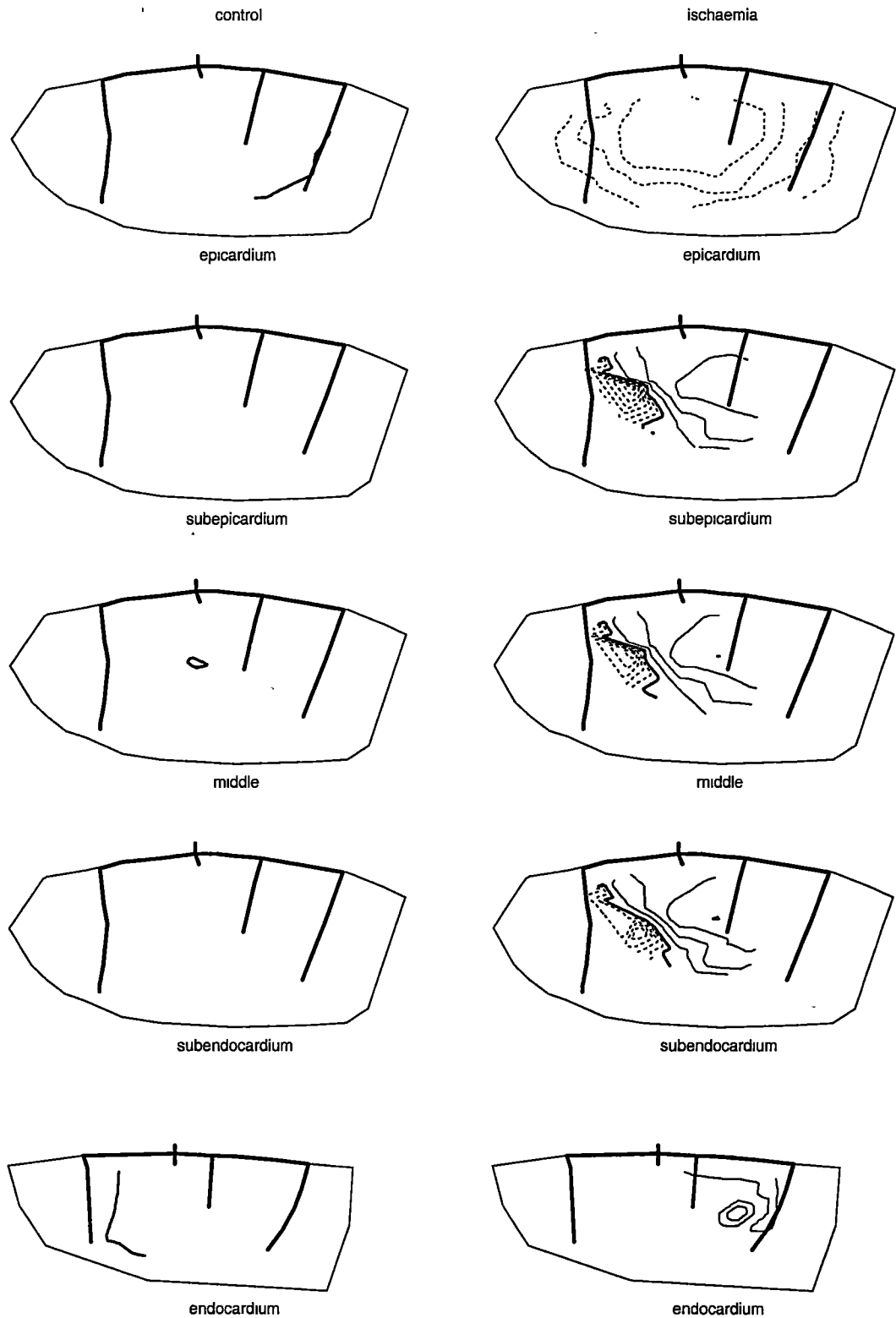


Fig. 4.5 ST potential distributions in different layers of the heart before and at 20min of subendocardial ischaemia of LCX area. The thickest solid lines reflect the position of the coronary arteries, the thick solid lines indicate zero potential, the thin solid and the dashed lines indicate ST elevation and ST depression respectively, with the occluded arteries indicated by bars across the coronary arteries. Maps are plotted from data of one of the animals in group 3. For negative ST, contour interval=0.2mV; for positive ST, contour interval=0.2mV in endocardium, contour interval=0.5mV in epicardium and intramyocardium (subepicardium, middle and subendocardium).

Time course of ST potential distribution in subendocardial ischaemia in either the LAD or LCX area

Fig. 4.6.1, Fig. 4.6.2, Fig. 4.7.1, and Fig. 4.7.2 illustrate the potential distributions in different layers of the heart at different times during subendocardial ischaemia in either the LAD or the LCX area. Epicardial ST depression was seen on the surface of the heart, with the maximal ST depression occurring on the lateral wall. Epicardial ST depression distribution changed little with progression of the ischaemia. Endocardial ST elevation occurred on the lateral wall, but as the ischaemia was maintained, it spread to the surrounding areas. The magnitude of ST elevation increased as well. Intramyocardial ST potential showed a stable distribution as the ischaemia progressed.

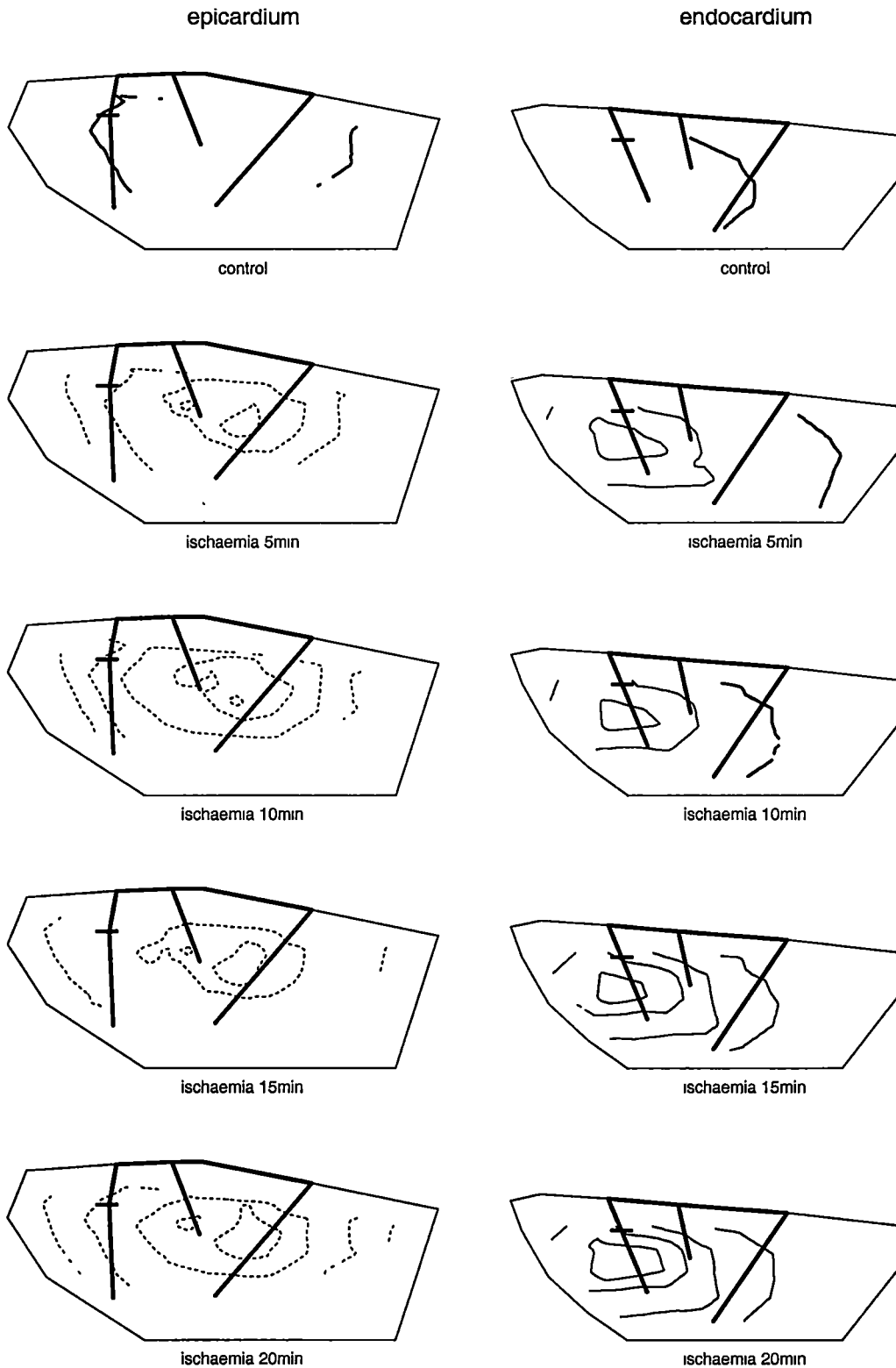


Fig. 4.6.1 ST potential distributions in epicardium and endocardium at control and at various time periods in subendocardial ischaemia of LAD ligation. The thickest solid lines reflect the position of coronary arteries, the thick solid lines indicate zero potential, the thin solid and dashed lines indicate ST elevation and ST depression respectively, with the occluded arteries indicated by bars across the coronary arteries. Maps are plotted from the data of one animal from group 2. Contour interval = 0.2 mV.

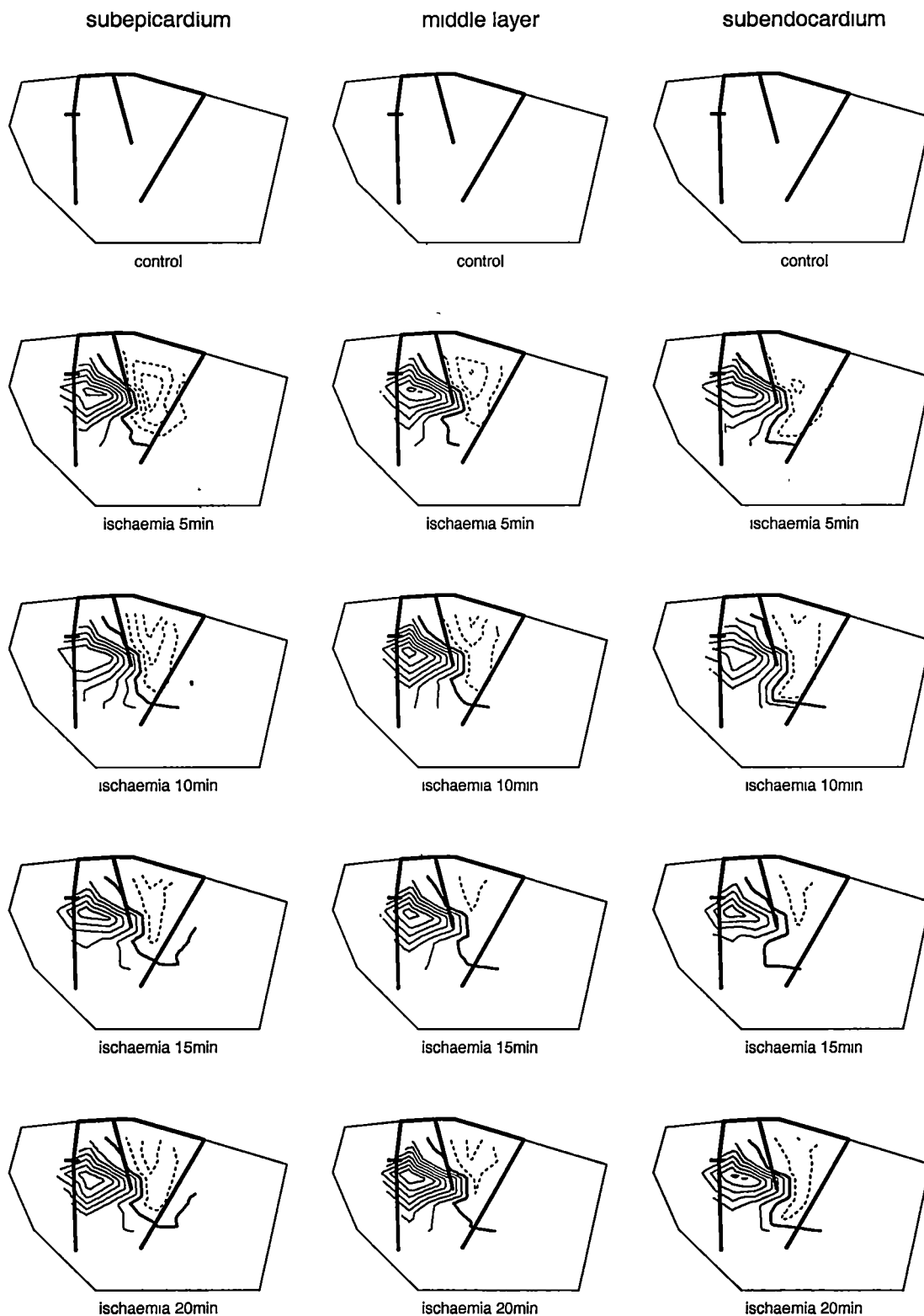


Fig. 4.6.2 ST potential distributions in different depth of intramyocardium at control and at various time periods in subendocardial ischaemia of LAD ligation. The thickest solid lines reflect the position of coronary arteries, the thick solid lines indicate zero potential, the thin solid and dashed lines indicate ST elevation and ST depression respectively, with the occluded arteries indicated by bars across the coronary arteries. Maps are plotted from the data of one animal from group2. Contour interval=0.5mV.

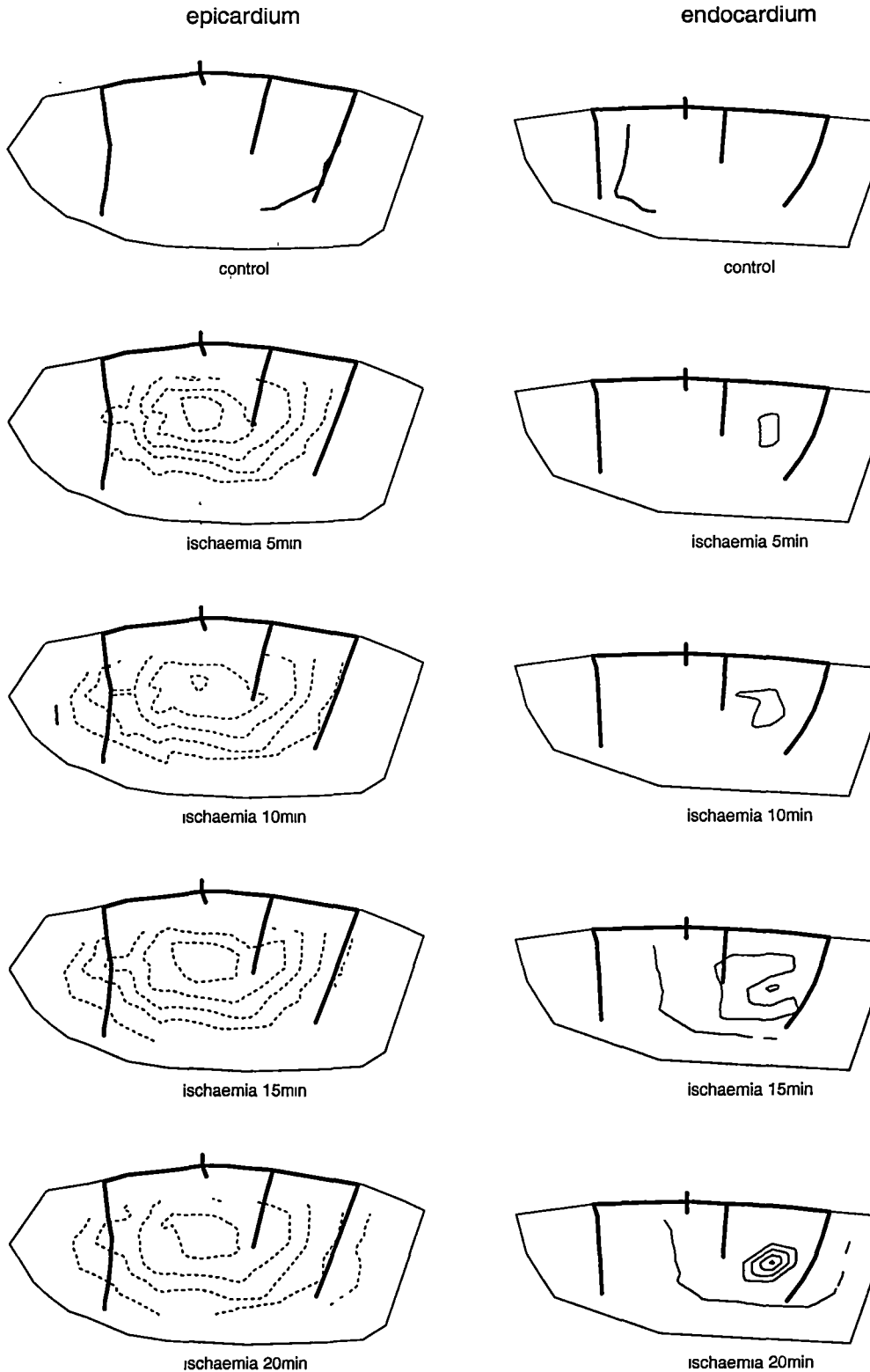


Fig. 4.7.1 ST potential distributions in epicardium and endocardium at control and at various time periods in subendocardial ischaemia of LCX ligation. The thickest solid lines reflect the position of coronary arteries, the thick solid lines indicate zero potential, the thin solid and dashed lines indicate ST elevation and ST depression respectively, with the occluded arteries indicated by bars across the coronary arteries. Maps are plotted from the data of one animal from group3. Contour interval=0.2mV.

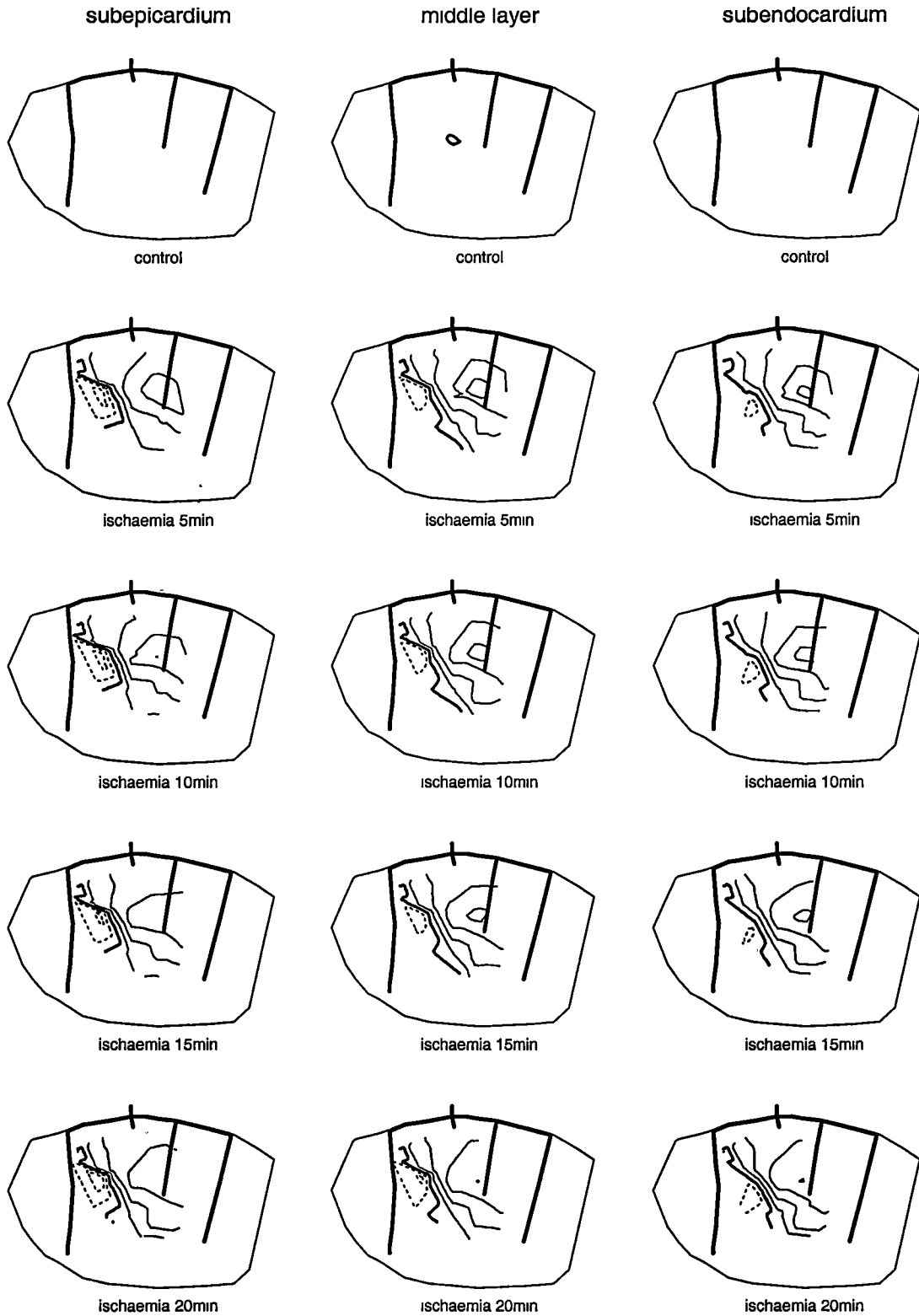


Fig. 4.7.2 ST potential distributions in different depth of intramyocardium at control and at various time periods in subendocardial ischaemia of LCX ligation. The thickest solid lines reflect the position of coronary arteries, the thick solid lines indicate zero potential, the thin solid and dashed lines indicate ST elevation and ST depression respectively, with the occluded arteries indicated by bars across the coronary arteries. Maps are plotted from the data of one animal from group 3. Contour interval = 0.5mV.

Intramyocardial transition of ST potential magnitude during subendocardial ischaemia

Table 4.7 showed intramyocardial transition of ST potential magnitude during subendocardial ischaemia at different time courses after ischaemia. It revealed that the ST potential magnitude at different time courses after ischaemia displayed no significant changes ($P>0.05$).

Comparison of ST potential magnitude among the three intramyocardial layers of the left ventricle showed that there were no significant changes of ST potential magnitude between the inner one-third and the mid one-third layers. Neither were there changes between the mid one-third and the outer one-third layers ($P>0.05$). At 5min, 10min and 15min after ischaemia, negative ST potential magnitude in the outer one-third layer was relatively lower than that in the inner one-third layer ($P<0.05$).

CHAPTER FOUR

Table 4.7 Intramyocardial transition of ST potential magnitude (millivolt) during subendocardial ischaemia (n=6)

	1min	5min	10min	15min	20min
positive ST-shift					
sub-epi	2.993±0.787	3.089±0.777	2.690±0.566	2.348±0.594	2.672±0.525
mid	2.431±0.472	2.744±0.606	3.187±0.799	3.088±0.663	3.186±0.588
sub-endo	2.442±0.474	2.514±0.538	2.435±0.430	2.368±0.402	2.506±0.302
negative ST-shift					
sub-epi	-1.236±0.384	-1.414±0.457	-1.352±0.451	-1.076±0.331	-1.004±0.386
mid	-1.030±0.246	-1.209±0.429	-1.275±0.478	-0.885±0.371	-0.874±0.414
sub-endo	-0.833±0.186	-0.874±0.170*	-0.860±0.230*	-0.675±0.232*	-0.617±0.242

sub-epi: ST potential magnitude from subepicardial recording

mid: ST potential magnitude from mid-layer of LV wall recording

sub-endo: ST potential magnitude from subendocardial recording

*Compared with sub-epi group at the same time: *P<0.05, others P>0.05*

Comparison between different time groups: P>0.05

4.2.3.3 ST potential distribution in subendocardial ischaemia in alternation of LAD and LCX area

ST potential distribution in subendocardial ischaemia in alternation of LAD and LCX area

Subendocardial ischaemia was produced by alternate LAD and LCX ligation in 6 sheep. Subendocardial ischaemia in either of the LAD or LCX area resulted in a similar ST potential distribution to that in subendocardial ischaemia of a single vessel. Epicardial ST depression occurred with maximum change in the anterolateral wall of the left ventricle, and the potential distribution was similar in various subendocardial ischaemic locations. The epicardial ST potential change in each individual electrode position during the LAD ligation was compared to that during the LCX ligation. The results showed that there was a significant relationship between epicardial ST potential distribution during LAD ligation and that during LCX ligation, the correlation coefficient was 0.769 ($P<0.001$), (Table 4.8).

Table 4.8 Relationship of epicardial ST potential distribution between LAD and LCX ligation in subendocardial ischaemia in alternate of LAD and LCX area.

sheep No	r	P value
1	0.807	$P<0.001$
2	0.696	$P<0.001$
3	0.923	$P<0.001$
4	0.543	$P<0.001$
5	0.794	$P<0.001$
6	0.859	$P<0.001$
mean \pm SD	0.769 \pm 0.135	$P<0.001$

Endocardial ST elevation occurred with the distribution corresponding to the partially occluded coronary artery. There was no significant relationship between endocardial ST potential distribution during LAD ligation and that during LCX ligation, the correlation coefficient was 0.017 ($P>0.01$), (Table 4.9).

Table 4.9 Relationship of endocardial ST potential distribution between LAD and LCX ligation in subendocardial ischaemia in alternate of LAD and LCX area.

sheep No	r	P value
1	0.007	P>0.01
2	0.021	P>0.01
3	0.032	P>0.01
4	0.009	P>0.01
5	0.025	P>0.01
6	0.010	P>0.01
mean±SD	0.017±0.010	P>0.01

Both ST depression and ST elevation occurred in the intramyocardium, with maximal ST elevation in the ischaemic centre and ST depression on the boundary of the ischaemic and non-ischaemic areas. The distribution of ST depression extended slightly towards the ischaemic area from subendocardium to subepicardium. The intramyocardial region with ST depression during subendocardial ischaemia in the LAD area converted to ST elevation during subendocardial ischaemia in the LCX area. The intramyocardial region with ST elevation during subendocardial ischaemia in the LAD area converted to ST depression during subendocardial ischaemia in the LCX area (Fig. 4.8).

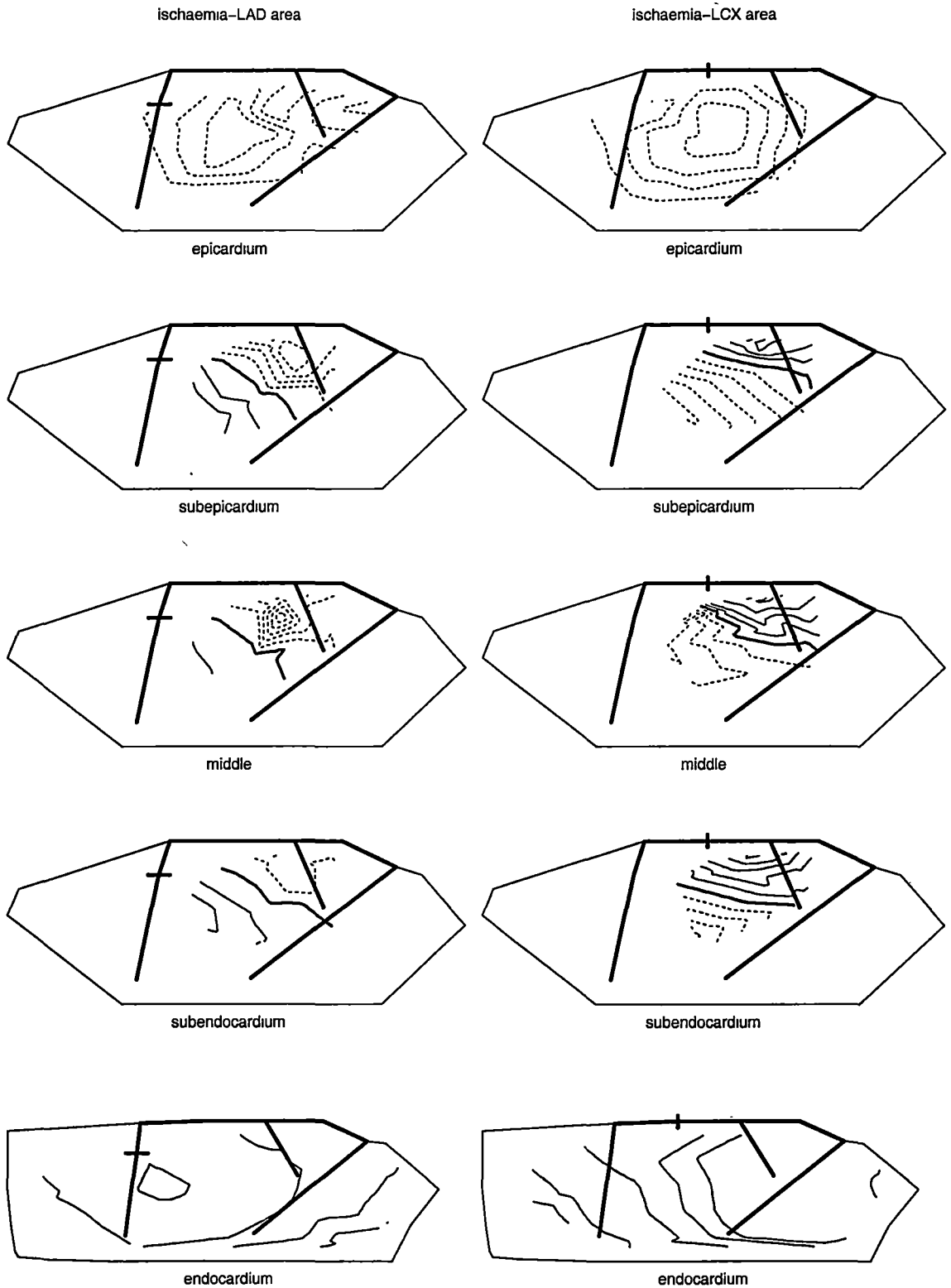


Fig. 4.8 ST potential distributions in different layers of the heart at 20min of subendocardial ischaemia of alternative occlusion of LAD or LCX. The thickest solid lines reflect the position of the coronary arteries, the thick solid lines indication zero potential, the thin solid and dashed lines indicate ST elevation and depression respectively, with the occluded arteries indicated by bars across the coronary arteries. Maps are plotted from the data of one of the animals in group 4. For endocardium, contour interval=0.2mV, for epicardium and intramyocardium, contour interval=0.5mV.

Time course of ST potential distribution in subendocardial ischaemia in alternation of LAD and LCX areas

Fig. 4.9.1~Fig. 4.9.5 illustrate the potential distributions in different layers of the heart at different times of alternate subendocardial ischaemia in the LAD and LCX areas.

Epicardial ST depression in LAD ligation started on the lateral wall. As the ischaemia progressed, the ST depression spread to the whole heart, with the maximal ST depression occurring on the lateral wall. Epicardial ST depression in LCX ligation showed a more stable distribution at different times of ischaemia.

The distribution of intramyocardial ST potential was constant in both the LAD and LCX ligation as ischaemia developed. There was a mild increase in magnitude of the ST potential in both the LAD and LCX ligation.

Endocardial ST elevation distribution in LAD ligation varied with the progression of ischaemia. The maximal ST elevation occurred in the centre of the ischaemic area. Endocardial ST elevation in the LCX ligation showed a more stable distribution with time.

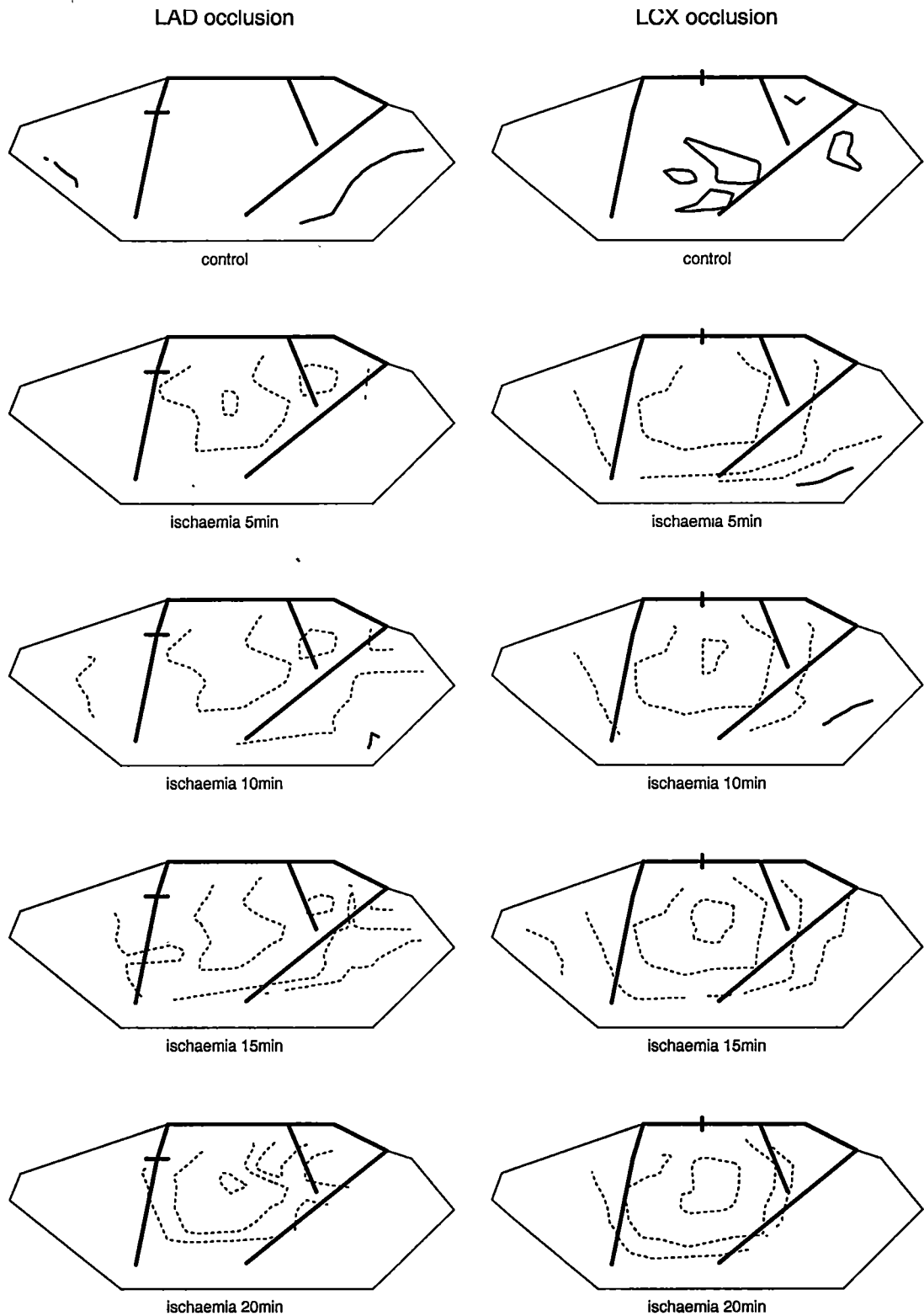


Fig. 4.9.1 Epicardial ST potential distributions at control and at various time periods in subendocardial ischaemia in alternation of LAD and LCX area. The thickest solid lines reflect the position of coronary arteries, the thick solid lines indicate zero potential, the thin solid and dashed lines indicate ST elevation and ST depression respectively. The occluded arteries are indicated by bars across the coronary arteries. Maps are plotted from the data of one animal from group 4. Contour interval=0.5mV.

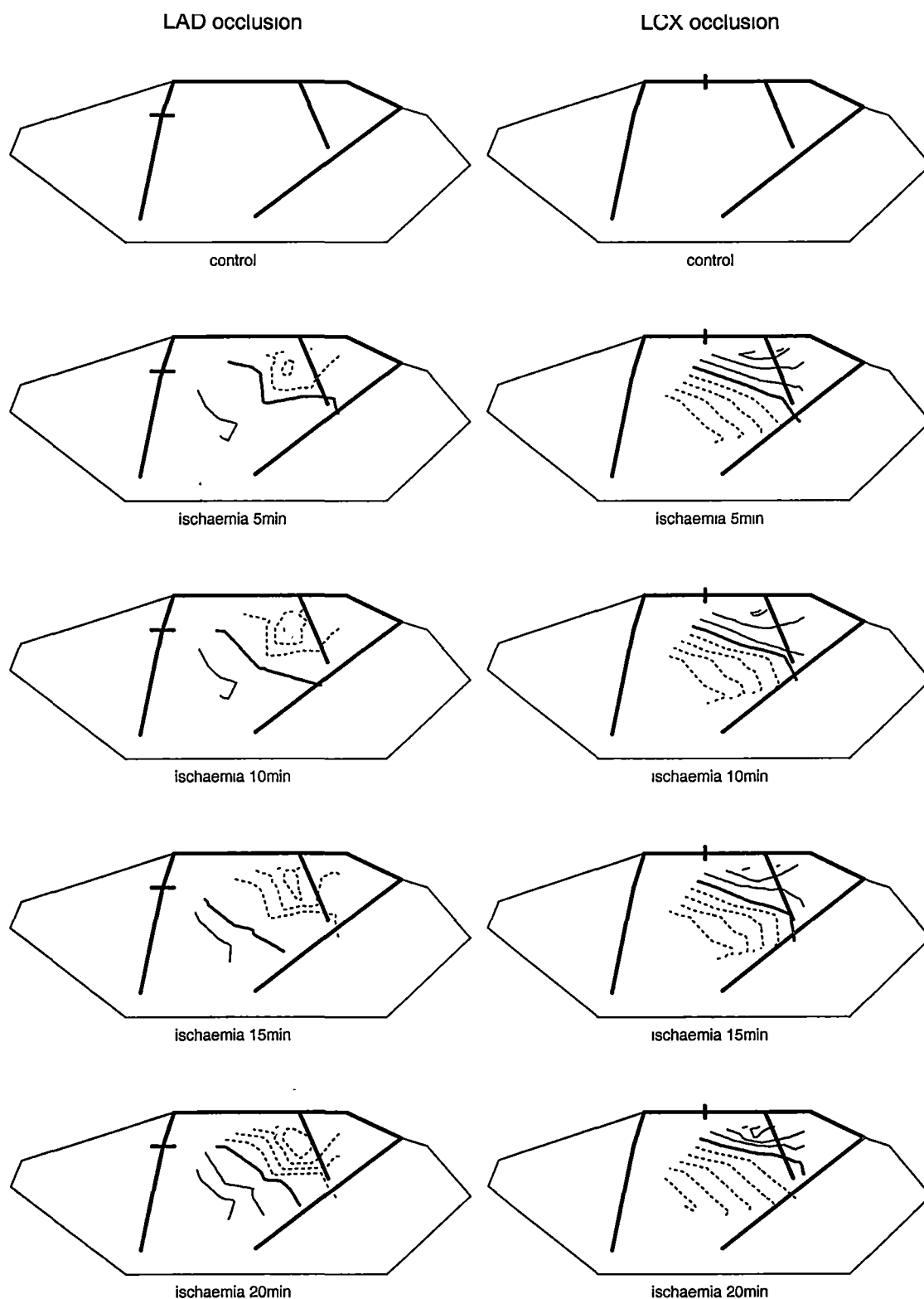


Fig. 4.9.2 Subepicardial ST potential distributions at control and at various time period in subendocardial ischaemia in alternation of LAD and LCX area. The thickest solid lines reflect the position of coronary arteries, the thick solid lines indicate zero potential, the thin solid and dashed lines indicate ST elevation and ST depression respectively. The occluded arteries are indicated by bars across the coronary arteries. Maps are plotted from the data of one animal from group 4. Contour interval=0.5mV.

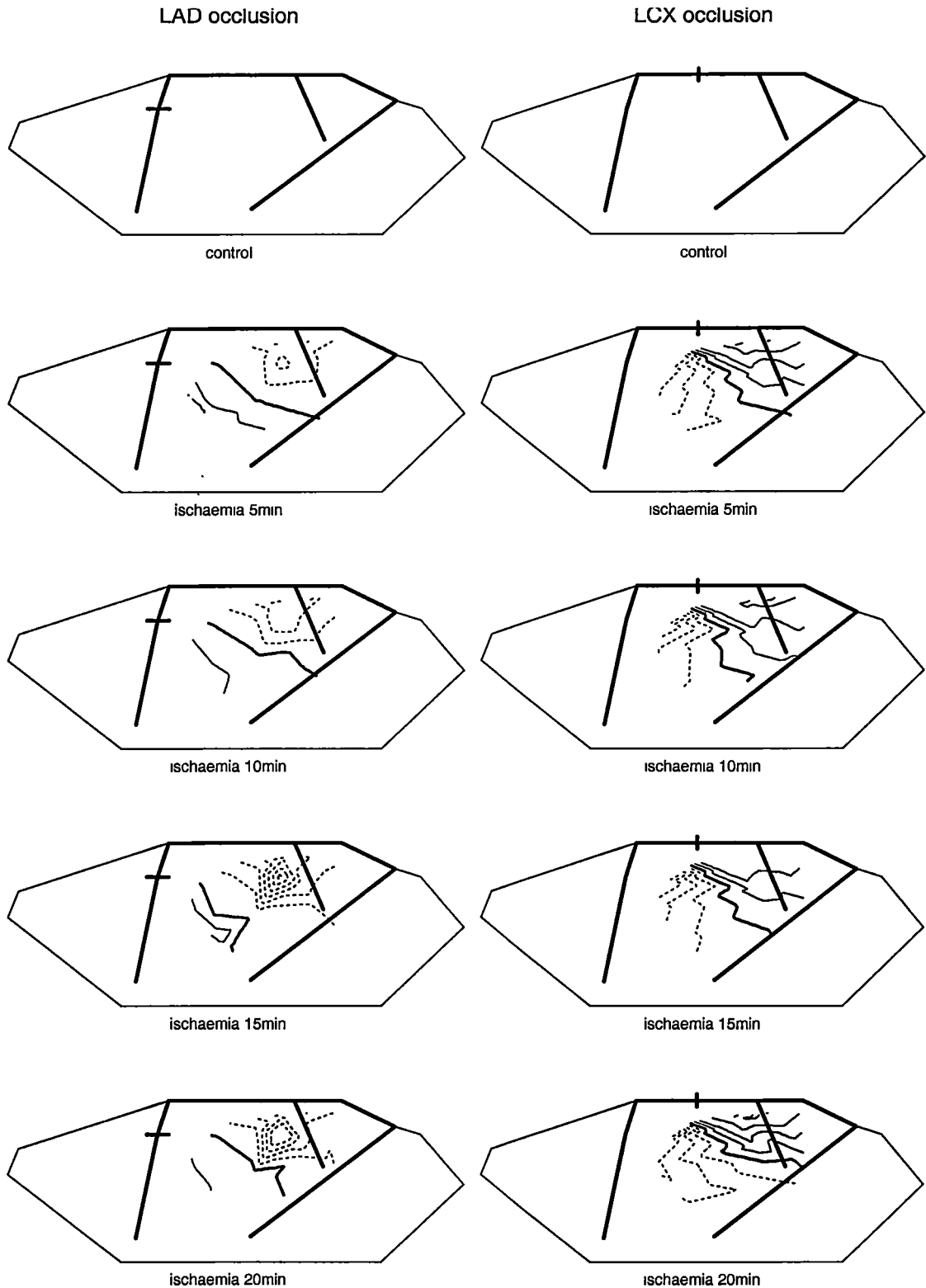


Fig. 4.9.3 ST potential distributions in middle layer of the heart at control and at various time periods in subendocardial ischaemia in alternation of LAD and LCX area. The thickest solid lines reflect the position of coronary arteries, the thick solid lines indicate zero potential, the thin solid and dashed lines indicate ST elevation and ST depression respectively. The occluded arteries are indicated by bars across the coronary arteries. Maps are plotted from the data of one animal from group 4. Contour interval=0.5mV. 140

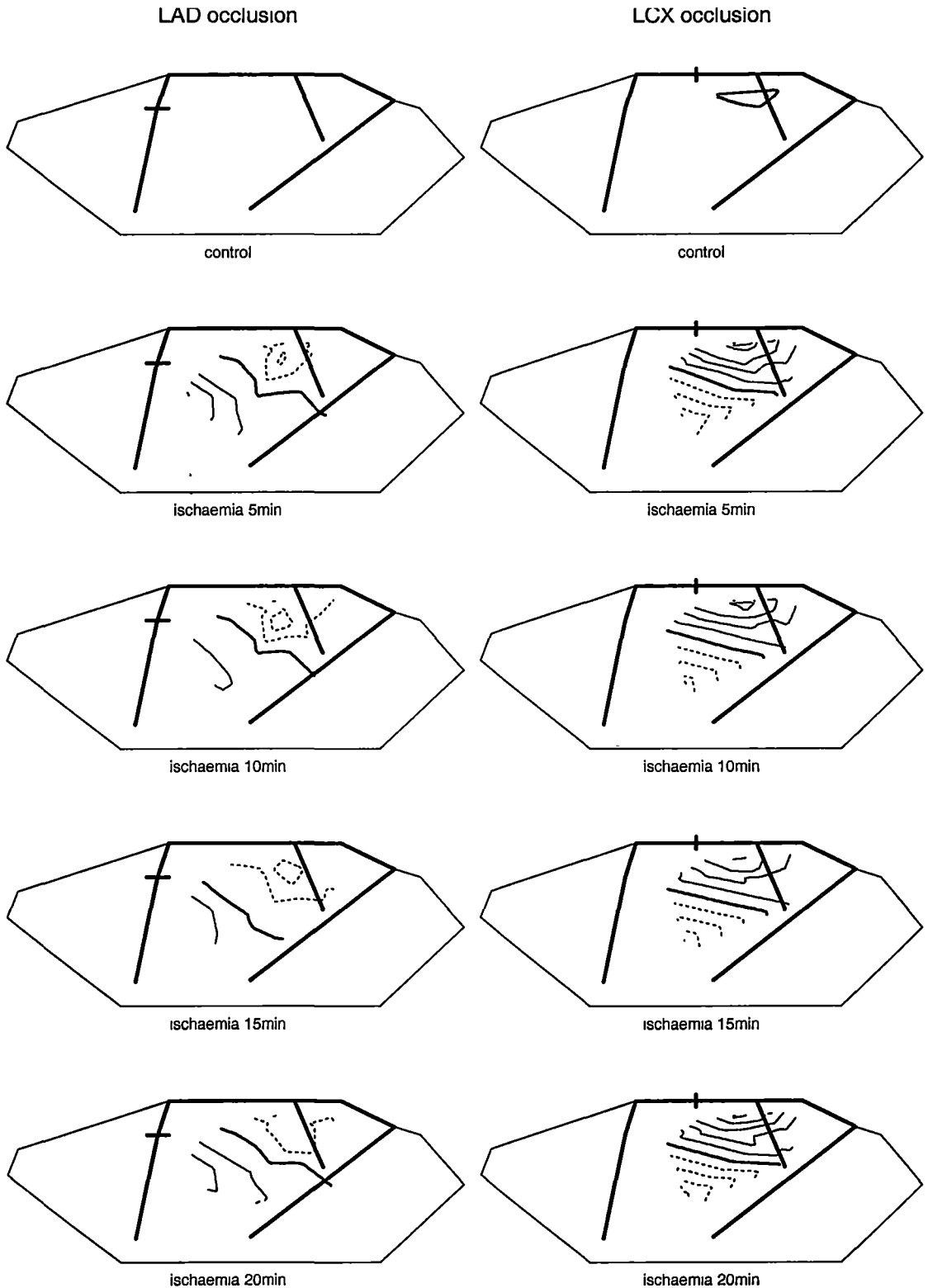


Fig. 4.9.4 Subendocardial ST potential distributions at control and at various time periods in subendocardial ischaemia in alternation of LAD and LCX area. The thickest solid lines reflect the position of coronary arteries, the thick solid lines indicate zero potential, the thin solid and dashed lines indicate ST elevation and ST depression respectively. The occluded arteries are indicated by bars across the coronary arteries. Maps are plotted from the data of one animal from group 4. Contour interval=0.5mV.

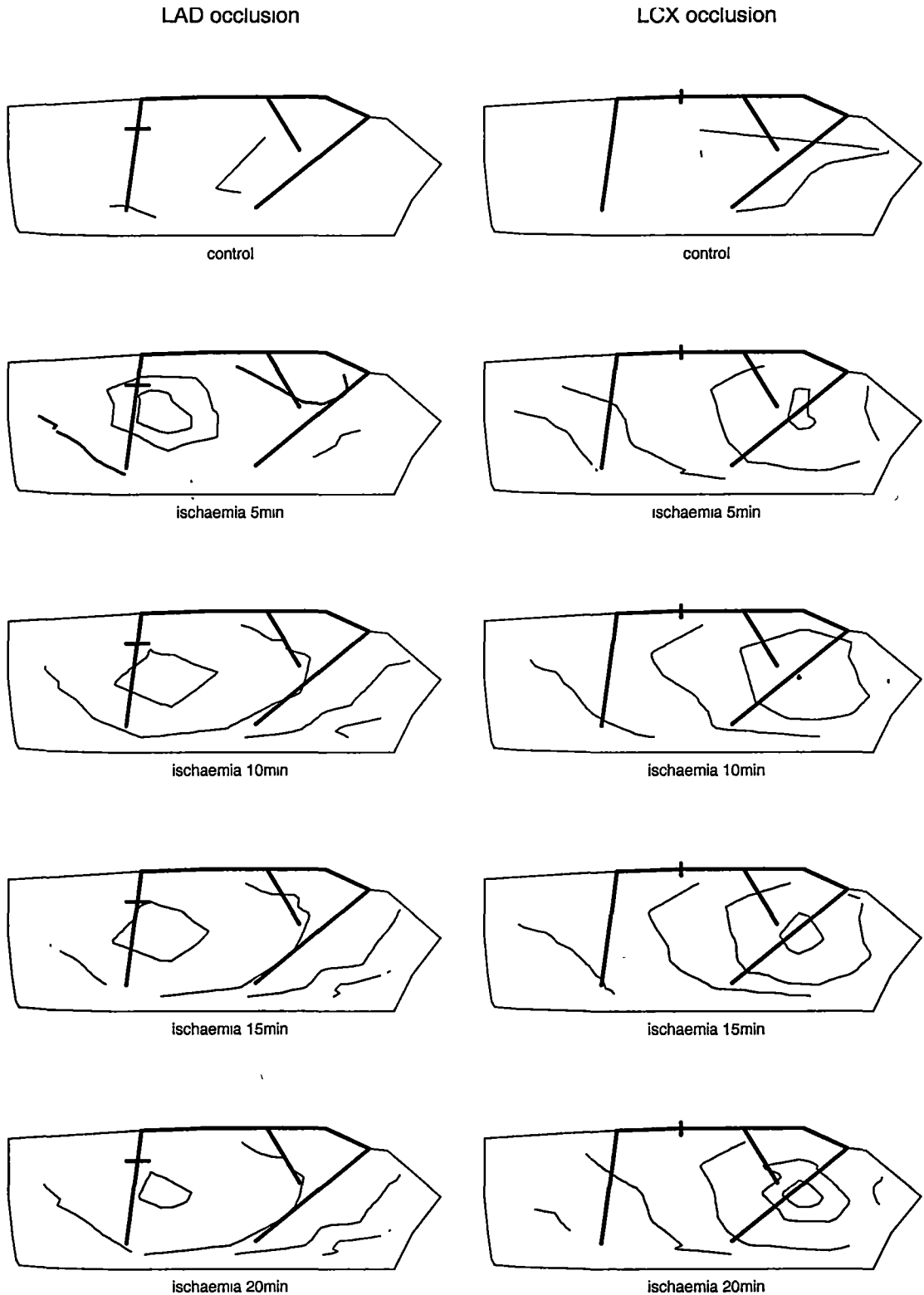


Fig. 4.9.5 Endocardial ST potential distributions at control and at various time periods in subendocardial ischaemia in alternation of LAD and LCX area. The thickest solid lines reflect the position of coronary arteries, the thick solid lines indicate zero potential, the thin solid and dashed lines indicate ST elevation and ST depression respectively. The occluded arteries are indicated by bars across the coronary arteries. Maps are plotted from the data of one animal from group 4. Contour interval=0.2mV.

4.2.3.4 Relationship between ST potential distribution and RMBF in subendocardial ischaemia

Relationship between ST potential distribution and RMBF in subendocardial ischaemia in either LAD or LCX area

RMBF was measured before and after 20min of ischaemia in every one-third layer of the heart. RMBF distribution image maps were plotted and combined with ST potential distribution contour maps. Epicardial and subepicardial ST potential distribution maps were combined with maps of RMBF of the outer one-third layer. Intramyocardial ST potential distribution maps of the mid one-third layer were combined with maps of RMBF of the mid one-third layer. Subendocardial and endocardial ST potential distribution maps were combined with maps of RMBF of the inner one-third layer. From Fig. 4.10 and Fig. 4.11, it can be seen that before subendocardial ischaemia, RMBF in every layer had an even distribution over the whole ventricle, and there were no significant ST potential shifts on any layer of the heart. At 20min of subendocardial ischaemia, RMBF in the ischaemic region was lower than that in the nonischaemic region, endocardial and intramyocardial ST elevation occurred in areas of reduced RMBF, intramyocardial ST depression occurred at the boundary of the ischaemic and nonischaemic areas, while epicardial ST depression was not related to RMBF change.

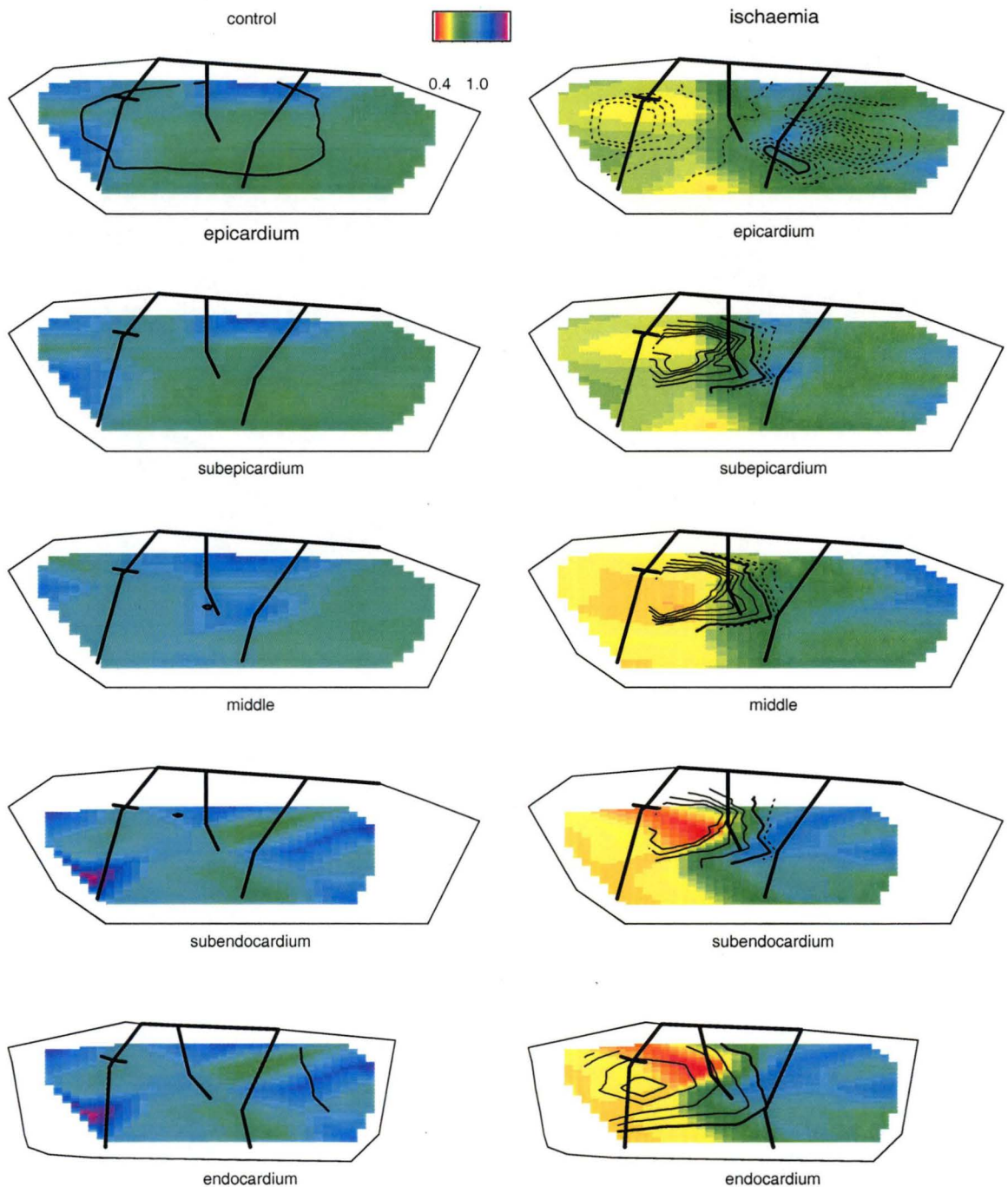


Fig. 4.10 Combination of ST potential distributions (contour lines) and RMBF distributions (shaded area, ml/min/g) in different layers of the heart at control and at 20min of subendocardial ischaemia in LAD area. From top to bottom:

Combination of epicardial ST potential distribution and RMBF distribution of outer 1/3 layer;

Combination of subepicardial ST potential distribution and RMBF distribution of outer 1/3 layer;

Combination of mid layer ST potential distribution and RMBF distribution of mid 1/3 layer;

Combination of subendocardial ST potential distribution and RMBF distribution of inner 1/3 layer;

Combination of endocardial ST potential distribution and RMBF distribution of inner 1/3 layer.

The intensities of the shade indicate the quantity of flow. The thickest solid lines reflect the position of the coronary arteries, the thick solid lines indicate zero potential, the thin solid and the dashed lines indicate ST elevation and ST depression respectively, with the occluded arteries indicated by bars across the coronary arteries. Maps are plotted from data of one of the animals in group 2. Contour interval is same as Fig. 4.4.

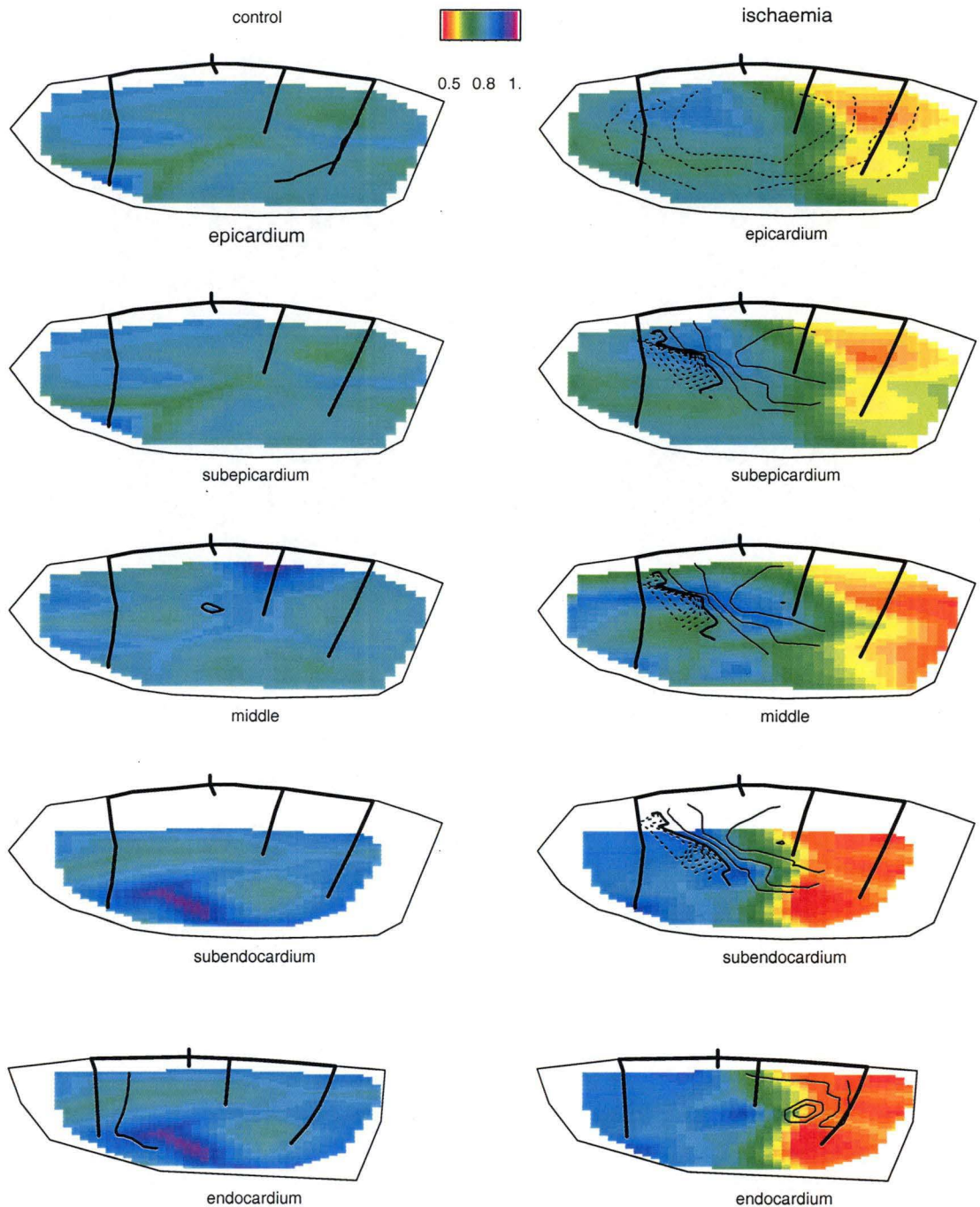


Fig. 4.11 Combination of ST potential distributions (contour lines) and RMBF distributions (shaded area, ml/min/g) in different layers of the heart at control and at 20min of subendocardial ischaemia in LCX area. From top to bottom:

Combination of epicardial ST potential distribution and RMBF distribution of outer 1/3 layer;

Combination of subepicardial ST potential distribution and RMBF distribution of outer 1/3 layer;

Combination of mid layer ST potential distribution and RMBF distribution of mid 1/3 layer;

Combination of subendocardial ST potential distribution and RMBF distribution of inner 1/3 layer;

Combination of endocardial ST potential distribution and RMBF distribution of inner 1/3 layer.

The intensities of the shade indicate the quantity of flow. The thickest solid lines reflect the position of the coronary arteries, the thick solid lines indicate zero potential, the thin solid and the dashed lines indicate ST elevation and ST depression respectively, with the occluded arteries indicated by bars across the coronary arteries. Maps are plotted from data of one of the animals in group 3. Contour interval is same as Fig. 4.5.

Relationship between ST potential distribution and RMBF in subendocardial ischaemia during alternative ligation of the LAD and LCX

RMBF was measured after 20min of ischaemia in both the LAD and LCX ligation in every one-third layer of the heart. RMBF distribution image maps were plotted and combined with ST potential distribution contour maps in the same way as that in the previous section (Fig. 4.10 and Fig. 4.11). Fig. 4.12 shows RMBF in the ischaemic region is lower than that in the nonischaemic region, no matter whether the LAD or LCX was ligated. Endocardial and intramyocardial ST elevation occurred in areas of reduced RMBF. Intramyocardial ST depression occurred at the boundary of ischaemic and nonischaemic areas. Finally, epicardial ST depression was not related to RMBF change.

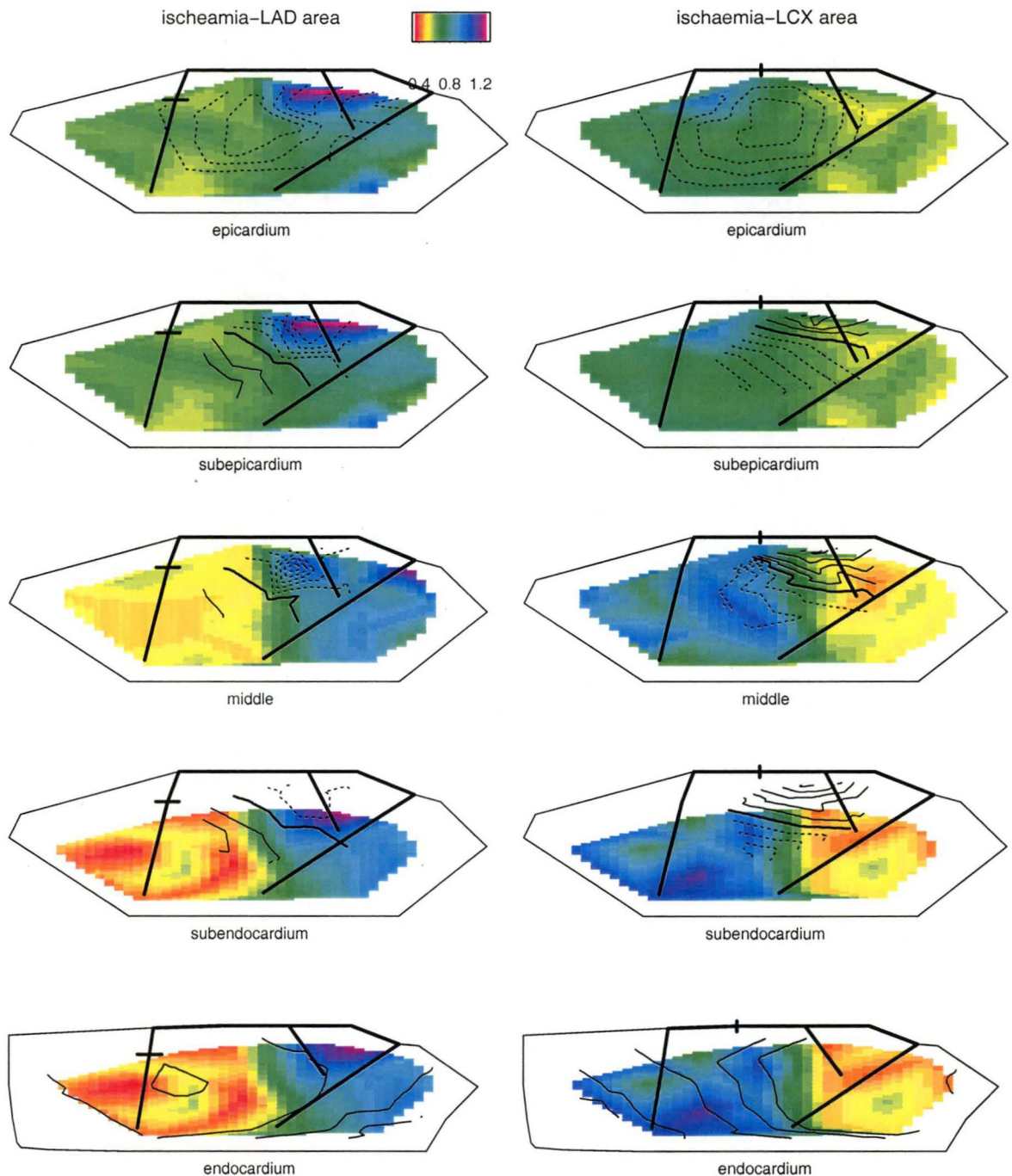


Fig. 4.12 Combination of ST potential distributions (contour lines) and RMBF distributions (shaded area, ml/min/g) in different layers of the heart at 20min of subendocardial ischaemia in alternation of LAD and LCX ischaemia. From top to bottom:

Combination of epicardial ST potential distribution and RMBF distribution of outer 1/3 layer;

Combination of subepicardial ST potential distribution and RMBF distribution of outer 1/3 layer;

Combination of mid layer ST potential distribution and RMBF distribution of mid 1/3 layer;

Combination of subendocardial ST potential distribution and RMBF distribution of inner 1/3 layer;

Combination of endocardial ST potential distribution and RMBF distribution of inner 1/3 layer.

The intensities of the shade indicate the quantity of flow. The thickest solid lines reflect the position of the coronary arteries, the thick solid lines indicate zero potential, the thin solid and the dashed lines indicate ST elevation and ST depression respectively, with the occluded arteries indicated by bars across the coronary arteries. Maps are plotted from data of one of the animals in group 4. Contour interval is same as Fig. 4.8.

4.3 DISCUSSION

4.3.1 SUBENDOCARDIAL ISCHAEMIA MODEL

This study was based on a successful subendocardial ischaemia model. The subendocardial ischaemia model in this study was constructed by partially occluding the coronary artery together with pacing the atrium at a rate of 180bpm, which was previously validated in our laboratory by fluorescent microspheres (Li et al., 1996). The design of this model was based on the principle of the clinical exercise stress test for detecting coronary artery disease. In circumstance of an insufficient coronary blood supply occurring, when the myocardial oxygen demand increases, then a transient subendocardial ischaemia will be produced. In animal experiments, pacing the heart at a specific rate reliably produces ischaemia of the subendocardium when the artery is narrowed to 50% of the original. These all increase the oxygen demand of the heart (Mirvis and Gordey, 1983; Heller et al., 1984).

Myocardial perfusion is spatially heterogeneous. Studies showed that the RMBF of subendocardium was about 20% to 40% higher than that of subepicardium in sheep and lamb (Archie et al., 1974; Fisher et al., 1980 and 1984; Li et al., 1996). However, cardiac ischaemia always begins from the subendocardium, with the increase of duration of coronary artery occlusion, a transmural “wavefront” of cell death progress from the subendocardium to the subepicardium (Reimer et al., 1977; Reimer and Jennings, 1979). Jennings (Jennings et al., 1985) observed in their study of coronary artery occlusion in dogs that the subendocardial region died quickly because it was severely ischaemic (flow $<0.15\text{ml/min/g}$ and that the epicardial region died more slowly because it was usually moderately ischaemic (flow $0.15\sim0.30\text{ml/min/g}$) or mildly ischaemic (flow $>0.3\text{ml/min/g}$). Similar temporal evolution of myocardial infarctions, beginning in the subendocardial region, and only later involving the subepicardial region, was observed in other experimental models of abrupt coronary occlusion of different species (Schaper et al., 1979; Baughman et al., 1981; Lee et al., 1981; Connelly et al., 1982; Fujiwara et al., 1982; Geary et al., 1982; Warltier et al., 1982; Kloner et al., 1983; Klein et al., 1984). In human studies of myocardial infarction, the ischaemic damage was either entirely subendocardial or, in transmural infarction, was confluent and maximal in the subendocardium and less extensive in the subepicardium (Freifeld et al., 1983).

By occluding the coronary artery to 50% of the original blood flow level, Li and co-workers (1996) produced subendocardial ischaemic sheep model, which was

evidenced by, as previously reported (Guyton et al., 1977; Mirvis et al., 1986; Mirvis and Kamanathan, 1987), the reduction in the endocardial/epicardial (endo/epi) flow ratio in the ischaemic area caused by a decrease in subendocardial flow without significant changes in subepicardial perfusion.

In this study, RMBF was measured in three different layers of the heart, i.e., inner one-third layer, middle one-third layer and outer one-third layer of the heart, by using fluorescent microspheres. After 20min of partial occlusion of coronary artery plus atrium pacing, RMBF in every layer of the heart in ischaemic area reduced, with endo/epi ratio reduced from 1.16 ± 0.08 before ischaemia to 0.77 ± 0.10 after ischaemia, suggested a more severe ischaemia in subendocardium. Although pacing the heart itself to 180bpm increased RMBF in every layer of the heart, especially blood flow in the inner layer, the differences were not significant.

Using fluorescent microspheres has been verified to be a reliable method to measure RMBF (Li et al., 1996), and it is comparable to radioactive microspheres method which has been regarded as a "gold standard" of measuring RMBF (Abel et al., 1993; Glenney et al., 1993).

From the results it can be seen that the subendocardium is more vulnerable to ischaemia. There is a tendency for greater oxygen usage or lower oxygen tensions in subendocardial than epicardial muscle. Subendocardial muscle might use more oxygen, it might be more easily damaged by a decreased oxygen supply, or it might more readily become underperfused. There is evidence that subendocardial oxygen consumption per unit weight is normally about 20% higher than that of subepicardial muscle (Weiss et al., 1978; Weiss, 1979). Some investigators have argued that this increase is due to greater work done by subendocardial muscle fibres, which shorten more in systole than do those in the subepicardium (Yoran et al., 1973). Compared with subepicardial muscle, subendocardial muscle has lower venous oxygen saturations (Weiss et al., 1978) and oxygen tensions (Winbury et al., 1971). Apart from the effect of blood flow, biochemical studies also indicated a transmural gradient of metabolites during coronary artery occlusion in the dog, where the subendocardium was more vulnerable biochemically to ischaemic injury than was the subepicardium (Griggs et al., 1972). And, in studies in which myocardium was made totally ischaemic in vivo with no transmural blood flow gradient, ultrastructure and metabolic features of cell injury occurred more quickly in the subendocardial region than in the subepicardial region (Lowe, 1983).

4.3.2. POTENTIAL RECORDING METHOD

In this study, potential distributions were recorded simultaneously from epicardium, endocardium and three different layers in the intramyocardium.

A 64-electrode sock, with each electrode constructed with a fine silver wire mounted on a nylon sock, was used to record the epicardial potential distributions (Cardiovascular Research and Training Institute, the University of Utah, USA).

Epicardial potential recording was first used to define patterns of ventricular activation in the Wolff-Parkinson-White syndrome (Gallagher et al., 1975). Similar procedures were employed in investigations of other disturbances of rhythm such as ventricular tachycardia (Gallagher, 1978; Harken et al., 1979). The initial epicardial potential recording approach was a single hand-held recording electrode which was positioned over an area of myocardium and electrical activity was recorded from that area. By moving the electrode sequentially to a series of sites over the entire ventricular surface, eventually enough data could be gathered. However, the data gathered was from different cardiac cycles and might be misleading, and it took at least 5min to get enough data to construct a map.

The use of the sock electrodes made it possible to obtain data simultaneously from numerous epicardial sites during a single cycle. The usefulness of the sock electrode array has been enhanced by the development of the computer system for rapid analysis and display of cardiac potentials (Smith et al., 1980; Walker et al; 1983). In this study, the cardiac potentials were recorded by a home-made 256-channel system (BDDD-Binary Data Delivery Device). A sample and hold on the output of each amplifier allowed the signal at all electrodes to be sampled simultaneously, and an immediate display of the sampled electrocardiographic signals enabled a check on the quality of the data.

The sock electrode is a useful tool in both experimental and clinical studies. It is flexible and easily positioned around the heart. The nylon mesh can closely envelop the heart without damaging the epicardium, and it can be quickly applied to the heart and can remain in place throughout the experiment. The arrangement of the electrodes provides coverage of the epicardial surface of the whole left and right ventricles.

Endocardial mapping data is essential for localizing some arrhythmia site and for the study of ischaemic heart disease. Invasive needles inserted through the myocardial wall and anchored on the endocardial surface were used in the earliest study of arrhythmia (Scherlay et al., 1963; Smith et al., 1979). This method had great disadvantage for the following reasons. Apart from causing damage to the heart muscle, a limited number of endocardial electrodes can be used. Multiple-electrode array catheters were introduced later and could be introduced percutaneously to the endocardial site (Josephson et al., 1982; Browne et al., 1983). This method avoided damage to the heart, but again, a limited number of electrodes can be used, and further more, the electrodes did not cover the whole surface of the endocardium.

By using an endocardial basket which had 8 arms, each arm with five electrodes on it, Li and co-workers (1999) successfully recorded the global endocardial potential distributions by inserting the basket from the cardiac apex to the cavity where the basket became inflated. A similar basket catheter was used by Zrenner (Zrenner et al., 1999) in his study of atrial arrhythmias.

In present study, the endocardial potentials were recorded by an oval basket similar to Li's (Li et al., 1999). The 40-electrode on the basket covered nearly the whole surface of the endocardium and the information provided by the electrodes should be enough to analyse the cardiac activity. The electrodes on the basket were not in direct contact to the endocardial surface to avoid potential disturbance. Although insertion of the basket from the heart apex would cause damage to the heart, the hydrodynamics did not deteriorate while inserting the basket, and it did not provoke cardiac arrhythmias, no injury current occurred during the entire process.

Information from intramyocardial electrodes is vital in understanding the current flowing at the ischaemic boundaries in this study. Intramyocardial needles with a diameter of 0.9mm were used in our laboratory to record potentials in previous experiments but were always subject to injury currents which prevented their use for ST segment analysis (Li, 1997). Techniques were tried to partially insulate the needle to prevent the metal from direct contact with the heart muscle, but this manipulation did not avoid the injury currents. Plunge needles made of different materials including: nickel, tungsten, silver, copper and stainless steel were tested to record the intramyocardial potentials. It was found that the tungsten, nickel and the silver needle electrodes caused less injury currents. Compared to tungsten and nickel, silver seemed to be a better material for the plunge needles in our experiments. As the sock

electrodes and the basket electrodes were all made of isolated silver wire, so isolated silver wire of a diameter of 0.147mm was chosen for the construction of the plunge needle. A series of research designed to study the mechanism of cardiac arrhythmia, the intramyocardial plunge needles were usually made of tungsten material (Kasell and Gallagher, 1977; Kramer et al., 1985; Pogwizd and Corr, 1987, Wu et al., 1995). Whatever material was used, the purpose was to minimize the injury currents.

Haemodynamic measurements during experiments suggested that the insertion of the needles into cardiac wall did not cause significant haemodynamic deterioration and did not provoke cardiac arrhythmia.

Recently, a fiberglass needle electrode for transmural cardiac mapping has been constructed by Rogers (Rogers et al., 2002). These needles had 12-electrode with 1mm spacing apart and were fabricated from fiberglass-reinforced epoxy. The characters of these needles were: They were much thinner than the traditional plunge needles (Kasell and Gallagher, 1977; Witkowski and Penkoske, 1988; Moore et al., 1990), and were stiff enough to be easily inserted into the heart and durable enough to be reused, and they were also nonconductive. These needles were well suited to record intramyocardial electrical activities from high-resolution arrays. However, the construction of these needles was technically difficult. We have looked at optical methods but these are currently not suitable because the interface of interest is intramyocardial and would be disturbed by implanting optical arrays. Multiple optic fibre sensors may become available but the voltage sensitive dyes are relatively toxic and not appropriate at this stage.

4.3.3 POTENTIAL DISTRIBUTIONS AND INTRAMYOCARDIAL ELECTRICAL CURRENT PATH

The main finding of this study is that even though epicardial ST depression can not predict ischaemic area as previously validated (Li et al., 1998), ST distribution patterns in different layers of intramyocardium during subendocardial ischaemia can be predicted from electrocardiographic theory. The ST potential distributions between epicardium and subepicardium are markedly different.

It was well accepted that ST elevation in ECG over the ischaemic area is a sign of myocardial ischaemia. Classic electrocardiographic theories offered to explain the changes which occur in the ST segments during myocardial ischaemia based on the supposition that a boundary might exist between a region of normal and damaged

cells and that an abnormal current might flow between the ischaemic area and normal area. Wilson (Wilson et al., 1933b) and Bayley (1942) proposed that ST elevation during myocardial ischaemia was a manifestation of this injury current, and Wilson (Wilson et al., 1933a) classified injury currents into two types: injury current at rest or diastolic injury current, and injury current of action or systolic injury current. At a cellular level, two major mechanisms are considered to underlie the injury currents: (1) a localized shortening of action potential duration and diminishing of the amplitude of the action potential and (2) a localized decrease in resting membrane potential. The former generates a systolic injury current flowing from the normal tissue to the injured tissue, produces “primary ST elevation” in the surface ECG. The latter generates a steady injury current that is interrupted during the ST segment when all the cells are depolarized. The injury current produces a TQ segment depression, which can not be directly detected on the surface ECG because the amplifiers are AC-coupled, and it is represented by ST elevation (secondary ST elevation)

The origin of ST depression is far from clear from up to date research. Early work (Wolferth et al., 1945; Bayley, 1946; Pruitt and Valencia, 1948) in isolated hearts suggested that the ST segment response to myocardial injury was elevation and that the ST depression recorded at the epicardium was the reciprocal of ST elevation in the underlying subendocardium. This verified the dipole theory (Wilson et al., 1933b; Pruitt and Valencia, 1948). The dipole model considered the active myocardial event as a single dipole source that contained both the maximum and the minimum potentials. Accordingly, an injured region of the myocardium acts in systole as the positive pole of a layer of dipoles situated on its boundary with normal myocardium, whereas the latter acts as the negative pole.

According to the dipole theory, in the event of subendocardial ischaemia, the epicardium over the ischaemic region faces the negative pole of the dipole; the cavity faces the positive pole. Thus, the electrodes over the ischaemia should record depressed ST segments, and the cavity should recorded elevated ST segments (Bayley, 1946; Yu, 1950; Cook et al., 1958). However, clinically, it is difficult to localize the ischaemic region by surface ST depression. In the present study of subendocardial ischaemia, even though ST depression occurred on epicardium and ST elevation occurred on endocardium, the epicardial ST depression was scattered on the left ventricular surface and could not localize the ischaemic area. Either LAD or LCX ischaemia gave a similar epicardial ST distribution pattern, whereas endocardial ST potential distribution pattern showed that ST elevation was directly associated

with the ischaemic area. These results are consistent with previous studies in this laboratory (Li et al., 1998). Thus, using the dipole theory to explain the ST depression in subendocardial ischaemia has its limitation. The limitations of the single dipole model have been demonstrated (Schmitt et al., 1953; Okada et al., 1959; Scher et al., 1960) and discussed (Holland and Arnsdorf, 1977; Okada, 1963; Horan and Flowers, 1972; Clark and Plonsey, 1966).

Prinzmetal and coworkers (Prinzmetal et al., 1959 and 1961, Ekmekci et al., 1961; Toyoshima et al., 1964) proposed that ST depression was a primary effect of abnormal membrane polarization rather than a reciprocal effect of ST elevation. Using a canine model, Prinzmetal and co-workers recorded relative ST segment depression (true TQ segment elevation) from the epicardium of “mild” ischaemic areas produced by severe haemorrhagic hypotension. The TQ segment elevation coincided with the increase in membrane resting potential. They suggested that mild subepicardial ischaemia might generate ST depression independent of subendocardium damage. But their model was not a real subendocardial ischaemia model and the “mild” ischaemia could not be validated.

The present study showed that during subendocardial ischaemia, RMBF of ischaemic area decreased, particularly in the inner one-third layer of the left ventricular wall. The endocardial ST elevation was related to the ischaemic area, while the epicardial ST depression had no relation to RMBF of subepicardium. It suggested that the source of the ischaemic ECG was related to the endocardium, that was, the ischaemic source was related to the endocardial ST change but not the epicardial ST change, which was consistent with our previous model study (Li et al., 1998) and Kleber’s (Kleber et al., 1978) work on intracellular recording. However, this finding can not be interpreted by the solid angle theory.

The solid angle theory, by taking into account the geometry of the ischaemic boundaries, the degree of transmembrane or action potential duration differences, and alterations in intracellular and extracellular conductivities, has provided a geometrical ischaemic heart model that quantitatively links changes in ST shifts to the distribution of transmembrane potential changes in the ischaemic region. This model predicts that subendocardial ischaemia would cause relative depression of the ST segment in the epicardium and precordium due to the reversed current flow at the boundary of the normal and the ischaemic myocardium (Holland and Brooks, 1975 and 1977) and that this ST depression should provide the means for localizing ischaemia, which can not

be verified by previous study (Li et al., 1998) and the present study. Li's experiment was replicated by a mathematical model of the whole heart. This model showed that there was a powerful current sink at the boundary of the ischaemic and non-ischaemic areas. It was this current sink that caused the epicardial ST depression. When the ischaemia was subendocardial, no matter which side of the boundary, there was ST depression over the boundary on the epicardium. This model gave no clue as to why the currents were concentrated at the boundary. A further bidomain model was constructed by Johnson (Johnson et al., 2001). In this model, a slab of cardiac tissue was presented where tissue anisotropy and fibre rotation were considered and it was concluded that it would be possible to predict the region of subendocardial ischaemia from the epicardial potential distribution, which was contrary to the experimental data.

Insulating the heart from surrounding tissue showed that the source of the ST depression was intramyocardial (Green et al., 1991; Li et al., 1998). These researchers showed that when the heart was surrounded by an insulating medium, the magnitude of QRS or ST potentials increased while the QRS or ST potential distribution pattern had not change. Further research was done by the transition of subendocardial ischaemia to transmural ischaemia, the results indicated that epicardial ST depression increased gradually over the boundary region as ischaemia progressed and ST elevation ensued over the ischaemic region as ischaemia became transmural (Guyton et al., 1977; Li et al., 1998). The electrical transition from ST depression to ST elevation was consistent with the contention that the current path was in the myocardium.

Thus, detailed information of the electrical field around the ischaemic boundary was needed. To record the potential distributions around the ischaemic boundary, intramyocardial electrodes are needed. Our self-made plunge needles enable us to record intramyocardial potential distributions from different layers of the left ventricle. The needles were randomly plunged into the left ventricle muscle of the experimental sheep, with a high density around the boundary of the ischaemic and non-ischaemic regions. The needle positions were marked at the end of each experiment, which were used for the potential distribution maps construction. The total 29 needles used in the experiments gave enough information from the intramyocardium for potential mapping purpose. Even though insertion of the needles into the heart muscle resulted in injury current initially, this injury current decreased with time, and approached to the isoelectrical line at least 1~1.5 hours following the insertion. Potentials were recorded after 1.5 hours of insertion of the needles. The

present study was carried out to measure potentials from intramyocardial electrodes together with the epicardial and endocardial electrodes. Our results showed that in the intramyocardium, both ST elevation and ST depression occurred in different layers from subendocardium to subepicardium, with the source appeared in the ischaemic area and the sink appeared in the non-ischaemic area, and the peak ST elevation occurred in the center of the ischaemic area, the distributions of the ST potential among the three intramyocardial layers were quite similar, only that ST depression extended slightly towards the ischaemic area from subendocardium to subepicardium. Analyses of ST potential magnitude in different intramyocardial layers showed that ST potential magnitude did not change significantly after the onset of ischaemia. Only negative ST potential magnitude in outer one-third layer at 5min, 10min and 15min after ischaemia was relatively lower compared to that in inner one-third layer. The similarity of ST potential distributions and magnitudes in different intramyocardial layers is beyond our understanding. When subendocardial ischaemia was alternated between the LAD and LCX areas, ST potential distributions and magnitude were similar to that of subendocardial ischaemia in either LAD or LCX area. These results suggested that the intramyocardial current path had little change in different intramyocardial layers. The different manifestation of epicardial and subepicardium ST distributions to ischaemia leads us to postulate that there might be an electrically different structure under the epicardium, which might result in the distortion of current path.

The different potential distributions between the epicardium and intramyocardium lead us further to a hypothesis that there might be an electrically different structure under the epicardium. As has been proposed by Wilensky (Wilensky et al., 1986) in their study of acute ischaemia in rabbit, they found that an endocardial zone of a 40~60 cell layer existed in which transmembrane potentials were affected relatively little by ischaemia, and extracellular K^+ , pH and content of phosphocreatine were quite different than that in the rest of the myocardium. Our hypothesized subepicardial structure might have different electrical characteristics which might disturb the electrical current path. However, no studies have been shown that this hypothetical structure existed yet.

We propose that the anisotropy of the cardiac muscle may result in the electrical current path diversion. By considering the impedance difference between ischaemic and normal heart tissues during ischaemia, it is likely that the injury current might divert its way when spreads outwards.

It is known that the cardiac muscle is anisotropic. The human cardiac cells are branched at their ends, the branching cardiac cells set up a complex three-dimensional geometry. At the gross anatomical level, the ventricles of the heart are composed of spiraling layers of fibres running in different directions. Even though the sheep cardiac cells might have different orientation as human's, from postmortem observation, it was found that the sheep cardiac fibres' orientation is also spiral from subendocardium to subepicardium. As a consequence, histological sections of ventricular muscle inevitably contains the profiles of cells cut in a variety of orientations.

It was reported that wavefront velocity would be influenced by fibre direction (Sano et al., 1959; Draper and Mya-Tu, 1959; Clerc, 1976; Roberts et al., 1979). Early work by Rush (Rush et al., 1963) showed a slight anisotropy of about 2:1 with a high resistivity value of 563ohm-cm and a low resistivity value of 252ohm-cm. Gorbin and Scher (1977) found that the fibre direction was important in determining potentials at a distance from the electrical source. Using an empirical axial hypothesis model, Gorbin and Scher predicted a strong dependence of wavefront voltage on fibre orientation. Roberts (Roberts et al., 1978) further analysed the influence of cardiac fibre orientation on wavefront voltage, conduction velocity and tissue resistivity in the dog. Their study disclosed that when the canine epicardium was stimulated, the spread of epicardial excitation was 2.4 times faster along the long axes of the cardiac fibres than perpendicular to them, the gross tissue resistivity was lower parallel to fibres by a factor of 3.2, and the voltage across the depolarization wave was approximately three times as great in the longitudinal direction. It indicated that there was a strong dependence between epicardial fibre direction, conduction velocity, resistivity of the myocardium and the surrounding potential field generated by a wave of depolarization.

Further study by Roberts and Scher (1982) by taking into account the tissue anisotropy in a mathematical model showed that the anisotropy of the electrical conductivity of cardiac muscle had important effects on the propagation of waves of depolarization and on the potential fields produced by depolarization in the intact heart. They found that the extracellular voltage drop across a propagating depolarization wave depends on the direction of propagation. The measured extracellular voltage across a longitudinal wave was 1.75 ± 0.12 times greater than the voltage across a transverse wave.

Recently, it was found that the myocardial electrical impedance varied in normal, ischaemic and infarcted tissue. Fallert (Fallert et al., 1993) measured the electrical impedance of myocardial tissue in a sheep model of infarction by using a four-electrode probe, it showed that the impedance was a bulk electrical property of tissue that varied with the evolution of myocardial infarction. Impedance mapping revealed significantly different values for normal, ischaemic and infarcted tissues. Previous studies also showed that hypoxia would lead to an increase in longitudinal resistance (Woitczak, 1979; Hiramatsu et al., 1988).

However, if the tissue anisotropy and impedance would play an important role on electrical current path, the potential distribution in different layers of the heart should show regular change, which is not apparent in present study. This postulation is not supported by the fact that ST distribution and magnitude in different intramyocardial layers were quite similar.

CHAPTER FIVE

INTRAMYOCARDIAL ST SEGMENT POTENTIAL
DISTRIBUTIONS: TRANSITION FROM MILD
SUBENDOCARDIAL ISCHAEMIA TO SEVERE
SUBENDOCARDIAL ISCHAEMIA

Intramyocardial ST potential distributions in subendocardial ischaemia were described fully in chapter 4. It can be concluded that the intramyocardial ST potential distributions were quite different from that of epicardium and endocardium, the negative ST potential originated on the boundary of the ischaemic and non-ischaemic regions in intramyocardium, the positive ST potential of intramyocardium was blocked when trying to spread along the path to epicardium. To further understand what happened in the intramyocardium during subendocardial ischaemia, a series of experiments were performed to convert mild subendocardial ischaemia to severe subendocardial ischaemia.

5.1 MATERIALS AND METHODS

5.1.1 EXPERIMENTAL ANIMALS AND PROTOCOLS

A total of 6 (Polworth/Comeback cross) sheep weighing between 27~35kg of both genders were used. All the sheep were bred in the University of Tasmania’s animal farm. Table 5.1 shows the groups of animals subjected to different experimental protocols.

Table 5.1 Experimental protocol

group	animal number	experimental protocol
1	3	transition from mild subendocardial ischaemia to severe subendocardial ischaemia in LAD area.
2	3	transition from mild subendocardial ischaemia to severe subendocardial ischaemia in LCX area.

group 1: Transition from mild subendocardial ischaemia to severe subendocardial ischaemia in LCX area (n=3).

group 2: Transition from mild subendocardial ischaemia to severe subendocardial ischaemia in LAD area (n=3).

5.1.2 EXPERIMENTAL PROCEDURES AND SUBENDOCARDIAL ISCHAEMIA

Experimental procedures were the same as in chapter 4. A sheep model of subendocardial ischaemia was made by combining pacing with partial occlusion of a coronary artery. Mild subendocardial ischaemia was produced by reducing either LAD or LCX blood flow by 30% of the original blood flow plus left atrial pacing at a rate of 180bpm, and was continued for 20 minutes. After a stable period of 30 minutes, severe subendocardial ischaemia was produced by reducing either LAD or LCX blood flow by 70% of the original blood flow plus left atrial pacing at a rate of 180bpm, and also lasted for 20 minutes. 30 minutes after severe ischaemia, either LAD or LCX was totally occluded for another 20 minutes. One sheep developed ventricular fibrillation after severe subendocardial ischaemia and was unable to be rescued. The left atrium was paced by a stimulator starting with a rate of 120bpm, and increased gradually by 10bpm every 2 minutes until it reached 180bpm.

5.1.3 RMBF MEASUREMENT

As described in chapter 4, RMBF were measured before ischaemia, 20min after mild subendocardial ischaemia, 20min after severe subendocardial ischaemia and 20min after total occlusion of a coronary artery.

5.1.4 POTENTIAL RECORDINGS AND MAP CONSTRUCTION

Potential recordings and map construction are described as in chapter 3 and chapter 4. ST potentials were simultaneously recorded before and 5min, 10min, 15min, 20min after ischaemia of varying degrees on epicardium, endocardium and three different depth of intramyocardium.

5.2 RESULTS

5.2.1 HAEMODYNAMIC RESPONSE

In mild subendocardial ischaemia group, LVDP, LVSP, LAP and CAP did not change with ischaemia. In the severe subendocardial ischaemia group, LVDP and LAP were significantly increased ($P<0.05$), LVSP and CAP were significantly decreased from control ($P<0.05$). Complete occlusion of the coronary artery resulted in a significant LVDP and LAP increase ($P<0.001$, 0.05 respectively) and also significant LVSP and CAP decrease ($P<0.001$), (Table 5.1).

Table 5.1 Haemodynamic response to subendocardial ischaemia from mild to severe degree (n=6)

	control	mild subendocardial ischaemia	severe subendocardial ischaemia	full thickness ischaemia
LVDP, mmHg	-5.17 ± 3.54	-2.33 ± 3.14	$-0.17 \pm 3.49^*$	$12.00 \pm 5.10^{**}$
LVSP, mmHg	112.00 ± 10.30	97.50 ± 22.08	$90.00 \pm 16.73^*$	$51.00 \pm 19.34^{**}$
LAP, mmHg	1.39 ± 3.90	5.01 ± 5.04	$8.81 \pm 6.17^*$	$16.33 \pm 11.26^*$
CAP, mmHg	96.39 ± 7.56	83.89 ± 21.18	$71.39 \pm 17.43^*$	$45.20 \pm 16.00^{**}$

LVDP: left ventricular diastolic pressure

LVSP: left ventricular systolic pressure

LAP: left atrial pressure

CAP: carotid artery pressure

*Compared to control group: * $P<0.05$, ** $P<0.001$.*

5.2.2 RMBF RESPONSE

In the mild subendocardial ischaemic group, the RMBF in the inner one-third layer and endo/epi ratio decreased significantly from control ($P<0.05$, 0.001 respectively), while the RMBF in the mid and outer one-third layers showed no significant change ($P>0.05$). In the severe subendocardial ischaemic group, the RMBF in every layer of the heart and endo/epi ratio were significantly decreased from control ($P<0.001$). Compared with the mild ischaemic group, the RMBF in every layer in severe ischaemia group decreased significantly in the ischaemic area ($p<0.001$), while the endo/epi ratio had no significant difference between these two groups ($p>0.05$). In the non-ischaemic area, the RMBF were unchanged, and the endo/epi ratio was identical between different groups ($P>0.05$) (Table 5.2, Fig. 5.1).

Fig. 5.2 and Fig. 5.3 show the RMBF distributions in subepicardium, mid and subendocardium layers during mild and severe ischaemia of either LAD or LCX occlusion respectively. It showed that there was a relatively distinct border of RMBF in the ischaemic and non-ischaemic regions.

Table 5.2 RMBF in mild and severe subendocardial ischaemia (n=6)

	control	mild ischaemia	severe ischaemia
ischaemic area			
epi	0.80±0.15	0.70±0.09	0.39±0.05**#
mid	0.82±0.15	0.67±0.08	0.37±0.05**#
endo	0.89±0.16	0.62±0.09*	0.34±0.05**#
trans	0.84±0.15	0.67±0.09*	0.37±0.05**#
ratio	1.11±0.04	0.89±0.05**	0.88±0.06**
non-ischaemic area			
epi	0.69±0.09	0.73±0.08	0.73±0.07
mid	0.76±0.07	0.76±0.07	0.76±0.07
endo	0.80±0.07	0.78±0.06	0.78±0.07
trans	0.75±0.06	0.76±0.06	0.75±0.06
ratio	1.17±0.19	1.07±0.11	1.07±0.10

epi. RMBF in outer one-third layer of LV wall mid. RMBF in middle one-third layer of LV wall

endo: RMBF in inner one-third layer of LV wall trans RMBF in full thickness of LV wall

ratio: ratio of RMBF of inner one-third layer and outer one-third layer of LV wall

*Compared with control group: * P<0.05, ** P<0.001*

Compared with mild ischaemic group: # P<0.001

Others: P>0.05

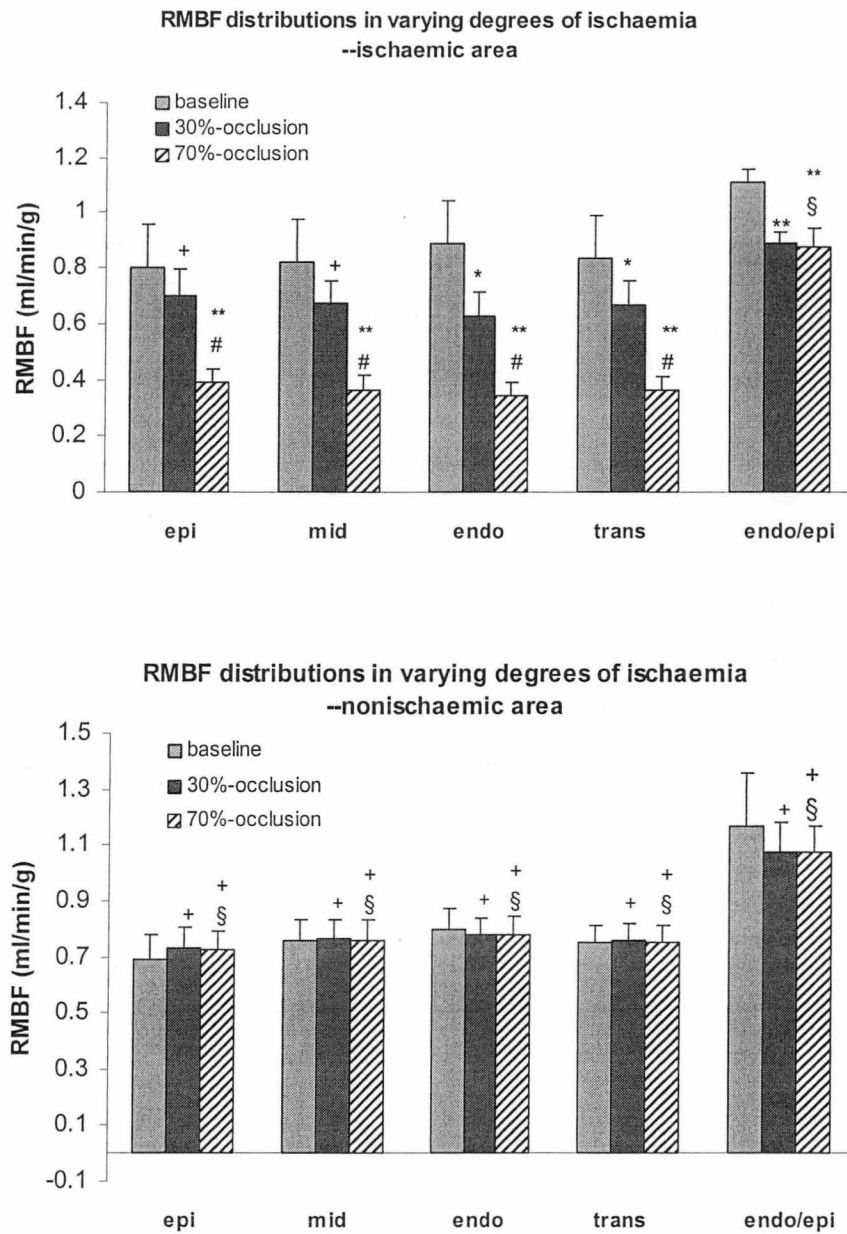


Fig. 5.1 EMBF distributions in mild subendocardial ischaemia, severe subendocardial ischaemia (see Table 5.2 for explanation).

Compared with baseline: ⁺ $p > 0.05$, ^{*} $p < 0.05$, ^{**} $p < 0.001$.

Compared with mild group: [§] $p > 0.05$, [#] $p < 0.001$.

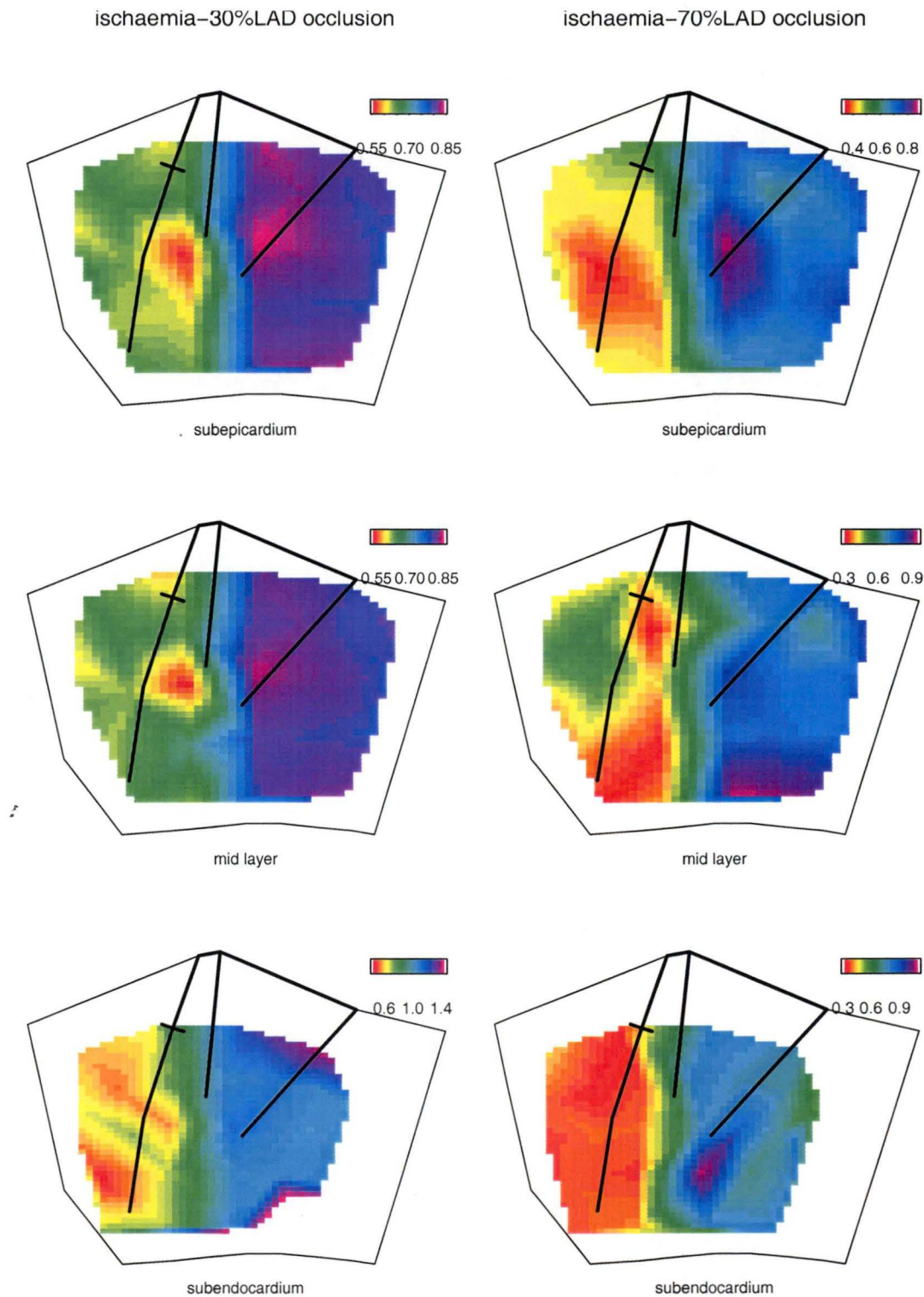


Fig. 5.2 Blood flow (ml/min/g) distributions in subepicardium, mid and subendocardium layers during mild and severe ischaemia of LAD occlusion. Notice the remarkable border at the ischaemic and non-ischaemic regions. Maps are plotted with data from group 1.

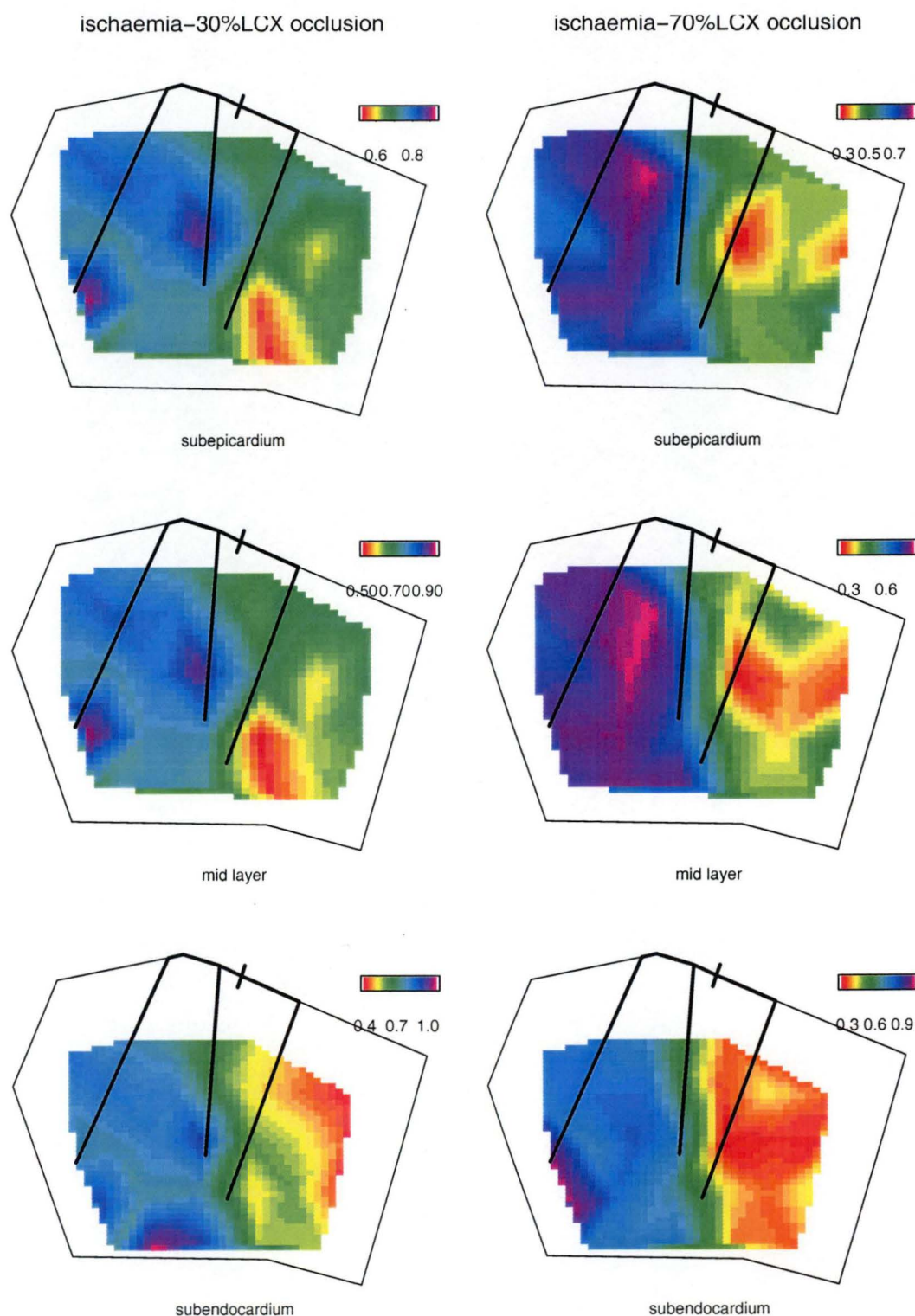


Fig. 5.3 Blood flow(ml/min/g) distributions in subepicardium, mid and subendocardium layers during mild and severe ischaemia of LCX occlusion. Notice the distinguish border at the ischaemic and non-ischaemic regions. Maps are plotted with data from group 2.

5.2.3 ST POTENTIAL DISTRIBUTIONS IN TRANSITION OF MILD SUBENDOCARDIAL ISCHAEMIA TO SEVERE SUBENDOCARDIAL ISCHAEMIA

Fig. 5.4 and Fig. 5.7 are contour maps showing ST distributions under three different degree of ischaemia. The imaging maps of Fig. 5.5, Fig. 5.8 give a more comparable view of the three groups. It showed that ST distribution pattern was quite similar in mild and severe ischaemia, except that in the mild ischaemic group, there was no ST elevation on epicardium. However, when ischaemia became full thickness, the ST distribution pattern was totally different. Fig. 5.6 and Fig. 5.9 showed the different patterns of ST distribution.

The results showed that in mild subendocardial ischaemia of either LAD or LCX ligation, ST potential distributions in different layers were similar to that in subendocardial ischaemia of 50% occlusion of coronary artery (results in chapter 4). In mild subendocardial ischaemic group, epicardial ST depression occurred after ischaemia, the epicardial ST depression was quite similar in either LAD or LCX group, and were not related to ischaemic region. Simultaneously recorded endocardial potentials showed ST elevation related to the area supplied by the culprit coronary artery. Intramyocardial ST potential recordings showed that ST elevation occurred in the ischaemic centre and ST depression occurred on the boundary of the ischaemic and non-ischaemic areas.

In severe subendocardial ischaemia of either LAD or LCX area, both ST elevation and ST depression occurred on epicardium and different layers of intramyocardium, ST elevation appeared in the ischaemic area, with the maximal magnitude occurred in the ischaemic centre; ST depression appeared in the non-ischaemic area. Endocardial ST elevation in severe ischaemia occurred in the ischaemic region.

When the ischaemia became full thickness, no matter which region was involved, there was a strong dipole in each layer of the heart. The distribution of the dipole was similar to that in severe subendocardial ischaemia. However, the highest magnitude of both ST elevation and ST depression occurred on the ischaemic boundary (Fig. 5.4~Fig. 5.9).

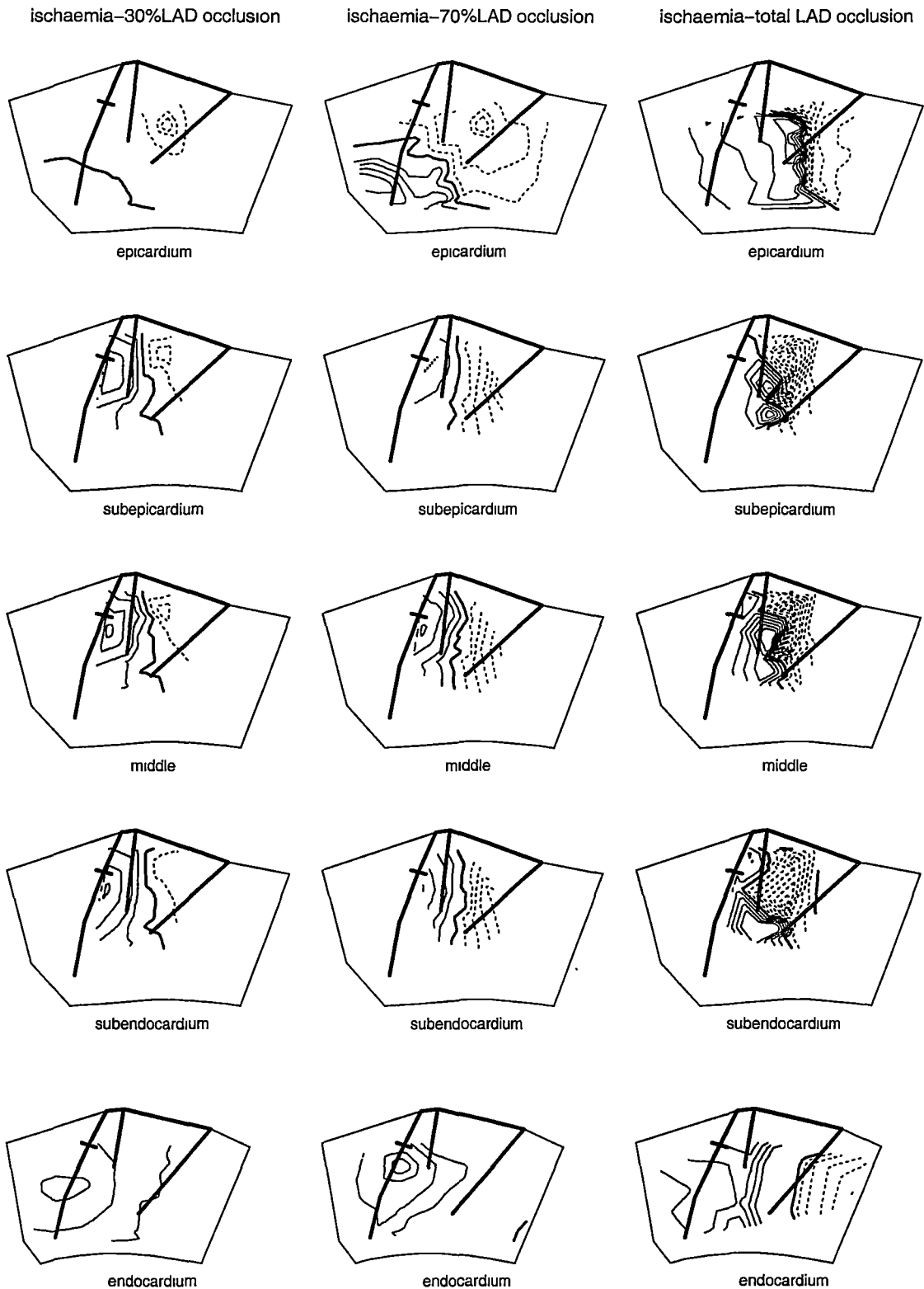


Fig. 5.4 ST potential distributions in different layers of the heart at 20min of mild subendocardial ischaemia, 20min of severe subendocardial ischemia and 20min of full thickness ischemia of LAD area. The thickest solid lines reflect the position of the coronary arteries, the thick solid lines indicate zero potential, the thin solid and dashed lines indicate ST elevation and ST depression respectively, with the occluded arteries indicated by bars across the coronary arteries. Maps are plotted from the data of one of the animals in group 1. For epicardium and intramyocardium (subepicardium, middle and subendocardium), contour interval=0.5mV; for endocardium in 30% occlusion, contour interval=0.2mV, for endocardium in 70% and total occlusion, contour interval=0.4mV.

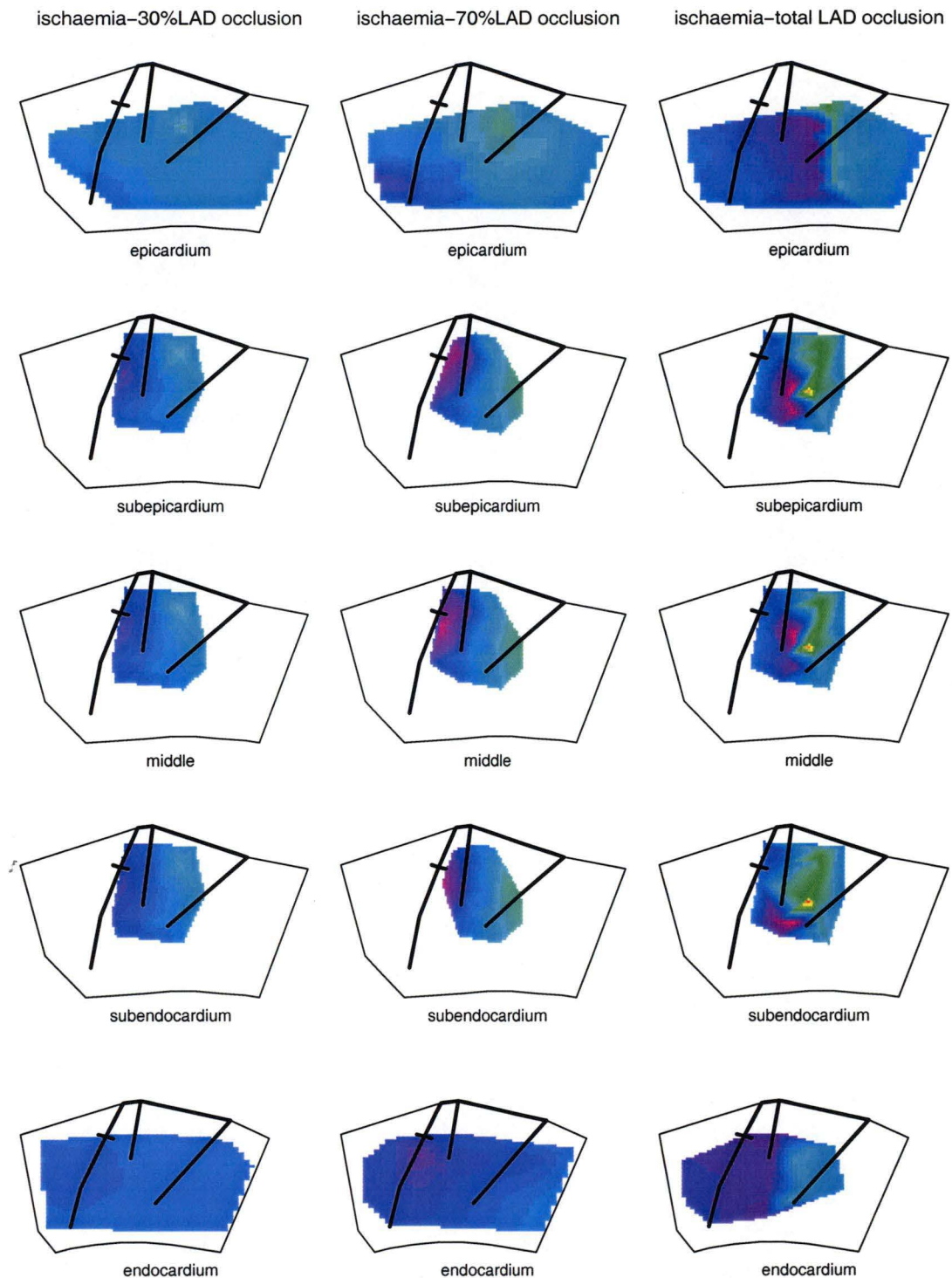


Fig. 5.5 Imaging view of ST potential distributions in different layers of the heart at 20min of mild, severe and full thickness ischemia of LAD area. The intensities of the shade indicate the quantity of ST potentials. The thickest solid lines reflect the position of the coronary arteries, with the occluded arteries indicated by bars across the coronary arteries. Maps are plotted from the data in Fig. 5.4

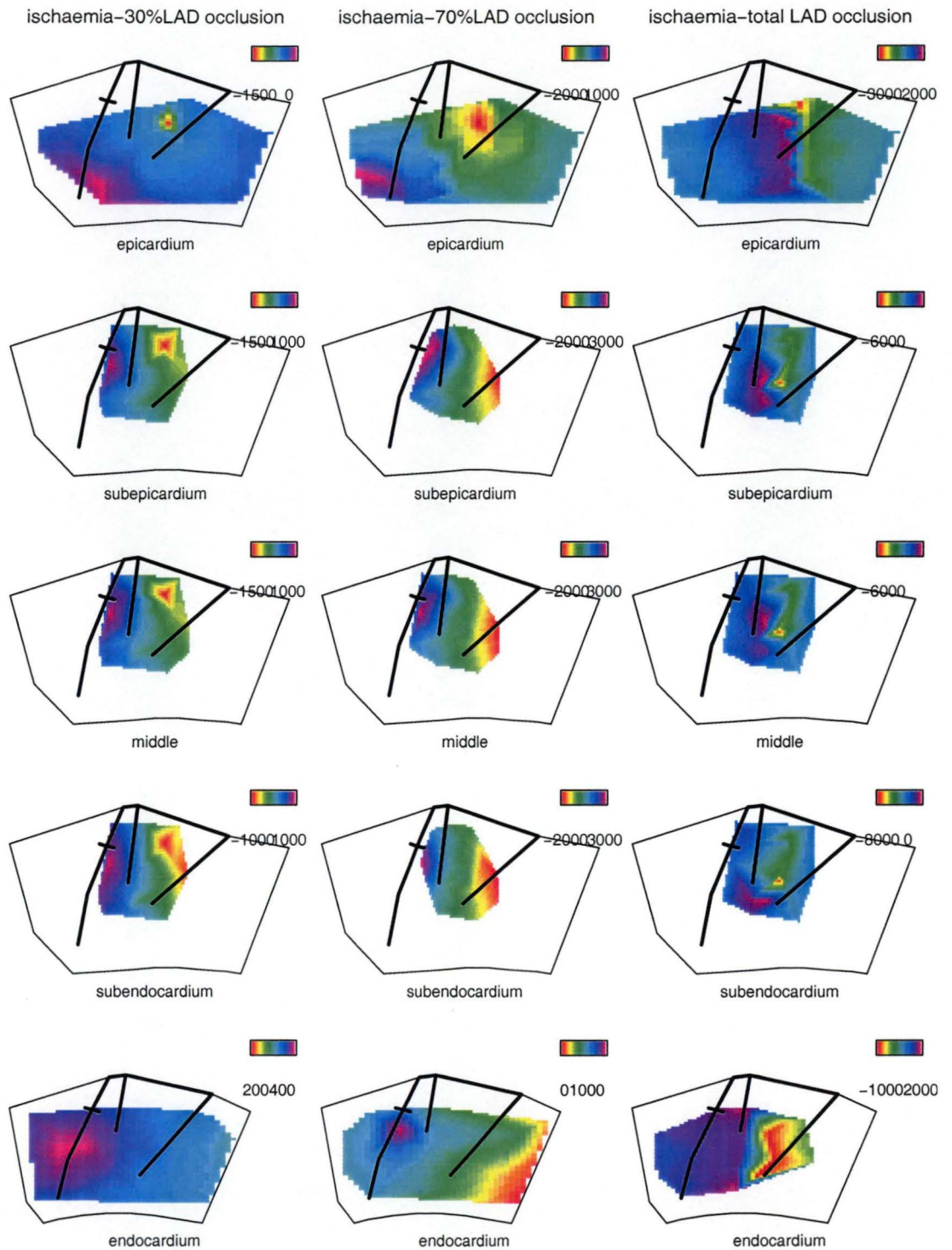


Fig. 5.6 Same imaging as in Fig. 5.5 except that the legend scales are different in each sub-graph, which gives a better view of ST potential distribution pattern.

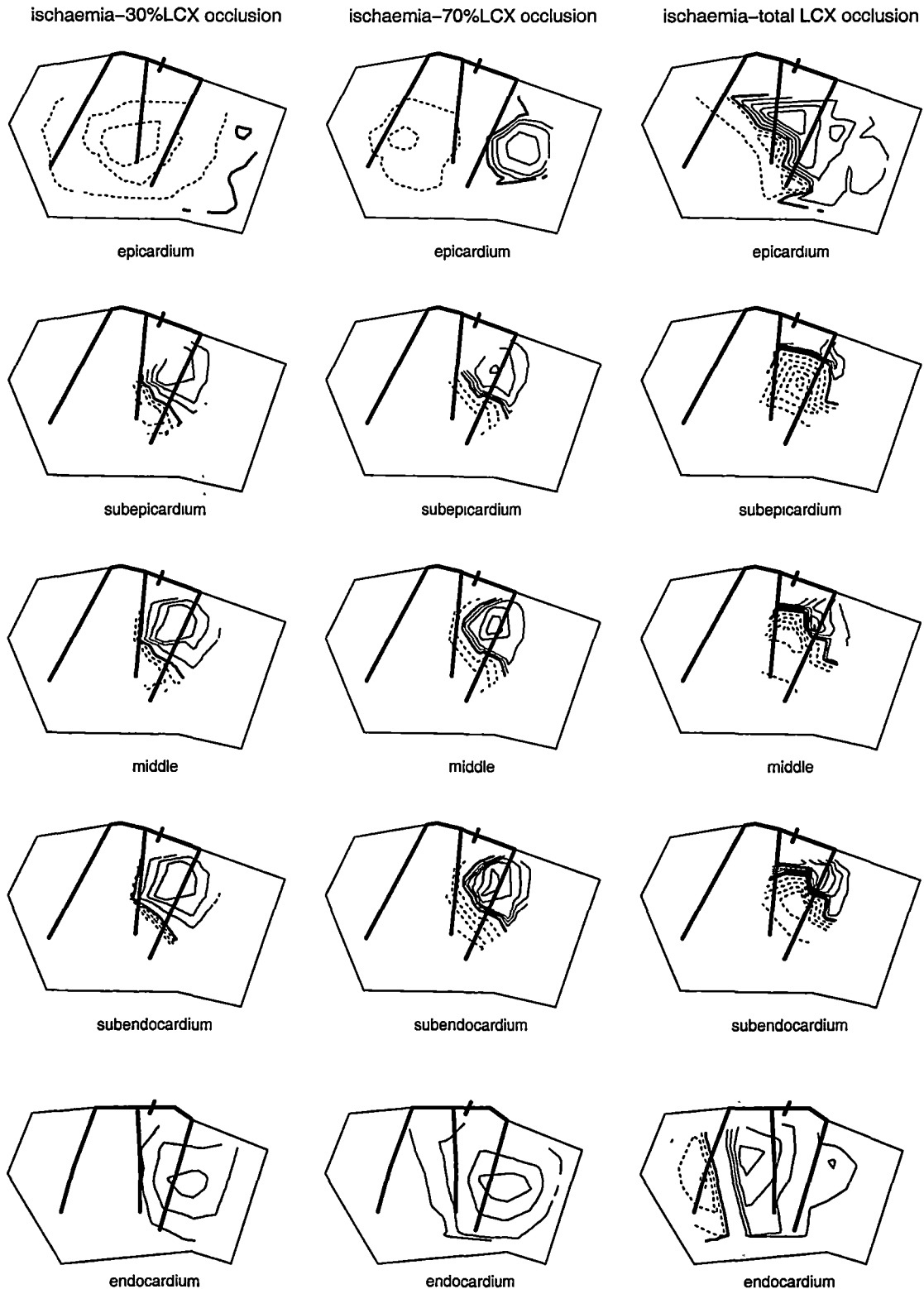


Fig. 5.7 ST potential distributions in different layers of the heart at 20min of mild subendocardial ischaemia, 20min of severe subendocardial ischemia and 20min of full thickness ischemia of LCX area. The thickest solid lines reflect the position of the coronary arteries, the thick solid lines indicate zero potential, the thin solid and dashed lines indicate ST elevation and ST depression respectively, with the occluded arteries indicated by bars across the coronary arteries. Maps are plotted from the data of one of the animals in group 2. For epicardium and intramyocardium, contour interval=0.5mV; for endocardium, contour interval=0.2mV.

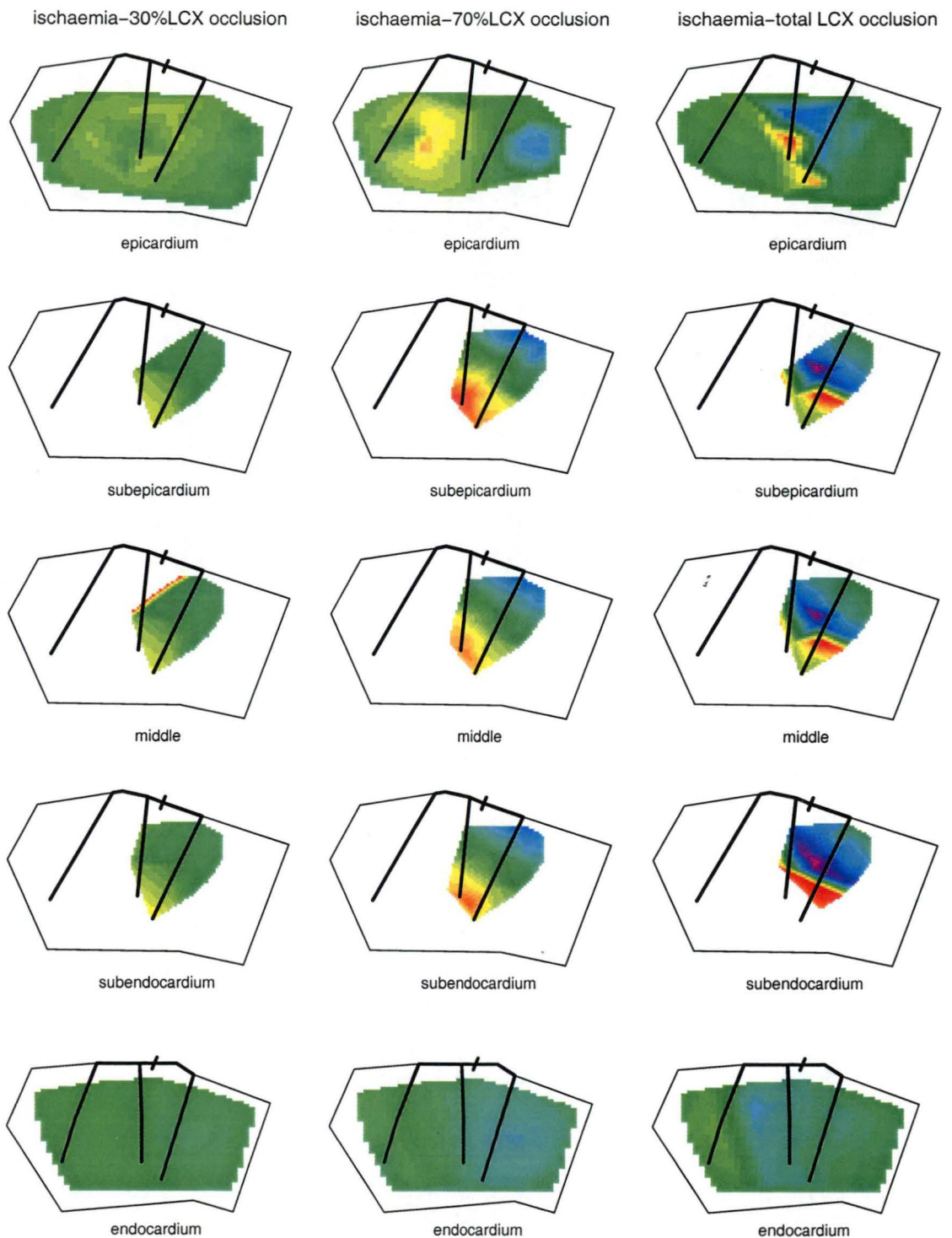


Fig. 5.8 Imaging view of ST potential distributions in different layers of the heart at 20min of mild, 20min of severe and 20min of full thickness ischemia of LCX area. The intensities of the shade indicate the quantity of ST potentials. The thickest solid lines reflect the position of the coronary arteries, with the occluded arteries indicated by bars across the coronary arteries. Maps are plotted from the data in Fig. 5.7.

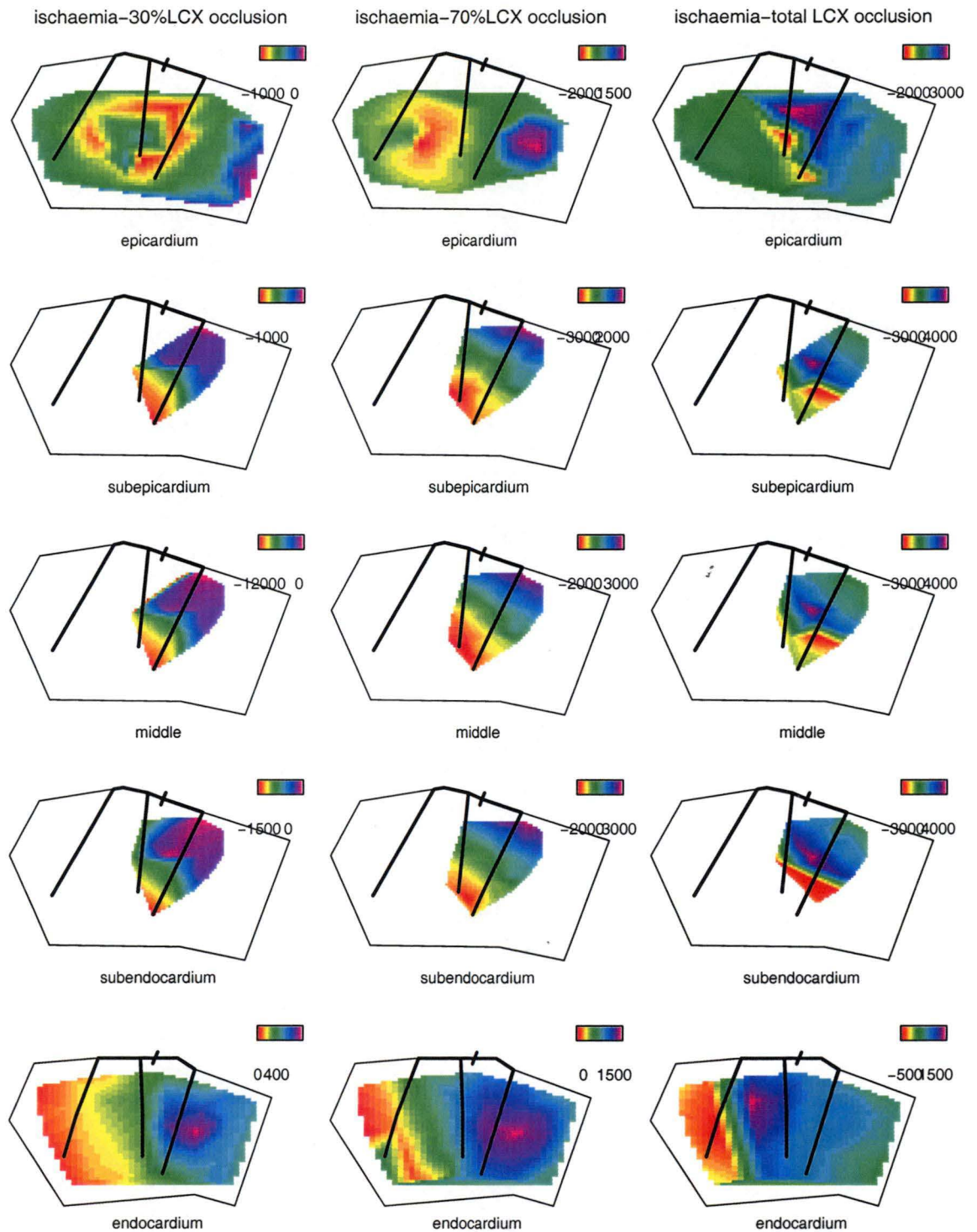


Fig. 5.9 Same imaging as in Fig. 5.7 except that the legend scales are different in each sub-graph, which gives a better view of ST potential distribution pattern.

5.2.4 RELATIONSHIP BETWEEN ST POTENTIAL DISTRIBUTIONS AND RMBF IN MILD AND SEVERE ISCHAEMIA IN EITHER LAD OR LCX AREA

RMBF were measured before and after 20min of ischaemia in every one-third layer of the heart. RMBF distribution image maps were plotted and combined with ST potential distribution contour maps. Epicardial and subepicardial ST potential distribution maps were combined with maps of RMBF of the outer one-third layer; intramyocardial ST potential distribution maps of the mid one-third layer were combined with maps of RMBF of the mid one-third layer; Subendocardial and endocardial ST potential distribution maps were combined with maps of RMBF of the inner one-third layer.

Fig. 5.10 and Fig. 5.11 showed that RMBF in the ischaemic region was lower than that in the non-ischaemia region, and RMBF in the ischaemic area decreased when the severity of ischaemia increased.

In mild ischaemia, epicardial ST depression scattered on the surface of the heart and had no relationship to the ischaemic area; endocardial and intramyocardial ST elevation occurred in area of reduced RMBF, intramyocardial ST depression occurred at the boundary of the ischaemic and nonischaemic areas.

In sever ischaemia, ST elevation in different layers occurred in the low blood flow areas, while ST depression in different layers occurred in relatively high blood flow areas (Fig. 5.10 and Fig. 5.11).

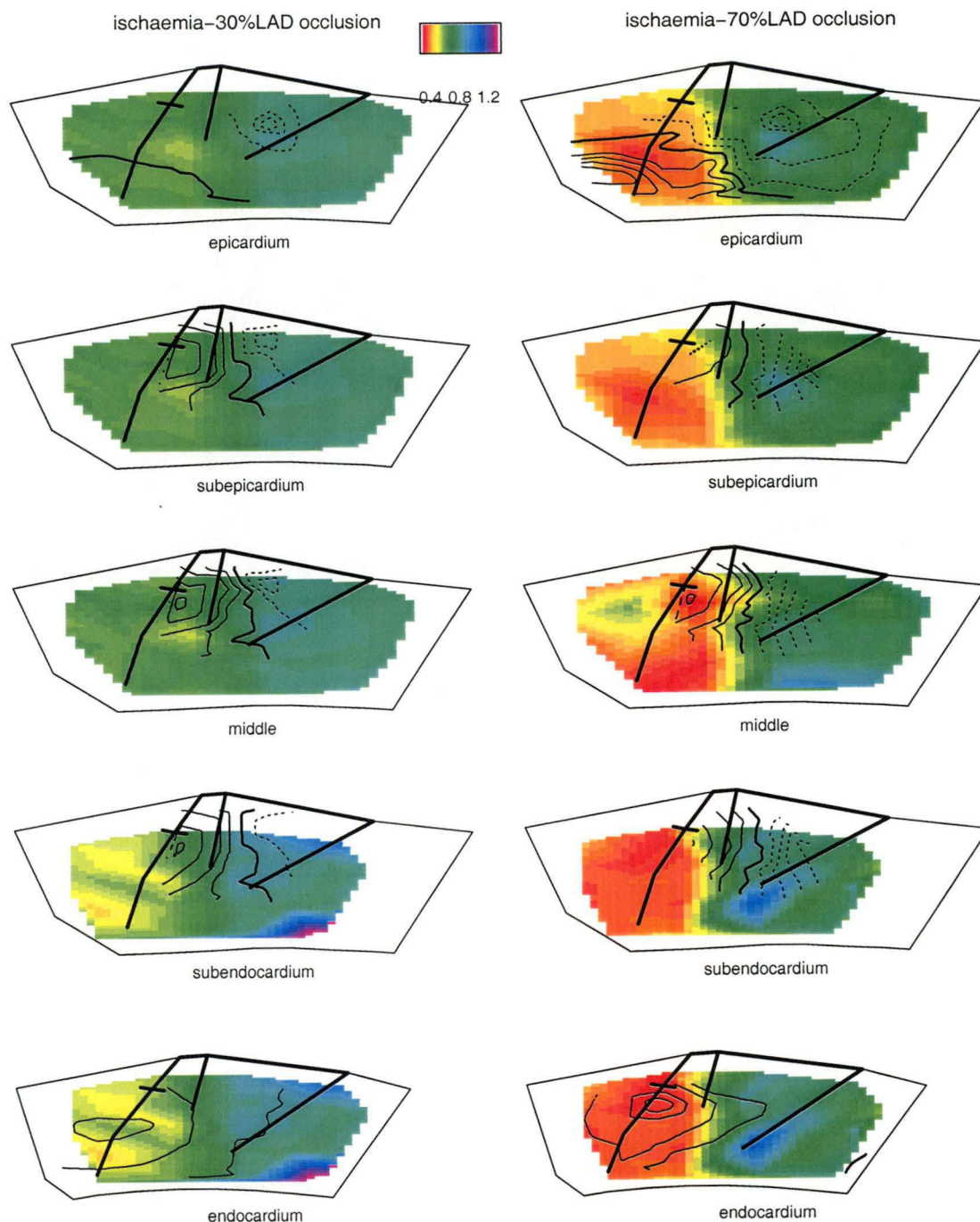


Fig. 5.10 Combination of ST potential distributions (contour lines) and RMBF distributions (shaded area, ml/min/g) in different layers of the heart at 20min of mild and 20min of severe ischaemia in LAD ligation. From top to bottom:

- Combination of epicardial ST potential distribution and RMBF distribution of outer 1/3 layer;
- Combination of subepicardial ST potential distribution and RMBF distribution of outer 1/3 layer;
- Combination of mid layer ST potential distribution and RMBF distribution of mid 1/3 layer;
- Combination of subendocardial ST potential distribution and RMBF distribution of inner 1/3 layer;
- Combination of endocardial ST potential distribution and RMBF distribution of inner 1/3 layer.

The intensities of the shade indicate the quantity of flow. The thickest solid lines reflect the position of the coronary arteries, the thick solid lines indicate zero potential, the thin solid and the dashed lines indicate ST elevation and ST depression respectively, with the occluded arteries indicated by bars across the coronary arteries. Maps are plotted from data of one of the animals in group 1. Contour interval is same as Fig. 5.4.

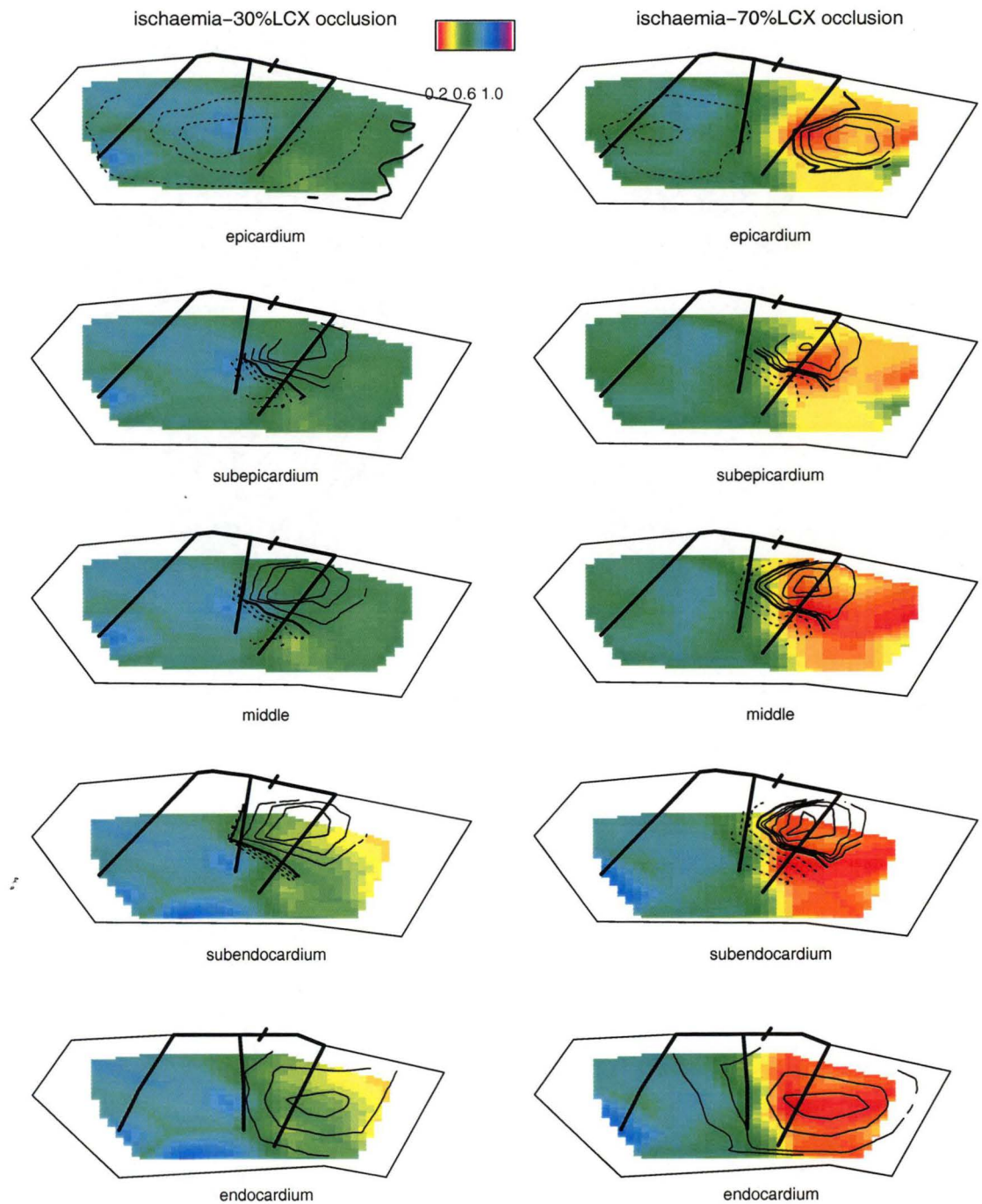


Fig. 5.11 Combination of ST potential distributions (contour lines) and RMBF distributions (shaded area, ml/min/g) in different layers of the heart at 20min of mild and 20min of severe ischaemia in LCX ligation. From top to bottom:

- Combination of epicardial ST potential distribution and RMBF distribution of outer 1/3 layer;
- Combination of subepicardial ST potential distribution and RMBF distribution of outer 1/3 layer;
- Combination of mid layer ST potential distribution and RMBF distribution of mid 1/3 layer;
- Combination of subendocardial ST potential distribution and RMBF distribution of inner 1/3 layer;
- Combination of endocardial ST potential distribution and RMBF distribution of inner 1/3 layer.

The intensities of the shade indicate the quantity of flow. The thickest solid lines reflect the position of the coronary arteries, the thick solid lines indicate zero potential, the thin solid and the dashed lines indicate ST elevation and ST depression respectively, with the occluded arteries indicated by bars across the coronary arteries. Maps are plotted from data of one of the animals in group 2. Contour interval is same as Fig. 5.6.

5.3 DISCUSSION

The main finding of this study is that the ST distribution patterns of intramyocardium and endocardium were quite similar in mild and severe ischaemia, and the ST distribution patterns of epicardium were different, i.e., in severe ischaemia, apart from ST depression, minor ST elevation also occurred. However, when ischaemia became full thickness, the ST distribution pattern was totally different.

The present results showed that in both mild and severe subendocardial ischaemia, both ST elevation and ST depression coexisted, ST elevation appeared in the ischaemic area, with the maximal magnitude occurred in the ischaemic centre; ST depression appeared in the non-ischaemic area. However, when the ischaemia became full thickness, even though ST elevation still appeared in the ischaemic area and ST depression appeared in non-ischaemic area, the highest magnitude of both ST elevation and ST depression occurred on the ischaemic boundary (Fig. 5.4~Fig. 5.9).

Occurrence of ischaemia is dependent on oxygen required and blood flow reserve of a particular organ, as well as the blood supply to that organ. The heart is one of the highest oxygen consumption organs, whereas, the cardiac blood flow reserve is relatively low. Any increase in the myocardial oxygen requirement will normally result in a proportional increase in coronary blood flow. In circumstances of coronary occlusion, blood supply to the heart is reduced. When oxygen requirement increases, the coronary blood supply fails to meet the needs of the heart muscle for oxygen and metabolic substrate. As a result, myocardial ischaemia may occur. The narrower the coronary artery is, the less blood supplies to the heart. The degree of subendocardial ischaemia increases as the degree of coronary artery obstruction increases (Ball and Bache, 1976; Bache et al., 1977).

It is well known that the myocardial perfusion is heterogeneous. In experimental animals, subendocardium of left ventricle at rest consumes 10 to 30 percent more oxygen than the epicardium and has a proportionately higher blood flow (Hoffman, 1978). However, when oxygen supply to the myocardium can't meet the requirement, cardiac ischaemia always begins from the subendocardium. The subendocardium is more likely to be compromised by ischaemia. With the increase of duration of coronary artery occlusion, a transmural wavefront of cell death progresses from subendocardium to epicardium (Reimer et al., 1977; Reier and Jennings, 1979). In the presence of low coronary artery perfusion and elevated myocardial oxygen demand, if

the collateral blood flow is low, the progression of the wavefront is accelerated when myocardial ischaemia becomes severe.

In the present study, two varying degrees of coronary artery blood flow reduction were performed: In mild coronary artery blood flow reduction group, coronary blood flow was reduced by 30% of the original flow; in severe coronary artery blood flow reduction group, coronary blood flow was reduced by 70% of the original flow. RMBF was measured in different layers of the left ventricular wall, i.e., inner one-third layer, mid one-third layer and outer one-third layer. The results showed that in the mild subendocardial ischaemic group, blood flow in the inner one-third layer decreased while blood flow in the mid and outer one-third layers remained unchanged. When coronary blood flow was reduced by 70% of the original flow, RMBF in every layer decreased. There were significant differences of RMBF in every layer between the mild ischaemic and severe ischaemic group, while endo/epi ratio between the mild ischaemic and severe ischaemic group had no significant difference. In both mild and severe subendocardial ischaemic groups, RMBF in endocardium was the lowest while RMBF in epicardium was the highest, with RMBF in mid layer being in between.

The effects of ischaemic injury on mechanical function, membrane potential, metabolism, and ultrastructure are all reversible if the duration of ischaemia is short (Bayley et al., 1944; Jennings et al., 1960). Only when the ischaemia persists for longer periods of time, the affected cells become irreversibly injured. Jennings (Jennings et al., 1975) found that during mild ischaemia in dogs (coronary blood flow reduced to 50~60% of control), no irreversible injury would occur. Although dogs usually have tiny collaterals existing, which is quite different from sheep, the mild degree and brief duration of partial coronary artery ligation should not cause severe injury to the myocardium, especially after a stable period of at least 30min. the outcome of the second ischaemia would not be interfered by the initial ischaemia.

In addition to a transmural flow gradient, there are also a lateral gradient in flow. This lateral gradient has been verified by high-speed cinematography of the surface of the heart following injection of tracers (Prinzmetal et al., 1948) and biochemical parameters (Sayen et al., 1958). However, unlike the gradual flow transition from the endocardium to the epicardium during subendocardial ischaemia, there was a sharp blood flow change from the ischaemic region to the nonischaemic region at the lateral boundary of the heart, producing a sharp lateral interface between the ischaemic and

normal regions (Li et al., 1998). Studies on transmural ischaemia also found a sharp lateral interface between the ischaemic and normal cells with severely ischaemic tissue lying adjacent to the normally well-perfused tissue (Reimer and Jennings, 1979; Factor et al., 1981; Harken et al., 1981). In ischaemic pig hearts, transmembrane action potential recordings using floating microelectrodes also demonstrated a sharp and distinct transition from electrophysiologically abnormal to normal cells (Janse et al., 1979).

Our results also showed this sharp blood flow transition from the ischaemic zone to nonischaemic zone in both mild and severe subendocardial ischaemia (Fig. 5.2 and Fig. 5.3). We expected that when mild subendocardial ischaemia was replaced by severe subendocardial ischaemia, the lateral boundary blood flow transition zone would move from ischaemic zone to nonischaemic zone, resulting in a large ischaemic area. However, this has not been found in our experiments. This might be explained as follows: the lack of collateral circulation in sheep makes ischaemia exist only in the area supplied by the culprit coronary artery and can not be compensated by other coronary artery supply; the mild and severe subendocardial ischaemia were produced by partially occluding the same site of the coronary artery at the proximate segment. Effort was tried to occlude the coronary artery at the proximal site as well as distal site, however, this was unsuccessful because of technique difficulties.

The different epicardial ST potential distributions in mild and severe ischaemia led to a postulation that the current path might breakthrough towards the epicardium during severe subendocardial ischaemia. During severe ischaemia, RMBF in every layer decreased, while in mild ischaemia, only the subendocardial RMBF decreased. Thus, the middle and outer one-third layers of the left ventricle might have vital effect on the different epicardial ST potential distributions during mild and severe ischaemia. Recent study of transmural differences in electrical properties of cardiac cells showed three different layers of left ventricular wall: epicardial cells, ventricular M and endocardial cells (Antzelevitch et al., 1999; Dumaine and Antzelevitch, 2000; Antzelevitch, 2001). Ventricular M and epicardial cells, but not endocardial cells, typically display action potentials with a prominent notch or phase 1, due to the presence of a large 4-aminopyridine (4-PA)-sensitive transient outward current (I_{to}). Transmural differences in the magnitude of the I_{to} -mediated action potential notch give rise to a transmural voltage gradient. Accentuation of this gradient leads to the appearance of pathophysiological J waves, ST segment elevation and the development of ventricular tachycardia and fibrillation in experimental models of the Brugada syndrome as well as under conditions of acute ischaemia. Whether this

transmural voltage gradient will affect the spread of electrical current path need further elaborate research, and might be important to understand the cardiac current path in ischaemia.

There were dipoles on intramyocardial layers during mild and severe ischaemia, and on epicardial during severe ischaemia, and there were also dipoles on each layer during full thickness ischaemia. We try to explain this by solid angle theory.

According to solid angle model, the potential (Φ) recorded at a specific site is as follows:

$$\Phi = \Omega/4\pi \cdot \Delta V_m \cdot K$$

Where Ω is the solid angle subtended by the ischaemic boundary at the electrode site, ΔV_m denotes the transmembrane potential difference of the normal and ischaemic regions, and K is a term correcting for differences in intracellular and extracellular conductivity and the occupancy of much of the heart muscle by interstitial tissue. The electrocardiographically recorded potential is directly proportional to both Ω and ΔV_m . The polarity of Ω is positive or negative depending on whether an observer at a specific site views first the positive or negative side of the surface enclosed by the boundary (Bayley, 1958). Thus, this model predicts that ischaemia would cause ST elevation over the ischaemic area whereas ST depression would occur on the non-ischaemic area. Our experimental model recorded potential distribution of dipoles all showed ST elevation over the ischaemic area, with ST depression occurred on the boundary of the ischaemic and non-ischaemic regions. Mild subendocardial ischaemia, severe subendocardial ischaemia and full thickness ischaemia all showed the same results, which is consistent with the solid angle theory.

In either mild or severe subendocardial ischaemia, the maximal intramyocardial ST elevation in present study occurred in the centre of the ischaemic area, the magnitude of ST elevation decreased gradually towards the ischaemic border (Fig. 5.5, Fig. 5.6, Fig. 5.8, Fig. 5.9), which is contrary to solid angle theory. However, in full thickness ischaemia, the maximal ST shift in each layer occurred on the ischaemic boundary, which was totally different with mild and severe ischaemia, and is consistent with the solid angle theory. As predicted by solid angle theory, when the solid angle Ω increases the recorded potential increases as well.

In the circumstance of subendocardial ischaemia, the solid angle of an intramyocardial electrode should increase with the ischaemic area. Thus the boundary potential recorded by a specific intramyocardial electrode should be higher compared

to the central potential recorded at the same intramyocardial site. The former should have a larger solid angle than that of the central one. In a previous (Holland and Brooks, 1975) experimental ischaemia model of swine, Holland and Brooks' recorded a higher epicardial ST elevation in the central of a small size ischaemia and a lower epicardial ST elevation in the central of a large size ischaemia. Their ischaemia model was later verified by thioflavin S fluorescence that the ischaemic area was confluent and maximal in subepicardium, this is contrary to previous studies which suggested that subendocardium is vulnerable to ischaemia (Reimer et al., 1977; Reimer and Jennings, 1979; Jennings et al., 1985). Furthermore, in Holland and Brooks' animal experiment, epicardial potentials were recorded by one electrode fixed on a epicardial site, and central potentials of different ischaemic sizes were recorded by two experimental protocols. The similarity of ST distribution in mild and severe ischaemia might resulted from the same blood flow distributions in both groups, even though RMBF in severe ischaemic group was lower than that in mild ischaemic group. However, RMBF in full thickness ischaemia was not measured. On the basis of the solid angle theory, electrodes located near the border of the ischaemia would be expected to record potentials different from those recorded by more centrally located electrodes. In addition, when the electrode moves away from the center, whether the potential decreases or increases depends on the size of the ischaemia. Thus, the relationship between ischaemic size and ST potential should be analyzed by multiple recording sites which should include not only the central ischaemic area but especially the ischaemic border as well. The discrepancy between our experimental results and their relationship with the theoretical deduction might be able to seek a solution by further modeling study. The solid angle theory is a "classic" theory for electrocardiograph, even though it has been recently ignored by growing insight in the essentially anisotropic nature of the ventricular myocardium, its role in source descriptions that relate directly to cardiac electrophysiology was re-emphasized by Van Oosterom (2002).

CHAPTER SIX

INTRAMYOCARDIAL ST SEGMENT POTENTIAL DISTRIBUTION IN ACUTE TRANSMURAL ISCHAEMIA

ST segment elevation has been accepted as being a bona fide marker of acute transmural ischaemia. However, the origin and significance of ST segment depression in acute transmural ischaemia had long been controversial. It was recently found that ST depression always accompanied ST elevation in large size of acute transmural ischaemia whereas in small size of acute transmural ischaemia, ST depression was almost invisible (Li et al., 1999). This study was analysed from the data of epicardial and endocardial ST potential. From the previous chapters we know that the intramyocardial ST potential distributions were quite different from those on epicardium and endocardium, the data of ST potential from the intramyocardium might be essential to explain the significance of ST depression in acute transmural ischaemia. In this chapter, epicardial, endocardial and intramyocardial ST potential distributions were recorded simultaneously in acute transmural ischaemia.

6.1 MATERIALS AND METHODS

6.1.1 EXPERIMENTAL ANIMALS AND PROTOCOLS

A total of 6 (Polworth/Comeback cross) sheep weighing between 26~35kg of both genders were used. All the sheep were bred in the University of Tasmania's animal farm. Table 6.1 shows the groups of animals subjected to different experimental protocols.

Table 6.1 Experimental protocol

animal		
group	number	experimental protocol
1	5	acute transmural ischaemia in LAD area.
2	4	acute transmural ischaemia in LCX area.

group 1: Acute transmural ischaemia in LCX area (n=5).

group 2: Acute transmural ischaemia in LAD area (n=4).

6.1.2 EXPERIMENTAL PROCEDURES AND ACUTE TRANSMURAL ISCHAEMIA

Experimental procedures were the same as in chapter 4. Instead of partially occluding the coronary artery plus LA pacing, acute transmural ischaemic sheep model was made by ligating either LAD or LCX for 20min. One sheep developed ventricular fibrillation after 15min of LAD occlusion, thus data recorded only for 15minutes. Two sheep in LAD group and one sheep in LCX group developed ventricular fibrillation caused by hypoxia during the early stage of the experiments, so no data were available in these three sheep.

6.1.3 RMBF MEASUREMENT

RMBF were measured as described in chapter 4. RMBF were measured before acute transmural ischaemia and at 15min after acute transmural ischaemia.

6.1.4 POTENTIALS RECORDING AND MAP CONSTRUCTION

Potentials recording and map construction are described as in chapter 3, chapter 4 and chapter 5. ST potentials were simultaneously recorded before and 5min, 10min, 15min, 20min after acute transmural ischaemia on epicardium, endocardium and three different depths of intramyocardium. (One sheep developed ventricular fibrillation after 15min of LAD occlusion, ST potentials were recorded before and 5min, 10min, 15min after its ligation).

6.2 RESULTS

6.2.1 HAEMODYNAMIC CHANGES IN ACUTE TRANSMURAL ISCHAEMIA

Haemodynamic parameters as LVDP, LVSP, LAP and CAP were recorded during the whole process of experiments.

Table 6.2 showed LVDP, LVSP, LAP and CAP recorded before and 15min after acute transmural ischaemia. The results showed that LVDP and LAP during acute ischaemia were significantly higher than that before ischaemia, LVSP and CAP during acute ischaemia were significantly lower than that before ischaemia ($P<0.01$).

Table 6.2 Haemodynamic response to acute transmural ischaemia (n=6)

	baseline	acute ischaemia
LVDP, mmHg	-8.83 ± 3.76	$-0.33 \pm 0.82^*$
LVSP, mmHg	106.67 ± 11.69	$81.67 \pm 19.15^*$
LAP, mmHg	2.21 ± 2.77	$8.97 \pm 2.90^*$
CAP, mmHg	85.83 ± 8.87	$61.50 \pm 15.32^*$

LVDP: left ventricular diastolic pressure LAP: left atrial pressure

LVSP: left ventricular systolic pressure CAP: carotid artery pressure

*Compared to baseline: * $P<0.05$.*

6.2.2 RMBF CHANGES IN ACUTE TRANSMURAL ISCHAEMIA

Table 6.3 and Fig. 6.1 illustrated that RMBF in every one-third layer of the heart and the endo/epi ratio at 15min after acute transmural ischaemia decreased significantly than that before ischaemia in ischaemic region ($P<0.001$). Table 6.4 and Fig. 6.2 illustrated that RMBF and the endo/epi ratio in mid and inner one-third layers of the heart at 15min after acute transmural ischaemia also decreased significantly than that of before ischaemia in non-ischaemic region ($P<0.05$); RMBF in outer one-third layer of the heart at 15min after acute transmural ischaemia had no significant change compared with that of before ischaemia in non-ischaemic region ($P>0.05$), resulted in a decreased endo/epi ratio in non-ischaemic region ($P=0.05$).

Table 6.3 RMBF response to acute transmural ischaemia in ischaemic area (n=6)

sheep	baseline					acute ischaemia				
	No	epi	mid	endo	trans	ratio	epi	mid	endo	trans
1	0.928	0.946	0.962	0.945	1.037	0.216	0.202	0.192	0.203	0.889
2	0.702	0.767	0.879	0.783	1.252	0.295	0.226	0.180	0.234	0.610
3	0.753	0.796	0.836	0.795	1.110	0.235	0.195	0.161	0.197	0.685
4	0.596	0.612	0.630	0.613	1.057	0.191	0.178	0.166	0.178	0.869
5	0.694	0.745	0.781	0.740	1.125	0.269	0.200	0.136	0.202	0.506
6	0.539	0.567	0.600	0.569	1.113	0.285	0.211	0.162	0.219	0.568
mean	0.702	0.739	0.781	0.741	1.116	0.249	0.202	0.166	0.206	0.688
SD	0.135	0.136	0.142	0.136	0.075	0.041	0.016	0.019	0.019	0.159
P value						0.0002	0.0002	0.0001	0.0002	0.0005

epi: RMBF in outer one-third layer of LV wall mid: RMBF in middle one-third layer of LV wall

endo RMBF in inner one-third layer of LV wall trans RMBF in full thickness of LV wall

ratio: ratio of RMBF of inner one-third layer and outer one-third layer of LV wall

Table 6.4 RMBF response to acute transmural ischaemia in non-ischaemic area (n=6)

sheep	baseline					acute ischaemia					
	No	epi	mid	endo	trans	ratio	epi	mid	endo	trans	ratio
1		0.870	0.892	0.910	0.891	1.046	0.770	0.760	0.745	0.758	0.968
2		0.665	0.741	0.805	0.737	1.211	0.614	0.602	0.584	0.600	0.951
3		0.726	0.764	0.804	0.765	1.107	0.657	0.640	0.612	0.636	0.932
4		0.715	0.733	0.750	0.733	1.049	0.640	0.614	0.598	0.617	0.934
5		0.796	0.840	0.893	0.843	1.122	0.680	0.655	0.660	0.665	0.971
6		0.539	0.573	0.600	0.571	1.113	0.498	0.482	0.490	0.490	0.984
mean		0.719	0.757	0.794	0.756	1.108	0.643	0.626	0.615	0.628	0.957
SD		0.113	0.109	0.112	0.110	0.060	0.089	0.090	0.085	0.088	0.021
P value							0.231	0.047	0.012	0.050	0.001

epi: RMBF in outer one-third layer of LV wall mid: RMBF in middle one-third layer of LV wall

endo: RMBF in inner one-third layer of LV wall trans: RMBF in full thickness of LV wall

ratio: ratio of RMBF of inner one-third layer and outer one-third layer of LV wall

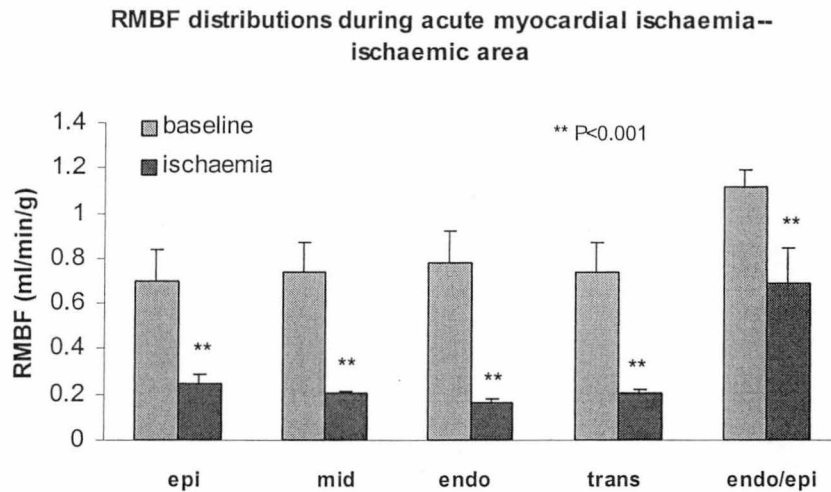


Fig. 6.1 RMBF distribution in different layers of the heart and endo/epi ratio before and at 15min after acute ischaemia in the ischaemic area (see Table 6.2 for abbreviation).

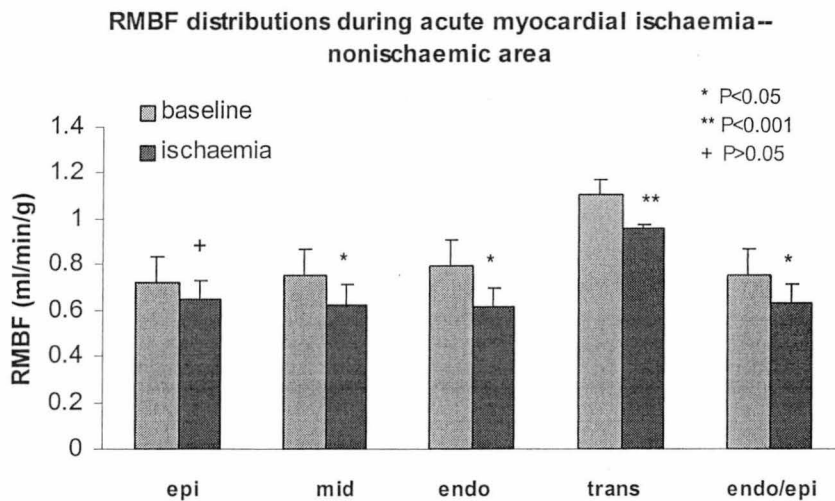


Fig. 6.2 RMBF distribution in different layers of the heart and endo/epi ratio before and at 15min after acute ischaemia in the non-ischaemic area (see Table 6.3 for abbreviation).

6.2.3 ST POTENTIAL DISTRIBUTION IN ACUTE TRANSMURAL ISCHAEMIA

6.2.3.1 ST potential distributions in acute transmural ischaemia in LAD ligation

Fig. 6.3 showed ST potential distributions at different layers of the heart before and 15min after total LAD occlusion. The epicardial ST potential distributions showed that ST elevation occurred on the acute ischaemic region while ST depression occurred on the non-ischaemic region. Similar ST potential distribution occurred in different layers of intramyocardium, with the magnitude of ST elevation and ST depression higher than that on epicardium. Endocardial ST elevation occurred on the ischaemic region, while endocardial ST depression occurred on the non-ischaemic region, which was different from that of during subendocardial ischaemia. In subendocardial ischaemia, only ST elevation appeared, and mostly on the ischaemic region. The highest magnitude of maximal and minimal ST potential occurred on the boundary of the ischaemic and non-ischaemic areas (Fig. 6.4).

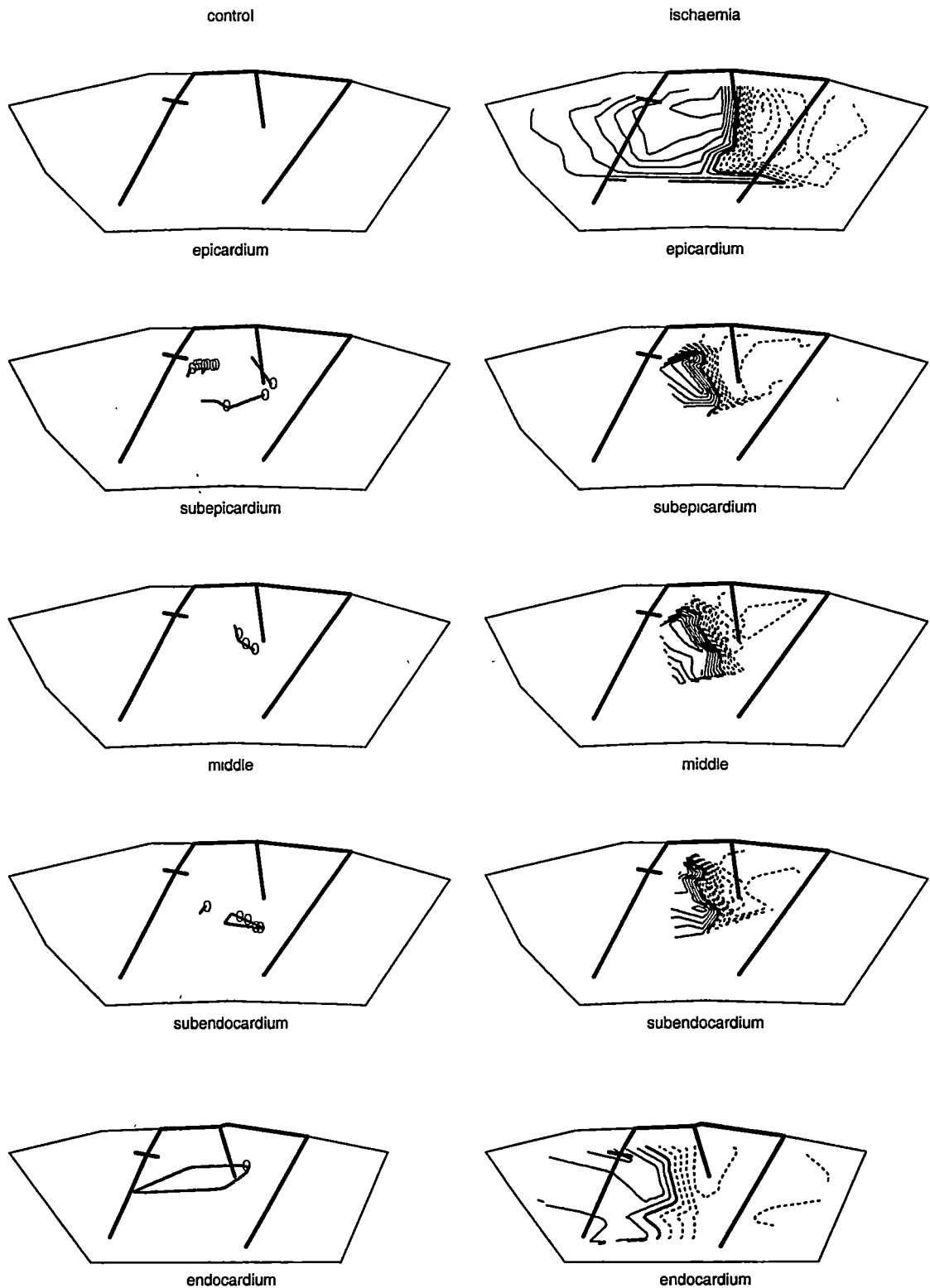


Fig. 6.3 ST potential distributions in different layers of the heart before and at 15min of acute transmural ischaemia of LAD ligation. The thickest solid lines reflect position of the coronary arteries, the thick solid lines reflect zero potential, the thin solid and the dashed lines indicate ST elevation and ST depression respectively, with the occluded arteries indicated by bars across the coronary arteries. Maps are plotted from data of one of the animals in group 1. Contour interval=0.5mV.

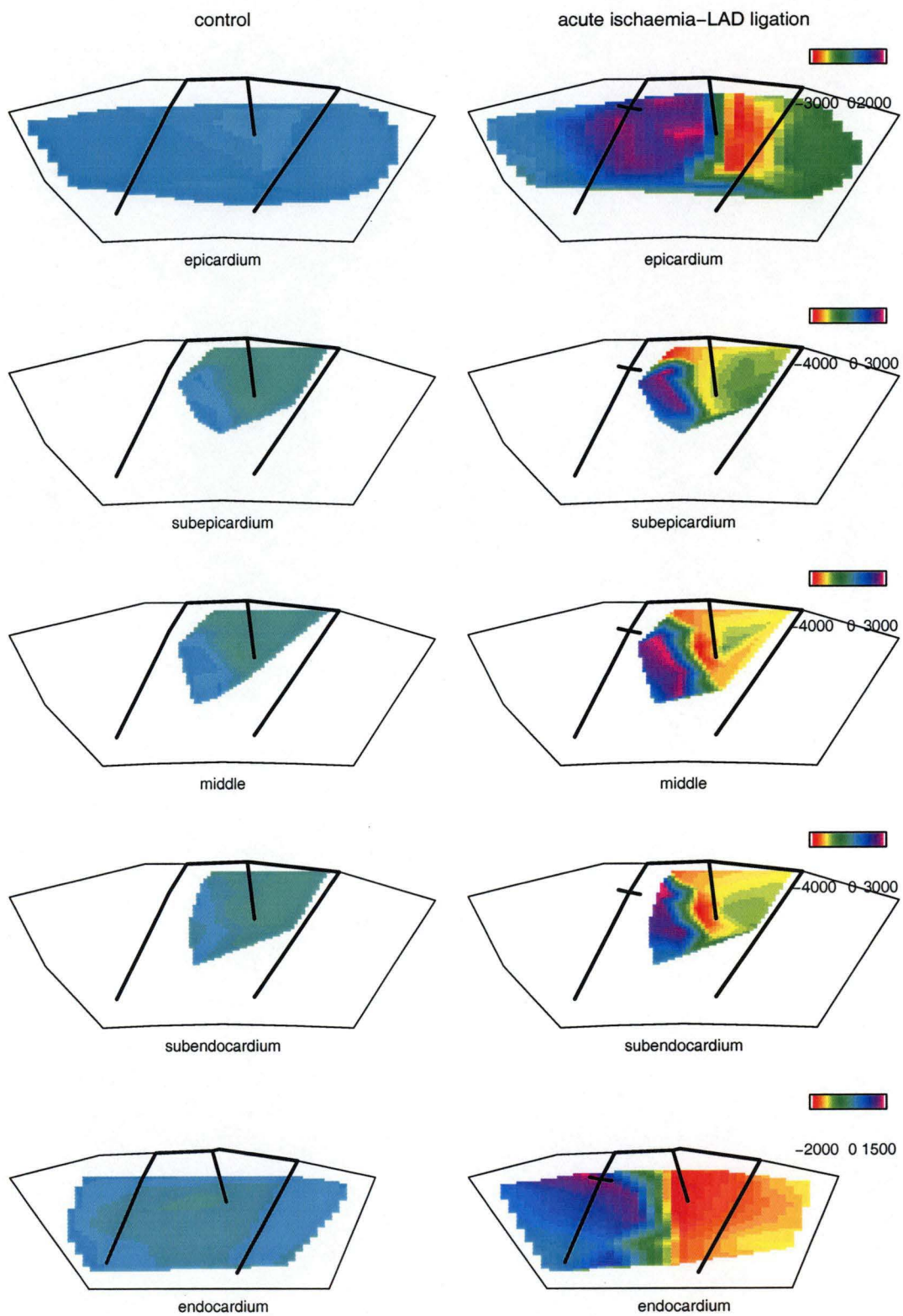


Fig. 6.4 Imaging view of ST potential distributions in different layers of the heart before and at 15min of acute ischaemia in LAD area. The intensities of the shade indicate the quantity of ST potentials. The thickest solid lines reflect the position of the coronary arteries, with the occluded arteries indicated by bars across the coronary arteries. Maps are plotted from data in Fig. 6.3.

6.2.3.2 ST potential distributions in acute transmural ischaemia of LCX ligation

ST potential distributions in acute transmural ischaemia of LCX ligation were quite similar to that of LAD ligation. Fig. 6.5 showed the ST potential distributions at different layers of the heart before and at 15min after total LCX occlusion. On the epicardium and three different layers of intramyocardium, ST elevation occurred on the acute ischaemic region while ST depression occurred on the non-ischaemic region. ST elevation occurred on endocardium of the ischaemic region, while ST depression occurred on endocardium of non-ischaemic region. The highest magnitude of maximal and minimal ST potential occurred on the boundary of the ischaemic and non-ischaemic areas (Fig. 6.6).

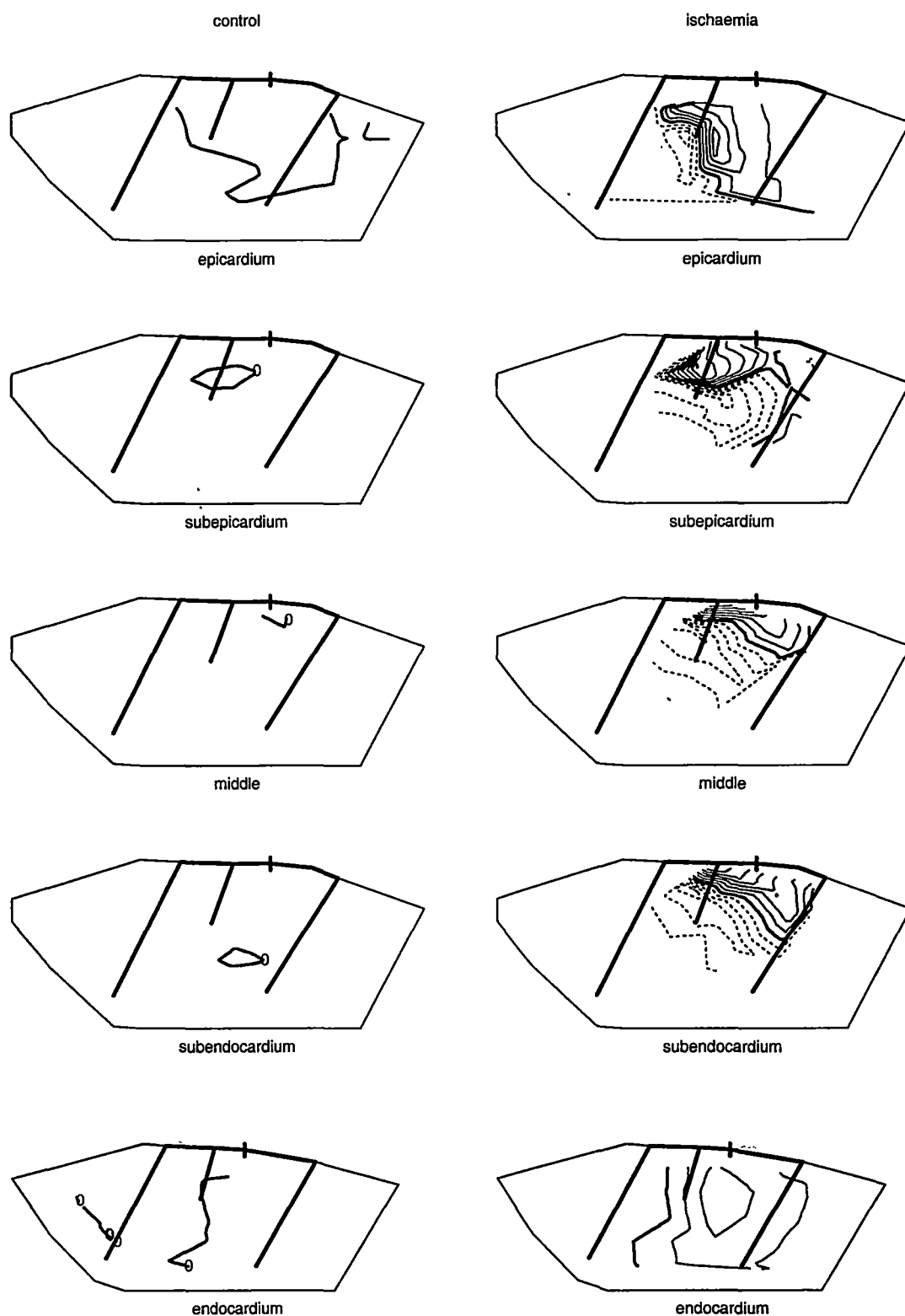


Fig. 6.5 ST potential distributions in different layers of the heart before and at 15min of acute transmural ischaemia of LCX ligation. The thickest solid lines reflect position of the coronary arteries, the thick solid lines reflect zero potential, the thin solid and the dashed lines indicate ST elevation and ST depression respectively, with the occluded arteries indicated by bars across the coronary arteries. Maps are plotted from data of one of the animals in group 2. Contour interval=0.5mV.

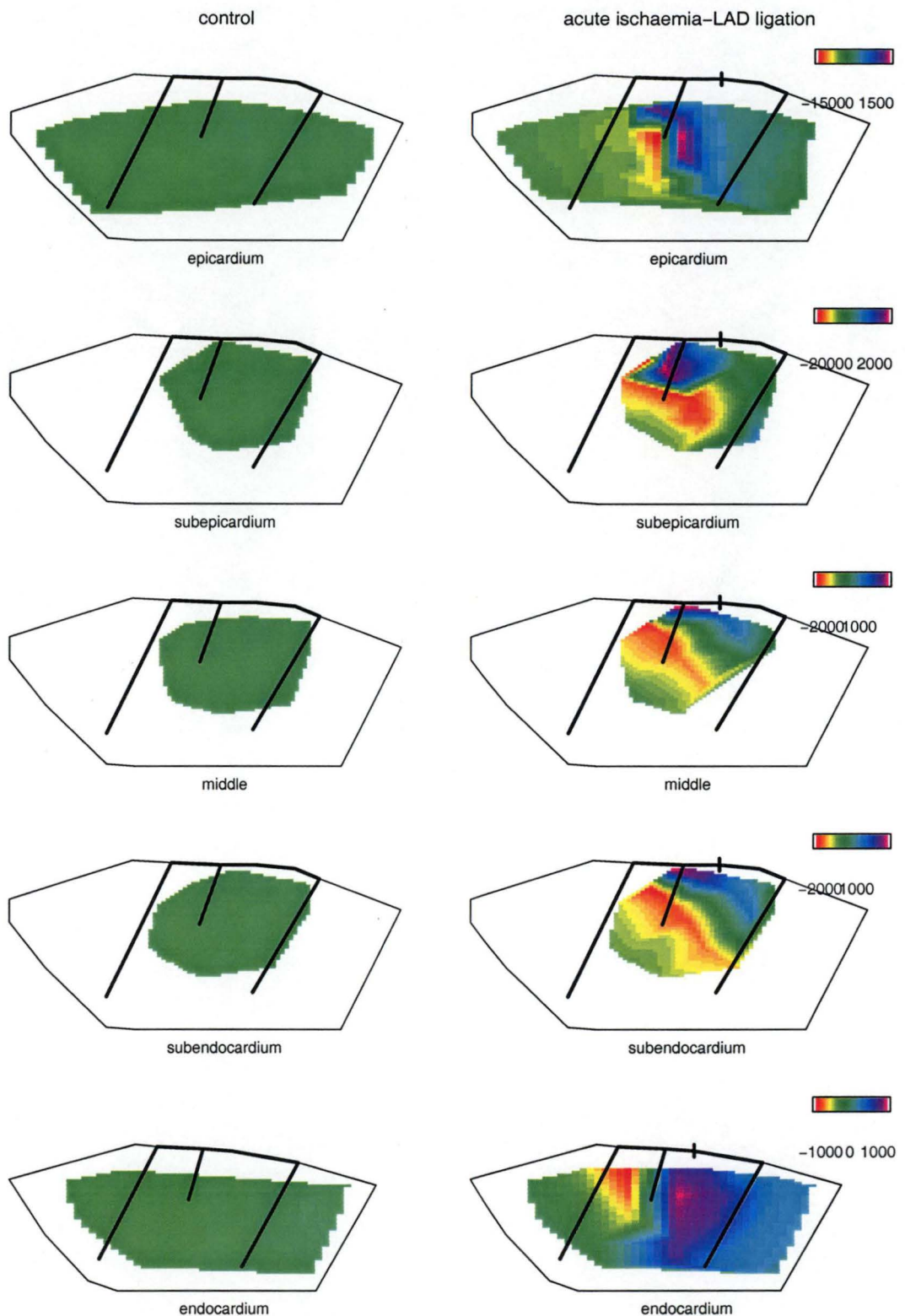


Fig. 6.6 Imaging view of ST potential distributions in different layers of the heart before and at 15min of acute ischaemia in LCX area. The intensities of the shade indicate the quantity of ST potentials. The thickest solid lines reflect the position of the coronary arteries, with the occluded arteries indicated by bars across the coronary arteries. Maps are plotted from data in Fig. 6.5.

6.2.4 TIME COURSE OF ST POTENTIAL DISTRIBUTIONS IN ACUTE TRANSMURAL ISCHAEMIA

6.2.4.1 Time course of ST potential distributions in acute transmural ischaemia of LAD ligation

ST potential distributions were recorded before, 5min, 10min, 15min and 20min after acute transmural ischaemia of LAD ligation. 5 minutes after acute ischaemia, ST elevation and ST depression appeared on every layer of the heart, with maximal and minimal ST potential occurred on the ischaemic and non-ischaemic boundary. 10 to 15 minutes after acute ischaemia, the magnitude of ST shifts reached the highest peak, and then decreased with the development of ischaemia (Fig. 6.7.1 and Fig. 6.7.2).

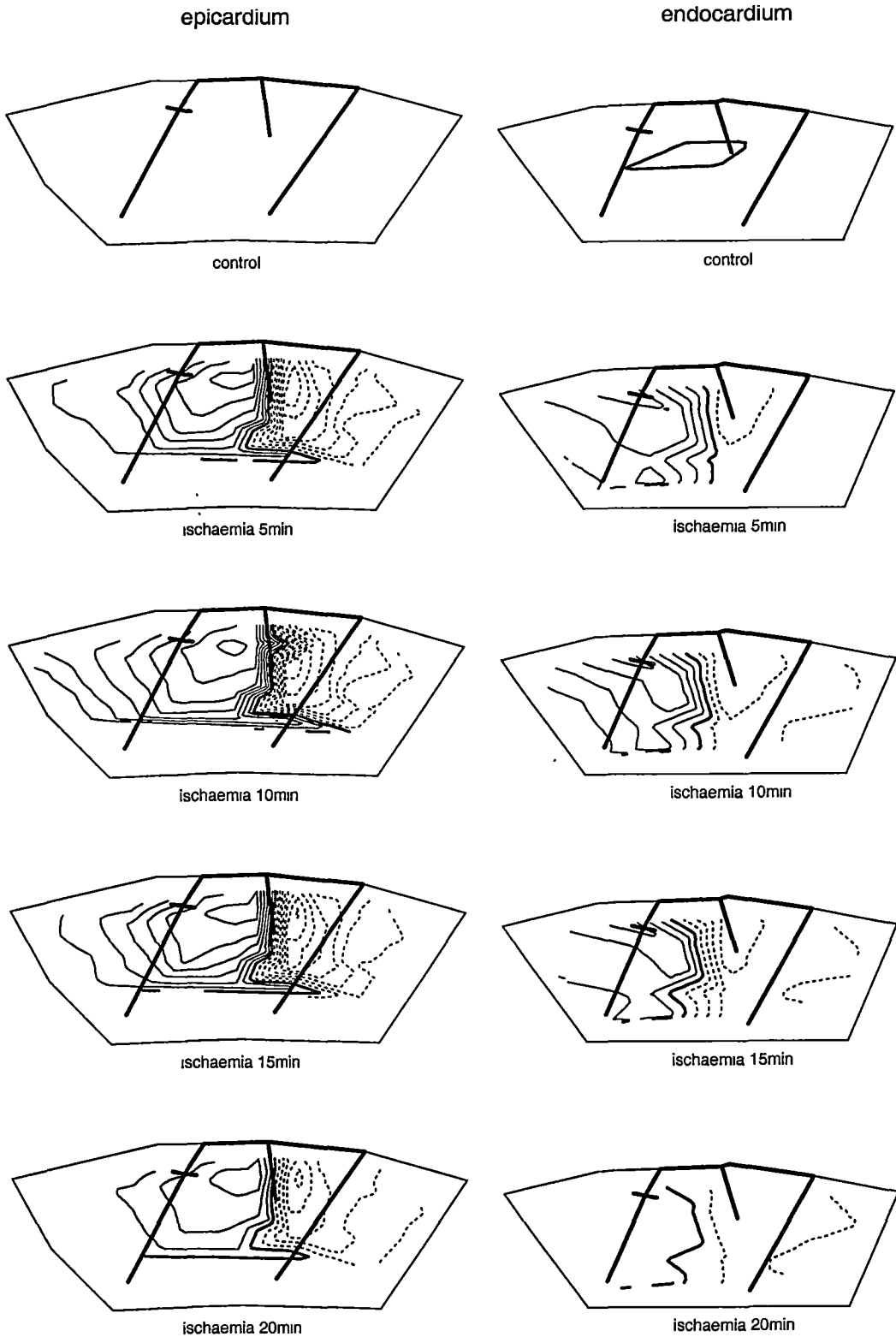


Fig. 6.7.1 ST potential distributions in epicardium and endocardium at control and at various time periods in acute transmural ischaemia of LAD ligation. The thickest solid lines reflect the position of coronary arteries, the thick solid lines indicate zero potential, the thin solid and dashed lines indicate ST elevation and ST depression respectively, with occluded arteries indicated by bars across the coronary arteries. Maps are plotted from data of one animal from group 1. Contour interval=0.5mV.

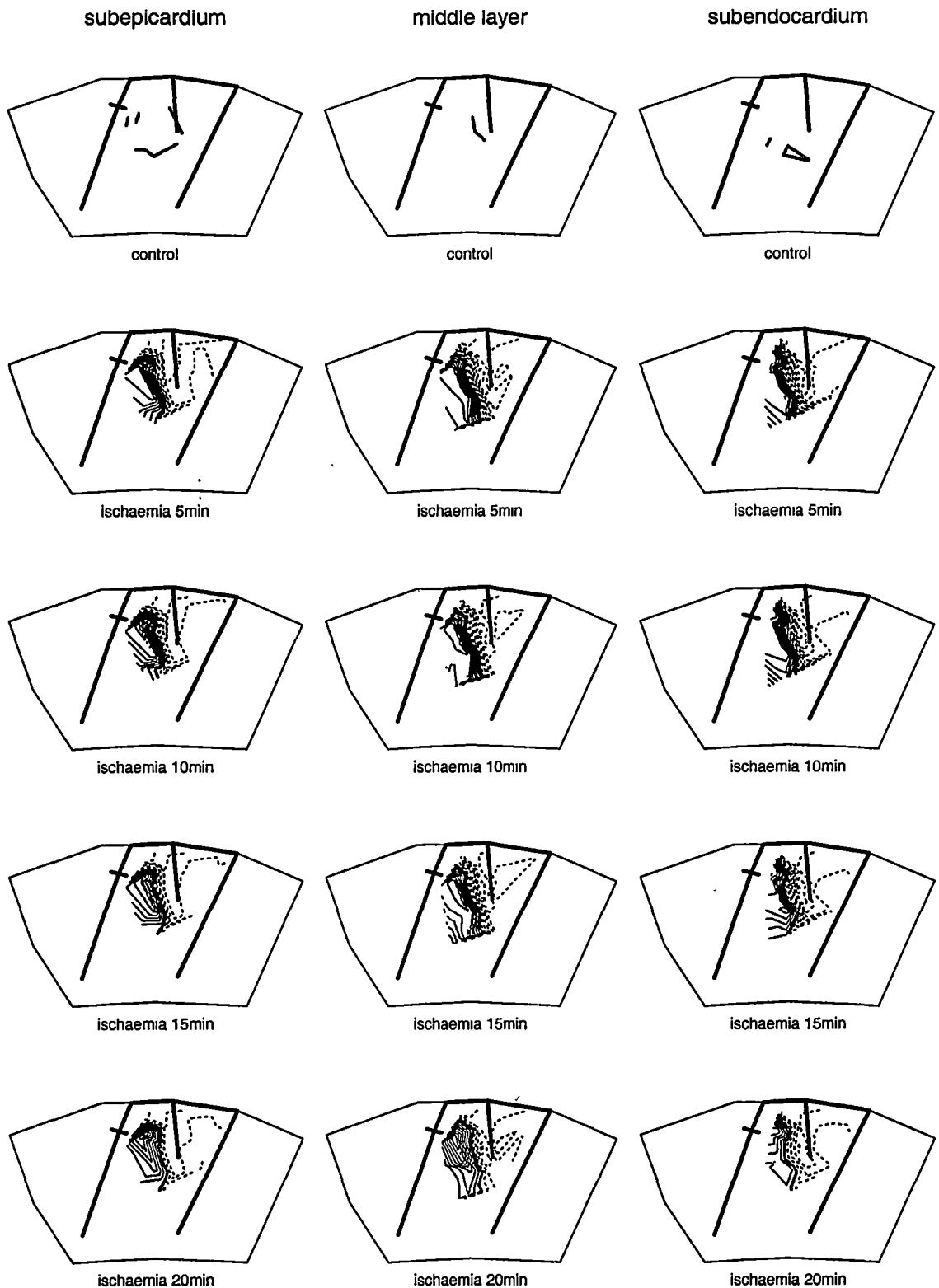


Fig. 6.7.2 ST potential distributions in different depth of intramyocardium at control and at various time periods in acute transmural ischaemia of LAD ligation. The thickest solid lines reflect the position of coronary arteries, the thick solid lines indicate zero potential, the thin solid and dashed lines indicate ST elevation and ST depression respectively, with the occluded arteries indicated by bars across the coronary arteries. Maps are plotted from the data of one animal from group 1. Contour interval=0.5mV.

6.2.4.2 Time course of ST potential distributions in acute transmural ischaemia of LCX ligation

ST potential distributions were recorded before, 5min, 10min, 15min and 20min after acute transmural ischaemia of LCX ligation. Compared to acute LAD ligation, maximal magnitude of ST shifts in acute LCX ligation occurred earlier. 5 to 10 minutes after acute ischaemia, highest magnitude of ST elevation and ST depression appeared on every layer of the heart, with ST elevation occurred in the ischaemic area, ST depression occurred in the non-ischaemic area, and maximal and minimal ST potential occurred on the ischaemic and non-ischaemic boundary. As the ischaemia developed, the magnitude of ST elevation and ST depression decreased (Fig. 6.8.1 and Fig. 6.8.2).

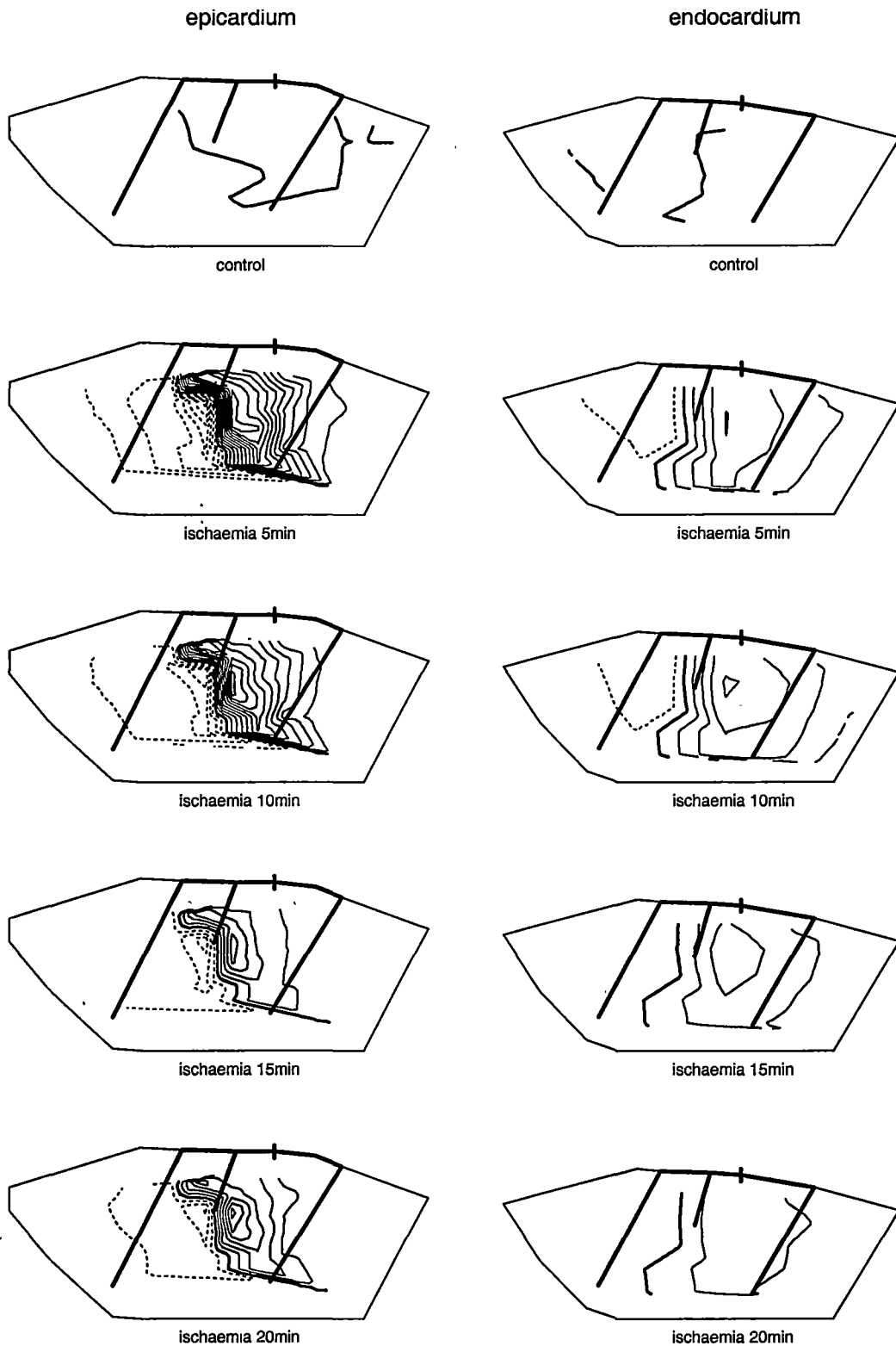


Fig. 6.8.1 ST potential distributions in epicardium and endocardium at control and at various time periods in acute transmural ischaemia of LCX ligation. The thickest solid lines reflect the position of coronary arteries, the thick solid lines indicate zero potential, the thin solid and dashed lines indicate ST elevation and ST depression respectively, with the occluded arteries indicated by bars across the coronary arteries. Maps are plotted from data of one animal from group 1. Contour interval=0.5mV.

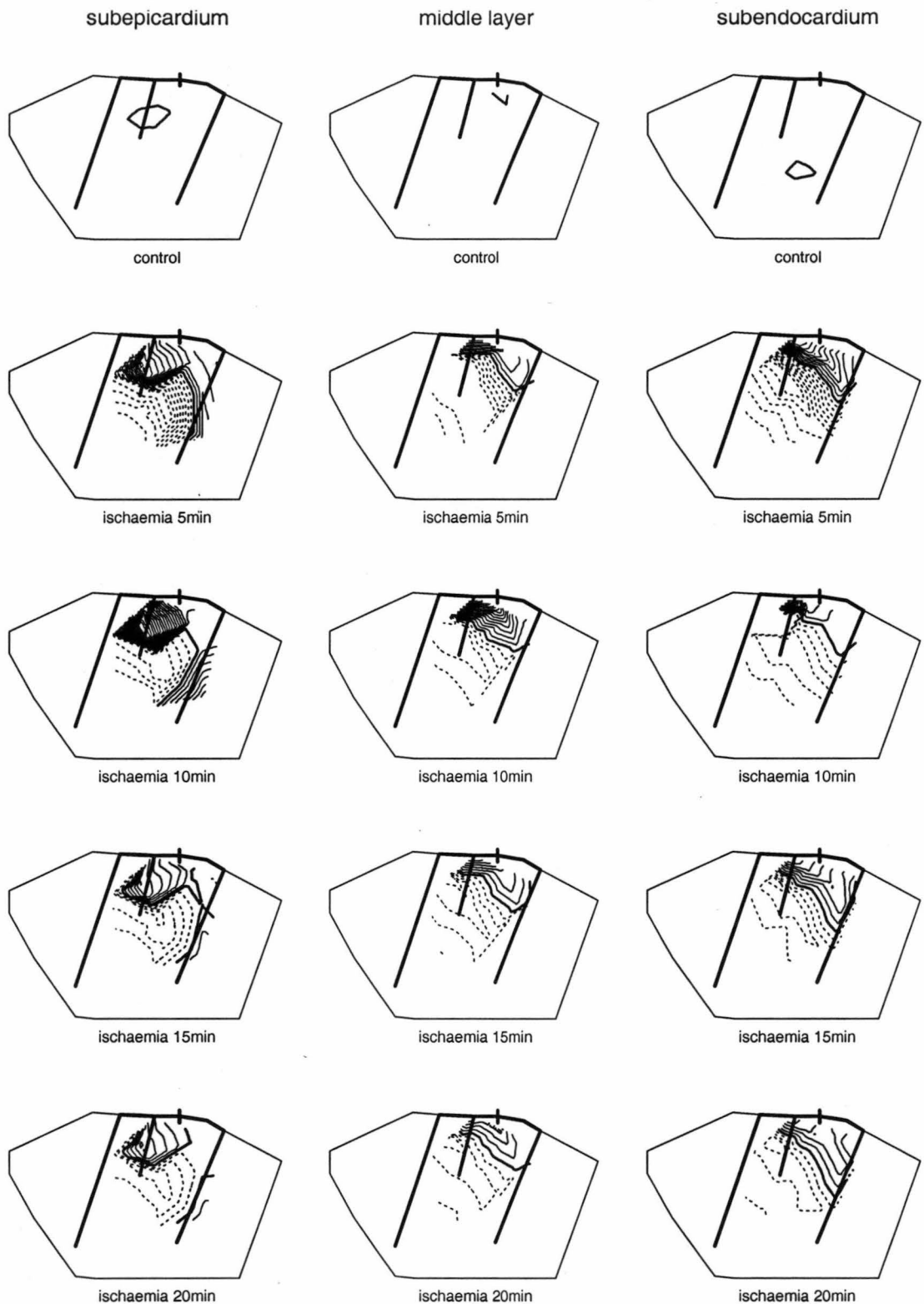


Fig. 6.8.2 ST potential distributions in different depth of intramyocardium at control and at various time periods in acute transmural ischaemia of LCX ligation. The thickest solid lines reflect the position of coronary arteries, the thick solid lines indicate zero potential, the thin solid and dashed lines indicate ST elevation and ST depression respectively, with the occluded arteries indicated by bars across the coronary arteries. Maps are plotted from the data of one animal from group 1. Contour interval=0.5mV.

6.2.5 RELATIONSHIP BETWEEN ST POTENTIAL DISTRIBUTIONS AND RMBF IN ACUTE TRANSMURAL ISCHAEMIA

6.2.5.1 Relationship between ST potential distributions and RMBF in acute transmural ischaemia of LAD ligation

RMBF were measured before and after 15min of acute transmural ischaemia in every one-third layer of the heart. RMBF distribution image maps were plotted and combined with ST potential distribution contour maps. Epicardial and subepicardial ST potential distribution maps were combined with maps of RMBF of the outer one-third layer; intramyocardial ST potential distribution maps of the mid one-third layer were combined with maps of RMBF of the mid one-third layer; Subendocardial and endocardial ST potential distribution maps were combined with maps of RMBF of the inner one-third layer. Fig. 6.9 illustrated that before acute transmural ischaemia, RMBF in every layer had an even distribution over the whole ventricle; there were no ST potential drift. 15min after acute transmural ischaemia, RMBF in the ischaemic region was significantly lower than that of the non-ischaemic region, ST elevation occurred in lower RMBF region every layer of the heart, ST depression occurred at the boundary of the ischaemic and non-ischaemic areas in every layer of the heart.

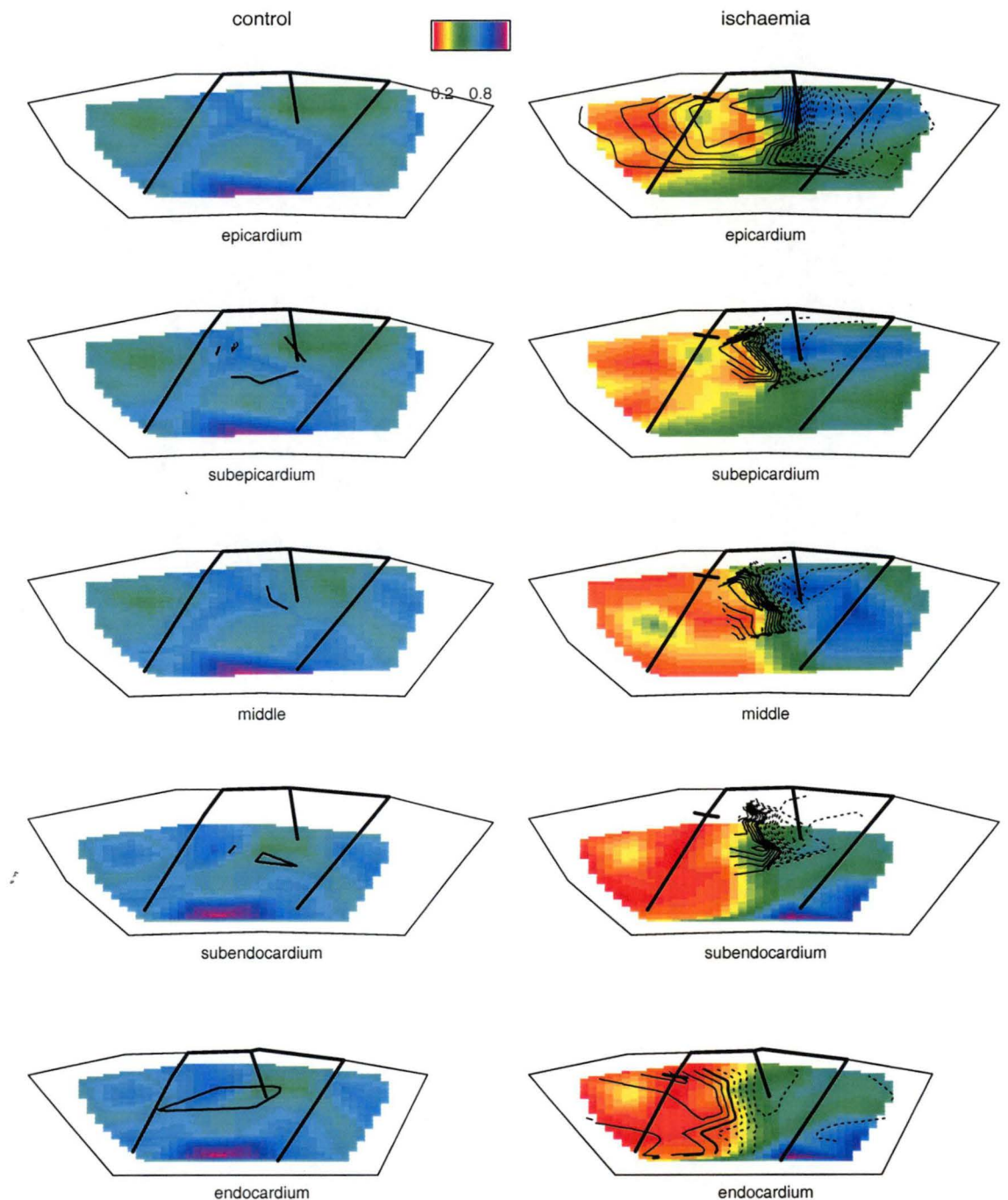


Fig. 6.9 Combination of ST potential distributions (contour lines) and RMBF distributions (shaded area, ml/min/g) in different layers of the heart at control and at 15min of acute transmural ischaemia of LAD ligation. From top to bottom:

Combination of epicardial ST potential distribution and RMBF distribution of outer 1/3 layer;

Combination of subepicardial ST potential distribution and RMBF distribution of outer 1/3 layer;

Combination of mid layer ST potential distribution and RMBF distribution of mid 1/3 layer;

Combination of subendocardial ST potential distribution and RMBF distribution of inner 1/3 layer;

Combination of endocardial ST potential distribution and RMBF distribution of inner 1/3 layer.

The intensities of the shade indicate the quantity of flow. The thickest solid lines reflect the position of the coronary arteries, the thick solid lines indicate zero potential, the thin solid and the dashed lines indicate ST elevation and ST depression respectively, with the occluded arteries indicated by bars across the coronary arteries. Maps are plotted from data of one of the animals in group 1. Contour interval is same as Fig. 6.3.

6.2.5.2 Relationship between ST potential distributions and RMBF in acute transmural ischaemia of LCX ligation

Measurement and maps construction of RMBF were similar to that of LAD ligation. RMBF distribution image maps were combined with ST potential distribution contour maps in the same way as in LAD ligation. Fig. 6.10 illustrated that before acute transmural ischaemia, RMBF in every layer had an even distribution over the whole ventricle, there were no ST potential drift. 15min after acute transmural ischaemia, RMBF in the ischaemic region was significantly lower than that of the non-ischaemic region, ST elevation occurred in every layer of the heart with reduced RMBF, ST depression occurred at the boundary of the ischaemic and non-ischaemic areas in every layer of the heart.

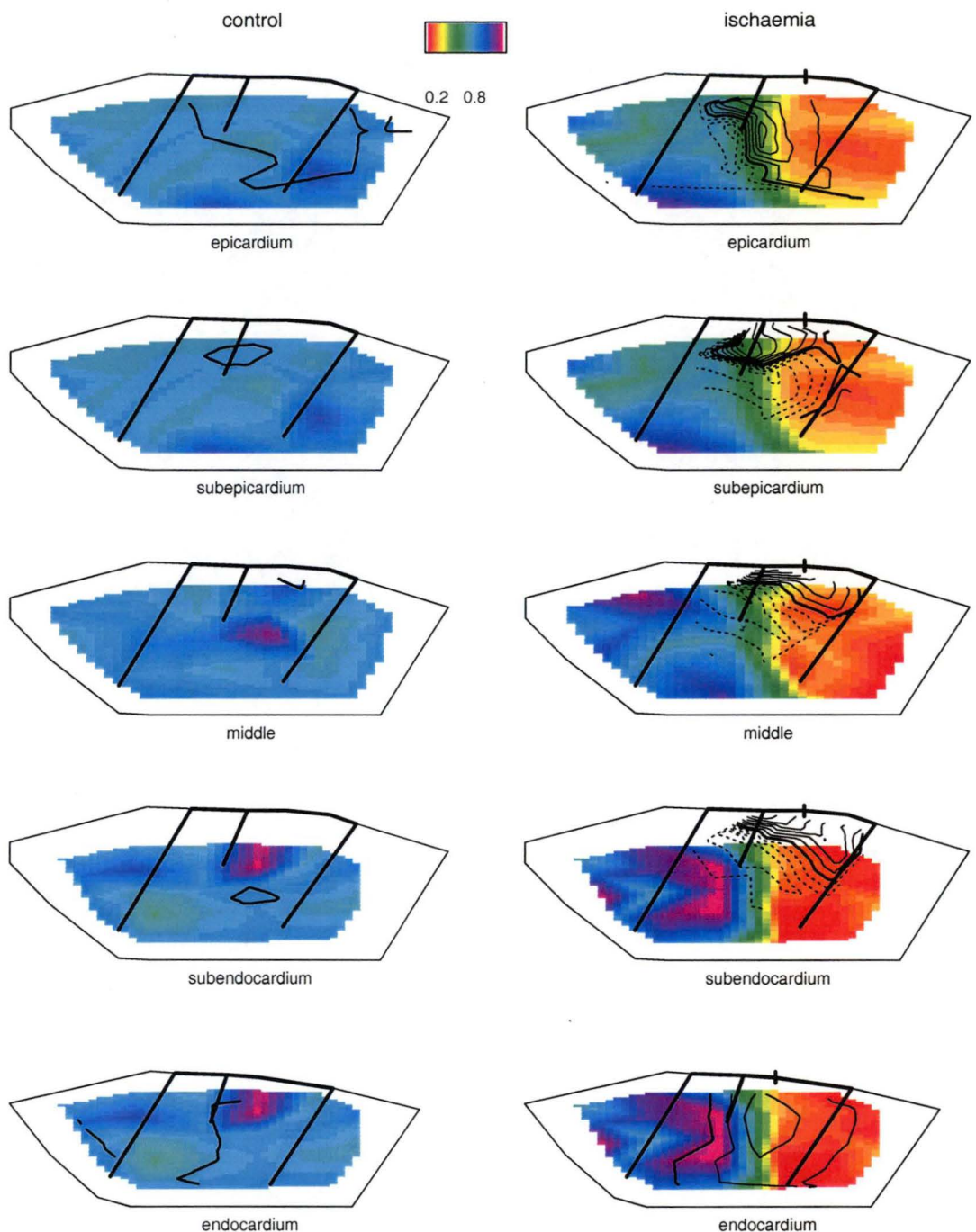


Fig. 6.10 Combination of ST potential distributions (contour lines) and RMBF distributions (shaded area, ml/min/g) in different layers of the heart at control and at 15min of acute transmural ischaemia of LCX ligation. From top to bottom:

Combination of epicardial ST potential distribution and RMBF distribution of outer 1/3 layer;

Combination of subepicardial ST potential distribution and RMBF distribution of outer 1/3 layer;

Combination of mid layer ST potential distribution and RMBF distribution of mid 1/3 layer;

Combination of subendocardial ST potential distribution and RMBF distribution of inner 1/3 layer;

Combination of endocardial ST potential distribution and RMBF distribution of inner 1/3 layer.

The intensities of the shade indicate the quantity of flow. The thickest solid lines reflect the position of the coronary arteries, the thick solid lines indicate zero potential, the thin solid and the dashed lines indicate ST elevation and ST depression respectively, with the occluded arteries indicated by bars across the coronary arteries. Maps are plotted from data of one of the animals in group 2. Contour interval is same as Fig. 6.5.

6.2.5.3 Correlation between ST potential shift and RMBF in acute transmural ischaemia

RMBF was measured in the inner one-third layer, mid one-third layer and outer one-third layer of the left ventricular wall at 15min of acute myocardial ischaemia. ST potentials were recorded from epicardium, subepicardium, mid layer of left ventricular wall, subendocardium and endocardium. The relationships between the mean RMBF and the mean ST potential from the same region at 15min after acute ischaemia were shown in Fig. 6.11.

Panel A showed the relationship between epicardial ST potential shift and RMBF of the outer one-third layer of the left ventricular wall. Panel B showed the relationship between subepicardial ST potential shift and RMBF of the outer one-third layer of the left ventricular wall. Panel C showed the relationship between mid layer ST potential shift and RMBF of the mid one-third layer of the left ventricular wall. Panel D showed the relationship between subendocardial ST potential shift and RMBF of the inner one-third layer of the left ventricular wall. Panel E showed the relationship between endocardial ST potential shift and RMBF of the inner one-third layer of the left ventricular wall.

All the results showed that ST elevation occurred on the area of reduced RMBF, and ST depression occurred on the relatively high RMBF area. However, when ST depression was correlated with RMBF in the non-ischaemic area, it showed no significant relationship ($r=0.004\sim0.145$, $P>0.05$) (Figures were not shown).

To further understand ST depression in acute myocardial ischaemia, the relationship between epicardial, subepicardial, mid layer and subendocardial ST depression and subendocardial RMBF at 15min of ischaemia in the non-ischaemic area were analysed (Fig. 6.12). Although it showed a positive relationship between ST depression of different layer and subendocardial RMBF, the relationship had no statistical significance.

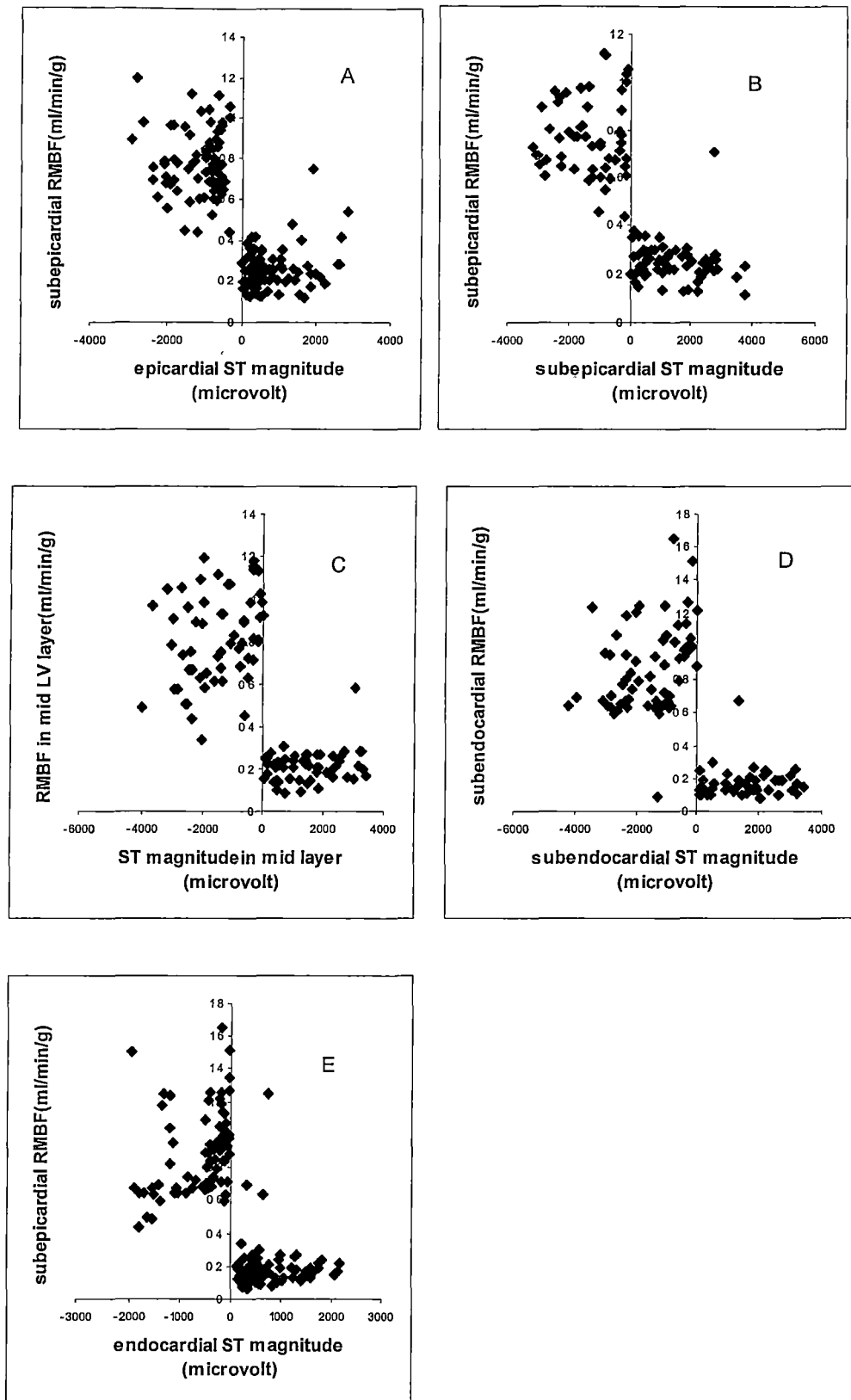


Fig. 6.11 Relationship between ST potential shift and RMBF in different LV layer at 15 min of acute myocardial ischaemia.

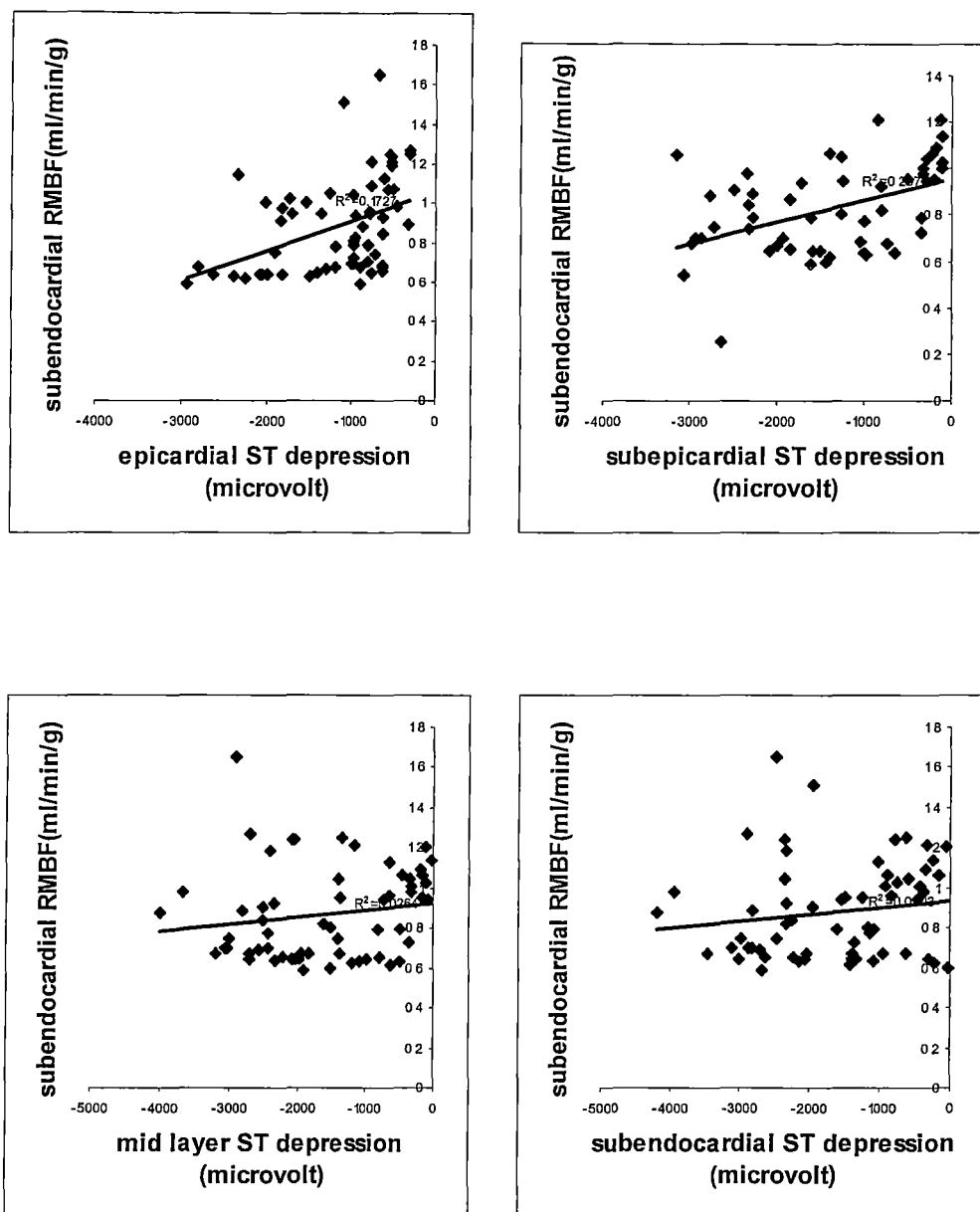


Fig. 6.12 Relationship between epicardial, subepicardial, mid layer and subendocardial ST depression and RMBF of the inner one-third layer of the LV wall at 15min of acute myocardial ischaemia in the non-ischaemic area ($r=0.02\sim0.173$, $P>0.05$).

6.2.6 RELATIONSHIP BETWEEN ST ELEVATION AND ST DEPRESSION

Linear correlation analysis was used to examine the relationship between ST elevation and ST depression in every layer of the heart. Fig. 6.13 showed that there were significant negative correlation between mean ST depression and mean ST elevation in different layer of the heart ($r=0.386\sim0.684$, $P<0.05\sim0.001$).

The results suggested that ST depression over the non-ischaemic area during acute myocardial ischaemia was a result of ST elevation over the ischaemic area.

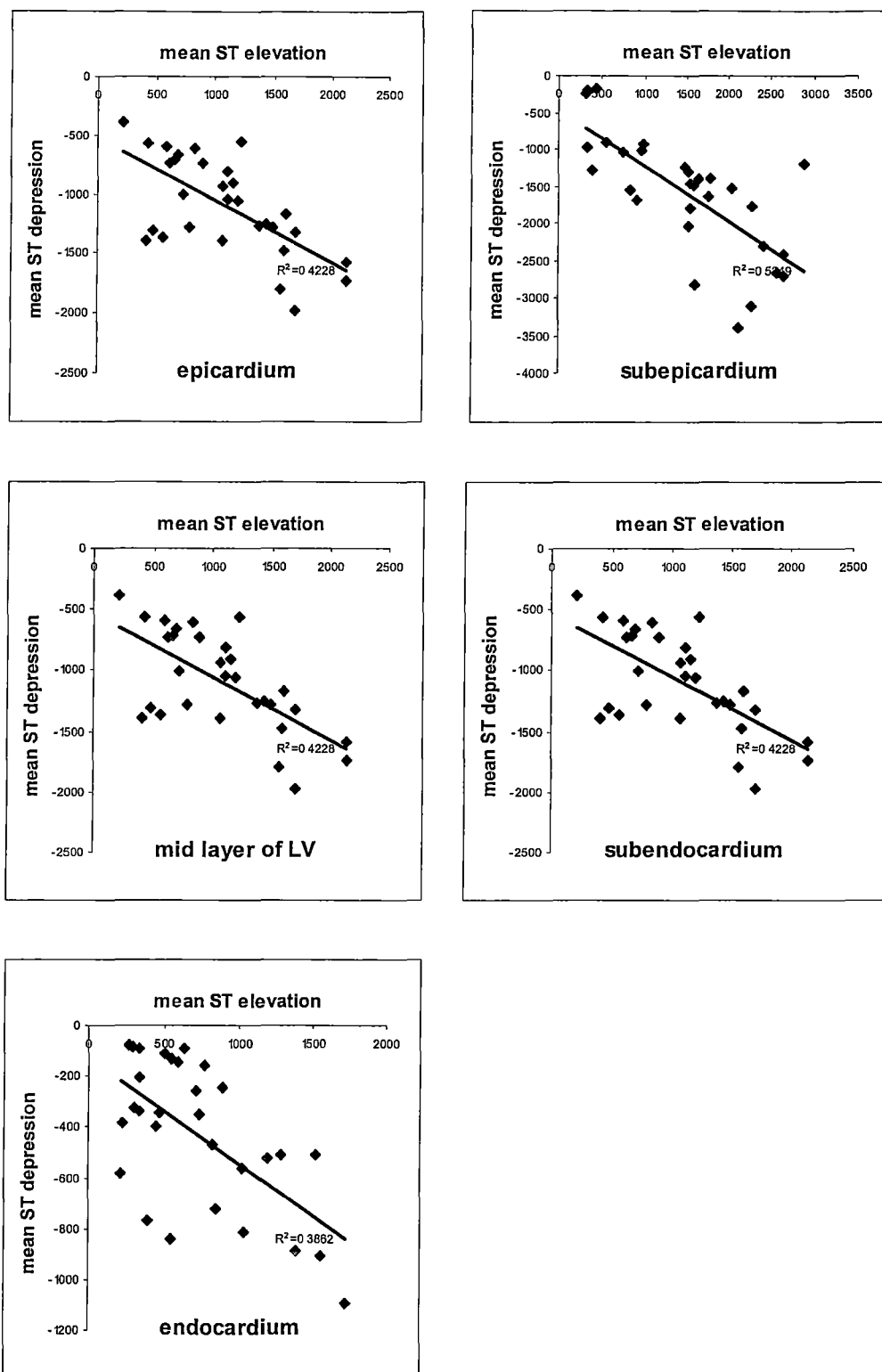


Fig. 6.13 Relationship between mean ST elevation over the ischaemic area and mean ST depression over the non-ischaemic area in every layer of the heart ($r=0.386\sim0.684$, $P<0.05\sim0.001$).

6.3 DISCUSSION

6.3.1 HAEMODYNAMIC RESPONSE IN ACUTE MYOCARDIAL ISCHAEMIA

Clinically, acute coronary syndromes refer to acute obstruction of coronary artery by abrupt rupture of plaque. In the present study, one of the coronary artery was ligated for 20min, which had the same effect as an acute coronary syndrome. The complete occlusion of a coronary artery typically leads to a well described sequence of events. There is rapid decline in myocardial oxygen tension, accompanied by loss of contractile performance; the affected area appears cyanotic and bulging, and the occlusion of the coronary artery further leads to a large zone of necrosis involving the full or nearly full thickness of the ventricular wall in the myocardial bed subtended by the affected coronary artery. The ultrastructure changes in cardiac muscle in experimental infarction following ligation of a coronary artery are noted within 20min, which consist of reduction in the size and number of glycogen granules, intracellular oedema, and swelling and distortion of the transverse tubular system, the sarcoplasmic reticulum, and the mitochondria. Early after the onset of ischaemia, contractile dysfunction in ischaemic zone is observed which is believed to be due in part to the shortening of the action potential duration, reduced cytosolic free calcium levels, and intracellular acidosis. Four abnormal contraction patterns develop in sequence: (1) dyssynchrony (i.e., dissociation in the time course of contraction of adjacent segments), (2) hypokinesis (reduction in the extent of shortening), (3) akinesis (cessation of shortening), and (4) dyskinesis (paradoxical expansion, systolic bulging) (Swan et al., 1972; Forrester et al., 1976). Myocardial contractile function in the non-ischaemic zone is also reduced.

When a sufficient quantity of myocardium undergoes ischaemic injury, it could result in left ventricular pump function depression, reduction of cardiac output, stroke volume, blood pressure and peak dp/dt , and increase of end-systolic volume; these will eventually cause elevation of left ventricular end-diastolic pressure and volume. Haemodynamic indexes were monitored during the whole process of present experiments. Our results showed that left ventricular end-diastolic pressure and left atrial pressure increased significantly during acute ischaemia, while left ventricular systolic pressure and carotid artery pressure decreased significantly during ischaemia. The systolic and diastolic myocardial dysfunction causes deterioration circle of myocardial dysfunction if the ischaemia remains unattended.

6.3.2 RMBF IN ACUTE MYOCARDIAL ISCHAEMIA

Immediately after a coronary artery ligation and cessation of coronary artery blood flow, the RMBF in every layer of the heart begin to decrease, especially in subendocardial layer which has a higher energy requirement (Dunn and Griggs, 1975). Studies revealed that the ovine left ventricle is exclusively supplied by the left main coronary artery and its branches; the LAD supplies the anterior wall and the apex, and the anterior two-thirds of the septum; the LCX supplies the remainder of the left ventricle (Markovitz et al., 1989). In contrast to other mammalian species, the ovine heart lacks an intrinsic coronary collateral circulation (Euler et al., 1983), and thus the ischaemic size and the transmural extent are mainly determined by the size of the occluded vascular bed. Therefore, either the LAD or LCX ligation would produce extensive ischaemia involving the myocardium supplied by the related coronary artery. RMBF is an early and important indicator of ischaemia. It detects both the extent and location of ischaemia, and also reflects the degree of ischaemia.

RMBF was measured in the inner one-third, mid one-third and outer one-third layers of the left ventricular wall before and after 15min of either LAD or LCX ligation in present study. During acute ischaemia, RMBF of every layer in the ischaemic area significantly decreased, especially that in the inner one-third layer, which was represented by decreased endo/epi ratio. RMBF of each layer in the non-ischaemic area also slightly decreased; again with subendocardial blood flow decreased the most. ST elevation occurred on each layer in the areas with reduced RMBF, and ST depression occurred on each layer in the relatively high RMBF area.

6.3.3 EPICARDIAL, ENDOCARDIAL AND INTRAMYOCARDIAL ST POTENTIAL DISTRIBUTIONS DURING ACUTE MYOCARDIAL ISCHAEMIA

Early ST mapping studies have been concentrated on the epicardial potential (Holland and Brooks, 1975; Kleber et al., 1978; Smith et al., 1979). The recording electrodes in these studies were distributed only in the ischaemic and the surrounding regions, the transition in electrophysiological measurements with respect to the distance from an ischaemic border were not examined and therefore the spatial features of the electrophysiological changes in the infarcted and non-infarcted areas were not estimated. A recent study explored ST potential distribution on both epicardium and endocardium during acute coronary artery ligation (Li et al., 1999). In Li's study, the

epicardial ST potentials were recorded from the whole surfaces of both left and right ventricles, the endocardial ST potentials were recorded from the entire endocardium of the left ventricle, and thus it is possible to record detailed signals from both the infarcted and the non-infarcted areas. However, intramyocardial ST potentials were not able to be recorded in those studies. Intramyocardial ST potential was recorded by Wendt (Wendt et al., 1974) as a part of study relate to various interventions effects on acute myocardial ischaemia, but only three intramyocardial electrodes each with one potential recording site were used in the ischaemic area. To map the ST potential distribution in acute myocardial ischaemia information from both the ischaemic and non-ischaemic areas are needed especially on the ischaemic boundary. 29 intramyocardial needles, each having 3 electrodes with different depth were used in this study. The intramyocardial needles were scattered on the ischaemic and non-ischaemic areas, with higher density on the ischaemic boundary.

The present study recorded ST potential distributions simultaneously from epicardium, endocardium and three different layers of left ventricular wall in acute myocardial ischaemia of either LAD or LCX ligation. The results showed a strong dipole on each of the individual layer of the left ventricular wall in either coronary artery ligation. The epicardial potential distributions showed ST elevation over the ischaemic area and ST depression over the non-ischaemic area, with maximal ST potential occurred on the boundary of the ischaemic side and minimal ST potential occurred on the boundary of the non-ischaemic side (Fig. 6.4, Fig. 6.6). The typical epicardial potential distributions of ST changes of the three different coronary arteries damages correspond well to the derived epicardial maps of humans with acute infarction (Kilpatrick et al., 1989). The intramyocardial ST distributions were similar to that of the epicardium, except that the magnitude of ST elevation and ST depression was slightly higher than that of the epicardium (Fig. 6.4, Fig. 6.6). The distribution and magnitude of endocardial ST potential were also similar to that of the epicardium (Fig. 6.4, Fig. 6.6). Thus, in every layer of the heart after acute myocardial ischaemia, there was a dipole with ST elevation occurred on the ischaemic area and ST depression occurred on the non-ischaemic area (Fig. 6.11). The process of this dipole was also recorded for 20min after the coronary artery ligation (data was recorded for 15min in one of six animals due to occurrence of ventricular fibrillation, from which the sheep died within 2min after ventricular fibrillation). During LAD ligation, ST elevation and ST depression appeared on every layer of the heart after 30 seconds of LAD ligation (This is not shown on the graph. Fig. 6.7.1 and Fig. 6.7.2 showed ST potential distributions after 5min of LAD

ligation). 10 to 15min after LAD ligation, the absolute magnitude of ST elevation and ST depression reached the highest value, and then decreased with the progression of ischaemia. During LCX ligation, maximal and minimal magnitude of ST potentials occurred slightly earlier than that of during LAD ligation, the highest absolute magnitude of ST elevation and ST depression on each layer occurred 5 to 10min after LCX ligation, and then decreased (Fig. 6.8.1 and Fig. 6.8.2).

Previous studies showed that following ligation of a coronary artery, epicardial ST elevation occurred within 30 to 60 seconds, and tended to reach a maximum in 5 to 10min (Rakita et al., 1954; Ekmekci et al., 1961a; Li et al., 1999). Ligation of either LAD or LCX resulted in a powerful electrical dipole with ST elevation over the ischaemic region and ST depression over the non-ischaemic region (Li et al., 1999). Early experimental work (Rakita et al., 1954) reported “reciprocal” ST depression in leads taken from the posterior wall of the heart following the ligation of the LAD. Posterior wall ST depression was also observed following LAD occlusion in an isolated, perfused rabbit heart (Brody et al., 1973) and in an in-situ baboon model (Crawford et al., 1984). However, Kleber’s work (Kleber et al., 1978) showed uniform ST elevation over the infarcted region and little change over the border region following the LAD ligation in the isolated pig heart. The different results may be due to the lack of the epicardial electrodes in the non-infarcted region in this study (Kleber et al., 1978).

An early study of mapping the entire surface of the endocardium of left ventricle also showed an electrical dipole after ligation of either LAD or LCX. This endocardial electrical dipole had the similar distribution to the simultaneously recorded epicardial ST potential (Li et al., 1999), but was quite different from those of the endocardial ST potentials in the subendocardial ischaemia (Li et al., 1998). There was little information from literature about intramyocardial ST potential mapping. In Wendt’s study (Wendt et al., 1974), intramyocardial ST potentials were recorded from three different sites in the ischaemic area which showed a highest ST elevation on the ischaemic boundary, the magnitude of ST elevation subsided in the ischaemic center. This was similar to present results. However, no ST potential information from non-ischaemic area was recorded in Wendt’s study.

6.3.4 ST DEPRESSION IN ACUTE MYOCARDIAL ISCHAEMIA

The present study showed exclusively ST depression over the non-ischaemic area in different layers of the left ventricular wall after acute coronary artery ligation. ST shift in acute myocardial ischaemia are attributed to injury currents flowing between the ischaemic area and the normal myocardium (Kleber et al., 1978; Samson and Scher, 1960); electrodes directly overlying the injured zones usually recorded ST elevation (Kleber et al., 1978; Samson and Scher, 1960), which was believed to be resulting from intracellular action potential change during ischaemia (Samson and Scher, 1960). However, electrocardiographic ST depression associated with acute myocardial infarction has not been explained satisfactorily. Two mechanisms are generally discussed. Firstly, ST depression may reflect reciprocal changes of the ST elevation. Secondly, it may also be produced by added ischaemia of adjacent myocardium. Many studies have suggested that ST depression was an indicator of a poor prognosis (Shah, 1980; Billadello et al., 1983; Mukharji et al., 1984; Haraphongse et al., 1984; Kilpatrick et al., 1989; Bates et al., 1990). Others considered that ST depression was only “reciprocal” to ST elevation (Wolferth et al., 1945; Putini et al., 1993; Fletcher et al., 1993; Stevenson et al., 1993 and 1994; Birnbaum et al., 1994).

According to classic electrocardiographic theory, ST depression should be expected during acute myocardial ischaemia as a “reciprocal” change of ST elevation. Our results showed exclusively ST depression over the non-ischaemic area and ST elevation over the ischaemic area in each individual layer of the left ventricular wall following acute coronary artery ligation, and the ST depression corresponded well with the ST elevation (Fig. 6.13). The significant positive relationship between the mean ST depression over the non-ischaemic area and the mean ST elevation over the ischaemic area suggested that ST depression in acute myocardial ischaemia is a reciprocal change of ST elevation.

Ferguson (Ferguson et al., 1984) performed coronary angiography on a group of patients with acute myocardial infarction. Patients with concomitant ST depressions in inferior ECG leads had similar degrees of anterior segmental wall motion abnormalities when compared with patients without ST depression, there were no abnormalities in the wall motion of the inferior or posterior myocardium. Furthermore, the extent of inferior ST depression correlate well with the degree of ST elevation in the anterior precordial leads, thereby suggested that the ST depression was an ECG phenomenon. However, other investigators (Lembo et al., 1986; Hlatky et al., 1985) suggested that inferior infarctions with anterior ST depression of 0.1mV or more were

associated with a larger area of infarction, poorer residual left ventricular function, and a higher in-hospital and 1-year mortality. The greater degree of left ventricular dysfunction observed in this subgroup may be the result of more extensive involvement of the inferior myocardium as well as the posterior and lateral walls (Gibson et al., 1982; Pierard et al., 1986; Ruddy et al., 1986). By analysing derived epicardial potential distribution patterns, Kilpatrick (Kilpatrick et al., 1989) found that epicardial electrical dipoles were present in patients with single vessel disease as well as in those with triple vessel disease and that the dipole predicted the death of those with single vessel disease. Further analysis showed that the degree of ST elevation and ST depression, and the negative ST segment area voltage integral were significantly related to mortality. They concluded that the dipole reflects major subendocardial ischaemia in other territories and suggested that this ischaemia be a result of mechanical stress secondary either to the size of the inferior infarction producing high wall stress in the remaining ventricle or to a mechanical dysfunction such as mitral regurgitation, ventricular septal defect or cardiac rupture.

A recent animal study showed that epicardial ST depression over the non-ischaemic area after acute coronary ligation correlated to the endocardial flow reduction (Li 1997), suggesting that ST depression during acute myocardial ischaemia might reflect remote ischaemia secondary to a reduced perfusion pressure. However, conflicting results were recorded from Li's study (Li, 1997). Even though epicardial ST depression was considered to be caused by subendocardial ischaemia in non-infarcted area, endocardial ST depression was recorded on the non-infarcted region. In stead of predicted ST elevation, the endocardial ST potential distribution patterns were similar to that of the epicardial, i.e., a dipole formed by ST depression over the non-infarcted region and ST elevation over the infracted region. Furthermore, Li found that there was a good correlation between the magnitude of epicardial ST depression in the non-infarcted regions and the magnitude of epicardial ST elevation in the infracted regions. They suggested that the epicardial ST depression was not purely secondary to subendocardial ischaemia of the non-infarcting myocardium.

It seemed both classic ECG theory and experimental results could not explain ST depression during acute myocardial ischaemia. By constructing a concentric spheres model, Li and co-workers (1999) suggested that some basic balance between ST elevation and ST depression exist, the total current flowing out of the heart must flow back into the heart. The basic property of physics dictates that the overall current out of the heart must be zero; all ST balances between ST elevation and ST depression

are subject to this. The ST depression was part of the source, and the balance between elevation and depression was dependent on the zero line set by the requirement that the overall current from the heart was zero. Li (Li et al., 1999) suggested that any large infarction will have both ST elevation and ST depression generated at the ischaemic boundary on the epicardium.

The present results also showed that there were an overall linear relationship between ST potential shift and RMBF in each individual layer of the left ventricular wall, i.e., ST elevation occurred on the area of low RMBF and ST depression occurred on the relatively high RMBF area. Nevertheless, when only ST depression correlated with RMBF in corresponded area, there was no significant relationship between ST depression and RMBF. This result suggested that ST depression is not a direct consequence of decreased RMBF. As we know, the endocardial RMBF decreased further than the epicardial RMBF in acute myocardial ischaemia in non-ischaemic area, we hypothesized that ST depression might relate to endocardial RMBF. However, our result did not show any statistical relationship between epicardial and intramyocardial ST depression and endocardial RMBF, which is contrary to Li's study (Li et al, 1999), (Fig. 6.12).

Thus the intramyocardial and the endocardial potential distribution patterns in present study might also be explained by this proposal. According to Li's (Li et al., 1999) analysis, it is clear that the dipole in every layer of the heart reflected the overall size of the infarction. Because the overall current from the heart was zero, ST elevation is always expected to be accompanied by ST depression. Although additional ischaemia existed in remote region, this will also be constrained by the need to have the overall current from the heart be zero. The presence of additional ischaemia will probably increase the ST elevation as well as increase the ST depression. The intramyocardial ST potential distribution at present study supported Li's model analysis (Li et al., 1999) and should be a clue for future study.

CHAPTER SEVEN CONCLUSION

7.1 SUMMARY OF THE STUDY

Subendocardial ischaemia

- 1) Epicardial ST potential mapping showed that the epicardial ST potential distributions were independent of the ischaemic region, whether they were in different animals or in the same sheep.
- 2) The endocardial ST elevation occurred on the ischaemic area in either the LAD or LCX occlusion. When the LAD and LCX were occluded alternatively, ST elevation occurred alternately on the ischaemic surface.
- 3) Intramyocardial ST potential distributions showed that the ST elevation occurred on the ischaemic centre, and the ST depression occurred on the boundary of the ischaemic and non-ischaemic areas, which is also in dependant of the ischaemic region. The distributions of ST potential in different intramural layers were quite similar.

Transition from mild to severe subendocardial ischaemia

- 4) Epicardial ST potential distributions in mild subendocardial ischaemia in either the LAD or LCX area showed similar pattern. Simultaneously recorded endocardial potential showed ST elevation related to the ischaemic area. Intramyocardial ST potential recording showed a dipole in different layers of the heart, with ST elevation occurring in the ischaemic centre and ST depression occurring on the boundary of the ischaemic and non-ischaemic areas.
- 5) In severe subendocardial ischaemia of either LCX or LAD area, ST elevation occurred in the ischaemic area, ST depression appeared in the non-ischaemic area. Endocardial ST elevation in severe ischaemia occurred in the ischaemic region.
- 6) When the severe ischaemia developed to full thickness, no matter which region was involved, there occurred a strong dipole in each layer of the heart, with ST elevation appeared in the ischaemic area, and ST depression appeared in the non-ischaemic area.

Acute myocardial ischaemia

- 7) Similar ST potential distributions pattern presented in acute myocardial ischaemia, with strong dipoles occur on each of the individual layers of the left ventricular wall in either coronary artery ligation.

- 8) The ST potential distributions showed ST elevation over the ischaemic area and ST depression over the non-ischaemic area, with maximal ST potential occurring on the boundary of the ischaemic side and minimal ST potential occurring on the boundary of the non-ischaemic side.

7.2 SUBENDOCARDIAL ISCHAEMIA MODEL

The primary aim of this study is to detect the transmural ST potential distribution on the ischaemic boundary during subendocardial ischaemia and to give a clue to explain why electrical current flows in such a manner as to cause epicardial ST depression over the ischaemic boundary.

A subendocardial ischaemic sheep model was produced by partially occluding the coronary artery together with pacing the left atrium at a rate of 180bpm in the anaesthetised sheep. Subendocardial ischaemia was produced in either the LAD area or the LCX area in different sheep, or in both LAD and LCX areas alternately in the same sheep. Measurement of RMBF showed that partially occluding a coronary artery plus atrial pacing resulted in a significant decrease of RMBF in the subendocardium, represented by a decreased endo/epi blood flow ratio.

ST potential distributions were recorded from the epicardium, endocardium and three different layers of the intramyocardium. Epicardial and endocardial ST potentials were recorded in a previous study. Intramyocardial ST potentials were recorded by self-made intramyocardial needles. Each needle has three electrodes on it, which enable the recording of intramyocardial potentials from three different depth of the left ventricular wall. The results were as following:

- (1) Epicardial ST potential mapping showed that the epicardial ST potential distributions were independent of the ischaemic region, whether they were in different animals or in the same sheep. When ischaemia of different regions was produced alternately in the same animal, it showed similar epicardial ST potential distributions in ischaemia of various regions ($r=0.769\pm0.135$). This result was consistent with previous studies which suggested that epicardial ST can not localise the ischaemic region. This explains the clinical difficulty in identifying stenosed arteries from body surface ST depression.

(2) The endocardial ST elevation occurred on the ischaemic area in either the LAD or LCX occlusion. When the LAD and LCX were occluded alternatively, ST elevation occurred alternately on the ischaemic surface.

(3) Intramyocardial ST potential recording showed dipoles in different layers of the left ventricular wall. Whichever coronary artery was occluded, or if both arteries were occluded in turn, it showed the ST elevation occurred on the ischaemic centre, and the ST depression occurred on the boundary of the ischaemic and non-ischaemic areas, the distributions of ST potential in different intramyocardial layers were quite similar.

We hypothesize that the epicardial ST depression should be compensation for the endocardial ST elevation. The different potential distributions between the epicardium and intramyocardium leads us to a further hypothesis that there might be an electrical structure under the epicardium, this hypothesized subepicardial structure might have different electrical characters as to disturb the electrical current path.

7.3 TRANSITION FROM MILD TO SEVERE SUBENDOCARDIAL ISCHAEMIA

To further understand the intramyocardial path of ST potential during ischaemia, a series of experiments were performed to convert mild subendocardial ischaemia to severe, and eventually to full thickness ischaemia. Different degrees of coronary artery blood flow reduction were performed: In the mild coronary artery blood flow reduction group, coronary blood flow was reduced by 30% of the original flow; In severe coronary artery blood flow reduction group, coronary blood flow was reduced by 70% of the original flow; after severe ischaemia, the coronary artery was totally occluded, resulted in a full thickness ischaemia. RMBF was measured in three layers of the left ventricular wall during mild and severe ischaemia. ST potential distributions were recorded from epicardium, endocardium and three different layers of the intramyocardium. The results showed that:

(1) In the mild subendocardial ischaemia group, blood flow in the inner one-third layer decreased significantly; in the severe subendocardial ischaemia group, blood flow in every layer decreased significantly.

(2) Mild subendocardial ischaemia in either the LAD or LCX area caused similar epicardial ST potential distributions. Simultaneously recorded endocardial potential

showed ST elevation related to the area supplied by the culprit coronary artery. Intramyocardial ST potential recording showed a dipole in different layers of the heart, with ST elevation occurring in the ischaemic centre and ST depression occurring on the boundary of the ischaemic and non-ischaemic areas.

(3) In severe subendocardial ischaemia of either LCX or LAD area, both ST elevation and ST depression occurred on the epicardium and different layers of intramyocardium, ST elevation appeared in the ischaemic area, with the maximal magnitude occurring in the ischaemic centre; ST depression appeared in the non-ischaemic area, the magnitude of ST depression decreased towards the ischaemic boundary. Endocardial ST elevation in severe ischaemia occurred in the ischaemic region.

(4) When the ischaemia became full thickness, no matter which region was involved, there occurred a strong dipole in each layer of the heart. As in severe subendocardial ischaemia, ST elevation appeared in the ischaemic area, and ST depression appeared in the non-ischaemic area. However, the highest magnitude of both ST elevation and ST depression occurred close to the ischaemic boundary.

The different epicardial ST potential distributions during mild and severe ischaemia led to a postulate that the current path might break through towards the epicardium during severe subendocardial ischaemia. During severe ischaemia, the RMBF in every layer decreased, while in mild ischaemia, only the subendocardial RMBF decreased. Thus, the middle and outer one-third layers of the left ventricle might have a vital effect on the different epicardial ST potential distributions during mild and severe ischaemia.

The similarity of intramyocardial ST distributions in mild and severe ischaemia might result from the same blood flow distribution in both groups. Even though RMBF in every layer of the heart in severe subendocardial ischaemia was lower than that in mild subendocardial ischaemia, the RMBF distributions were the same. The different distributions of ST potential between severe and full thickness ischaemia are not easily explained. It might suggest that with the progress of ischaemia, the current path follows a regular way to spread out towards the epicardium. When the ischaemia becomes full thickness, a quantitative to qualitative transit occurs in this current path, resulting in a vital current path distortion.

7.4 ACUTE MYOCARDIAL ISCHAEMIA MODEL

Another aim of this study was to investigate the electrophysiologic and pathophysiologic mechanism of ST depression occurring with ST elevation during acute myocardial ischaemia. Acute myocardial ischaemia was produced by totally occluding either the LAD or LCX. RMBF was measured in three layers of the left ventricular wall. ST potential distributions were also recorded simultaneously from epicardium, endocardium and three different transmural layers of left ventricular wall. The following results were obtained:

- (1) During acute myocardial ischaemia, RMBF of every layer in the ischaemic area significantly decreased. This was especially so in the inner one-third layer, which was represented by decreased endo/epi ratio. RMBF of each layer in the non-ischaemic area also slightly decreased, again the subendocardial blood flow decreased the most. ST elevation occurred on each layer in the area of low RMBF, and ST depression occurred on each layer in the area of relatively high RMBF.
- (2) The results of ST potential distributions showed a strong dipole on each of the individual layers of the left ventricular wall in either coronary artery ligation. The epicardial potential distributions showed ST elevation over the ischaemic area and ST depression over the non-ischaemic area, with maximal ST potential occurring on the boundary of the ischaemic side and minimal ST potential occurring on the boundary of the non-ischaemic side. The intramyocardial ST distributions were similar to that of the epicardium, except that the magnitude of ST elevation and ST depression was much higher than that of the epicardium. The distribution and magnitude of endocardial ST potential were also similar to that of the epicardium.

The ST depression in acute myocardial ischaemia can not be explained by classical ECG theory. A concentric spheres model suggested that some basic balance between ST elevation and ST depression exists. According to this model, the total current flowing out of the heart must flow back into the heart. The basic property of physics dictates that the overall current out of the heart must be zero; all ST balances between ST elevation and ST depression are subject to this. Thus the ST potential distribution patterns in present study might be explained by this proposal. Because the overall current from the heart was zero, ST elevation is always expected to be accompanied by ST depression.

References

- Abel FL, Cooper RH, Beck RR. Use of fluorescent latex microspheres to measure coronary blood flow distribution. *Circ Shock*,41:156~161,1993
- Abildskov JA, Burgess MJ, Lux RL, Wyatt RF. Experimental evidence for regional cardiac influence in body surface isopotential maps of dogs. *Circ Res*,38(5) 386~391,1976
- Abraham NG. A suction electrode net for precordial ECG mapping. *J Med Eng Tech*,7:285~287,1983.
- Antzelevitch C. Molecular basis for the transmural distribution of the transient outward current. *J Physiol*,15,533(Pt 1):1,2001.
- Antzelevitch C, Shimizu W, Yan GX, Sicouri S, Weissenburger J, Nesterenko VV, Burashnikov A, Di Diego J, Saffitz J, Thomas GP. The M cell: its contribution to the ECG and to normal and abnormal electrical function of the heart. *J Cardiovasc Electrophysiol*,10:1124~1152,1999.
- Archie JP, Fixler DE, Ulliyot DJ, Buckberg GD, Hoffman JJ. Regional myocardial blood flow in lambs with concentric right ventricular hypertrophy. *Circ Res*,34(2) 143~154,1974.
- Arthur RM. Evaluation and use of a human dipole plus quadrupole equivalent cardiac generator. PhD Dissertation, University of Pennsylvania,1968
- Bache RJ, McHale PA, Greenfield JC. Transmural myocardial perfusion during restricted coronary inflow in the awake dog. *Am J Physiol*,232:H645~651,1977.
- Ball RM, Bache RJ. Distribution of myocardial blood flow in the exercising dog with restricted coronary artery inflow. *Circ Res*,38:60~66,1976.
- Barker PS, Macleod AG, Alexander J. The excitatory process observed in the exposed human heart. *Am Heart J*,5:720~742,1930.
- Barlow CH, Harken AH, Chance B. Evaluation of cardiac ischaemia by NADH fluorescence photograph. *Ann Surg*,186(6):734~740,1977
- Barnes AR, Whitten MB. Study of the RT interval in myocardial infarction. *Am Heart J*,5:142~171,1929.
- Barr RC, Spach MS. Inverse calculation of QRS-T epicardial potentials from body surface potential distributions for normal and ectopic beats in the intact dog. *Circ Res*,42(5):661~675,1978a.
- Barr RC, Spach MS. A comparison of measured epicardial potentials with epicardial potentials computed from body surface measurements in the intact dog. *Adv Cardiol*,21:19~22,1978b.
- Bates ER, Clemmensen PM, Califf RM, Gorman LE, Aronson LG, George BS, Kereiakes DJ, Topol EJ. Precordial ST segment depression predicts a worse prognosis in inferior infarction despite reperfusion therapy. The thrombolysis and Angioplasty in Myocardial Infarction (TAMI) Study Group. *J Am Coll Cardiol*,16(7):1538~1544,1990.
- Baughman KL, Maroko PR, Vatner SF. Effects of coronary artery reperfusion on myocardial infarct size and survival in conscious dogs. *Circulation*,63(2):317~323,1981.
- Bayley RH. Biophysical principles of electrocardiography. New York, Hoeber, pp19~34, 184~196, 207~222, 1958.
- Bayley,RH.. The electrocardiographic effects of injury at the endocardial surface of the left ventricle. *Am Heart J*,31:677~684,1946.
- Bayley,RH, LaDue JS, York DJ. Electrocardiographic changes produced in the dog by temporary occlusion of a coronary artery showing a new stage in the evolution of myocardial infarction. *Am Heart J*, 27:164~169,1944.
- Bayley RH. An interpretation of the injury and ischaemic effects of myocardial infarction in accordance with the laws which determine the flow of electric currents in homogeneous volume conductors and in accordance with relevant pathologic changes. *Am Heart J*,24:514~528,1942
- Bayley RH, Berry PM. The arbitrary electromotive double layer in the eccentric "heart" of the nonhomogeneous circular lamina. *IEEE Trans Biomed Eng*,11(4):137~147,1964
- Beatty GE, Adler SW, Benditt DG. Non-contact measurement of endocardial potentials with a percutaneously introduced multi-electrode array catheter. *Circulation*,90(4 pt 2) I-280,1994
- Becker LC, Fortuin NJ, Pitt B. Effect of ischaemia and antianginal drugs on the distribution of radioactive microspheres in the canine left ventricle. *Circ Res*,28(2):263~269,1971.
- Biheimer DW, Buja LM, Parkey RW, Bonte FJ, Willerson JT. Fatty acid accumulation and abnormal lipid deposition in peripheral and border zones of experimental myocardial infarcts. *J Nucl Med*,19(3):276~283,1978.
- Birnbaum Y, Solodky A, Herz I, Kusnec J, Rechavia E, Sulkas J, Sclarovsky S. Implications of inferior ST-segment depression in anterior acute myocardial infarction: electrocardiographic and angiographic correlation. *Am Heart J*,127:1467~1473,1994

- Bodenheimer MM, Banka VS, Levites. Temporal relation of epicardial electrographic, contractile and biochemical changes after acute coronary occlusion and reperfusion. *Am J Cardiol*, 37(4):486-492, 1976.
- Boineau JP, Spach MS. The relationship between the electrocardiogram and the electrical activity of the heart. *J Electrocardiol*, 1(1):117-124, 1968.
- Brandt G, Fam WM, McGregor M. Measurement of coronary flow in local areas of myocardium using xenon¹³³. *J Appl Physiol*, 24(3):446-450, 1968.
- Brody DA, Terry FH, Ideker RE. Eccentric dipole in a spherical medium: generalized expression for surface potentials. *IEEE Trans Biomed Eng*, 20(2):141-143, 1973.
- Brooks H, Al-Sadir J, Schwartz J, Rich B, Harper P, Resnekov L. Biventricular dynamics during quantitated anteroseptal infarction in the porcine heart. *Am J Cardiol*, 36(6):765-775, 1975.
- Browne KF, Chilson DA, Waller BF, Zipes DP. Use of a spatially distributed multielectrode catheter to activation map the left ventricular endocardium simultaneously and destroy selected areas. *Circulation*, Suppl 1:1-84, 1983.
- Brusca A, Rosettani E. Activation of the human fetal heart. *Am Heart J*, 86(1):79-87, 1973.
- Burchell HB, Frye RL, Anderson MW, McGoon DC. Atrioventricular and ventriculoatrial excitation in Wolff-Parkinson-White syndrome (type B). Temporary ablation at surgery. *Circulation*, 36(5):663-672, 1967.
- Caldwell PC. Factors governing movement and distribution of inorganic ions in nerve and muscle. *Physiol Rev*, 48(1):1-64, 1968.
- Camara EJ, Chandra N, Ouyang P, Gottlieb SH, Shapiro EP. Reciprocal ST change in acute myocardial infarction: assessment by electrocardiography and echocardiography. *J Am Coll Cardiol*, 2:251-257, 1983.
- Camici P, Ursini F, Galiazzo F, Bellitto L, Pelosi G, Marzilli M, L'Abbate A, Barsacchi R. Different respiratory activities of mitochondria isolated from the subendocardium and subepicardium of the canine heart. *Basic Res Cardiol*, 79(4):454-460, 1984.
- Chung EK. *Electrocardiography. Practical application with vectorial principles*. New York, Harper & Row, pp89-133, 1980.
- Cinca J, Figueras J, Senador G, Garcia-Moreno E, Salas A, Rius J. Transmural DC electrograms after coronary artery occlusion and latex embolization in pigs. *Am J Physiol*, 246(4 pt 2):H475-482, 1984.
- Cinca J, Janse MJ, Morena H, Candell J, Valle V, Durrer D. Mechanism and time course of the early electrical changes during acute coronary artery occlusion. *Chest*, 77(4):499-505, 1980.
- Clark J, Plonsey R. A mathematical evaluation of the core conductor model. *Biophys J*, 6:95-112, 1966.
- Clerc L. Directional differences of impulse spread in trabecular muscle from mammalian heart. *J Physiol*, 255:335-346, 1976.
- Cohen D, Kaufman LA. Magnetic determination of the relationship between the ST segment shift and the injury current produced by coronary artery occlusion. *Cir Res*, 36(3):414-424, 1975.
- Cohen D, Savard P, Rifkin RD, Lepeschkin E, Strauss WE. Magnetic measurement of ST and TQ segment shift in humans. Part II. Exercise induced ST segment depression. *Cir Res*, 53(2):274-279, 1983.
- Colli-Franzone P, Guerni L, Taccardi B. Modeling ventricular excitation: axial and orthotropic anisotropy effects on wavefronts and potentials. *Math Biosci*, 188:191-205, 2004.
- Connelly C, Vogel WM, Hernandez YM, Apstein CS. Movement of necrotic wavefront after coronary artery occlusion in rabbit. *Am J Physiol*, 243(5):H682-690, 1982.
- Cook RW, Edwards JE, Pruitt RD. Electrocardiographic changes in acute subendocardial infarction, I: large subendocardial and large non-transmural infarcts. *Circulation*, 18:603-612, 1958.
- Corbin LV 2nd, Scher AM. The canine heart as an electrocardiographic generator. Dependence on cardiac cell orientation. *Circ Res*, 41:58-67, 1977.
- Cox JL, McLaughlin VW, Flowers NC, Horan LG. The ischaemic zone surrounding acute myocardial infarction. Its morphology as detected by dehydrogenase staining. *Am Heart J*, 76(5):650-659, 1968.
- Crawford MH, O'Rourke RA, Grover FL. Mechanism of inferior electrocardiographic ST-segment depression during acute anterior myocardial infarction in a baboon model. *Am J Cardiol*, 54(8):1114-1117, 1984.
- Crystal GJ, Downey HF, Bashour FA. Small vessel and total coronary blood volume during intracoronary adenosine. *Am J Physiol*, 241(2):H194-201, 1981.
- Cuppen JJ, VanOosterom A. Model studies with the inversely calculated isochrones of ventricular depolarisation. *IEEE Trans Biomed Eng*, BME-31(10):652-659, 1984.
- D'Alche P. Experimental and theoretical methods for studying the genesis of the electrocardiograms. *Adv Cardiol*, 16:47-51, 1976.

- Daniel TM, Boineau JP, Cox JL, Sabiston DC Jr. Mapping of epicardial and intramural activation of the heart: a technique for localization of chronic infarction during myocardial revascularization. *J Thorac Cardiovasc Surg*,60(5):704-709,1970.
- Daniel TM, Boineau JP, Sabiston DC Jr. Comparison of human ventricular activation with a canine model in chronic myocardial infarction. *Circulation*,44(1) 74-89,1971
- Datta BN, Gupta BB. Morphological study of coronary venous system in cardiac disorders. *Br Heart J*,34(12):1227-1231,1972.
- De Ambroggi L, Bertoni T, Rabbia C, Landolina M. Body surface potential maps in old inferior myocardial infarction. Assessment of diagnostic criteria. *J Electrocardiol*,19(3):225-234,1986
- De Ambroggi L, Macchi E, Brusoni B, Taccardi B. Electromaps during ventricular recovery in angina patients with normal resting ECG. *Adv Cardiol*,19:88-90,1977.
- de Bakker JM, Janse MJ, Van Capelle FJ, Durrer D. Endocardial mapping by simultaneous recording of endocardial electrograms during cardiac surgery for ventricular aneurysm. *J Am Coll Cardiol*,2(5):947-953,1983.
- DeMello WC "Intercellular Communication". Plenum, New York, 1977.
- Dick M 2nd, Norwood WI, Chipman C, Castaneda AR. Intraoperative recording of specialized atrioventricular conduction tissue electrograms in 47 patients. *Circulation*,59(1):150-160,1979.
- Deussen A, Lauer T, Loncar R, Kropp J. Heterogeneity of metabolic parameters in the left ventricular myocardium and its relation to local blood flow. *Basic Res Cardiol*,96:564-574,2001.
- Domenech RJ, Hoffman JL, Noble MJ, Saunders KB, Henson JR, Subijanto S. Total and regional coronary blood flow measured by radioactive microspheres in conscious and anesthetized dogs. *Circ Res*,25(5):581-596,1969.
- Draper MH, Mya-Tu M. A comparison of the conduction velocity in cardiac tissues of various mammals. *Q J Exp Physiol Cogn Med Sci*,44(1) 91-109,1959.
- Dumaine R, Antzelevitch C. Molecular mechanisms underlying the long QT syndrome. *Curr Opin Cardiol*, 7(1):36-42,2002.
- Dunn RB, Griggs DM Jr. Transmural gradients in ventricular tissue metabolites produced by stopping coronary blood flow in the dog. *Circ Res*,37(4) 438-445,1975.
- Dunn RF, Bailey IK, Uren R, Kelly DT. Exercise-induced ST segment elevation. correlation of thallium-201 myocardial perfusion scanning and coronary arteriography. *Circulation*,61(5):989-995,1980.
- Dunn RF, Freedman B, Bailey IK, Uren RF, Kelly DT. Localisation of coronary artery disease with exercise electrocardiography. Correlation with thallium-201 myocardial perfusion scanning. *Am J Cardiol*,48(5):837-843,1981.
- Dunn RF, Freedman B, Kelly DT, Bailey IK, McLaughlin A. Exercise-induced ST segment elevation in leads V1 or VL: a predictor of anterior myocardial ischaemia and left anterior descending coronary artery disease. *Circulation*,63(6):1357-1363,1981
- Durrer D, van Dam RT, Freud GE, Janse MJ, Meijler FL, Arzbaecher RC. Total excitation of the isolated human heart. *Circulation*,41(6) 899-912,1970.
- Durrer D, van Der Tweel LH. Spread of activation in the left ventricular wall of the dog. *Am Heart J*,46:683-687,1953.
- Edmunds JJ, Gibbons RJ, Bresnahan JF, Clements IP. Significance of anterior ST depression in inferior wall acute myocardial infarction. *Am J Cardiol*,73:143-148,1994.
- Einthoven W., Fahr G., De Waart A. On the direction and manifest size of the variations of potential in the human heart and on the influence of the position of the heart on the form of the electrocardiogram. *Pflügers Arch*,150:275-315,1913. (Translated by Hoff PE and Sekelj P. *Am Heart J*,40:163-211,1950)
- Ekmekci A, Toyoshima H, Kwoczynski JK, Nagaya T, Prinzmetal M. Angina pectoris. IV. Clinical and experimental difference between ischaemia with ST elevation and ischaemia with ST depression. *Am J Cardiol*,7:412,1961a.
- Ekmekci A, Toyoshima H, Kwoczynski JK, Nagaya T, Prinzmetal M. Angina pectoris. V: Giant R and receding S wave in myocardial ischaemia and certain nonischaemic conditions. *Am J Cardiol*,7:521-532,1961b.
- El-Sherif N, Caref EB, Yin H, Restivo M. The electrophysiological mechanism of ventricular arrhythmias in the long QT syndrome. Tridimensional mapping of activation and recovery patterns. *Circ Res*,79(3):474-492,1996.
- Ergin MA, Dastgır G, Butt KMH, Stuckey JH. Prolonged epicardial mapping of myocardial infarction. the effects of propranolol and intra-aortic balloon pumping following coronary artery occlusion. *J Thorac Cardiovasc Surg*,72(6):892-899,1976.
- Euler DE, Prood CE, Spear JF, Moore EN. The interruption of collateral blood flow to the ischaemic canine myocardium by embolization of a coronary artery with latex effects on conduction delay and ventricular arrhythmias. *Circ Res*,49(1):97-108,1981
- Euler DE, Spear JF, Moore EN. Effect of coronary occlusion on arrhythmias and conduction in the ovine heart. *Am J Physiol*,245:H82-H89,1983.

- Evans AK, Lux RL, Burgess MJ, Wyatt RF, Abildskov JA. Redundancy reduction for improved display and analysis of body surface potential maps II Temporal compression. *Circ Res*,49(1):197-203,1981.
- Factor SM, Okun EM, Kirk ES. The histological lateral border of acute canine myocardial infarction. A function of microcirculation. *Circ Res*,48(5):640-649,1981.
- Fallert MA, Mirotznik MS, Downing SW, Savage EB, Foster KR, Josephson ME, Bogen DK. Myocardial electrical impedance mapping of ischemic sheep hearts and healing aneurysms. *Circulation*,87(1):199-207,1993.
- Ferguson DW, Pandian N, Kioschos JM, Marcus ML, White CW. Angiographic evidence that reciprocal ST-segment depression during acute myocardial infarction does not indicate remote ischemia: analysis of 23 patients. *Am J Cardiol*,53:55-62,1984.
- Fletcher WO, Gibbons RJ, Clements IP. The relationship of inferior ST depression, lateral ST elevation, and left precordial ST elevation to myocardium at risk in acute anterior myocardial infarction. *Am Heart J*,126(3 Pt 1):526-535,1993.
- Fisher DJ. Increased regional myocardial blood flows and oxygen deliveries during hypoxemia in lambs. *Pediatr Res*,18:602-606,1984.
- Fisher DJ, Heymann MA, Rodolph AM. Effects of hemorrhage on myocardial consumption of oxygen and carbohydrate in fetal sheep in utero. *J Dev Physiol*,2(3):151-159,1980.
- Forrester JS, Wyatt HL, Da Luz PL, Tyberg JV, Diamond GA, Swan HJ. Functional significance of regional ischemic contraction abnormalities. *Circulation*,54:64-70,1976.
- Fox KM, Deanfield J, Ribero P, England D, Wright C. Projection of ST segment changes on to the front of the chest. Practical implications for exercise testing and ambulatory monitoring. *Br Heart J*,48(6):555-559,1982.
- Fox KM, Jonathan A, Selwyn AP. Significance of exercise induced ST segment elevation in patients with previous myocardial infarction. *Br Heart J*,49(1):15-19,1983.
- Fox KM, Selwyn AP, Shillingford JP. A method for precordial surface mapping of the exercise electrocardiogram. *Br Heart J*,40(12):1339-1343,1978.
- Frasure-Smith N, Lesperance F, Talajic M. Depression following myocardial infarction. Impact on 6-month survival. *JAMA*,270(15):1819-25,1993.
- Freedman B, Dunn RF, Bailey IK, McLaughlin A, Kelly DT. ST elevation in V1 or VL on exercise: a non-invasive predictor of severe LAD disease and anterior myocardial ischaemia (abstr). *Circulation*,62(Suppl III):III-269,1980.
- Freifeld AG, Schuster EH, Bulkley BH. Nontransmural versus transmural myocardial infarction. A morphologic study. *Am J Med*,75(3):423-432,1983.
- Fuchs RM, Achuff SC, Grunwald L, Yin FC, Griffith LS. Electrocardiographic localisation of coronary artery narrowings: Studies during myocardial ischaemia and infarction in patients with one-vessel disease. *Circulation*,66(6):1168-1176,1982.
- Fujiswara H, Ashraf M, Sato S, Millard RW. Transmural cellular damage and blood flow distribution in early ischaemia in pig hearts. *Circ Res*,51(6):683-693,1982.
- Gallagher JJ. Surgical treatment of arrhythmias: current status and future directions. *Am J Cardiol*,41:1035-1044,1978.
- Gallagher JJ, Cox JL. Status of surgery for ventricular arrhythmias. *Circulation*,60(7):1440-1442, 1979.
- Gallagher JJ, Gilbert M, Svenson RH, Sealy WC, Kasell J, Wallace AG. Wolff-Parkinson-White syndrome. The problem, evaluation, and surgical correction. *Circulation*,51:767-785,1975.
- Gallagher JJ, Kasell JH, Cox JL, Smith WM, Ideker RE, Smith WM. Technique of intraoperative electrophysiologic mapping. *Am J Cardiol*,49(1):221-240,1982.
- Geary GG, Smith GT, McNamara JJ. Quantitative effect of early coronary artery reperfusion in baboons. Extent of salvage of the perfusion bed of an occluded artery. *Circulation*,66(2):391-396,1982.
- Gelman JS, Saltups A. Precordial ST segment depression in patients with inferior myocardial infarction: clinical implications. *Br Heart J*,48:560-565,1982.
- Geselowitz DB. Dipole theory in electrocardiography. *Am J Cardiol*,14:301-306,1964.
- Gibson RS, Crampton RS, Watson DD, Taylor GJ, Carabello BA, Holt ND, Beller GA. Precordial ST-segment depression during acute inferior myocardial infarction: clinical, scintigraphic and angiographic correlations. *Circulation*,66:732-741,1982.
- Glenny RW, Bernard S, Brinkley M. Validation of fluorescent labelled microsphere for measurement of regional organ perfusion. *J Appl Physiol*,74(5):2585-2597,1993.
- Goldman MJ. Electrophysiology of the heart. In: Principles of clinical electrocardiography, Goldman MJ, ed. California, Lange Medical Publications, pp16-22,1986.

- Goldschlager N, Goldman MJ. Electrophysiology of the heart. In Principles of clinical electrocardiography. California, New York, Connecticut/San Mateo, pp11~14, 1989.
- Green LS, Taccardi B, Ershler PR, Lux RL. Epicardial potential mapping Effects of conducting media on isopotential and isochrone distributions. *Circulation*,84(6):2513~2521,1991.
- Griffith L, Grunwald L, Aschuff S. Electrocardiographic changes in single vessel disease (abstr). *Circulation*,58,II-238 1978.
- Griggs DM Jr, Tchokoev VV, Chen CC. Transmural differences in ventricular tissue substrate levels due to coronary constriction. *Am J Physiol*,22705~709,1972.
- Groeneveld ABJ, van Beek JHGM, Alders DJ. Assessing heterogenous distribution of blood flow and metabolism in the heart. *Basic Res Cardiol*,96:575~581,2001.
- Guyton RA, McClenathan JH, Newman GE, Michaelis CC. Significance of subendocardial ST segment elevation caused by coronary stenosis in the dog. *Am J Cardiol*,40:373~380, 1977.
- Guyton RA. Subendocardial ST segment changes during acute coronary occlusion. *The Annals of Thoracic Surgery*, 20:52~55, 1975.
- Hale SI, Alker KJ, Kloner RA. Evaluation of non-radioactive, coloured microspheres for measurement of regional myocardial blood flow in dogs. *Circulation*,78(2):428~434,1988.
- Hanninen H, Takala P, Mäkiärvä M, Korhonen P, Okikarinen L, Simelius K, Nenonen J, Katila T, Toivonen L. ST segment level and slope in exercise-induced myocardial ischaemia evaluated with body surface potential mapping. *Am J Cardiol*,88(10):1152~1156,2001a.
- Haraphongse M, Tanomsup S, Yugdutt BI. Inferior ST segment depression during acute anterior myocardial infarction. clinical and angiographic correlations. *J Am Coll Cardiol*,4(3):467~476,1984.
- Harken AH, Josephson ME, Horowitz LN. Surgical endocardial resection for the treatment of malignant ventricular tachycardia. *Ann Surg*,190 456~460,1979.
- Harken AH, Simson MB, Haselgrove J, Wetstein L, Harden WR 3rd, Barlow CH. Early ischemia after complete coronary ligation in the rabbit, dog, pig, and monkey. *Am J Physiol*, 241:H202~H210,1981.
- He B, Bansal S, Tsai A, Saul JP. A comparison of volume conductor effects on body surface Laplacian and potential ECGs: a model study. *Comput Biol Med*,27(2):117-27,1997.
- Hearse DJ, Opie LH, Katzeff IE, Lubbe WF, Van Der Werff TJ, Peisach M, Boule G. Characterization of the "border zone" in acute regional ischaemia in the dog. *Am J Cardiol*,40(5):716~726,1977.
- Hearse DJ, Yellon DM. The "border zone" in evolving myocardial infarction: controversy or confusion? *Am J Cardiol*,47(6):1321~1334,1981.
- Heller GV, Aroesty JM, McKay RG, Parker JA, Silverman KJ, Come PC, Grossman W. The pacing stress test: a reexamination of the relation between coronary artery disease and pacing-induced electrocardiographic changes. *Am J Cardiol*,54:50~55,1984.
- Herman MV, Elliott WC, Gorlin R. An electrocardiographic, anatomic and metabolic study of zonal myocardial ischaemia in coronary heart disease. *Circulation*,35(5):834~846,1967.
- Hirai M, Ohta T, Kinoshita A, Toyama J, Nagaya T, Yamada K. Body surface isopotential maps in old anterior myocardial infarction undetectable by 12-lead electrocardiograms. *Am Heart J*,108(4 pt 1):975~982,1984.
- Hiramatsu Y, Buchanan JW, Knisley SB, Gettes LS. Rate-dependent effects of hypoxia on internal longitudinal resistance in guinea pig papillary muscles. *Circ Res*,63(5):923~929,1988.
- Hirzel HO, Sonnenblick EH, Kirk ES. Absence of a lateral border zone of intermediate creatine phosphokinase depletion surrounding a central infarct 24 hours after acute coronary occlusion in the dog. *Circ Res*,41(5):673~683,1977.
- Hlatky MA, Califf RM, Lee KL, Pryor DB, Wagner GS, Rosati RA. Prognostic significance of precordial ST-segment depression during inferior acute myocardial infarction. *Am J Cardiol*,55:325~329,1985.
- Hoffman JIE. Determinants and prediction of transmural myocardial perfusion. *Circulation*,58(3Pt 1):381~391,1978.
- Hoffman JIE, Payne BD, Heymann MA. The use of microspheres to measure blood flow, in Linden RJ (ed). *Techniques in Cardiovascular Physiology*. Amsterdam,Elsevier,p304,1~36,1983.
- Holland RP, Arnsdorf MF. Solid angle theory and the electrocardiogram: physiologic and quantitative interpretations. *Prog Cardiovasc Dis*,19(6):431~457,1977.
- Holland RP, Brooks H. Precordial and epicardial surface potentials during myocardial ischaemia in the pig. A theoretical and experimental analysis of the TQ and ST segments. *Circ Res*,37(4):471~480,1975.
- Holland RP, Brooks H. The QRS complex during myocardial ischaemia: An experimental analysis in the porcine heart. *J Clin Invest*,57(3):541~550,1976.

- Holland RP, Brooks H. TQ-ST segment mapping: critical review and analysis of current concepts. *Am J Cardiol*, 40:110~129, 1977a.
- Holland RP, Brooks H, Lidl B. Spatial and non-spatial influences on the TQ-ST segment deflection of ischaemia. Theoretical and experimental analysis in the pig. *J Clin Invest*, 60(1):197~214, 1977b.
- Holt JH Jr, Barnard AC, Lynn MS, Svendsen P. A study of the human heart as a multiple dipole electrical source. I. Normal adult male subjects. *Circulation*, 40(5):687~696, 1969.
- Hopenfeld B, Stinstra JG, MacLeod RS. Mechanism of ST-depression associated with contiguous subendocardial ischaemia. *J Cardiovasc Electrophysiol*, 15: 1200~1206, 2004.
- Hopenfeld B, Stinstra JG, MacLeod RS. The effect of conductivity on ST-segment epicardial potentials arising from subendocardial ischaemia. *Annals of Biomedical Engineering*, 33(6): 751~763, 2005.
- Horan LG, Flowers NC. Electrocardiography and vectorcardiography. In: heart Disease, Braunwald E, ed. W.B. Saunders Company, pp198~250, 1980.
- Horan LG, Flowers NC. Limitations of the dipole concept in electrocardiographic interpretation, in Schlant RC, Hurst JW (eds) *Advances in Electrocardiography*. New York, Grune & Stratton. Pp9~18, 1972.
- Horan LG, Sridharan MR, Hand RC, Flowers NC. Non-invasive prediction of ventriculographic contours from surface voltage measurements in coronary artery disease (abstract). *Circulation*, 78(suppl II):II-33, 1988.
- Howe BB, Winbury MM. Effect of pentritinol, nitroglycerin and propranolol on small vessel blood content of the canine myocardium. *J Pharmacol Exp Ther*, 187(3):465~474, 1973.
- Ikeda K, Kubota I, Igarashi A, Yamaki M, Tsukikawa K, Yasui S. Detection of local abnormalities in ventricular activation sequence by body surface isochrone mapping in patients with previous myocardial infarction. *Circulation*, 72(4):801~809, 1985.
- Iskandrian AS, Segal BL. Structure and function of the coronary arteries: how are they related? *Cathet Cardiovasc Diagn*, 5(2):101~105, 1979.
- Iwai S, Markowitz SM, Stein KM, Mittal S, Slotwimer DJ, Das MK, Cohen JD, Hao SC, Lerman BB. Response to adenosine differentiates focal from macroreentrant atrial tachycardia: validation using three-dimensional electroanatomic mapping. *Circulation*, 106(22):2793~2799, 2002.
- Janse MJ, Cinca J, Morena H, Fiolet JW, Kleber AG, de Vries GP, Becker AE, Durrer D. The "border zone" in myocardial ischaemia. An Electrophysiological, Metabolic and Histochemical correlation in the pig heart. *Circ Res*, 44(4):576~588, 1979.
- Janse MJ, van Capelle FJ, Morsink H, Kleber AG, Wilson-Schopman F, Cardinal R, d'Almoncourt CN, Durrer D. Flow of "injury" current and patterns of excitation during early ventricular arrhythmias in acute regional myocardial ischaemia in isolated porcine and canine hearts. Evidence for two different arrhythmogenic mechanisms. *Circ Res*, 47(2):151~165, 1980.
- Jennings RB, Ganote CE, Reimer KA. Ischaemic tissue injury. *Am J Pathol*, 81:179~193, 1975.
- Jennings K, Reid DS, Julian DG. "Reciprocal" depression of the ST segment in acute myocardial infarction. *Br Med J (Clin Res Ed)*, 287(6393):634~637, 1983.
- Jennings RB, Sommers HM, Smyth GA, Flack HA, Linn H. Myocardial necrosis induced by temporary occlusion of a coronary artery in the dog. *Arch Pathol*, 70:68~78, 1960.
- Jennings RB, Schaper J, Hill ML, Steenbergen C Jr, Reimer KA. Effect of reperfusion late in the phase of reversible ischaemic injury. Changes in cell volume, electrolytes, metabolites and ultrastructure. *Circ Res*, 56(2):262~278, 1985.
- John Ross JR. Electrocardiographic ST segment analysis in the characterization of myocardial ischaemia and infarction. *Circulation*, 53,3(suppl I):I73~81, 1976.
- Johnston PR, Kilpatrick D. The effect of conductivity values on ST segment shift in subendocardial ischaemia. *IEEE Trans Biomed Eng*, 50(2):150~8, 2003.
- Johnston PR, Kilpatrick D, Li CY. The importance of anisotropy in modelling ST segment shift in subendocardial ischaemia. *IEEE Transactions Biomedical Engineering*, 48(12), 2001.
- Josephson ME, Horowitz LN, Spielman SR, Waxman HL, Greenspan AM. Role of catheter mapping in the preoperative evaluation of ventricular tachycardia. *Am J Cardiol*, 49(1):207~220, 1982.
- Kasell J, Gallagher JJ. Construction of a multipolar needle electrode for activation study of the heart. *Am J Physiol*, 233: H312~317, 1977.
- Kato K, Fukuda H, Koyama S. Depression of the ST segment in epicardial electrocardiogram associated with experimental major coronary artery constriction. *J Electrocardiol*, 1(2):167~174, 1968.
- Katz AM. Membrane structure. In "Handbook of cardiac electrophysiology" Fozzard HA., Haber H., Jennings A., Katz AM., Margan HE, eds. Raven, New York, pp101~110, 1986.
- Kennamer R, Bernstein J, Maxwell M, Prinzmetal M, Shaw CM. Studies on mechanism of ventricular activity: V. Intramural depolarisation potentials in the normal heart with a consideration of currents of injury in coronary artery disease. *Am Heart J*, 46:379~400, 1953.

- Kleber, A.G., Janse, M.J., Capelle, F.J.C. Van, Durrer, D.. Mechanism and time course of ST and TQ segment changes during acute regional myocardial ischemia in the pig heart determined by extracellular and intracellular recordings. *Circ Res* 1978, 42:603-613
- Khoury DS, Rudy Y. A model study of volume conductor effects on endocardial and intracavitary potentials. *Circ Res*, 71(3):511-25, 1992.
- Kilpatrick D, Bell AJ, Walker SJ. Derived epicardial potentials differentiate ischemic ST depression from ST depression secondary to ST elevation in acute inferior myocardial infarction in humans. *J Am Coll Cardiol*, 14:695-702, 1989.
- Kilpatrick D, Walker SJ, Bell AJ. Importance of the great vessels in the genesis of the electrocardiogram. *Circ Res*, 66:1081-1087, 1990.
- Kimura S, Bassett AL, Kohya T, Kozlovskis PL, Myerburg RJ. Simultaneous recording of action potentials from endocardium and epicardium during ischaemia in the isolated cat ventricle: relation of temporal electrophysiologic heterogeneities to arrhythmias. *Circulation*, 74(2):401-409, 1986.
- Kjekshus JK, Maroko PR, Sobel BE. Distribution of myocardial injury and its relation to epicardial ST-segment changes after coronary artery occlusion in the dog. *Circ Res*, 6(5):490-499, 1972.
- Kleber AG. Resting membrane potential, extracellular potassium activity and intracellular sodium activity during acute global ischaemia in isolated perfused guinea pig hearts. *Circ Res*, 52(4):442-450, 1983.
- Kleber AG, Janse MJ, Van Capelle FJ, Durrer D. Mechanism and time course of ST and TQ segment changes during acute regional myocardial ischaemia in the pig heart determined by extracellular and intracellular recordings. *Circ Res*, 42(5):603-613, 1978.
- Klein HH, Schubotho M, Nebendahl K, Kreuzer H. Temporal and spatial development of infarcts in porcine hearts. *Basic Res Cardiol*, 79(4):440-447, 1984.
- Kleinert HD, Scales JL, Weiss HR. Effects of carbon monoxide or low oxygen gas mixture inhalation on regional oxygenation, blood flow, and small vessel blood content of the rabbit heart. *Pflugers Arch*, 383(2):105-111, 1980.
- Kloner RA, Ellis SG, Lange R, Braunwald E. Studies of experimental coronary artery reperfusion: Effects on infarct size, myocardial function, biochemistry, ultrastructure and microvascular damage. *Circulation*, 68(2 pt 2):18-15, 1983.
- Kornreich F, Montague TJ, Rautaharju PM. Body surface potential mapping of ST segment changes in acute myocardial infarction. Implications for ECG enrolment criteria for thrombolytic therapy. *Circulation*, 87(3):773-782, 1993.
- Kowallik P, Schulz R, Guth BD, Schade A, Paffhausen W, Gross R, Heusch G. Measurement of regional myocardial blood flow with multiple coloured microspheres. *Circulation*, 83(3):974-982, 1991.
- Kramer JB, Saffitz JE, Witkowski FX, Corr PB. Intramural reentry as a mechanism of ventricular tachycardia during evolving canine myocardial infarction. *Circ Res*, 56:736-754, 1985.
- Krone RJ, Greenberg H, Dwyer EM Jr, Kleiger RE, Boden WE. Long-term prognostic significance of ST segment depression during acute myocardial infarction. The Multicenter Diltiazem Postinfarction Trial Research Group. *J Am Coll Cardiol*, 22:361-367, 1993.
- Kroll K, Wilke N, Jerosch-Herold M, Wang Y, Zhang Y, Bache RJ, Bassingthwaite JB. Modeling regional myocardial flows from residue functions of an intravascular indicator. *Am J Physiol*, 271(4 Pt 2):H1643-655, 1996.
- Kushmerick MJ, Podolsky RJ. Ionic mobility in muscle cells. *Science*, 166(910):1297-1298, 1969.
- Ladwig KH, Kieser M, König J, Breithardt G, Borggrefe M. Affective disorders and survival after acute myocardial infarction. Results from the post-infarction late potential study. *Eur Heart J*, 12(9):959-964, 1991.
- Lee JT, Ideker RE, Reimer KA. Myocardial infarct size and location in relation to the coronary vascular bed at risk in man. *Circulation*, 64(3):526-534, 1981.
- Lekven J, Semb G. Effect of dopamine and calcium on lipolysis and myocardial ischaemic injury following acute coronary occlusion in the dog. *Circ Res*, 34(3):349-359, 1974.
- Lembo NJ, Starling MR, Dell'Italia LJ, Crawford MH, Chaudhuri TK, O'Rourke RA. Clinical and prognostic importance of persistent precordial (V1-V4) electrocardiographic ST segment depression in patients with inferior transmural myocardial infarction. *Circulation*, 74(1):56-63, 1986.
- Leon LJ, Horacek BM. Computer model of excitation and recovery in the anisotropic myocardium. I. Rectangular and cubic arrays of excitable elements. *J Electrocardiol*, 24(1):1-15, 1991.
- Levick JR. Excitation and contraction of a cardiac myocyte. In: An introduction to cardiovascular physiology. Levick JR. eds. Butterworth-Heinemann Ltd, pp25-43, 1995.
- Lewis T, Rothschild MA. The excitatory process in the dog's heart. II. The ventricles. London: Philosophical Transactions of the Royal Society, 206:181, 1915.
- Li DS. Epicardial and endocardial ST mapping in ischaemia. PhD Dissertation, pp126-128, 147-148, 155-160, 181-185, 1997.

- Li DS, Li CY, Yong AC, Johnston PR, Kilpatrick D Epicardial ST depression in acute myocardial infarction. *Circ Res*,85(10):959-964,1999.
- Li DS, Li CY, Yong AC, Kilpatrick D Source of electrocardiographic ST changes in subendocardial ischaemia. *Circ Res*,82(9) 957-970,1998.
- Li DS, Yong AC, Kilpatrick D Validation of a subendocardial ischaemic sheep model by intracoronary fluorescent microspheres. *Clinical and Experimental Pharmacology and Physiology*,23(2):111-118,1996
- Li RA, Leppo M, Miki T, Seino S, Marban E Molecular basis of electrocardiographic ST-segment elevation *Circ Res*,87(10):837-839,2000.
- Li Z, Yipintsoi T, Bassingthwaite JB. Nonlinear model for capillary-tissue oxygen transport and metabolism. *Ann Biomed Eng*, 25(4):604-619,1997.
- Lie JT, Pairolero PC, Holley KE, McCall JT, Thompson HK Jr, Titus JL Time course and zonal variations of ischaemia-induced myocardial cationic electrolyte derangements. *Circulation*,51(5).860-866,1975.
- Liebman J, Rudy Y, Diaz P, Thomas CW, Plonsey R. The spectrum of right bundle branch block as manifested in electrocardiographic body surface potential maps. *J Electrocardiol*,17(4).329-346,1984.
- Lipman BS, Dunn M, Massie E. Basic physiologic principles. In: *Clinical electrocardiography*, 7th. Ed. Chicago, Year Book Medical Publishers, INC., pp34-49,1984
- Lipman BS, Massie E. *Clinical scalar electrocardiography* Chicago, Year Book ,pp216-274,1956.
- Little SE, Bassingthwaite JB. Plasma-soluble marker for intraorgan regional flows. *Am J Physiol*,245:H707-712,1983.
- Little WC, Rogers EW, Sodums MT, Texas SA, Florida P. Mechanism of anterior ST segment depression during acute inferior myocardial infarction. *Annals of Internal Medicine*,100.226-229,1984.
- Lowe JE, Cummings RG, Adams DH, Hull-Ryde EA Evidence that ischaemic cell death begins in the subendocardium independent of variations in collateral flow or wall tension. *Circulation*,68(1):190-202,1983.
- Lundsgaard-Hansen P, Meyer C, Riedwyl H Transmural gradients of glycolytic enzyme activities in left ventricular myocardium. I. The normal state. *Pflügers Arch Gesamte Physiol Menschen Tiere*,297(2):89-106,1967.
- Lux RL, Evans AK, Burgess MJ, Wyatt RF, Abildskov JA Redundancy reduction for improved display and analysis of body surface potential maps. I Spatial compression *Circ Res*,49(1):186-196,1981.
- MacDonald RG, Hill JA, Feldman RL ST segment response to acute coronary occlusion. coronary hemodynamic and angiographic determinants of direction of ST segment shift. *Circulation*,74(5):973-979,1986.
- Maehara K, Kyono H, Shimizu Y, Maruyama Y, Kitaoka S, Nishioka O, Yoshikata S, Ishiki Y, Kanazuka H, Watanabe J, Ino-Oka E, Takishima T A theoretical analysis of ST segment deviation during acute regional ischaemia in the isolated canine heart by subendocardial, epicardial and precordial ST segment mapping. *Japanese Heart Journal*,23:394-396,1982.
- Maehara K, Kyono H, Kitaoka S, Shimizu Y, Maruyama Y, Ashikawa K, Ino-Oka E, Takishima T. A comparison of ST segment deviation and calculated solid angle during acute regional ischaemia in the isolated canine heart at precordial, epicardial and intramyocardial lead surfaces. *J Electrocardiology*,19(3) 235-246,1986.
- Marcus ML, Kerber RE, Ehrhardt J, Abboud FM. Three dimensional geometry of acutely ischaemic myocardium. *Circulation*,52(2):254-263,1975
- Markovitz LJ, Savage EB, Ratcliffe MB, Bavaria JE, Kreiner G, Iozzo RV, Hargrove WC 3rd, Bogen DK, Edmunds LH Jr. Large animal model of left ventricular aneurysm. *Ann Thorac Surg*,48:838-845,1989.
- Mark DB, Hlatky MA, Lee KL, Harrell FE Jr, Califf RM, Fryer DB. Localizing coronary artery obstructions with the exercise treadmill test. *Ann Intern Med*,106(1).53-55,1987
- Markham RV, Winniford MD, Firth BG, Nicod P, Dehmer GJ, Lewis SE, Hillis LD. Symptomatic, electrocardiographic, metabolic, and hemodynamic alterations during pacing-induced myocardial ischaemia. *Am J Cardiol*,51(10):1589-1594,1983
- Maroko PR, Braunwald E. Modification of myocardial infarction size after coronary occlusion. *Ann Intern Med*,79(5):720-733,1973
- Maroko PR, Kjekshus JK, Sobel BE, Watanabe T, Covell JW, Ross J Jr, Braunwald E. Factors influencing infarct size following experimental coronary occlusion *Circulation*,43(1).67-82,1971.
- Massie BM, Schwartz GG, Garcia J, Wisneski JA, Weiner MW, Owens T Myocardial metabolism during increased work states in the porcine left ventricle in vivo. *Circ Res*,74(1) 64-73,1994.
- Massumi RA, Goldman A, Rakita L, Kuramoto K, Prinzmetal M Studies on the mechanism of ventricular activity. XVI Activation of the human ventricle. *Am J Med*,19:832-848,1955.
- Matsumoto T, Goto M, Tachibana H, Ogasawara Y, Tsujiooka K, Kajiyama F. Microheterogeneity of myocardial blood flow in rabbit hearts during normoxic and hypoxic states. *Am J Physiol*,270(2 Pt 2):H435-441,1996.

- May-Newman K, Mathieu-Costello O, Omens JH, Klumb K, McCulloch AD. Transmural distribution of capillary morphology as a function of coronary perfusion pressure in the resting canine heart. *Microvasc Res*,50(3):381-96,1995.
- Menown IB, Allen J, Anderson J, Adgey AA. Early diagnosis of right ventricular or posterior infarction associated with inferior wall left ventricular acute myocardial infarction. *Am J Cardiol*,85(8):934-938,2000.
- Menown I, Allen J, Anderson J, Adgey AA. ST depression only on the initial 12-lead ECG early diagnosis of acute myocardial infarction. *Eur Heart J*,22(3):218-227,2001.
- Miller AJ. The lymphatics of the heart. *Arch Intern Med (Chicago)*,112:501-511,1963.
- Miller WT, Geselowitz DB. Simulation studies of the electrocardiogram I. The normal heart II. Ischaemia and infarction. *Circ Res*,43(2):301-315, 315-323,1978.
- Miller WT 3rd, Spach MS, Warren RB. Total body surface potential mapping during exercise: QRS-T-Wave changes in normal young adults. *Circulation*,62(3):632-645,1980.
- Minamide A, Takano S, Hashikawa T, Abiko Y. Transmural gradient of NAD⁺/NADH ratio in the canine left ventricular myocardium, and effects of coronary dilators on the transmural gradient. *Jpn J Pharmacol*,23(1):126-128,1973.
- Mirvis DM. Body surface distribution of exercise induced QRS changes in normal subjects. *Am J Cardiol*,46:988-996,1980.
- Mirvis DM. Differential electrocardiographic effects of myocardial ischaemia induced by atrial pacing in dogs with various locations of coronary stenosis. *Circulation*,68(5):1116-1126,1983.
- Mirvis DM. Physiologic bases for anterior ST segment depression in patients with acute inferior wall myocardial infarction. *Am Heart J*,116(5 pt 1):1308-1322,1988.
- Mirvis DM, Gordey RL. Electrocardiographic effects of myocardial ischaemia induced by atrial pacing in dogs with coronary stenosis I. Repolarization changes with progressive left circumflex coronary artery narrowing. *J Am Coll Cardiol*,1(4):1090-1098,1983.
- Mirvis DM, Ramanathan KB. Alterations in transmural blood flow and body surface ST segment abnormalities produced by ischemia in the circumflex and left anterior descending coronary arterial beds of the dog. *Circulation*,76:697-704,1987.
- Mirvis DM, Ramanathan KB, Wilson JL. Regional blood flow correlates of ST segment depression in tachycardia-induced myocardial ischaemia. *Circulation*,73(2):365-373,1986.
- Mirvis DM, Ramanathan KB, Wilson JL. Comparative electrocardiographic and myocardial blood flow effects of rapid atrial pacing and dipyridamole infusion in dogs with chronic coronary artery occlusion. *Am Heart J* 115(5):984-992,1988.
- Mittra B. Use of potassium, glucose, and insulin in the treatment of myocardial infarction. *Prog Cardiovasc Dis*,10:529-544,1968.
- Monro DM, Bones PJ, Stanbridge RD, Jones RW. Comparison of epicardial and body surface ECG potentials in man. *Cardiovasc Res*,20(3):201-207,1986.
- Montague TJ, Smith ER, Cameron DA, Rautaharju PM, Klassen GA, Fehnington GS, Horacek BM. Isointegral analysis of body surface maps: surface distribution and temporal variability in normal subjects. *Circulation*,63:1166-1172,1981.
- Montague TJ, Smith ER, Spencer CA, Johnstone DE, Lalonde LD, Bessoudo RM, Gardner MJ, Anderson RN, Horacek BM. Body surface electrocardiographic mapping in inferior myocardial infarction. Manifestation of left and right ventricular involvement. *Circulation*,67(3):665-673,1983.
- Montague TJ, Johnstone DE, Spencer CA, Miller RM, Mackenzie RB, Gardner MJ, Horacek BM. Body surface potential maps with low-level exercise in isolated left anterior descending coronary artery disease. *Am J Cardiol*,61(4):273-282,1988.
- Montague TJ, Witkowski FX, Miller RM, Johnstone DE, Mackenzie RB, Spencer CA, Horacek BM. Exercise body surface potential mapping in single and multiple coronary artery disease. *Chest*,97(6):1333-1342,1990.
- Moore KB, Kimball T, Steadman B. Silver-silver chloride plunge electrode needles and chloriding monitor. *IEEE Trans Biomed Eng*,37(5):532-535,1990.
- Muller JE, Maroko PR, Braunwald E. Evaluation of precordial electrocardiographic mapping as a means of assessing changes in myocardial ischemic injury. *Circulation*,52(1):16-27,1975.
- Musso E, Stilli D, Macchi E, Regolosi G, Brambilla C, Francescon P, Bo M, Rolli A, Botti G, Taccardi B. Body surface maps in left bundle branch block uncomplicated or complicated by myocardial infarction, left ventricular hypertrophy or myocardial ischemia. *J Electrocardiol*,20(1):1-20,1987.
- Nabel EG, Shook TL, Meyerovitz M, Ganz P, Selwyn AP, Friedman PL. Detection of pacing-induced myocardial ischaemia by endocardial electrograms recorded during cardiac catheterisation. *J Am Coll Cardiol*,11(5):983-992,1988.
- Nasmith JB, Pharand C, Dube B, Matteau S, LeBlanc AR, Nadeau R. Localization of maximal ST segment displacement in various ischaemic setting by orthogonal ECG. Implications for lead selection and the mechanism of ST shift. *Can J Cardiol*,17(1):57-62,2001.
- Okada RH. A critical review of vector electrocardiography. *IEEE Trans Biomed Eng*,10:95-98,1963.

- Okada RH, Langner PH, Briller SA. Synthesis of precordial potentials from the SVEC III vectorcardiographic system. *Circ Res*,7:185~191,1959.
- Oster HS, Taccardi B, Lux RL, Ershler PR, Rudy Y. Noninvasive electrocardiographic imaging: reconstruction of epicardial potentials, electrograms, and isochrones and localization of single and multiple electrocardiac events. *Circulation*,96(3) 1012~1024,1997.
- Osugi J, Ohta T, Toyama J, Takatsu F, Nagaya T, Yamada K. Body surface isopotential maps in old inferior myocardial infarction undetectable by 12 lead electrocardiogram. *J Electrocardiology*,17(1).55~62,1984.
- Otto, H L. The ventricular electrocardiogram. An experimental study. *Arch Int Med*,43 335~350,1929
- Page E. The electrical potential difference across the cell membrane of heart muscle. Biophysical consideration. *Circulation*,26: 582~595, 1962.
- Page E, Manjunath CK. Communicating junctions between cells. In "Handbook of cardiac electrophysiology" Fozzard HA., Haber H., Jennings A., Katz AM, Margan HE., eds. Raven, New York, pp573~600, 1986.
- Pardee HEB. An electrocardiographic sign of coronary artery obstruction. *Arch Intern Med*,26:244~257,1920.
- Parker JO, Chiong MA, West RO, Case RB. The effect of ischaemia and alterations of heart rate on myocardial potassium balance in man. *Circulation*,42(2):205~217,1970.
- Pierard LA, Sprynger M, Gilis F, Carlier J. Significance of precordial ST-segment depression in inferior acute myocardial infarction as determined by echocardiography. *Am J Cardiol*,57:82~85,1986.
- Plonsey R. An evaluation of several cardiac activation models. *J Electrocardiol*,7(3).237~244,1974.
- Plonsey R. Bioelectric phenomena. New York, McGraw-Hill, chap 5: pp202~275,1969.
- Pogwizd SM, Corr PB. Reentrant and non-reentrant mechanisms contribute to arrhythmogenesis during early myocardial ischaemia: results using three-dimensional mapping. *Circ Res*,61(3):352~371,1987.
- Pressler ML. Effects of pCai and PHi on cell-to-cell coupling. *Experientia*,43(10).1084~1091,1987.
- Prinzmetal M, Bergman HC, Kruger HE, Schwartz LL, Simkin B, Sobin SS. Studies on the coronary circulation III. Collateral circulation of beating human and dog hearts with coronary occlusion. *Am Heart J*,35:689~717,1948.
- Prinzmetal M, Goldman A, Shubin M, Bor N, Wada T. Angina pectoris. II. Observation on the classic form of angina pectoris. *Am Heart J*,57:530,1959.
- Prinzmetal M, Ishikawa K, Nakashima M, Oishi H, Ozkan E, Wakayama J, Barnes JM. Correlation between intracellular and surface electrograms in acute myocardial ischaemia. *J Electrocardiol*,1(2):161~166,1968.
- Prinzmetal M, Toyoshima H, Ekmekci A, Mizuno Y, Nagaya. Myocardial ischaemia. Nature of ischaemic electrocardiographic patterns in the mammalian ventricles as determined by intracellular electrographic and metabolic changes. *Am J Cardiol*,8:493~503,1961.
- Proceedings of the Tenth Bethesda Conference on Optimal Electrocardiography, Task Force VI: Future direction in electrocardiography. *Am J Cardiol*,41:74~81,1977.
- Pruitt RD, Valencia F. The immediate electrocardiographic effects of circumscribed myocardial injuries: An experimental study. *Am Heart J*,35:161~197,1948.
- Puech P, Esclaire M, Sodi-Pollares D, Cisneros F. Normal auricular activation in the dogs heart. *Am Heart J*,47:174~191,1954.
- Putini RL, Natale E, Ricci R, Minardi G, Tubaro M, Lioy E, Boccardi L, Pucci E, Di Segni M, Giovannini E, et al. Dipyridamole echocardiography evaluation of acute inferior myocardial infarction with concomitant anterior ST segment depression. *Eur Heart J*,14:1328~1333,1993.
- Quinn PJ. "The molecular biology of cell membranes". University park Press, Baltimore, Maryland, 1976.
- Raab W, VAN LITH P, LEFESCHKIN E, Herrlick HC. Catecholamine induced myocardial hypoxia in the presence of impaired coronary dilatibility independent of external cardiac work. *Am J Cardiol*,9:455~470,1962.
- Rakita L, Borduas JL, Rothman S, Prinzmetal M. Studies on the mechanism of ventricular activity XII. Early changes in the RS-T segment and QRS occlusion. Experimental study and clinical applications. *Am Heart J*,48:351~372,1954.
- Rall W. Distribution of potential in cylindrical coordinates and time constants for a membrane cylinder. *Biophys J*,9(12):1509~1541,1969.
- Reimer KA, Jennings RB. The "wavefront phenomenon" of myocardial ischaemic cell death II. Transmural progression of necrosis within the framework of ischaemic bed size (myocardium at risk) and collateral flow. *Lab Invest*,40(6):633~644,1979.
- Reimer KA, Lowe JE, Rasmussen MM, Jennings RB. The wavefront phenomenon of ischaemic cell death. I. Myocardial infarct size vs duration of coronary occlusion in dogs. *Circulation*,56(5) 786~794,1977.

- Reimer KA, Rasmussen MM, Jennings RB. Reduction by propranolol of myocardial necrosis following temporary coronary artery occlusion in dogs. *Circ Res*,33(3):353~363,1973.
- Ribisl PM, Liu J, Mousa I, Herbert WG, Miranda CP, Froning JN, Froelicher VF. Comparison of computed ST criteria for diagnosis of severe coronary artery disease. *Am J Cardiol*,71(7):546~551,1993
- Richeson JF, Akiyama T, Schenk E. A solid angle analysis of the epicardial ischaemic TQ-ST deflection in the pig: a theoretical and experimental study. *Circ Res*,43(6):879~888,1978
- Roberts DE, Hersh LT, Scher AM. Influence of cardiac fiber orientation on wavefront voltage, conduction velocity, and tissue resistivity in the dog. *Circ Res*,44(5):701~712,1979.
- Roberts DE, Scher AM. Effect of tissue anisotropy on extracellular potential fields in canine myocardium in situ. *Circ Res*,50(3):342~351,1982
- Robertson D, Kostuk WJ, Ahuja SP. The localization of coronary artery stenoses by 12 lead ECG response to graded exercise test: support for intercoronary steal. *Am Heart J*,91(4):437~444,1976
- Rogers JM, Melnick SB, Huang J. Fiberglass needle electrodes for transmural cardiac mapping. *IEEE Trans Biomed Eng*,2002,12 1639~1641.
- Rothberger CJ, Winterberg H. Studien über die Bestimmung des Ausgangspunktes ventrikulärer extrasystolen mit Hilfe des Elektrokardiogramms. *Pflügers Arch Physiol*,154:571~598,1913
- Roubin GS, Shen WF, Nicholson M, Dunn RF, Kelly DT, Harris PJ. Anterolateral ST segment depression in acute inferior myocardial infarction: angiographic and clinical implications. *Am. Heart J*,107(6):1177~1182,1984.
- Rudy Y, Plonsey R. A comparison of volume conductor and source geometry effects on body surface and epicardial potentials. *Circ Res*,46(2):283~91,1980.
- Ruddy TD, Yasuda T, Gold HK, Leinbach RC, Newell JB, McKusick KA, Boucher CA, Strauss HW. Anterior ST segment depression in acute inferior myocardial infarction as a marker of greater inferior, apical, and posterolateral damage. *Am Heart J*,112:1210~1216,1986.
- Salcedo JR, Baird MG, Chambers RJ, Beaulands DS. Significance of reciprocal ST segment depression in anterior precordial leads in acute inferior myocardial infarction: concomitant left anterior descending disease? *Am J Cardiol*,48:1003~1008,1981.
- Samson, W.E. and Scher, A.M.. Mechanism of ST segment alteration during acute myocardial injury. *Circ Res*,8:780~787,1960.
- Samson WE, Scher AM. Mechanism of ST segment alteration during acute myocardial injury. *Circ Res*,8:780~787,1960.
- Sano T, Takayama N, Shimamoto T. Directional difference of conduction velocity in the cardiac ventricular syncytium studied by microelectrodes. *Circ Res*,7(2):262~267,1959.
- Sasaki K, Yotsukura M, Sakata K, Yoshino H, Ishikawa K. Relation of ST-segment changes in inferior leads during anterior wall acute myocardial infarction to length and occlusion site of the left anterior descending coronary artery. *Am J Cardiol*, 87(12):1340~1345,2001.
- Savard P, Cohen D, Lepeschkin E, Cuffin BN, Madias JE. Magnetic measurement of ST and TQ segment shifts in humans. Part I: Early repolarization and left bundle branch block. *Circ Res*,53(2):264~273,1983.
- Sayen JJ, Sheldon WF, Peirce G, Kuo PT. Polarographic oxygen, the epicardial electrocardiogram and muscle contraction in experimental acute regional ischemia of the left ventricle. *Circ Res*, 6:779~798,1958.
- Sayen JJ, Peirce G, Katcher AH, Sheldon WF. Correlation of intramyocardial electrocardiograms with polarographic oxygen and contractility in the non-ischaemic and regionally ischaemic left ventricle. *Circ Res*,9:1268~1279,1961.
- Schaper W. Comparative arteriography of the collateral circulation. In: *The Collateral Circulation of the Heart*. Amsterdam: North Holland Publishing Company, pp29~50,1971a.
- Schaper W. Pathophysiology of coronary circulation. *Prog Cardiovasc Dis*,14(3):275~296,1971b.
- Schaper W, Frenzel H, Hort W, Winkler B. Experimental coronary artery occlusion. II. Spatial and temporal evolution of infarcts in the dog heart. *Basic Res Cardiol*,74(3):233~239,1979.
- Scher AM, Young AC. The pathway of ventricular depolarisation in the dog. *Circulation Res*,4:461~469,1956.
- Scher AM, Young AC, Meredith WM. Factor analysis of the electrocardiogram. Test of electrocardiographic theory. Normal hearts. *Circ Res*,8 619~626,1960.
- Scherlay BJ, Kosowsky BD, Damato AN. A technique for ventricular pacing from the His bundle of the intact heart. *J Appl Physiol*,22(3):584~687,1967.
- Schmitt OH, Levine RB, Simonson E. electrocardiographic mirror from pattern studies, experimental validity test of the dipole test and of central terminal theory. *Am Heart J*,45:416~428,1953

- Schwartz JS, Cohn JN, Bache RJ. Effects of coronary occlusion on flow in the distribution of a neighboring coronary artery in the dog. *Am J Cardiol*, 52:189-195, 1983.
- Selvester RH, Kalaba R, Collier CR, Bellman R, Kagiwada H. A digital computer model of the vector cardiogram with distance and boundary effects: Simulated myocardial infarction. *Am Heart J*, 74(6):792-808, 1967.
- Shaefer H, Hass HG. Electrocardiography. In: *Handbook of physiology* sect 2, Circulation Vol 1, edited by WF Hamilton, P Dow. Amer Physiol Soc, p379, 1962.
- Shah PK, Pichler M, Berman DS, Maddahi J, Peter T, Singh BN, Swan HJ. Noninvasive identification of a high risk subset of patients with acute inferior myocardial infarction. *Am J Cardiol*, 46(6):915-921, 1980.
- Shah PK, Pichler M, Berman DS, Singh BN, Swan HJ. Left ventricular ejection fraction determined by radionuclide ventriculography in early stages of first transmural myocardial infarction. Relation to short-term prognosis. *Am J Cardiol*, 45(3):542-546, 1980.
- Simoons ML, Block P. Toward the optimal lead system and optimal criteria for exercise electrocardiography. *Am J Cardiol*, 47((6):1366-1374, 1981.
- Smith GT, Geary G, Ruf W, Roelofs TH, McNamara JJ. Epicardial mapping and electrocardiographic models of myocardial ischaemic injury. *Circulation*, 60(4):930-938, 1979.
- Smith GT, Geary G, Blanchard W, Roelofs TH, Ruf W, McNamara JJ. An electrocardiographic model of myocardial ischaemic injury. *J Electrocardiol*, 16(3):223-233, 1983.
- Smith MF, Guzzo JA, Buonocore RV, Greenspon AJ. Endocardial activation mapping of ventricular tachycardia in swine using a percutaneous multielectrode "Basket" catheter. *Circulation*, 90(4 pt 2):I-485, 1994.
- Smith WM, Ideker RE, Kinckel RE, Harrison L. A computer system for the intraoperative mapping of ventricular arrhythmias. *Comput Biomed Res*, 13:61-72, 1980.
- Smith WM, Ideker RE, Smith WM, Kasell J, Harrison L, Bardy GH, Gallagher JJ, Wallace AG. Localization of septal pacing sites in the dog heart by epicardial mapping. *J Am Coll Cardiol*, 1(6):1423-34, 1983.
- Smith HJ, Singh BN, Norris RM, John MB, Hurley PJ. Changes in myocardial blood flow and ST segment elevation following coronary artery occlusion in dogs. *Circ Res*, 36(6):697-705, 1975.
- Spach MS, Barr RC. Ventricular intramural and epicardial potential distribution during ventricular activation and repolarization on the intact dog. *Circ Res*, 37(2):243-257, 1975.
- Spach MS, Barr RC. Origin of epicardial ST-T wave potentials in the intact dog. *Circ Res*, 39(4):475-487, 1976.
- Spach MS, Barr RC, Serwer GA, Kootsey JM, Johnson EA. Extracellular potentials related to intracellular action potentials in the dog Purkinje system. *Circ Res*, 30(5):505-519, 1972.
- Spielman SR, Michelson EL, Horowitz LN, Spear JF, Moore EN. The limitations of epicardial mapping as a guide to the surgical therapy of ventricular tachycardia. *Circulation*, 57(4):666-670, 1978.
- Stevenson RN, Ranjadayan K, Umachandran V, Timmis AD. Significance of reciprocal ST depression in acute myocardial infarction: a study of 258 patients treated by thrombolysis. *Br Heart J*, 69:211-214, 1993.
- Stevenson RN, Umachandran V, Ranjadayan K, Roberts RH, Timmis AD. Early exercise testing after treatment with thrombolytic drugs for acute myocardial infarction: importance of reciprocal ST segment depression. *British Medical Journal*, 308:1189-1192, 1994.
- Surawicz B. Relationship between electrocardiogram and electrolytes. *Am Heart J*, 73(6):814-834, 1967.
- Surawicz B. ST-T abnormalities. In: *Comprehensive Electrocardiology*, Macfarlane PW, Veitch Lawrie TD, eds. Pergamon Press, pp513-520, 1989.
- Swan HJ, Forrester JS, Diamond G, Chatterjee K, Parmley WW. Hemodynamic spectrum of myocardial infarction and cardiogenic shock. A conceptual model. *Circulation*, 45:1097-1110, 1972.
- Taccardi B. Changes in cardiac electrogenesis following coronary occlusion. In: Marchetti G, Taccardi B., eds., *Coronary circulation and Energetics of the myocardium*. Karger, Basel, pp259-267, 1967.
- Taccardi B. La distribution spatiale des potentiels cardiaques. *Acta Cardiol*, 13:173-189, 1958.
- Taccardi B. Present and future of body surface electrocardiographic mapping. In: *Electrocardiographic body surface mapping*. Van Dam RT and Van Oosterom A eds., 3rd edition, pp3-8, 1985.
- Taccardi B, Arisi G, Macchi E, Baruffi S, Spaggiari S. A new intracavitary probe for detecting the site of origin of ectopic ventricular beats during one cardiac cycle. *Circulation*, 75(1):272-281, 1987.
- Tanaka H, Yajima K, Thara T, Furukawa T. An inverse solution of electrocardiography---epicardial potential estimation by using the orthogonal expansion method. *Jap Heart J*, 23:352-354, 1982.

- Thompson PL, Katavatis V. Acute myocardial infarction. Evaluation of precordial ST segment mapping. *Br Heart J*, 38(10):1020-1024, 1976.
- Tiefenbacher CP, Chilian WM. Heterogeneity of coronary vasomotion. *Basic Res Cardiol*, 93:446-454, 1998.
- Tilg B, Hanser F, Modre-Osprian R, Fischer G, Messnarz B, Berger T, Hintringer F, Pachinger O, Roithinger FX. Clinical ECG mapping and imaging of cardiac electrical excitation. *J Electrocardiol*, 35 Suppl:81-87, 2002.
- Tonooka I, Kubota I, Watanabe Y, Tsuiki K, Yasui S. Isointegral analysis of body surface maps for the assessment of location and size of myocardial infarction. *Am J Cardiol*, 52(10):1174-1180, 1983.
- Tota B. On the regional metabolism of beef heart ventricles. *Acta Physiol Scand*, 87(3):289-295, 1973.
- Tota B. Vascular and metabolic zonation in the ventricular myocardium of mammals and fishes. *Comp Biochem Physiol*, 76(3):423-437, 1983.
- Toyama S, Suzuki K, Yoshino K, Fujimoto K. A comparative study of body surface isopotential mapping and the electrocardiogram in diagnosing of myocardial infarction. *J Electrocardiol*, 17(1):7-13, 1984.
- Toyama S, Suzuki K, Takahashi T, Yamashita Y. Myocardial infarction size and location: a comparative study of epicardial isopotential mapping, thallium-201 scintigraphy, Electrocardiography and vectorcardiography. *J Electrocardiol*, 20(3):203-211, 1987.
- Toyoshima H, Ekmekci A, Flamm E, Mizuno Y, Nagaya T, Nakayama R, Yamada K, and Prinzmetal M. Angina Pectoris. VII The nature of ST depression in acute myocardial ischemia. *Am J Cardiol*, 13:498-509, 1964.
- Toyoshima H, Takakuma K. ST segment displacement of intramural lead ECG in experimental hemorrhagic hypotension. *Ann Report of Inst of Environment Med*, 11:92, 1960.
- Tripp MR, Meyer MW, Einzig S, Leonard JJ, Swayze CR, Fox JJ. Simultaneous regional myocardial blood flows by tritiated water and microspheres. *Am J Physiol*, 232(2):H173-190, 1977.
- Tung T. "A bidomain model for describing ischaemic myocardial DC potentials," in PhD thesis, MIT, 1978.
- Tzivoni D, Chenzbraun A, Keren A, Benhorn J, Gottlieb S, Lonn E, Stern S. Reciprocal electrocardiographic changes in acute myocardial infarction. *Am J Cardiol*, 56(1):23-26, 1985.
- Tzivoni D, Gottlieb S, Keren A, Benhorn J, Chenzbraun A, Klein J, Stern S. Early right atrial pacing after myocardial infarction. II. Results in 77 patients with predischARGE angina pectoris, congestive heart failure, or age older than 70 years. *Am J Cardiol*, 53(4):418-420, 1984.
- Tzivoni D, Keren A, Gottlieb S, Benhorn J, Gazala E, Goldman JO, Stern S. Right atrial pacing ??? after myocardial infarction. *Circulation*, 65(2):330-335, 1982.
- van Oosterom A. Solidifying the solid angle. *J Electrocardiol*, 35 Suppl:181-192, 2002.
- Van Oosterom A, van Dam RT. Potential distribution in the left ventricular wall during depolarisation. *Adv Cardiol*, 16:27-31, 1976.
- Vincent MG, Abildskov JA, Burgess MJ. Mechanism of ischaemic ST-segment displacement. evaluation by direct current recordings. *Circulation*, 56:559-566, 1977.
- Von-Essen R, Schmidt W, Uebis R, Edelmann B, Effert S, Silny J, Rau G. Myocardial infarction and thrombolysis: Electrocardiographic short term and long term results using precordial mapping. *Br Heart J*, 54(1):6-10, 1985.
- Wallace AG, Sealy WC, Gallagher JJ, Svenson RH, Strauss HC, Kasei J. Surgical correction of anomalous left ventricular preexcitation: Wolff-Parkinson-White (type A). *Circulation*, 49(2):206-213, 1974.
- Walker SJ, Kilpatrick D. An automated system for modelling the electrical properties of the human torso. *IEEE Computers in Cardiology*, 409-412, 1985.
- Walker SJ, Kilpatrick D. Forward and inverse electrocardiographic calculations using resistor network models of the human torso. *Circ Res*, 61(4):504-513, 1987a.
- Walker SJ, Kilpatrick D. Studies of the regularisation method applied to the inverse calculation of epicardial potentials. *IEEE Computers in Cardiology*, 359-362, 1987b.
- Walker SJ, Lavercombe PS, Loughhead MG, Kilpatrick D. A body surface mapping system with immediate interactive data processing. *IEEE Computers in Cardiology*, 305-308, 1983.
- Wartier DC, Zyvoloski MG, Gross GJ, Brooks HL. Subendocardial versus transmural myocardial infarction: Relationship to the collateral circulation in canine and porcine hearts. *Can J Physiol Pharmacol*, 60(12):1700-1706, 1982.
- Wasserman AG, Ross AM, Bogaty DB, Richardson DW, Hutchinson RG, Rios JC. Anterior ST segment depression during acute inferior myocardial infarction: evidence for the reciprocal change theory. *Am Heart J*, 106(3):516-520, 1983.
- Wei K, Jayaweera AR, Firoozan S, Linka A, Skyba DM, Kaul S. Quantification of myocardial blood flow with ultrasound-induced destruction of microbubbles administered as a constant venous infusion. *Circulation*, 97(5):473-483, 1998.

- Weiss HR. Regional oxygen consumption and supply in the dog heart: effect of atrial pacing. *Am J Physiol*,236(2):H231~237,1979.
- Weiss HR, Sinha AK. Regional oxygen saturation of small arteries and veins in the canine myocardium. *Circ Res*,42(1):119~126,1978.
- Wellens HJJ, Janse MJ, van Dam RT, Durrer D. Epicardial excitation of the atria in a patient with atrial flutter. *Br Heart J*,33(2):233~237,1971.
- Wendt RL, Canavan RC, Michalak RJ. Effects of various agents on regional ischemic myocardial injury: electrocardiographic analysis. *Am Heart J*,87:468~482,1974.
- Wilde AA, Kleber AG. The combined effects of hypoxia, high K^+ , and acidosis on the intracellular sodium activity and resting potential in guinea pig papillary muscle. *Circ Res*,58(2):249~256,1986.
- Wilensky RL, Trantum-Jensen J, Coronel R, Wilde AA, Fiolet JW, Janse MJ. The subendocardial border zone during acute ischemia of the rabbit heart: an electrophysiologic, metabolic, and morphologic correlative study. *Circulation*,74:1137~1146,1986.
- Willeison JT, Powell WJ Jr, Guiney TE, Stark JJ, Sanders CA, Leaf A. Improvement in myocardial function and coronary blood flow in ischaemic myocardium after mannitol. *J Clin Invest*,51(12):2989~2998,1972.
- Wilson FN, Hill IGW, Johnston FD. The interpretation of the galvanometric curves obtained when one electrode is distinct from the heart and the other near or in contact with its surface. II. Observations on the mammalian heart. *Am Heart J*,10:163~175,1934.
- Wilson FN, MacLeod AG, Barker PS. The distribution of the action currents produced by heart muscle and other excitable tissue immersed in extensive conducting media. *J Gen Physiol*,16:423~456,1933a.
- Wilson FN, Macleod AG, Barker PS. The distribution of the currents of action and injury displayed by heart muscle and other excitable tissues. *Univ Mich Studies Sci Ser*,10:1~57,1933b.
- Wilson FN, Macleod AG, Barker PS. The distribution of the currents of action and of injury displayed by heart muscle and other excitable tissues. *Univ Mich Studies Sci Ser*,18:58~115,1933c.
- Wilson FM, Macleod AG, Johnston FD, Hill IGW. Monophasic electrical response produced by the contraction of injured heart muscle. *Proc Soc Exp Biol*,30:797~798,1933d.
- Wimbury MM, Howe BB, Weiss JR. Effect of nitroglycerin and dipyridamole on epicardial and endocardial oxygen tension--further evidence for redistribution of myocardial blood flow. *J Pharmacol Exp Ther*,176(1):184~199,1971.
- Witkowski FX, Penkoske PA. A new fabrication technique for directly coupled transmural cardiac electrodes. *Am J Physiol*,254(4 Pt 2):H804~810,1988.
- Witkowski FX, Corr PB. An automated simultaneous transmural cardiac mapping system. *Am J Physiol*,247(4 pt 2):H661~668,1984.
- Woitczak J. Contractures and increase in internal longitudinal resistance of cow ventricular muscle induced by hypoxia. *Circ Res*,44(1):88~95,1979.
- Wolferth C.C., Bellet S., Livezey M.M., and Murphy F. Negative displacement of the RS-T segment in the electrocardiogram and its relationships to positive displacement; an experimental study. *Am Heart J*,29:220~224,1945.
- Wong CK, Freedman SB. Usefulness of continuous ST monitoring in inferior wall acute myocardial infarction for describing the relation between precordial ST depression and inferior ST elevation. *Am J Cardiol*,72:532~537,1993.
- Wong CK, Freedman SB, Bautovich G, Bailey BP, Bernstein L, Kelly DT. Mechanism and significance of precordial ST-segment depression during inferior wall acute myocardial infarction associated with severe narrowing of the dominant right coronary artery. *Am J Cardiol*,71:1025~1030,1993.
- Woodbury JW. Interrelationships between ion transport mechanism and excitatory events. *Fed Proc*,22:31~35,1963.
- Wu G, Littmann L, Svenson RH, Nanney GA, Tatsis GP, Tuntelder JR, Chuang CH, Thompson M, Dezern KR. Computerized three-dimensional activation mapping study of spontaneous ventricular arrhythmias during acute myocardial ischemia in dogs. *J Electrocardiology*,28(2):115~130,1995.
- Wusten B, Buss DD, Deist H, Schaper W. Dilatory capacity of the coronary circulation and its correlation to the arterial vasculature in the canine left ventricle. *Basic Res Cardiol*,72(6):636~650,1977.
- Wyndham CR, Smith T, Meeran MK, Mammana R, Levitsky S, Rosen KM. Epicardial activation in patients with left bundle branch block. *Circulation*,61(4):696~703,1980.
- Yajima K, Thara T, Tanaka H, Hirayanagi K, Furukawa T. An inverse solution of electrocardiography---experimental evaluation of its accuracy by freezing degeneration of myocardium. *Jap Heart J*,23:349~351,1982.
- Yamaki M, Ikeda K, Kubota I, Nakamura K, Hanashima K, Tsuki K, Yasui S. Improved diagnostic performance on the severity of left ventricular hypertrophy with body surface mapping. *Circulation*,79(2):312~323,1989.

REFERENCES

- Yanowitz FG, Vincent M, Lux RL, Merchant M, Green LS, Abildskov JA. Application of body surface mapping to exercise testing: ST-80 isoarea maps in patients with coronary artery disease. *Am J Cardiol*,50(5):1109~1113,1982.
- Yasue H, Omote S, Takizawa A, Masao N, Hyon H, Nishida S, Horie M. Comparison of coronary arteriographic findings during angina pectoris associated with ST segment elevation or depression *Am J Cardiol*,47(3):539~546,1981.
- Yin FC Ventricular wall stress. *Circ Res*,49 829~842,1981.
- Yipintsoi T, Dobbs WA Jr, Scanlon PD, Knopp TJ, Bassingthwaighite JB. Regional distribution of diffusible tracer and carbonised microspheres in the left ventricle of isolated dog hearts. *Circ Res*,33(5):573~587,1973
- Yoran C, Covell JW, Ross J Jr. Structural basis for the ascending limb of left ventricular function *Circ Res*,32(2):297~303,1973
- Yu PNG, Stewart JM. Subendocardial myocardial infarction with special reference to the electrocardiographic changes. *Am Heart J*,39:862~880,1950.
- Zhou H, van Oosterom A. Application of the boundary element method to the solution of anisotropic electromagnetic problems *Med Biol Eng Comput*,32(4):399-405,1994.
- Zrenner B, Ndrepepa G, Schneider M, Karch M, Hofmann F, Schomig A, Schmitt C. Computer-assisted animation of atrial tachyarrhythmias recorded with a 64-electrode basket catheter. *J Am Coll Cardiol*,34(7).2051-60,1999.